PACIFIC EARTHQUAKE ENGINEERING RESEARCH CENTER

Seismic Performance of Masonry Buildings and Design Implications

Kerri Anne Taeko Tokoro
Stanford University

James C. Anderson
University of Southern California

Vitelmo V. Bertero
University of California, Berkeley

Sponsor:
California Energy Commission

PEER 2004/01
FEBRUARY 2004

Seismic Performance of Masonry Buildings and Design Implications

Kerri Anne Taeko Tokoro
Stanford University

James C. Anderson
University of Southern California

Vitelmo V. Bertero
University of California, Berkeley

Sponsor:

California Energy Commission

PEER Report 2004/01
Pacific Earthquake Engineering Research Center
College of Engineering
University of California, Berkeley

February 2004

ABSTRACT

The seismic response of three reinforced masonry buildings with flexible diaphragms is investigated, two buildings with instrumentation, and one without. An instrumented three-story building is investigated for its response during the Whittier Narrows (1989), Landers (1992), and Northridge (1994), California, earthquakes, and the response of an instrumented two-story building during the Loma Prieta (1989) earthquake is presented. Flexibility of the diaphragms of the two instrumented buildings was also studied by using the 1997 UBC criteria. Static and dynamic analyses were used to evaluate the code criteria for determining the flexibility of the diaphragms. It was found that for the two instrumented buildings, the classification of the diaphragm depended largely on the type of loading used in the analyses. A third building studied in this report is a one-story building lacking instrumentation and modeled using ETABS (version 7). Dynamic time history analyses were conducted on this model using a total of 6 sets of ground motions representative of strong ground motions, including motions containing multi-sided displacement pulses. Base shear and displacement time histories suggest that this building would not suffer significant structural damage in an earthquake having similar ground motion characteristics. However, damage to nonstructural components and equipment may occur due to high accelerations.

ACKNOWLEDGMENTS

This project was sponsored by the Pacific Earthquake Engineering Research Center's Program of Applied Earthquake Engineering Research of Lifeline Systems supported by the California Energy Commission, the California Department of Transportation, and the Pacific Gas and Electric Company.

This work made use of the Earthquake Engineering Research Centers Shared Facilities supported by the National Science Foundation under award number EEC-9701568 through the Pacific Earthquake Engineering Research Center (PEER).

Any opinions, findings, and conclusions or recommendations expressed in this material are those of the author(s) and do not necessarily reflect those of the National Science Foundation.

This report was prepared as a result of work sponsored by the California Energy Commission (Commission). It does not necessarily represent the views of the Commission, its employees, or the State of California. The Commission, the State of California, its employees, contractors, and subcontractors make no warranty, express or implied, and assume no legal liability for the information in this report; nor does any party represent that the use of this information will not infringe upon privately owned rights. This report has not been approved or disapproved by the Commission nor has the Commission passed upon the accuracy or adequacy of the information in this report.

Mr. Kent Ferre (PG&E) served as technical monitor for this project, and Mr. Chris Poland (Degenkolb Engineers) and Mrs. Maryann T. Phipps (ESTRUCTURE) served as project consultants. Their interest and constructive comments were greatly appreciated and made a significant contribution to the results presented in this report. Thanks are also due Dr. Tony Shakal and Dr. Moh Huang of the California Strong Motion Instrumentation Program for their assistance in providing much of the data used in this study.

CONTENTS

LIST OF FIGURES

LIST OF TABLES

1 Introduction

1.1 GENERAL REMARKS

Damaged observed following moderate to large earthquakes has shown that masonry buildings are vulnerable to lateral shaking (Abrams 1997). Fallen brick and mortar constitute a life-safety hazard that must be mitigated for future earthquakes. The two most important methods to prevent damage, destruction, and loss of life are to constantly improve the current standards by which buildings are designed, as well as to focus on developing effective methods for the rehabilitation and/or upgrading of buildings that have been shown to be vulnerable to lateral shaking.

In order to improve the design of new buildings and select effective new methods to assess the vulnerability and to retrofit existing facilities, the dynamic behavior of structures subjected to critical seismic excitations that may occur during their expected service life must be evaluated. One approach to this existing problem has been the construction and testing of reduced-scale masonry buildings subjected to an array of simulated earthquake ground motions (Abrams 1997). However, research has shown that existing instrumented buildings may provide invaluable insights into the understanding of the true seismic response of masonry buildings subjected to earthquake ground motions (Raggett and Rojahn 1991). When properly instrumented to record the response of the building to base accelerations, these data may be used as a basis for the development and calibration of analytical models and building code requirements.

Few experimental research studies have attempted to assess the dynamic response of masonry structures with wood diaphragms. An alternative to using either full-scale or reduced-scale experiments to evaluate the dynamic response of this class of buildings is to develop analytical models that can be shown to closely emulate the response obtained from instrumented buildings for which there are recorded acceleration data.

Though masonry is one of the oldest known forms of construction, a limited number of studies on the seismic response of reinforced masonry shear wall buildings with flexible diaphragms have been presented in the literature. Previous efforts have focused on the creation of a two-dimensional (2-D) multi-degree-of-freedom linear elastic dynamic model for the analytical analysis of such buildings (Tena-Colunga and Abrams 1992), (Tena-Colunga 1992). These previous efforts have been expanded to include a simplified three-dimensional (3-D) dynamic response analysis of masonry buildings with flexible diaphragms. In this simplified analysis, the 3-D response is approximated by superimposing the peak accelerations at a desired time of peak response of two 2-D linear elastic MDOF models created for the transverse and longitudinal building directions. Finally, a 3-D nonlinear static analysis, based upon the equivalent static forces obtained from the dynamic analyses of the two orthogonal MDOF discrete models using the ABAQUS finite element analysis program, was performed to obtain the quasi-dynamic response of the structure (Tena-Colunga and Abrams 1993, 1995). Recent increases in the computational speed and the data storage capacity of business computers coupled with enhanced capabilities of current structural analysis software make the use of more detailed structural models possible. Hence, the current study reported in this document describes the development of detailed 3-D models.

Although testing reduced-scale masonry structures is of great significance to understanding the behavior of such buildings, there is a great need to develop reliable and practical analytical models for predicting the seismic response of buildings for which instrumentation is not available, since it is not feasible nor practical to instrument a large number of reinforced masonry buildings. Therefore, general guidelines for the development of analytical models must be developed. To do this, analytical models for predicting the dynamic response of instrumented masonry buildings need to be created and the calculated response compared to the recorded response for verification.

In addition, prior analyses of strong motion data have shown that there is a need for more complete instrumentation of the existing instrumented masonry buildings in order to avoid ambiguity. Research has also shown that there is significant amplification of the ground acceleration at the roof level of stiff shear wall buildings with flexible diaphragms, particularly in the transverse building direction. However, the motions of such a building in the longitudinal direction show little amplification at the roof because the primary contributor to that amplification, diaphragm flexibility, is generally small.

Structures with flexible floor diaphragms behave intrinsically different under dynamic lateral loading than structures with rigid diaphragms. This has been recognized by building codes, including the 1997 Uniform Building Code (UBC, Section 1633.2.9), which specify provisions for the seismic design of newly constructed building systems considering flexible-diaphragm behavior (ICBO 1997). However, a clear criterion for determining when a diaphragm is flexible or rigid is not available for application in practice. Flexible-diaphragm systems continue to be analyzed using the same criteria and recommendations as developed for structures with rigid diaphragms, which may not necessarily be a conservative approach. Research has shown that structures with flexible diaphragms may experience higher accelerations and displacements than structures with rigid diaphragms, and their fundamental periods of vibration may be significantly longer (Tena-Colunga and Abrams 1996).

Although it is known that properly detailed reinforced masonry buildings can develop sufficient stiffness and strength, their seismic performance has not been well documented in the past. Therefore, the seismic behavior of masonry structures is still not completely understood. Certain masonry structures have performed well when subjected to strong ground motions and modern masonry construction has also had a satisfactory performance in recent earthquakes. Of the buildings with such modern characteristics are a three-story office building in Lancaster, California, and a two-story office building in Palo Alto, California. These buildings are of particular interest for analytical studies as they are among the few reinforced masonry buildings that have been instrumented by the California Strong Motion Instrumentation Program (CSMIP). Significant amplification of the peak ground acceleration was observed at the roof level of both buildings. Each building had satisfactory performance despite the intensity of the seismic shaking. The analytical study of the performance of each of these buildings is of interest, since they serve as a means for enhancing our understanding of how similar masonry structures may respond when subjected to moderate and strong ground motions.

1.2 OBJECTIVES AND SCOPE

The present work will investigate the seismic response of three masonry shear wall buildings. Two of these have plywood diaphragms and one has a metal deck diaphragm. The two existing buildings with plywood diaphragms are instrumented and have recorded the building response to seismic ground motion, making them valuable for analytical investigation. The California

Strong Motion Instrumentation Program (CSMIP) has instrumented each of the two buildings. Strong motion data for thirteen sensors were available to measure the accelerations of the Lancaster building during the Landers (1992), Northridge (1994), and Whittier Narrows (1987) earthquakes. Accelerations recorded during the Loma Prieta earthquake (1989) were available for the Palo Alto building that was instrumented by CSMIP with seven sensors. For the three-story building, analyses of its dynamic behavior during the 1987 Whittier Narrows, 1992 Landers, and 1994 Northridge earthquakes are presented. Additionally the behavior of the two-story office building in Palo Alto during the 1989 Loma Prieta earthquake will be examined. Two of the building systems consisted of lateral-force-resisting masonry walls, edge beams, and diaphragms of plywood and joist construction. Specific information regarding the degree of structural damage to each building as a result of the earthquakes was not available. The third building is a one-story building that houses equipment. Although it is not occupied during normal operation, it must remain functional following an earthquake. Three-dimensional linear elastic analytical models of the three buildings were created using ETABS (Computers and Structures, Inc. 1999) software to study the seismic response of each building.

Spectral analyses are performed on each building to determine the dynamic characteristics of the building using the recorded accelerations experienced by the building during the seismic ground shaking. Three-dimensional models are developed using the linear-elastic finite elements in ETABS, and the calculated dynamic response to the recorded base motion is compared to the accelerations and corresponding displacements derived from the accelerations. Base shear demands are also studied by comparing the 1997 UBC requirements for the design base shear to the values predicted by the analytical models. Data on soil profile and properties were not available. Since instruments were located in the base of the building, soil-structure interaction effects were not considered.

The objectives of this study are to (1) assess the applicability of the analytical models presently available for analyzing the elastic seismic performance of reinforced masonry buildings, (2) to estimate through dynamic analyses the linear elastic response and to infer the potential damage that each of the reference buildings may have experienced under the recorded ground motion, (3) to estimate the response of the reference buildings under more severe ground motions to which they may be exposed during their service life, (4) to evaluate the code criteria for considering a diaphragm as rigid or flexible, (5) to investigate the response modification factor specified by current building codes for these buildings and (6) to evaluate the implications of the obtained results regarding the reliability of present seismic code regulations for the design of such buildings.

2 Three-Story Office Building: Lancaster

2.1 BUILDING DESCRIPTION

2.1.1 General

The three-story office building considered in this investigation is shown below in Figures 2.1 and 2.2. The building has a rectangular plan that is 72′ x 129′ and a total height of 37.5′. A view of the east face is shown in Figure 2.1. Shear walls at the south end of the building are shown in Figure 2.2.

Figure 2.1 West exterior view, 3-story building.

The building was designed in 1975, and simplified plan views of the structural components of the building floors are presented in Figure 2.3. The building is rectangular in shape, with the exception of the two rectangular stairwells located at the north and south ends of the building. The longitudinal dimension of the building is aligned in a north-south direction.

The lateral-force-resisting system is composed of grouted concrete masonry unit block walls in the N-S and E-W directions, together with plywood diaphragm floor systems. In addition to the masonry walls, vertical loads are also supported by rectangular steel tube columns located on interior and exterior column lines having an equal number in each story of the building. The building foundation consists of concrete piers.

Figure 2.2 Northeast exterior view, 3-story building.

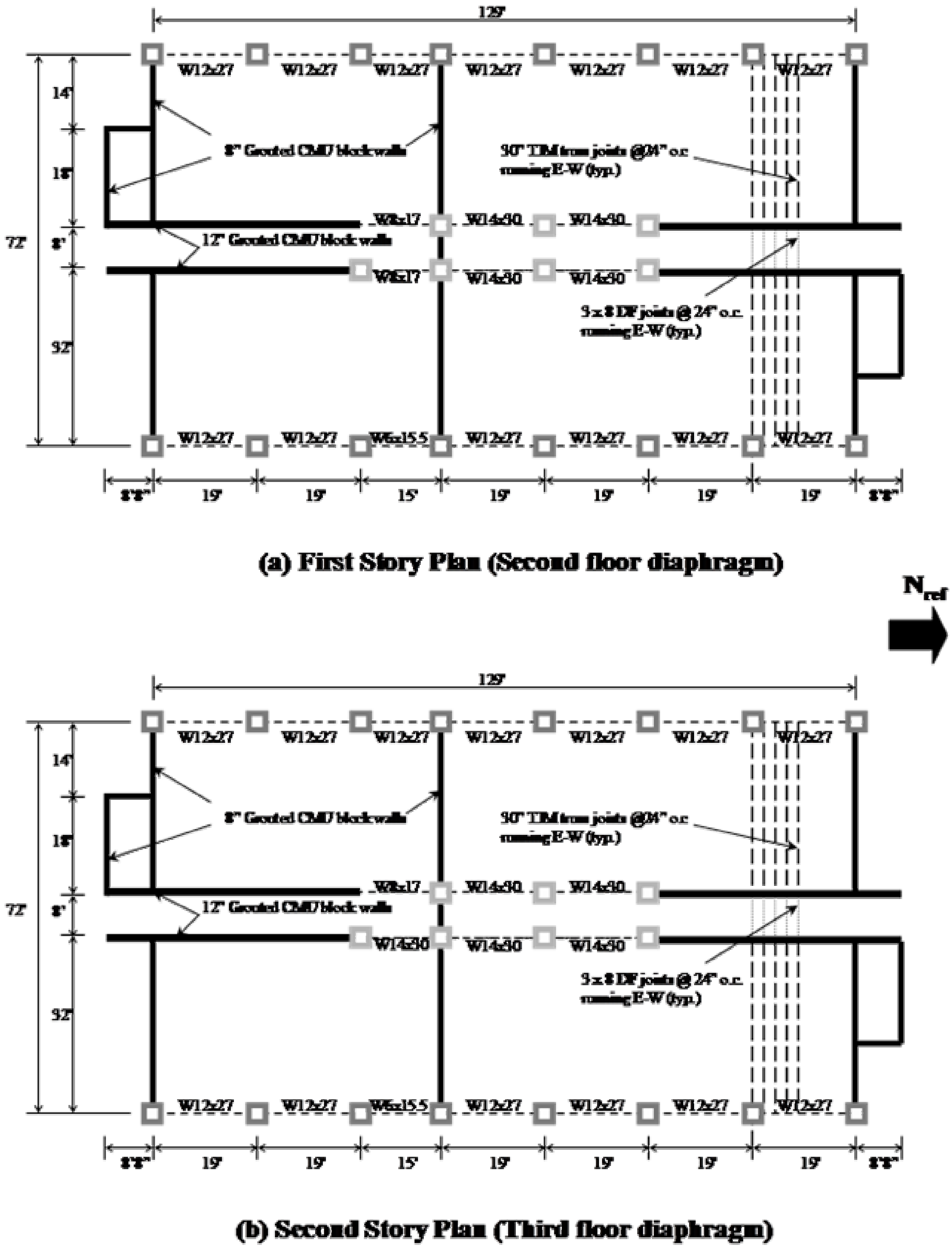

Figure 2.3 Plan views, 3-story building.

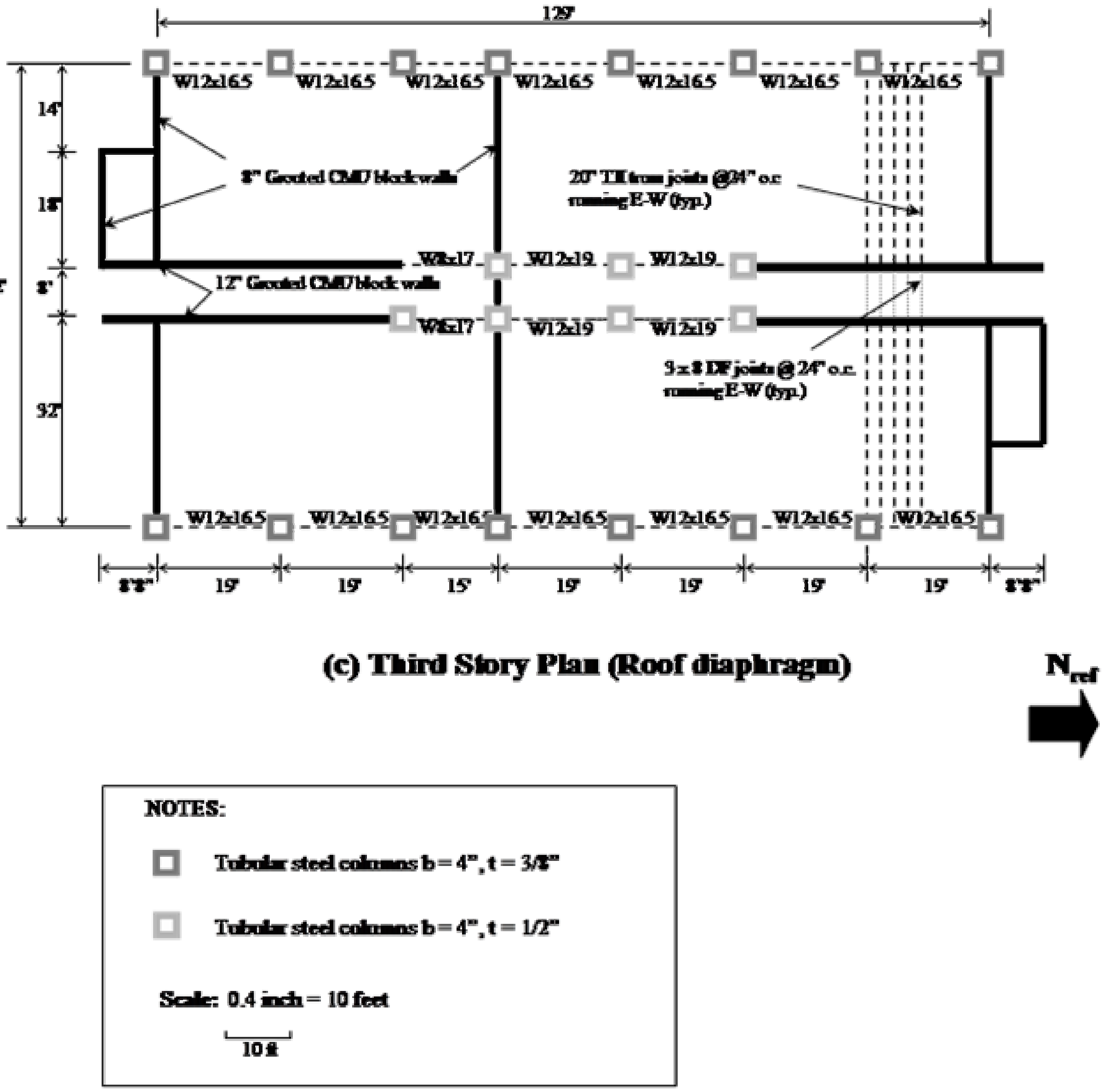

Figure 2.3 Plan views, 3-story building (cont'd.).

2.1.2 Diaphragms

The roof diaphragm of the three-story office building in Lancaster consists of 4′x 8′x ½″ thick structural I plywood mounted on 20″ TJI truss joists running in the E-W direction at 24″ o.c., while plywood edges were nailed to 2x4 Douglas fir studs at 48″ o.c. in the N-S direction. Wide flange W12 x 16 1/2 steel edge beams span between TS 4x4x3/8 steel tube columns along the longitudinal (N-S) edges of the roof, W12x27 steel beams span between similar columns at the edges of the third-floor diaphragm and W 12x27 steel beams span between TS 4x4x1/2 steel tube columns at the edges of the second floor. Wide flange W8x17 and W12x19 interior beams spanning between TS 4x4x3/8 steel tube columns in the N-S direction are used to connect the 12″ N-S masonry shear wall to the roof system. Wide flange W14x30 and W8x17 steel beams spanning between TS 4x4x3/8 steel tube columns in the N-S direction are used to connect the N-S shear walls to the diaphragms at the third-floor level and similar beams are connected to TS 4x4x1/2 steel tube columns at the second floor level. A typical detail of these connections is shown in Figure 2.4. The second and third floor diaphragms consisted of 1-1/8″ Structural I plywood mounted on 30″ TJI open web truss joists at every 24″ o.c. in the E-W direction, and on 2x4 Douglas fir studs in the N-S direction.

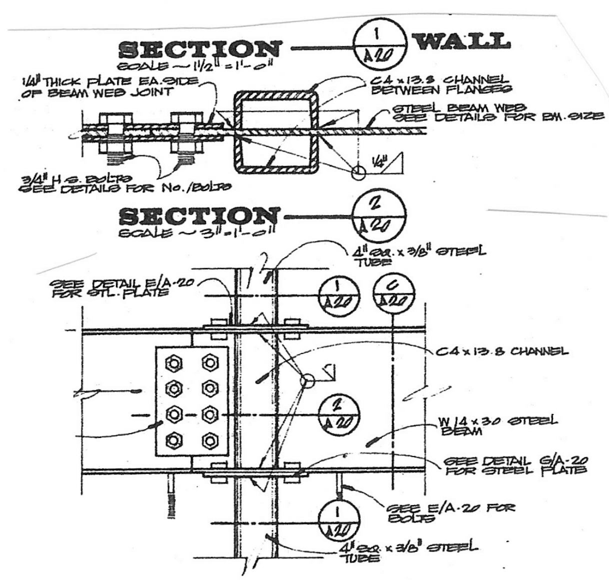

Figure 2.4 Beam to tube column connection detail, 3-story building.

2.1.3 Grouted Walls

The walls of the building are 8″ and 12″ grouted concrete masonry unit block walls. The primary lateral force resisting system in the N-S direction consists of four 12″ walls located four feet on either side of the N-S centerline of the building. Three 8″ walls were used in the E-W direction for lateral resistance with one near the E-W centerline and one at each end. Typical vertical and horizontal reinforcing in the 8″ walls of the building were 1-#5 spaced at 32″o.c. and

1-#4 spaced at 24″o.c., respectively. The 12″ walls contained 2-#4 bars spaced at 24″ o.c. in the horizontal direction, while 2-#4 bars spaced at 32″ were used as vertical reinforcing.

2.1.4 Connection between Diaphragms and Walls

Douglas fir (3x6), ledgers run along the E-W (transverse) reinforced CMU shear walls as a medium for connection of the 2x4 blocking that is perpendicular to the truss joists supporting the plywood diaphragms of the building. Ledgers of the diaphragms are anchored to the grouted walls by ¾″ ϕ steel rods embedded 5″ into the thickness of the CMU walls at 24″ o.c. along the length of 3x6 Douglas fir ledgers. Plywood structural panels are connected to the ledgers through 10d nails at 4″ o.c. along the length of the ledgers. Typical details of the connections of the E-W walls to the diaphragm at the roof and third-story levels are shown in Figures 2.5 and 2.6. Connection of the truss joists to the 12″ CMU walls in the N-S (longitudinal) walls is through a corbel at the top chord and a ledger block at the bottom chord. The corbel is formed by placing two 16″ CMU in the wall as shown in Figure 2.7.

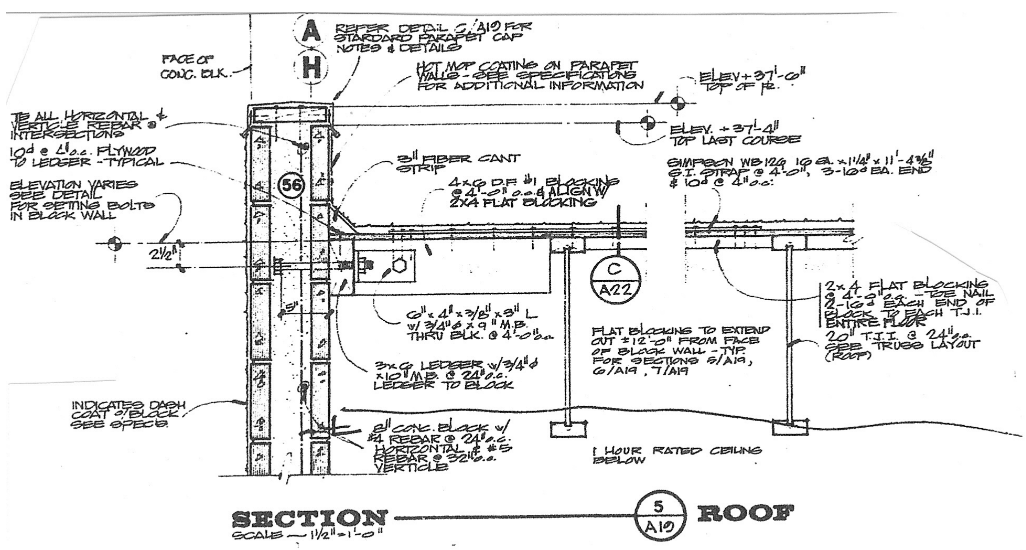

Figure 2.5 Diaphragm to E-W wall connection, roof, 3-story building.

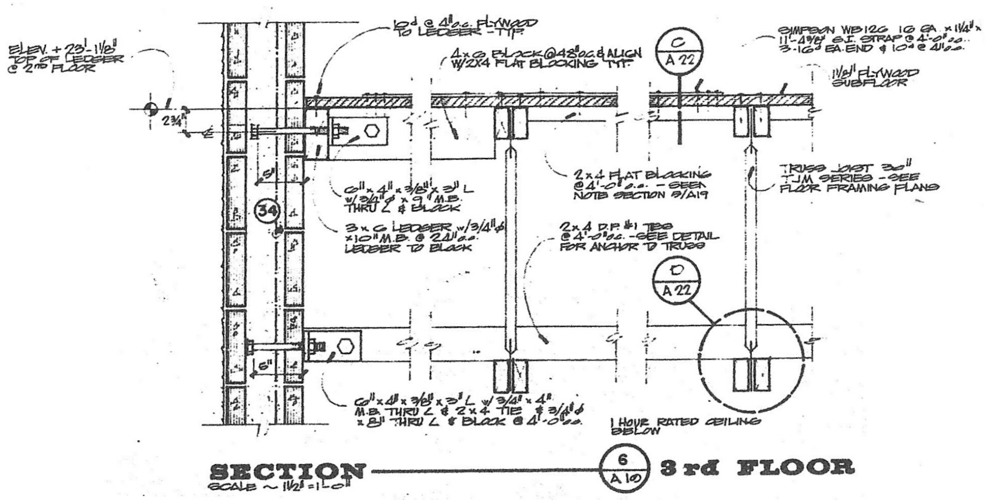

Figure 2.6 Diaphragm to E-W wall connection, 3rd floor, 3-story building.

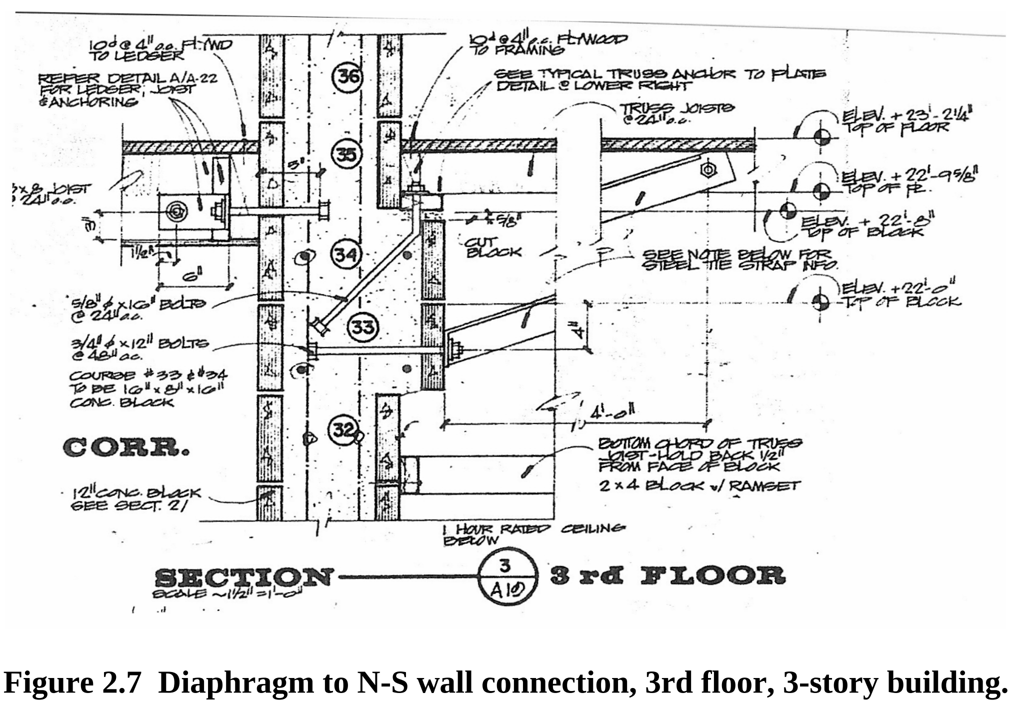

Figure 2.7 Diaphragm to N-S wall connection, 3rd floor, 3-story building.

2.1.5 Foundation System

At ground level, a 4″ thick reinforced concrete slab with welded wire mesh rests on a moisture barrier consisting of 2″ of sand over 4-mill visqueen. The foundation consists of 20″ diameter reinforced concrete piers that extend either 20 or 25 ft in depth. Reinforced concrete grade beams, 18″ x 30″ span between piers under the grouted CMU walls in both directions. Piers are also located at all interior and exterior steel tube columns. The base plate of the steel columns (10″ x 10″ x 1″) is connected to the pier with 4-¾-in. diameter anchor bolts. The concrete slab is thickened to a depth of 8″ and poured over the pier. The details of a typical column to pier connection and a typical grade beam to pier connection are shown in Figure 2.8.

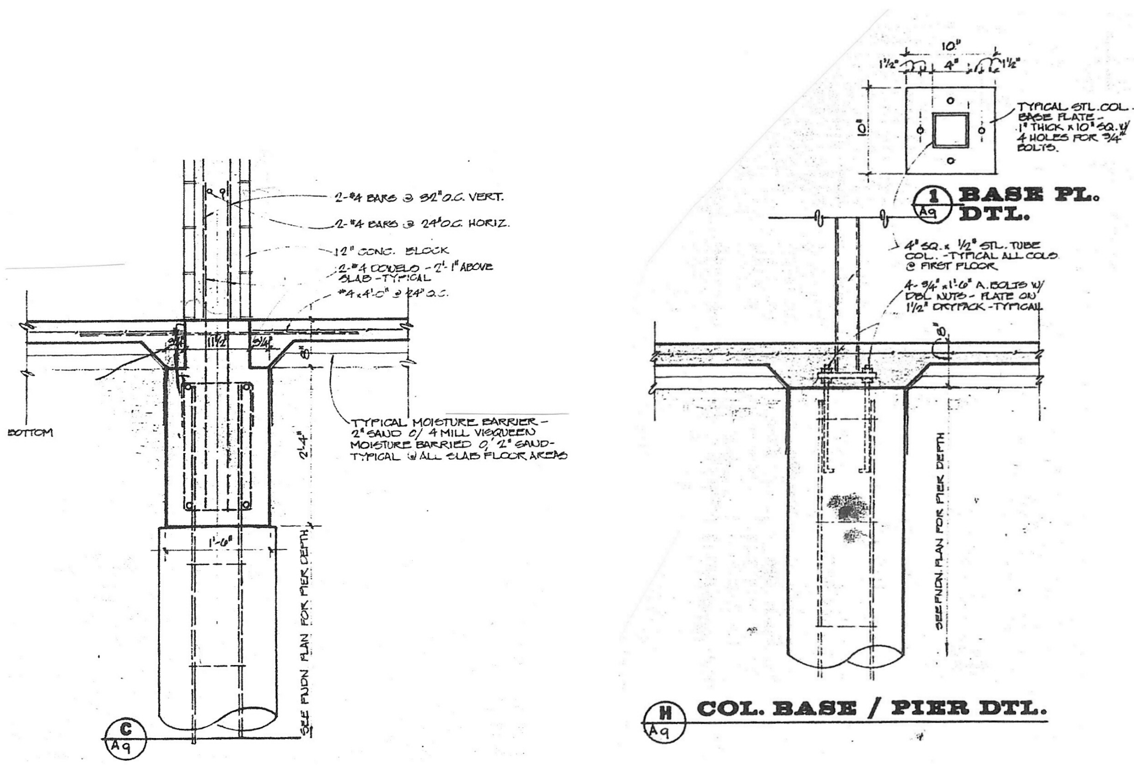

Figure 2.8 Foundation details, 3-story building.

2.2 WHITTIER NARROWS, LANDERS, AND NORTHRIDGE EARTHQUAKES

Instruments in the building have recorded the response to three major earthquakes over the past 15 years. These earthquakes and the recorded responses are described in the following sections.

2.2.1 The Whittier Narrows Earthquake (1987)

The Whittier Narrows Earthquake occurred at 7:42 am (PDT) on the morning of October 1, 1987 and was assigned a local Richter magnitude of 5.9 (M_L). The location of the epicenter was 34^0 03.68′ N, 118^0 04.71′ W, or 11 km (7 miles) southeast of Pasadena. The building site is approximately 52 miles north of the epicenter. This earthquake occurred on a previously unknown, concealed thrust fault approximately 20 km east of downtown Los Angeles, California. It resulted in eight fatalities and $358 million in property damage. Severe damage was confined mainly to communities east of Los Angeles and near the epicenter. No severe structural damage to high-rise structures in downtown Los Angeles was reported.

The most severe damage occurred in the "Uptown" district of Whittier, the old downtown section of Alhambra, and in the "Old Town" section of Pasadena. These areas had high concentrations of unreinforced masonry buildings. Residences that sustained damage usually were constructed of masonry and were not fully anchored to foundations, or were houses built over garages with large door openings. Many chimneys collapsed and in some cases, fell through roofs. Wood-frame residences sustained relatively little damage.

2.2.2 The Landers Earthquake (1992)

The Landers earthquake occurred at 4:57:31 am (PDT) June 28, 1992, and was assigned a Richter magnitude of 7.3 (M_w). The epicenter was 34^0 12′ N, 116^0 26′ W, or 6 miles north of Yucca Valley and 103 miles from the building site. Having a magnitude of 7.3, the Landers earthquake was the largest magnitude earthquake to occur in Southern California in 40 years. The epicenter was in the Mojave Desert, approximately 120 miles from Los Angeles. The earthquake caused relatively little damage for its size, since it occurred in a sparsely populated area. The total length of the ground rupture, 85 km, illustrated the power of this earthquake.

2.2.3 The Northridge Earthquake (1994)

The Northridge earthquake occurred at 4:30 am (PST) January 17, 1994, and was assigned a Richter magnitude of 6.7 (M_w). The epicenter was 34^0 $12.8^{0\prime}$ N, 118^0 32.22′ W, 20 miles west-northwest of Los Angeles, or one mile south-southwest of Northridge. The reference building is located 40 miles from the epicenter. At 4:30 am, on January 17, 1994, the strong shaking of the Northridge earthquake rudely awakened residents of the Greater Los Angeles area. This was the first earthquake to strike directly under an urban area of the United States since the 1933 Long Beach earthquake.

The Northridge earthquake occurred on a blind thrust fault, and produced the strongest ground motions ever instrumentally recorded in an urban setting in North America. Damage was widespread, sections of major freeways collapsed, parking structures and office buildings collapsed, and numerous apartment buildings suffered irreparable damage. Damage to wood-frame apartment houses was very widespread in the San Fernando Valley and Santa Monica areas, especially to structures with "soft" first floors or lower-level parking garages.

2.3 INSTRUMENTATION AND RECORDED RESPONSE

The California Strong Motion Instrumentation Program (CSMIP) instrumented the three-story office building with thirteen sensors [CSMIP, 1994]. The location of each sensor is shown schematically in Figure 2.9. Sensors 1, 9, and 13 recorded motions at the base. Sensors 8 and 12 recorded horizontal accelerations at the second-floor level. Sensors 5, 6, 7, and 11 recorded horizontal accelerations at the third-floor level, and sensors 2, 3, 4 and 10 measured the horizontal accelerations of the roof during the earthquakes. Acceleration data recorded at each of the 13 channels were available from CSMIP.

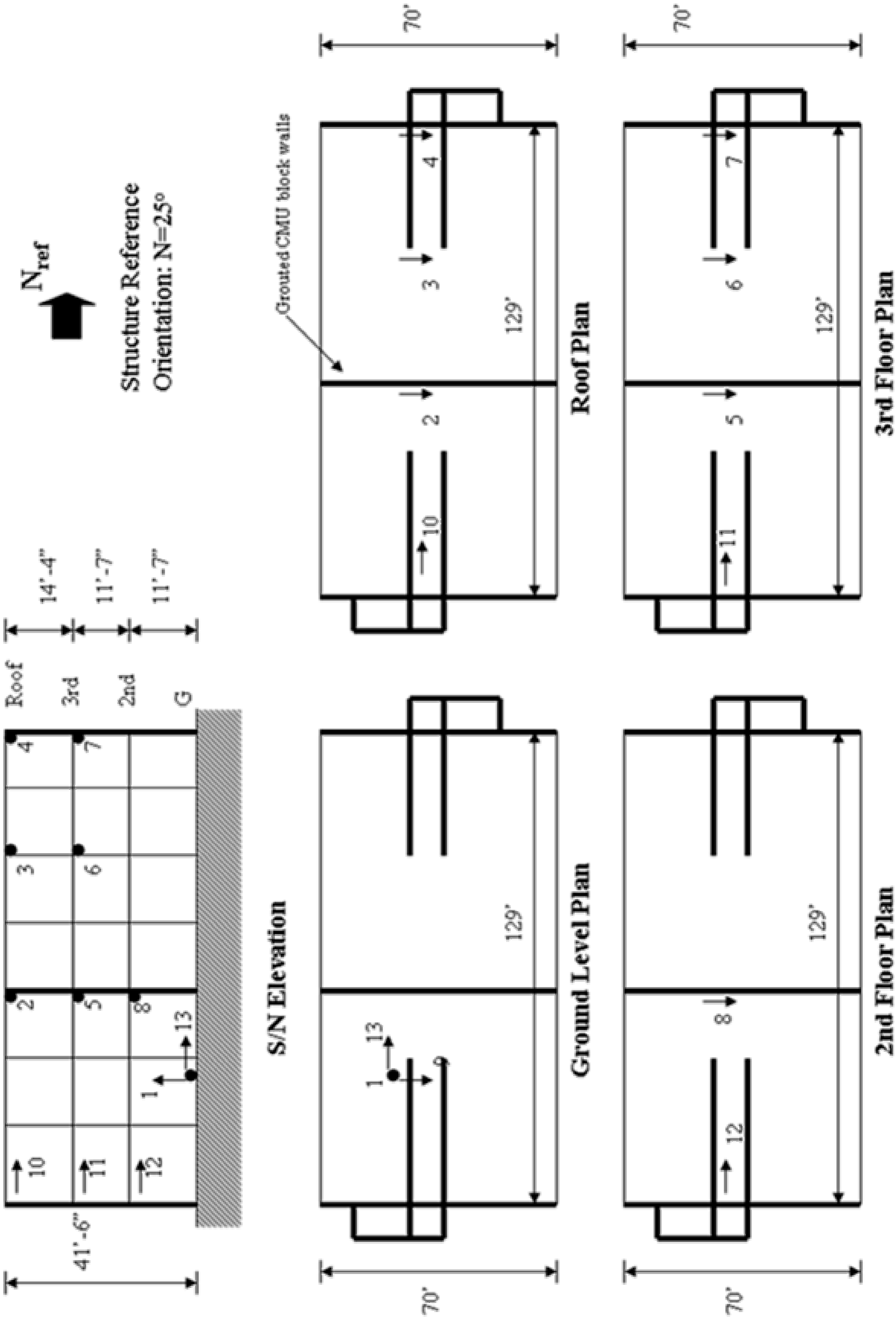

Figure 2.9 Location of strong motion instrumentation, 3-story building.

2.3.1 Observed Damage

Specific information regarding the extent to which the three-story building suffered damage after the Landers, Whittier Narrows, and Northridge earthquakes is not available in the public domain.

2.3.2 Recorded Motions during the Whittier Narrows Earthquake (1987)

The time histories showing the recorded accelerations and corresponding displacements at each of the 13 sensor locations during the Whittier Narrows earthquake are shown in Appendices A-1 and A-2, respectively. During the Whittier Narrows earthquake, the sensors measured a total of 40 sec of acceleration data, although only 9 sec were considered to be significant strong ground motion. Recorded peak accelerations and corresponding displacements for each sensor during the Whittier Narrows earthquake are summarized in Tables 2.1 and 2.2, respectively. Peak absolute displacement denotes the maximum displacement at a particular sensor location, which is the displacement relative to the base plus the base displacement of the building. Peak relative displacement refers to the maximum displacement of each sensor relative to the base.

From a preliminary inspection of the characteristics of the recorded acceleration response of the three-story building, it is apparent that the frequencies of the acceleration and computed displacement time histories at each channel appear to stay relatively constant even after the strongest portion of the motion. Such an occurrence suggests that the building remained essentially elastic during the Whittier Narrows earthquake.

These data also indicate that a significant amplification of the ground accelerations occurred in the transverse (E-W) building direction. The middle shear wall in the E-W direction experienced a peak acceleration at the roof level of 0.09g as measured by sensor 2, while a peak acceleration of 0.18g in the roof diaphragm was recorded between the middle and north walls by sensor 3. However, the peak ground acceleration in the E-W direction during the Whittier Narrows earthquakes was only 0.06g, as measured by sensor 9.

In the longitudinal (N-S) building direction, a smaller amplification of motion was observed. A peak acceleration of 0.06g at the roof level was recorded by sensor 10; however, the corresponding peak ground acceleration was measured by sensor 13 to be 0.04g. Significant ground motion amplifications are not expected to occur along the longitudinal direction of buildings with flexible diaphragms because the primary contributor to that amplification, diaphragm flexibility, in that direction is anticipated to be small (Raggett and Rojahn 1991).

Vertical accelerations are a concern in masonry structures, since they may adversely affect the stresses due to gravity loads, especially if these accelerations are high. The peak vertical ground acceleration of the three-story building during the Whittier Narrows earthquake was measured by sensor 1 to be 0.02g. Such vertical ground acceleration values are too low to have any significant impact on the magnitude of the stresses due to gravity load and thus were not considered in this study.

2.3.3 Recorded Motions during the Landers Earthquake (1992)

The time histories showing the recorded accelerations and calculated displacements at each of the 13 sensors during the Landers earthquake are shown in Appendices A-3 and A-4, respectively. During the Landers Earthquake, the sensors recorded a total of 80 sec of acceleration data, although only 7 sec were considered to be significant ground motion. Peak accelerations recorded for each sensor during the Landers earthquake and corresponding displacements are summarized in Tables 2.1 and 2.2, respectively.

An inspection of the acceleration and displacement time histories indicates that the frequency of the accelerations and displacements for each channel stays relatively constant even following the strongest portion of the base motion. Such a result suggests that the building responded in an essentially elastic manner during the Landers earthquake.

Amplification of the peak acceleration between the ground and roof levels was observed in the E-W direction during the Landers earthquake, due to the in-plane flexibility of the diaphragms in the transverse building direction. During the Landers earthquake, the middle wall of the E-W lateral-force-resisting system experienced a peak acceleration at the roof level of 0.09g was measured by sensor 2, while a peak acceleration in the roof diaphragm of 0.24g was measured midway between the middle and north walls by sensor 3. However, the peak ground acceleration in the E-W direction during the Landers earthquake was only 0.07g as measured by sensor 9. The recorded data show that only slight amplification of the peak acceleration between the ground and roof occurred in the N-S direction. A peak acceleration of 0.06g at the roof level was measured by sensor 10, whereas the peak N-S ground acceleration as measured by sensor 13 was 0.04g. The peak vertical ground acceleration of the three-story building during the Landers earthquake was 0.04g, which is not considered to be significant.

2.3.4 Recorded Motions during the Northridge Earthquake (1994)

Time histories showing the recorded accelerations and corresponding displacements at each of the 13 sensors during the Northridge earthquake are shown in Appendices A-5 and A-6, respectively. During the Northridge earthquake, the sensors measured a total of 80 sec of acceleration data, with 25 sec regarded as strong ground motion. Peak accelerations and displacements recorded for each sensor during the Northridge earthquake are summarized in Tables 2.1 and 2.2, respectively. The peak absolute and relative displacements in Table 2.2 refer to the peak values over the duration of the corresponding time history record. Therefore, the peak relative displacement and any associated peak absolute displacement do not occur at the same instant of time. The acceleration and displacement response of the three-story building show that the frequency of the recorded values stay relatively constant even after the strongest portion of the motion.

Table 2.1 Peak recorded accelerations, 3-story building.

Sensor I.D.	Location	Peak Absolute Acceleration (g)		
		Whittier Narrows	Landers	Northridge
1	Ground (UP)	0.02	0.04	0.04
2	Roof (E-W)	0.09	0.09	0.07
3	Roof (E-W)	0.18	0.24	0.12
4	Roof (E-W)	0.07	0.09	0.07
5	3RD (E-W)	0.08	0.09	0.06
6	3RD (E-W)	0.15	0.19	0.13
7	3RD (E-W)	0.07	0.09	0.06
8	2ND (E-W)	0.06	0.07	0.05
9	Ground (E-W)	0.06	0.07	0.04
10	Roof (N-S)	0.06	0.06	0.09
11	3RD (N-S)	0.05	0.05	0.08
12	2ND (N-S)	0.05	0.04	0.07
13	Ground (N-S)	0.04	0.04	0.07

Amplification of the ground motions was noticed in the E-W building direction, but the effect was not as prevalent along the N-S dimension. During the earthquake, the middle wall experienced a peak acceleration at the roof level of 0.07g as measured by sensor 2, while a peak diaphragm acceleration of 0.12g was experienced between the middle and north walls as measured by sensor 3. The peak ground acceleration in the E-W direction during the Northridge earthquake was 0.04g as measured by sensor 9. In the N-S direction, the building experienced a peak acceleration of 0.09g at the roof level as measured by sensor 10. The corresponding peak ground acceleration earthquake was 0.07g as measured by sensor 13.

The peak vertical ground acceleration of the three-story building during the Northridge earthquake was measured to be 0.04g and not considered to have any significant impact.

Table 2.2 Peak absolute and relative recorded displacements, Whittier Narrows, Landers and Northridge, 3-story building.

Sensor I.D.	Location	Peak Absolute Displacements (Inches)			Peak Relative Displacements (Inches)		
		Whittier Narrows	Landers	Northridge	Whittier Narrows	Landers	Northridge
1	Ground (UP)	0.53	0.02	0.68			
2	Roof (E-W)	1.02	0.08	1.48	0.01	0.14	0.16
3	Roof (E-W)	1.00	0.13	1.42	0.09	0.26	0.18
4	Roof (E-W)	1.04	0.08	1.47	0.03	0.16	0.15
5	3RD (E-W)	1.02	0.07	1.48	0.01	0.16	0.12
6	3RD (E-W)	0.98	0.11	1.41	0.08	0.23	0.13
7	3RD (E-W)	0.98	0.07	1.43	0.02	0.14	0.12
8	2ND (E-W)	0.97	0.07	1.45	0.01	0.12	0.10
9	Ground (E-W)	0.96	0.06	1.43			
10	Roof (N-S)	1.11	0.09	1.05	0.13	0.17	0.15
11	3RD (N-S)	0.96	0.08	1.01	0.01	0.12	0.14
12	2ND (N-S)	0.96	0.08	1.04	0.01	0.12	0.15
13	Ground (N-S)	1.04	0.07	1.06			

2.4 SPECTRAL ANALYSES

In order to better understand the recorded dynamic response of the building and to evaluate the dynamic characteristics of the building prior to performing the detailed response analyses, the recorded response data were processed using response spectra and moving window Fourier analyses. The results of these studies are discussed and presented in the following sections.

2.4.1 Whittier Narrows Earthquake

2.4.1.1 Linear Elastic Response Spectra (LERS)

LERS for 5% damping in all modes were generated and plotted for the recorded motion of the three-story building during the Whittier Narrows earthquake. The spectra were generated by passing the recorded base accelerations in the N-S and E-W directions, from channels 13 and 9, through a single-degree-of-freedom oscillator having 5% of critical damping. The resulting response spectra for the N-S and E-W directions of the three-story building are presented in Figure 2.10.

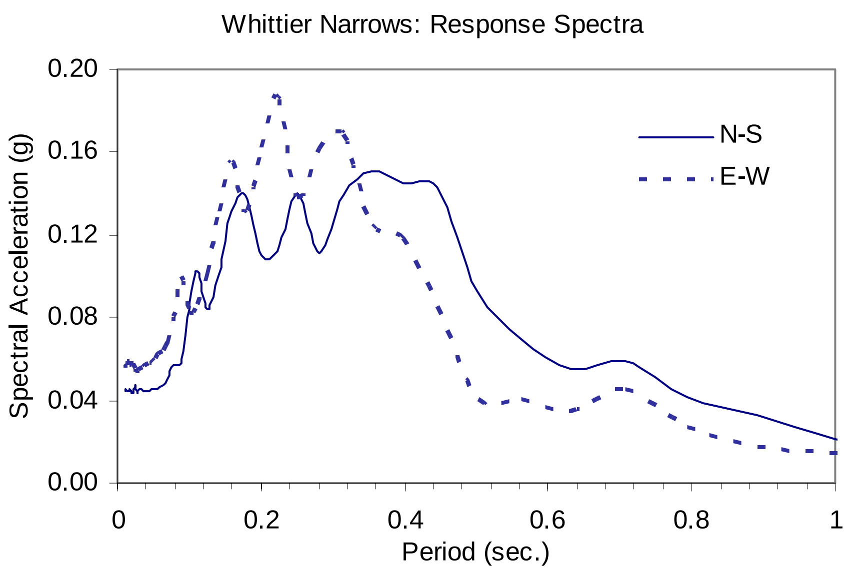

Figure 2.10 N-S and E-W response spectra, Whittier Narrows, 3-story building.

This figure indicates that for periods less than 0.35 sec the E-W motion produces higher spectral accelerations, whereas for periods above 0.35 sec the spectral accelerations due to the N-S motions are higher.

2.4.1.2 Fourier Analyses

Moving window Fourier transfer function (MWFTF) analyses were performed using the recorded base and roof motions in both the N-S and E-W directions of the building to obtain the variation of the first mode (translation) periods during the Whittier Narrows earthquake. The recorded data from sensors 2 and 9 were used to compute the moving window analyses in the E-W direction, while the recorded acceleration response from sensors 10 and 13 were used for the N-S direction. The Fourier transfer functions have been calculated for 10-sec window lengths with 5-sec window shifts, thus resulting in 14 windows. Moving window analyses were also conducted between the roof and base motions obtained from sensors 3 and 9. The resulting plots of the variation of the period for the fundamental translation mode of the building in each direction are shown in Figure 2.11.

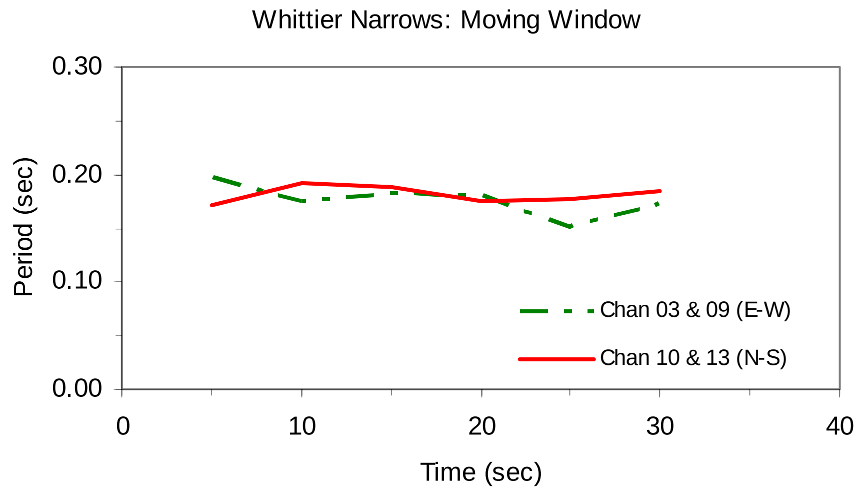

Figure 2.11 Temporal period variation, Whittier Narrows, 3-story building.

From inspection of the resulting moving window diagrams for the N-S direction, we may notice that the period of the three-story building varied between 0.17 and 0.19 sec, with an average value of approximately 0.18 sec. Similarly, in the E-W direction the period of the building varied between 0.15 and 0.20 sec. However, the average values in both directions are approximately 0.17 sec. From the moving window results, we see that the first translation mode periods of the building in both the E-W and N-S directions are approximately 0.18 sec during the Whittier Narrows earthquake. This lack of a significant change in the first mode period in the N-S and E-W directions suggest that the building did not experience appreciable inelastic behavior during the Whittier Narrows earthquake. Therefore, the conclusion can be made that the three-story building remained essentially linear elastic.

2.4.2 Landers Earthquake

2.4.2.1 Linear Elastic Response Spectra (LERS)

LERS for 5% damping were generated and plotted for the recorded motion of the three-story building in the N-S and E-W directions during the Landers earthquake. The spectra were generated by passing the recorded base accelerations in the N-S and E-W directions, from channels 13 and 9, through a single-degree-of-freedom oscillator having 5% of critical damping. The resulting response spectra for the N-S and E-W directions of the three-story building are presented in Figure 2.12. For this earthquake, the ground motions in the E-W direction produce the higher spectral accelerations.

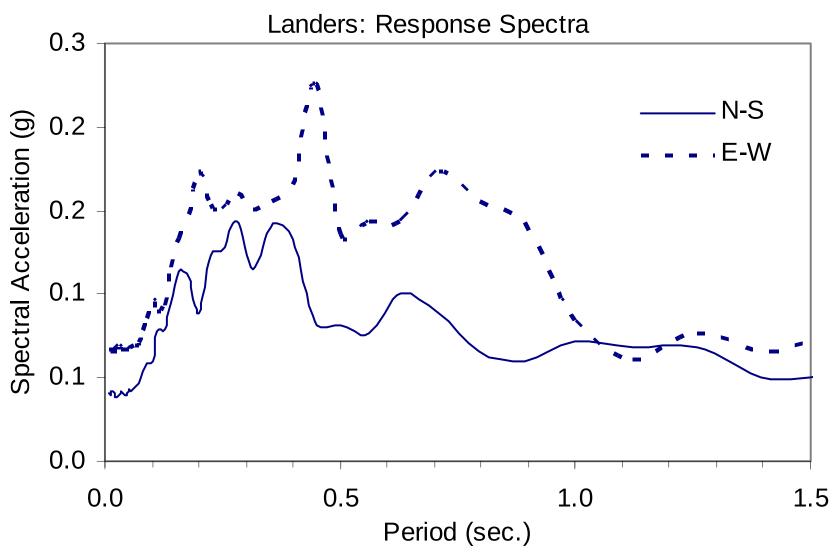

Figure 2.12 N-S and E-W response spectra, Landers, 3-story building.

2.4.2.2 Fourier Analyses on Landers Data

Moving window Fourier transfer function analyses were performed using the recorded base and roof motions in the N-S and E-W directions of the building during the Landers earthquake. The moving window results for the building in the N-S and E-W directions are shown in Figure 2.13. The resulting moving window diagrams for the N-S direction indicate that the period of the three-story building varied between 0.15 sec and 0.25 sec with an average of 0.20 sec during the entire duration of the earthquake record. Similarly, in the E-W direction, the period of the building varied between 0.15 sec and 0.22 sec. From the moving window results, it can be seen that the periods of the first translation mode of the building in both the E-W and N-S directions are approximately 0.2 sec during the Landers earthquake. This lack of a significant change in these first mode periods in the N-S and E-W directions suggest that the building behavior was primarily linear elastic and that the building did not suffer any appreciable structural damage during the Landers earthquake.

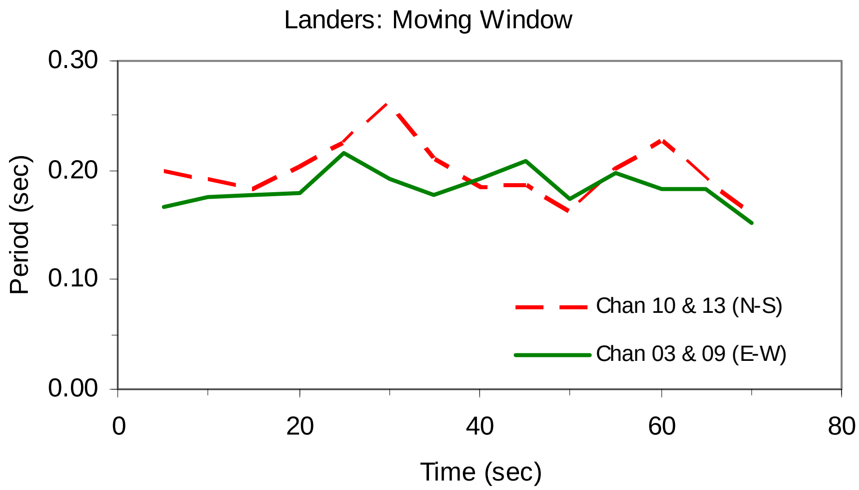

Figure 2.13 Temporal period variation, Landers, 3-story building.

2.4.3 Northridge Earthquake

2.4.3.1 Linear Elastic Response Spectra (LERS)

LERS for 5% damping in all modes were generated and plotted for the recorded motion of the three-story building in the N-S and E-W directions during the Northridge earthquake. The resulting response spectra for the N-S and E-W directions of the three-story building are presented in Figure 2.14. Here it can be seen that the N-S motions are predominate for periods less than 1.0 sec, but for periods above 1.15 sec, the E-W motions have higher spectral accelerations.

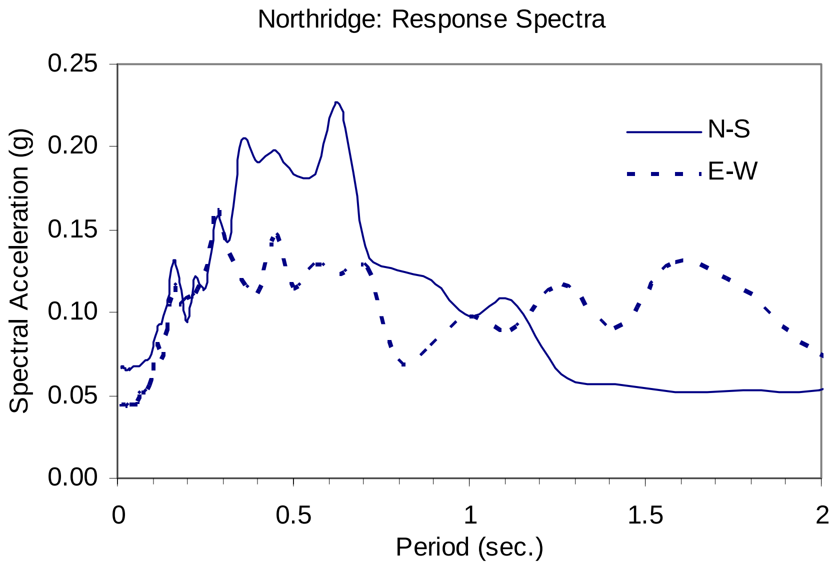

Figure 2.14 N-S and E-W response spectra, Northridge, 3-story building.

2.4.3.2 Fourier Analyses on Northridge Data

As for the Whittier Narrows and Landers earthquakes, moving window Fourier transfer function analyses were performed using the recorded base and roof motions for the N-S and E-W directions to evaluate any variation of the periods of the fundamental translation modes of the three-story building during the Northridge earthquake. The moving window results for the building in the N-S and E-W directions are shown in Figure 2.15. From the moving window results, it can be seen that the first translation mode periods of the building in the N-S and E-W directions all vary between 0.15 and 0.30 sec with an average approximately 0.22 sec throughout the record. This lack of a significant change of the first translation mode periods in both the N-S and E-W directions between the first window and the last window suggests that the building did not suffer any appreciable structural damage during the Northridge earthquake. However, it may have experienced some micro-cracking of the masonry walls. Therefore, the conclusion can be made that the three-story building remained essentially elastic during the Northridge earthquake.

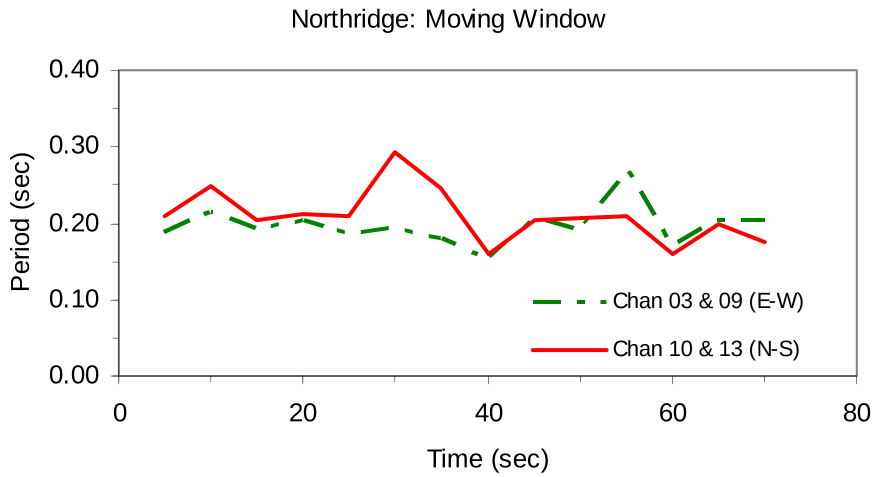

Figure 2.15 Temporal period variation, Northridge, 3-story building.

2.4.4 General Conclusions

The lack of a significant shift in the first mode periods in the E-W and N-S directions indicate that the behavior of the building during all three earthquakes remained essentially elastic. Variations in the translation periods during the earthquakes may be due to the opening and closing of cracks in the masonry walls. It can be observed that the smaller variation occurred during the weaker, Whittier Narrows earthquake.

One may argue that the time shift between successive windows of the moving window Fourier transfer function analyses (5 sec) is too long for a building with a short period. It could also be possible that the length of the window is too long (10 sec) for this type of structure. Both points need to be investigated further for such a rigid structure in order to refine this analysis technique. Cracking of the masonry walls can have a significant effect on the effective stiffness. If the buildings under study had exhibited inelastic behavior due to yielding or the reinforcing steel or a pull-out of the connections, the results of the MWFTF would have indicated an increase in the fundamental period which remained to the end of the time history. Therefore, it is reasoned that the MWFTF analyses conducted on these buildings was sufficient to show that (1) the period of the buildings remained fairly constant and that variations were mainly due to micro-cracking of the masonry shear walls and loosening of the nailed connections and (2) the building response was primarily in the elastic range during all three earthquakes.

2.5 ELASTIC DYNAMIC ANALYSES

Three-dimensional dynamic analyses of building structures have traditionally not been done because of high computational demands and memory requirements. However, with the surge in computational capabilities available to engineering offices, such analyses may be used for more conventional structural systems. A wide variety of general-purpose computer software is currently available for the static and dynamic structural analysis of complex frame structures. Most of these programs can be used for the analysis of multi-story frame and shear wall buildings. However, ETABS is a special-purpose computer program developed specifically for building systems. It has simplified input and output that reduces the time required for development of the analytical model and the time to evaluate the final results. ETABS, a finite-element-analysis-based software package that has been in development since the late 1960s, has proven to be an invaluable design and analysis aid to structural engineers (Computers and Structures, Inc. 1999).

2.5.1 Mathematical Model

Although masonry is known to be a highly nonlinear material, the moving window Fourier transfer function analyses of the recorded data of the building during each of the three earthquakes indicated that the three-story building remained essentially elastic during all three earthquakes. Therefore, it was deemed sufficient to develop a linear model to evaluate the dynamic response. Due to the expected interaction of the walls, base slab and diaphragms, a three-dimensional linear elastic finite element model of the three-story building was developed using ETABS (version 7) computer software, although other computer programs could also have been used. An isometric view of the 3-D linear elastic analytical model of the three-story building is shown in Figure 2.16. The model consists of a total of 5,112 nodal points. To accurately reproduce the flexibility of the diaphragms, 6,413 shell elements were used, which is well above the recommended minimum (Computers and Structures, Inc. 1999). The columns, edge beams, and interior beams were modeled using 824 frame elements.

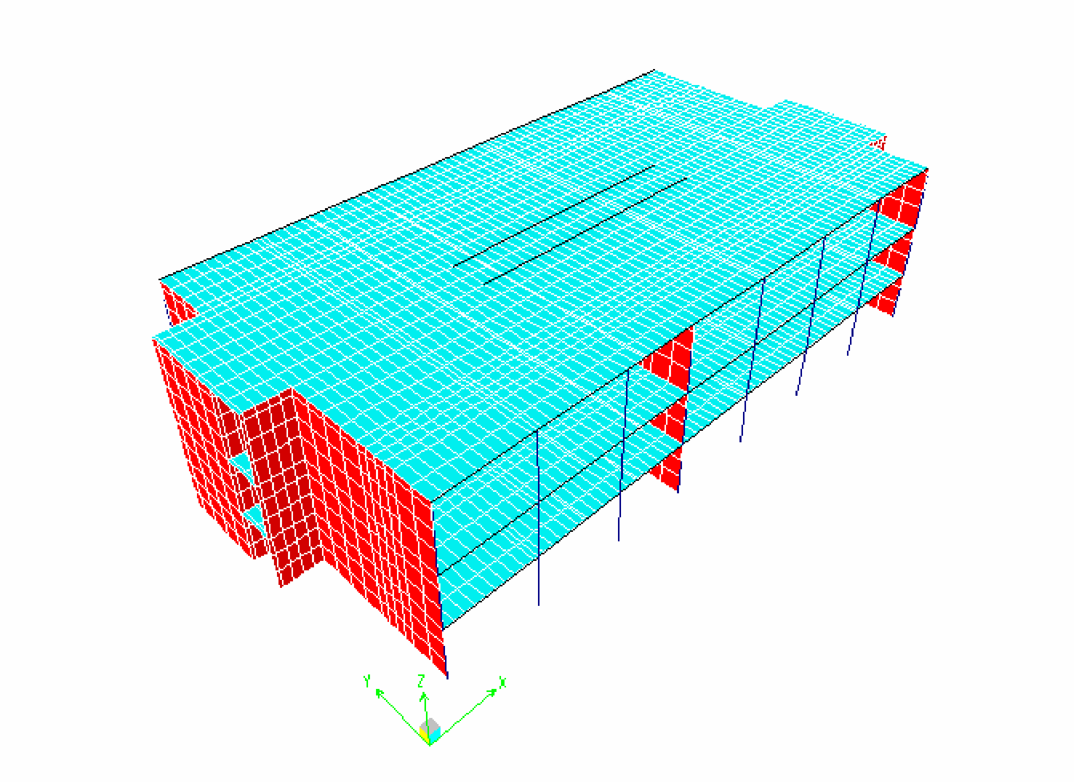

Figure 2.16 3-D linear elastic ETABS model, isometric view, 3-story building.

2.5.1.1 Modeling of Flexible Plywood Diaphragms

Thick shell elements were employed to model the roof and floor diaphragms. Use of such elements was necessary to sufficiently reproduce both the translation and the flexural movement of the diaphragms. The thick plate option was selected, so that the shear deformation of the diaphragm would also be considered. The plywood diaphragms of the three-story building consisted of structural plywood panels mounted on truss joists running in the E-W (transverse) direction of the building. The diaphragm was represented by shell elements having an equivalent uniform thickness that represented membrane and bending stiffness in each principal orthogonal direction of the building. The methodology for calculating the equivalent membrane and bending thickness for the floor and roof diaphragms is shown in Figure 2.17. For the membrane thickness, determining an equivalent thickness that resulted in the same cross-sectional area accomplished this. For the bending thickness, a uniform thickness was determined that resulted in the same moment of inertia as the actual cross section. The resulting equivalent section was rectangular in shape with a different thickness associated with each property in each principal direction of building. For simplicity, the stiffness of the diaphragms in the E-W and N-S directions was considered independent of one another.

Equivalent shell element thickness properties at the roof level in the E-W direction were based on ½″ plywood that was nailed to 20″ TJI trusses spaced at 2′ on center. In the N-S direction they were based on ½″ plywood panels with 2x4 Douglas fir (DF) flat blocking spaced at 4′ and used for nailing at the plywood edges. At a typical floor level, the equivalent thickness properties in the E-W direction were based on 1-1/8″ plywood mounted on 30″ TJM open web trusses spaced at 2′ on center. In the N-S direction they were based on 1-1/8″ plywood with 2x4 DF flat blocking at every 4′ at the plywood edges. The resulting values for the equivalent membrane and equivalent bending thickness in the E-W direction at the roof level were 1.25 in. and 12.24 in. respectively. Similarly, the values for the equivalent membrane and bending thickness calculated for the floor diaphragms of the building in the E-W direction were calculated to be 2.0 in. and 14.87 in., respectively. The large value for the equivalent bending thickness of the roof and floor diaphragms in the E-W direction is a direct result of considering the Trus Joists cross section in the calculations. In the N-S direction, the equivalent membrane thickness and equivalent bending thickness at the roof level were 0.61 in. and 1.13 in. respectively, while corresponding values of 1.29 in. and 1.85 in. were used at the floor levels.

Orthotropic material behavior was essential to model the difference in diaphragm material properties between the E-W and N-S directions. Material properties were calculated for the roof and floor diaphragms, to capture the combined interaction on the effects of the TJI trusses and the plywood. The average modulus of elasticity of plywood was taken to be 1700 ksi. The average modulus of elasticity of 20″ and 30″ TJI trusses was taken to be 1450 ksi, and 1905 ksi, respectively (Trus Joist MacMillan 1998). Equation (2.1) is the formula used to determine the modulus of elasticity of the open-web TJM trusses, where E is the effective modulus of elasticity, I is the actual moment of inertia of the truss section, and **d** is the average depth of the truss minus 3.5 in. (Trus Joist MacMillan 1998).

$$EI = 10.06\,x10^{6}\,d^{2} \tag{2.1}$$

The direction of the grain of the plywood was also considered in the calculations of the effective modulus of elasticity of the diaphragms. The modulus of elasticity of the plywood diaphragms in the weak direction was calculated according to Equation (2.2), where E_{weak} and E_{strong}, refer to the elastic moduli in the perpendicular and parallel to the direction of the grain

(Breyer et al. 1999). The equivalent elastic modulus of each diaphragm in each direction was taken as the average of each of the respective components used in the equivalent thickness calculations. Thus, the effective moduli of elasticity used at the roof level were 1700 ksi in the N-S direction, and 750 ksi in the E-W direction. For the floor diaphragm shell elements, an effective elastic modulus was taken as 1700 ksi in the N-S direction, and 975 ksi in the E-W direction. It is imperative that the modulus of elasticity of the TJI and TJM trusses be considered in the calculation of the equivalent modulus of elasticity for the shell elements used to model the diaphragm, because the trusses make a significant contribution (e.g., 1.85 in. to 12.24 in.) to the diaphragm bending stiffness.

$$E_{weak} \cong \frac{E_{strong}}{35} \tag{2.2}$$

Since no data were readily available regarding the shear modulus of TJI and TJM truss joists, the equivalent shear modulus value of each of the diaphragms was simply taken as the average shear modulus of plywood. Thus, a value of 90 ksi for the shear modulus was used for the shell elements in both principal directions of the building. In any case, it is reasonable to limit the shear modulus of each diaphragm to that of the plywood because the plywood serves as the only continuous media that provides resistance to shear deformation.

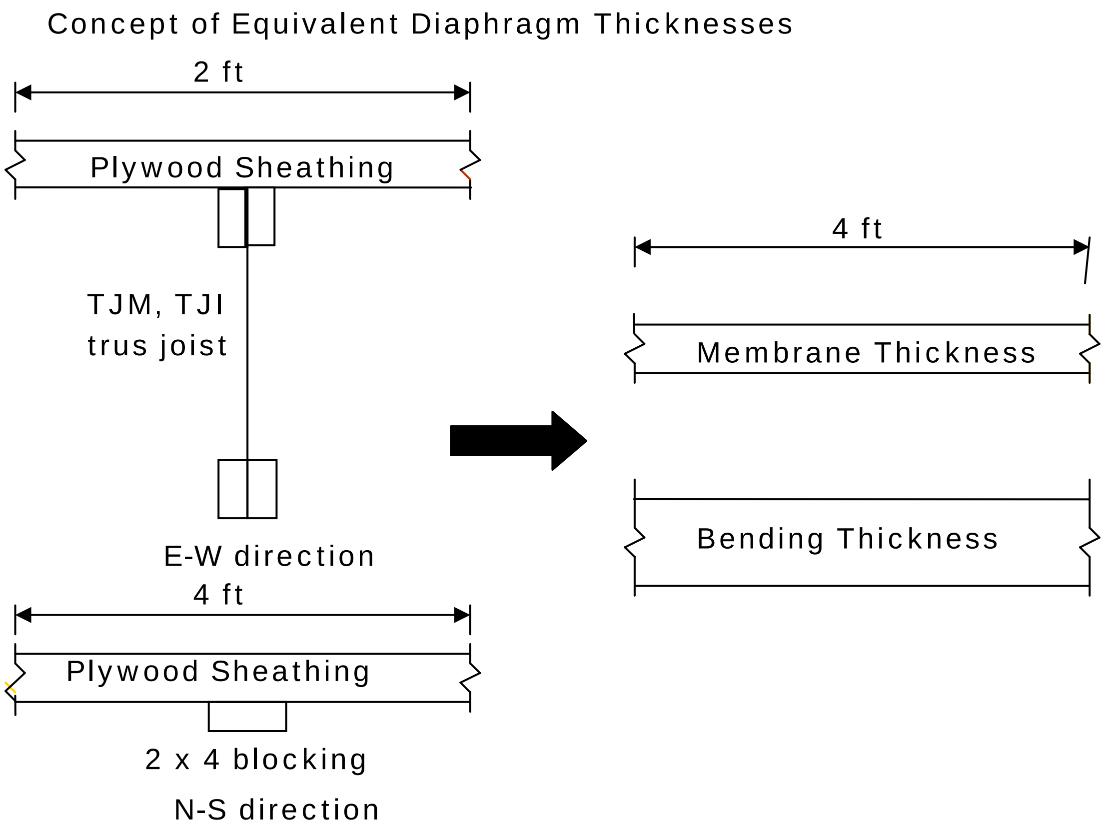

Figure 2.17 Concept of equivalent diaphragm thickness.

2.5.1.2 Modeling of Masonry Shear Walls

Thick plate shell elements were used to model both the 8″ and 12″ thick shear walls. Cracking of the masonry wall section was assumed and the equivalent thickness was computed based on the cracked section properties for a rectangular section under bending. The ACI Code (10.11.1) suggests an effective moment of inertia of $0.35I_g$ for beams and walls to account for cracking. For masonry, the reinforcement in the wall generally consists of a single curtain of steel placed on the center-line of the wall resulting in an effective depth of $0.5h$. The effective moment of inertia per inch becomes $\frac{0.35(h/2)^3}{12}$. Equating this value to that of the plate element results in an effective thickness for the element, $h_{eff} = 0.35h$. In this manner, the equivalent thickness properties for membrane and bending stiffness for the shell elements used to model the shear walls were taken as 35% of the uncracked section resulting in an equivalent thickness of 2.8″ for the 8″ walls and 4.2″ for the 12″ walls. Although the thickness of the walls were reduced for modeling purposes, the weight of the walls were calculated based on the original dimensions of the walls and used in the dynamic analyses of the building.

Isotropic material behavior was assumed for the masonry shear walls. The modulus of elasticity for masonry was calculated using Equation (2.3), where f'_m was taken to be 1500 psi (Brandow, Hart and Virdee 1997). Poisson's ratio for masonry was assumed to be 0.2, and the shear modulus was calculated internally by ETABS to be $G = 468.75\,\text{ksi}$, based on the dependence relation for an isotropic material as shown in Equation (2.4)

$$E = 750 f'_m \tag{2.3}$$

$$G = \frac{E}{2(1+\upsilon)} \tag{2.4}$$

2.5.1.3 Other Modeling Considerations

The connections of both interior and exterior wide flange steel beams to the tubular steel columns in the three-story building were considered to be simple shear-type. In the connection detail, shown in Figure 2.5, the steel beam rather than the steel tube column is continuous through the joint. The column has a cap plate that bolts to the bottom flange of the beam and a base plate that bolts to the top flange. Continuity of the column is provided by two channel sections welded to each side of the beam web. A bolted shear splice in the web of the beam is just outside the column. Therefore, end moment releases about the strong axis of the frame elements used to model these interior and edge beams were used to re-create the pinned end connection of the wide flange steel beams in the three-story building.

In modeling the building in ETABS, a few of the steel wide flange beam sizes listed on the structural drawings were modified slightly from the original sizes, since they were no longer included in the sections listed in the AISC steel design manual (AISC 1998). To model the W8x17 steel beams used in the connection between the masonry shear walls in the N-S direction, W8x18 sections were used in their place. W12x16 sections were used in the model to represent theW12x16.5 sections used as exterior edge beams at the roof level of the building. W12x26 sections were used to model the W12x27 sections used as exterior edge beams on the second and third floors of the building and finally, a W6x16 section was used to model the actual W6x15.5 edge beam beneath the canopy of the building at the second-floor level.

In the plane of the truss joists, the top chord is anchored to a small corbel to make the connection at the masonry wall as shown in Figure 2.7. The bottom chord is connected to a ledger block in the wall. In the out-of-plane direction, blocking connected to a ledger block anchored in the wall stabilizes the bottom chord. At the exterior on the east and west sides, the top flange of the edge beam supports the top chord of the truss joist. For this type of framing, simple, pinned connections were used at both ends of the truss joists.

2.5.1.4 Weight (Mass) Determination

The weight (mass) of the floor levels of each of the two buildings under study was estimated based on the information given on the structural drawings. However, it was necessary to estimate the weights of some of the finish materials of each building.

All weight calculations were based on the weight per unit area and on the outer dimensions of the building. This resulted in a plan area of 9,739 ft^2. The unit weight of the exterior glass was multiplied by the portion of the building perimeter not enclosed by the masonry shear walls. Estimations of the total weight (mass) of each floor level of the building were based on the heights tributary to each level. Architectural, framed 2x4 stud fin walls are located at the columns on the east and west sides of the building. The weight of these members was distributed along the total height of the exterior columns from ground to roof level.

For calculation of the total mass of the roof framing consisting of the trusses and plywood sheathing, the lineal weight of 4.5 lb/ft for a typical 20″ TJI truss was obtained from the Trus Joist McMillan Product Specifications Manual (Trus Joist MacMillan 1998). The ½″. plywood sheathing was covered with a 20-year bondable Class A roof. Table 2.3 documents the estimations made for the weight of the three-story building at the roof level.

An average lineal weight of 8.3 lb/ft for typical 30″ TJM trusses was obtained from the Trus Joist McMillan Product Specifications Manual. The truss weight was essential for estimating the weight of the roof floor diaphragms. The estimations made for the weight (mass) at the third-floor level of the building are summarized in Table 2.4.

Table 2.3 Roof weight (mass) calculations, 3-story building.

Component	Assumed Unit Weight (psf)	Weight (k)
Roof Framing	X	68
Roofing	6	58
Hung Ceiling	8	78
Exterior Glass	8	16
Exterior Wall	X	71
Elevator	50	11
Exterior Columns	X	2
Interior Columns	X	1
Edge Beams	X	4
Interior Beams	X	2
Shear Wall (lt. wt. CMU)	X	258
Total Roof Weight		569 kips
Roof Translational Mass		1.47 k-s^2/in

Table 2.4 Third-floor weight (mass) calculations, 3-story.

Component	Assumed Unit Weight (psf)	Weight (k)
Roof Framing	X	105
Roofing	2	19
Hung Ceiling	8	78
Exterior Glass	8	25
Exterior Wall	X	52
Exterior Columns	X	3
Interior Columns	X	1
Edge Beams	X	7
Interior Beams	X	3
Shear Wall (lt. wt. CMU)	X	524
Partitions	20	195
Total 3rd Floor Weight		1013 kips
3rd Roof Translational Mass		2.62 k-s^2/in

The estimations made for the weight (mass) at the second-floor level of the building are shown in Table 2.5. The total weight of the three-story building used for dynamic analyses was 2606 kips (6.74 k-s^2/in.).

Table 2.5 Second-floor weight (mass) calculations, 3-story building.

Component	Assumed Unit Weight (psf)	Weight (k)
Roof Framing	X	105
Roofing	2	19
Hung Ceiling	8	78
Exterior Glass	8	25
Exterior Wall	x	54
Exterior Columns	x	4
Interior Columns	x	2
Edge Beams	x	7
Interior Beams	x	3
Shear Wall (lt. wt. CMU)	x	532
Partitions	20	195
Total 2nd Floor Weight		1024 kips
2nd Roof Translational Mass		2.65 k-s^2/in

2.5.2 Modal Period Analyses

The 3-D finite element ETABS model of the three-story building was used to evaluate the first 20 mode shapes and frequencies of the structure. The deflected mode shapes of the translational mode of vibration in the N-S and E-W directions for the three-story building are shown in Figures 2.18 and 2.19, which corresponded to modes 1 and 2 from the ETABS output. The third mode shape was calculated to be a torsional mode shape and is displayed in Figure 2.20. The modal periods of the building corresponding to the first translational mode shapes in the N-S and E-W direction were 0.210 and 0.209 sec, respectively. The torsional mode shape of the building had a 0.189 sec period of vibration. Due to the lack of symmetry of the building, the deformed shape of the translational modes differ in each principal direction of the building. The translational mode in the E-W direction captures the in-plane bending of the diaphragm with the E-W direction shear walls acting as fixed diaphragm supports in the horizontal plane.

The values of the fundamental modal period of vibration for the building in each orthogonal direction predicted by the analytical model closely reproduced the values obtained from the spectral analyses of the recorded response of the building: approximately 0.175 sec in each direction. The translational periods calculated by the ETABS model neglect the effect of the nonstructural components, such as interior partitions. These elements would add some initial stiffness to the building as indicated by the period obtained from the recorded data being slightly less than the calculated period. Additionally, modeling the structural masonry walls with a reduced thickness decreases the stiffness of the model and hence lengthens the period obtained from the analysis of the analytical model. In running the dynamic analysis of the model, including 20 modes, allowed 93.1% of the translational mass to participate in the dynamic response, which is above the 90% required by the 1997 UBC. Since the period of the fixed-base model agrees reasonably well with the recorded period, additional flexibility at the base was not considered in this study.

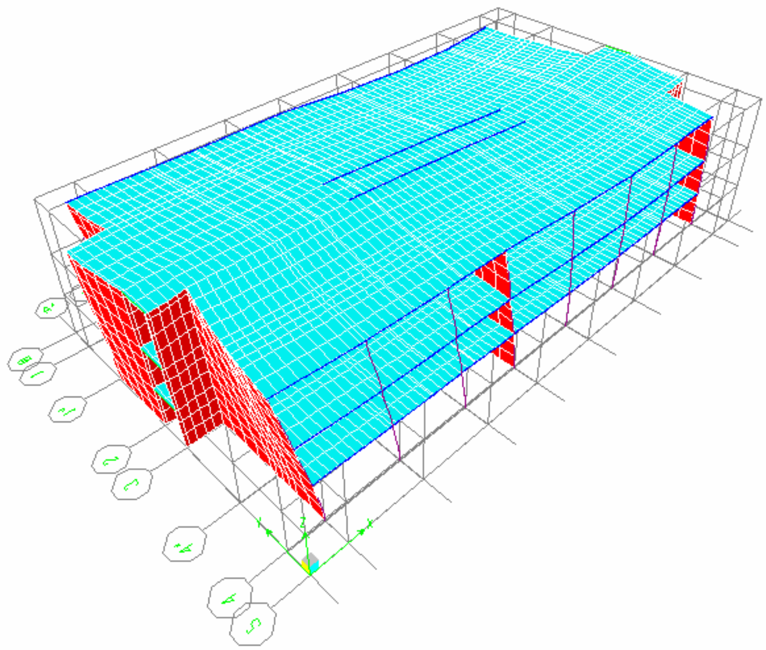

Figure 2.18 Translational mode shape, N-S (longitudinal), 3-story building.

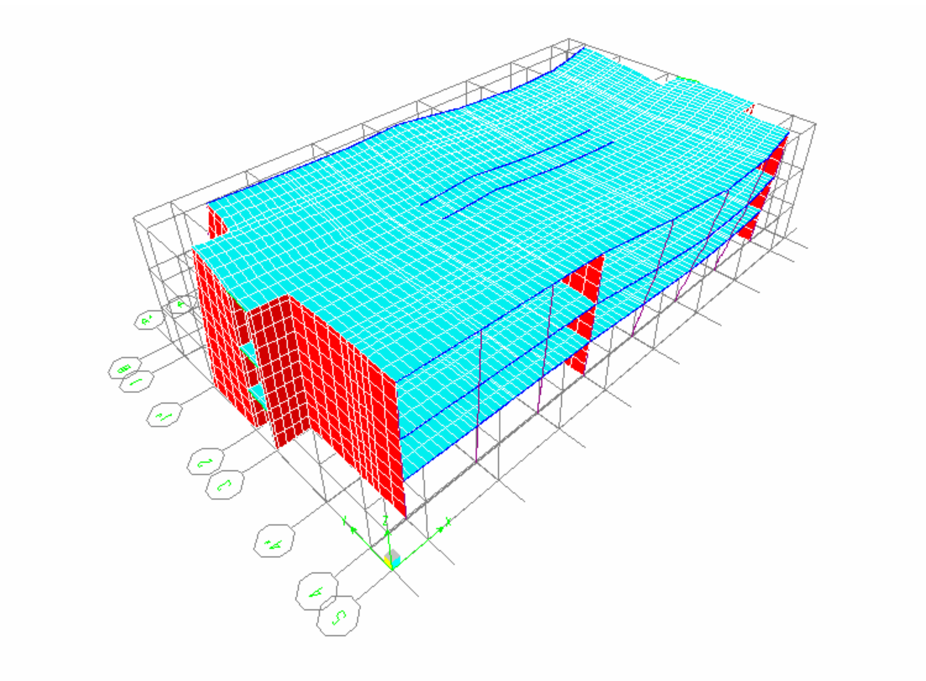

Figure 2.19 Translational mode shape, E-W (transverse), 3-story building.

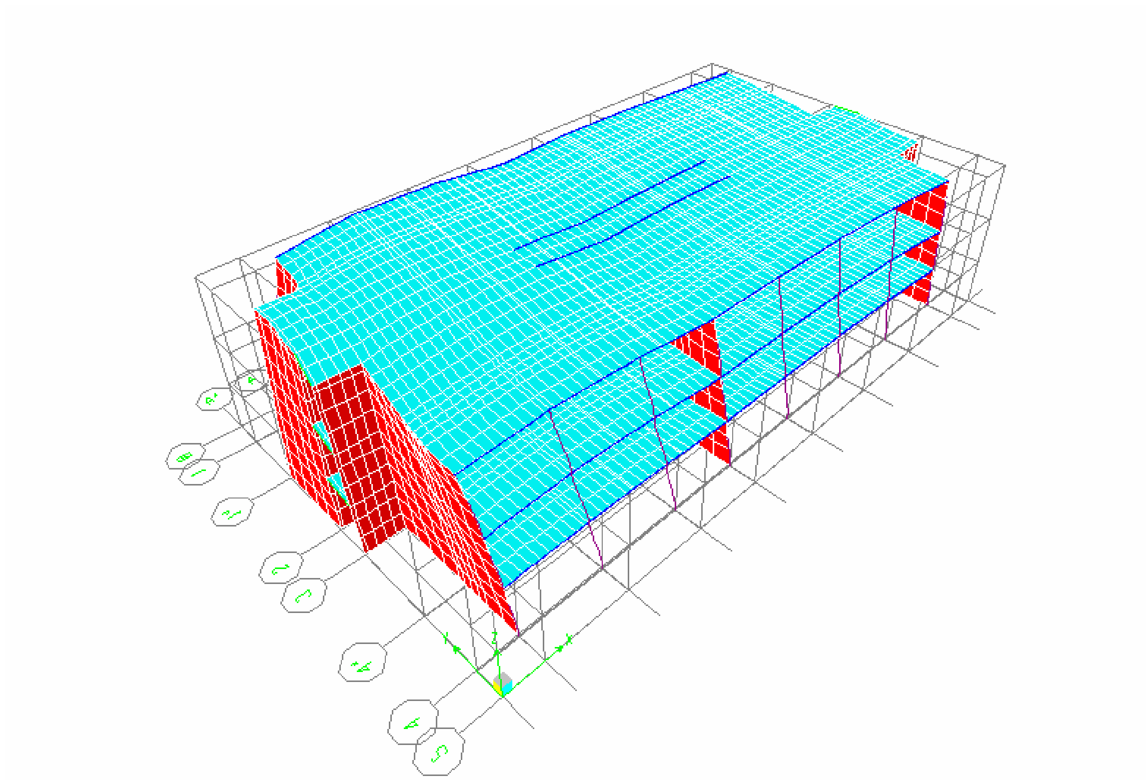

Figure 2.20 Torsional mode shape, 3-story building.

2.5.3 Calculated vs. Recorded Response

To study the dynamic time history response of the three-story Lancaster building subjected to the recorded motions at its base, the 3-D ETABS model was simultaneously subjected to base accelerations recorded in the N-S (record 13) and E-W (record 9) directions. A value of 5% critical damping for all 20 modes was used in the dynamic response analyses. Both the acceleration and displacement time histories for the building were computed using the analytical model and compared to the recorded data. It was decided that the comparison of the calculated building response with that recorded could more accurately be evaluated by studying the displacement response.

The three-dimensional analytical model was used to compute the dynamic displacement time history responses at each sensor location above ground level of the three-story building. The ETABS acceleration time history results were computed and integrated to obtain the corresponding displacement response of the building during each earthquake. Baseline corrections were then applied to the displacement data.

2.5.3.1 Whittier Narrows Displacement and Acceleration Comparisons

Acceleration and displacement comparisons between the predicted values from the analytical model and from the actual recorded response for sensor 3 of the three-story building during the Whittier Narrows earthquake are shown in Figures 2.21 and 2.22. From these figures, it is evident that aside from slightly overestimating the peak displacement at each sensor location, the model successfully reproduced the displacement response. The model tended to overestimate the magnitude of the peak acceleration values. However, the origin of this discrepancy is the result of high-frequency, short-duration acceleration spikes. The model was able to reproduce the general frequency of the recorded response. The time history acceleration and displacement comparisons were also computed for the remaining 9 sensors elsewhere (Tokoro 2001).

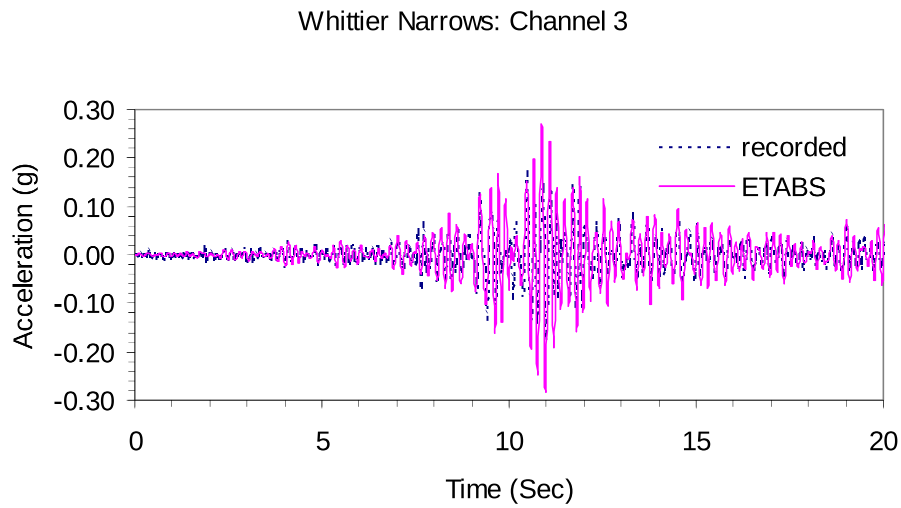

Figure 2.21 Calculated vs. recorded accelerations (ch. 3), Whittier Narrows.

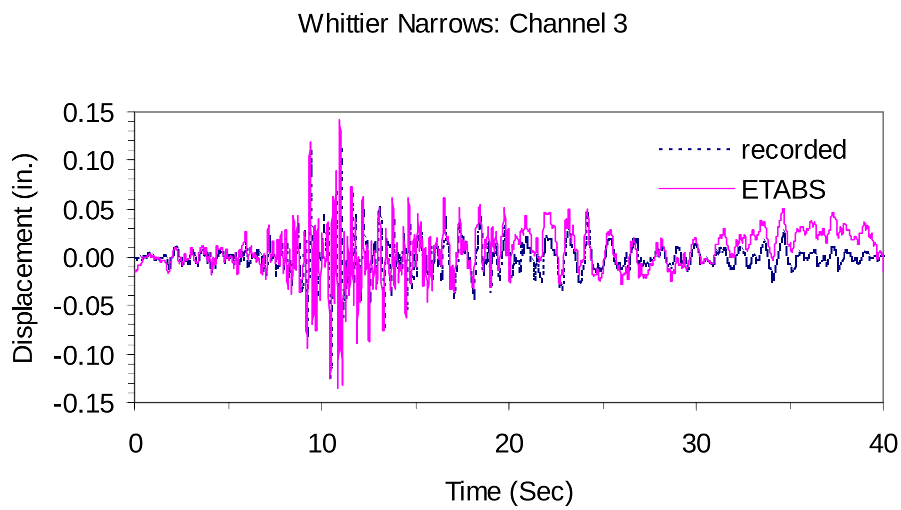

Figure 2.22 Calculated vs. recorded displacements (ch. 3), Whittier Narrows.

2.5.3.2 Landers Displacement and Acceleration Comparisons

Acceleration and displacement time history responses for sensor 3 at the roof level during the Landers earthquake are compared in Figures 2.23 and 2.24. In all cases, the 3-D ETABS model successfully approximated the recorded peak values, as well as the frequency of the response. The calculated and recorded acceleration and displacement responses for the remaining sensors of the three-story building are presented elsewhere (Tokoro 2001). The acceleration time histories of all 10 sensors located above ground level show a reasonable correlation to the actual recorded values. The model was especially accurate in predicting the acceleration time histories of the south wall in the N-S lateral force resisting system at the second, third, and roof levels.

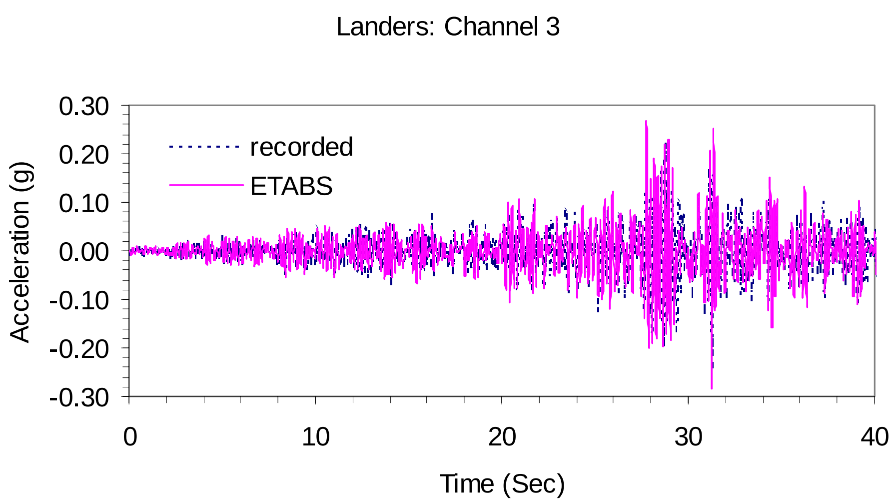

Figure 2.23 Calculated vs. recorded accelerations (ch. 3), Landers.

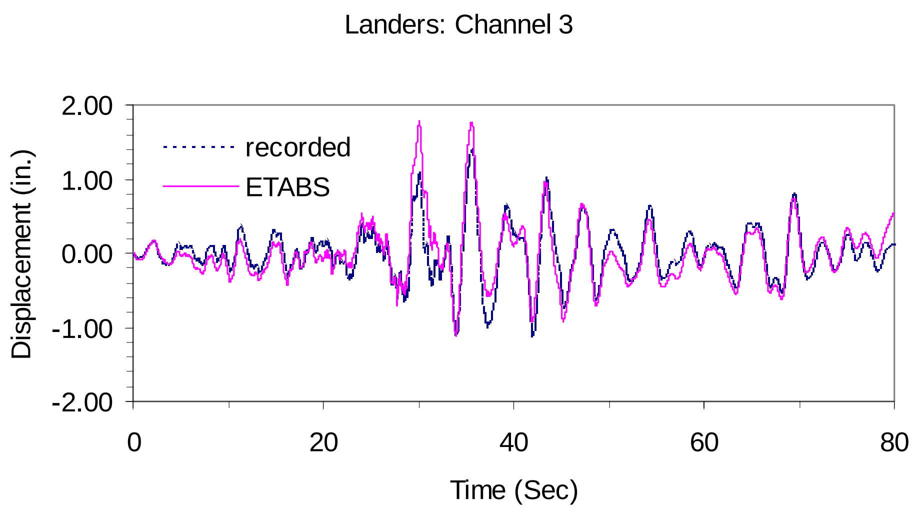

Figure 2.24 Calculated vs. recorded displacements (ch. 3), Landers.

2.5.3.3 Northridge Displacement and Acceleration Comparisons

Acceleration and displacement time history responses for sensor 3 at the roof level during the Northridge earthquake are compared in Figures 2.25 and 2.26. In all cases, the 3-D ETABS model was able to successfully approximate the recorded peak values, as well as the frequency of the response. The calculated and recorded acceleration and displacement responses for the remaining sensors for the three-story building are shown elsewhere (Tokoro 2001). The acceleration time histories of all 10 sensors located above ground level show a reasonably good correlation to the actual recorded values.

In general, the match between the recorded and calculated values of both displacement and acceleration are good. However, the displacement comparisons provide more insight into the physical response. The calculated acceleration amplitudes tend to overestimate the recorded response at the locations of all channels in the E-W and N-S directions. One source of error is due to the fact that the exact location of the recording instrument is unknown, which makes it hard to know if the calculated results represent the exact location of the sensor in the building.

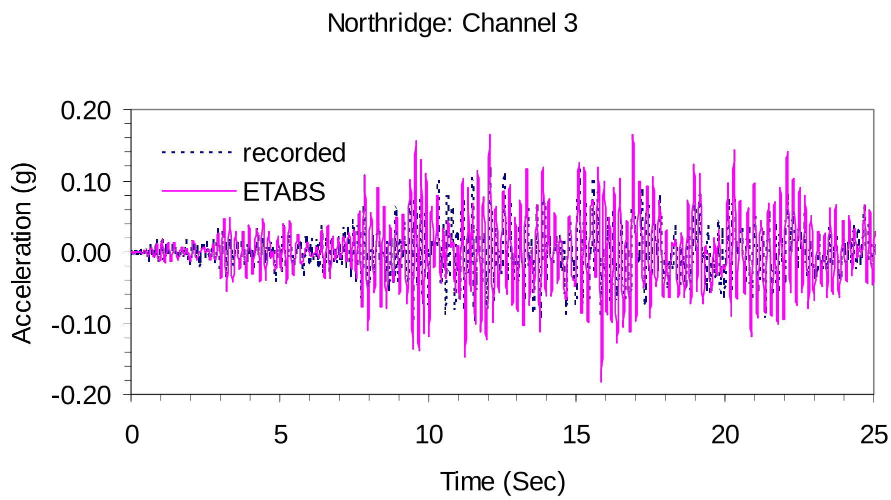

Figure 2.25 Calculated vs. recorded accelerations (ch. 3), Northridge.

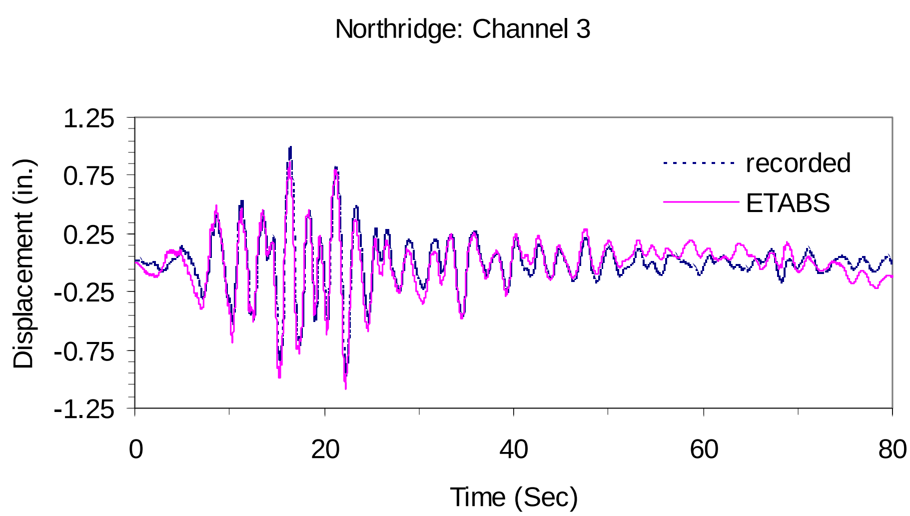

Figure 2.26 Calculated vs. recorded displacements (ch. 3), Northridge.

However, these comparison plots indicate that the calculated displacement response closely approximates the recorded displacement response of the building during each of these three earthquakes. A closer examination of the comparison plots indicates that the analytical model slightly overestimated the peak displacement at each sensor location. This occurrence may indicate that a slightly higher damping is required in the analytical model. The displacement comparisons cover the entire duration for which there were recorded data, and show extremely close results. Comparing the recorded and calculated displacement results over the significant portion of the recorded ground motion indicated that the linear elastic model was adequate to reasonably predict the displacement response of the building for each of the three earthquakes.

2.6 UNIFORM BUILDING CODE COMPARISON

The three-story office building in Lancaster, California, was designed in 1975, and it is assumed that the governing building code was the 1973 Uniform Building Code (ICBO 1973). Therefore, estimates of the nominal base shear capacity of the three-story building were made using the 1973 UBC. The design base shear was also calculated for the three-story building using the 1997 UBC in order to assess current code provisions for calculation of the design base shear.

2.6.1 Code Seismic Force Requirement (UBC 1973)

The three-story building was designed in 1975, and thus is assumed to have been designed according to the governing building code at that time. The UBC 1973 specified that the design base shear values were to be calculated along each principal dimension of the building. The base shear V in the longitudinal or transverse direction of the building may be calculated using Equation (2.5).

The seismic coefficient, C, is specified by Equation (2.6) and the period, T, can be estimated using the empirical formula in Equation (2.7), where H is the total height of the building in feet, and D is the plan dimension of the building in the direction of seismic loading parallel to a principal building dimension.

$$V = KCWZ \tag{2.5}$$

$$C = \frac{0.05}{\sqrt[3]{T}} \tag{2.6}$$

$$T = \frac{0.05H}{\sqrt{D}} \tag{2.7}$$

Due to the difference in longitudinal and transverse dimensions of the three-story building, the period, and hence the base shear had to be computed for loading along both directions. Using the Equation (2.7) in the N-S and E-W directions of the three-story building, the calculated periods are shown in Equations (2.8) and (2.9), respectively.

$$T_{NS} = \frac{0.05H}{\sqrt{D_{NS}}} = \frac{0.05(37.5\,ft)}{\sqrt{129\,ft}} = 0.17 \text{ sec} \tag{2.8}$$

$$T_{EW} = \frac{0.05H}{\sqrt{D_{EW}}} = \frac{0.05(37.5\,ft)}{\sqrt{72\,ft}} = 0.22 \text{ sec} \tag{2.9}$$

Similarly, using Equation (2.6) we find that the seismic coefficients may be computed in the N-S and E-W direction as shown in Equations (2.10) and (2.11).

$$C_{NS} = \frac{0.05}{\sqrt[3]{T_{NS}}} = \frac{0.05}{\sqrt[3]{0.17\,\text{sec}}} = 0.091 \tag{2.10}$$

$$C_{EW} = \frac{0.05}{\sqrt[3]{T_{EW}}} \frac{0.05}{\sqrt[3]{0.22\,\text{sec}}} = 0.083 \tag{2.11}$$

Using K=1.33, Z=1.0 (load bearing) and W to be the total weight of the three-story building above ground in Equation (2.5), the design seismic resistance coefficients for the N-S and E-W directions may be computed as shown in Equations (2.12) and (2.13).

$$V_{NS} = (ZKC_{NS})W = (1.0)(1.33)(0.091)W = 0.12W \tag{2.12}$$

$$V_{EW} = (ZKC_{EW})W = (1.0)(1.33)(0.083)W = 0.11W \tag{2.13}$$

Taking W to be the effective dead load of the building, the design base shears in the N-S and E-W directions are as shown in Equations (2.14) and (2.15).

$$V_{NS} = 0.12W = 0.12(2606\,kips) = 312.72\,kips \tag{2.14}$$

$$V_{EW} = 0.11W = 0.11(2606\,kips) = 286.66\,kips \tag{2.15}$$

2.6.2 Code Design Requirements (UBC 1997)

The period of the three-story building was calculated according to Method A of the 1997 UBC provisions, with the value of C_t equal to 0.020. According to the 1997 UBC, the period of the three-story building may be approximated by "Method A," and is given by the following empirical formula in Equation (2.16).

$$T = 0.020(h_n)^{3/4} = 0.02(41.5\,ft)^{3/4} = 0.3270\,\text{sec} \tag{2.16}$$

The actual soil profile at the location of the building is unknown, which made using the default soil profile S_D necessary in the code analysis calculations. Since the three-story building is located in California, it was necessary to use the seismic zone factor Z=0.4. Near-source factors were chosen based on a generating seismic source A and a distance to source greater than 15km, where N_a and N_v were each taken to be 1.0. The seismic coefficients C_a and C_v for a building in seismic zone 4 and sited on a soil of profile S_D are calculated using the 1997 UBC formulas shown in Equation (2.17).

$$\begin{aligned} C_a &= 0.44 N_a = 0.44(1.0) = 0.44 \\ C_v &= 0.64 N_v = 0.64(1.0) = 0.64 \end{aligned} \tag{2.17}$$

A structural system factor of R=5.5 (masonry shear wall building frame system) was used in the base shear calculations although according to the 1997 UBC, a strength reduction factor of 4.5 would be more appropriate (ICBO 1997).

The 1997 UBC specifies that the design base shear V in a given direction of a building should be determined from the Equation (2.18).

$$V = \left(\frac{C_v I}{RT}\right) W = \left(\frac{0.64 * 1.0}{5.5 * 0.3270 \sec}\right) W = 0.36W \tag{2.18}$$

However, the total design base shear need not exceed Equation (2.19).

$$V \leq \left(\frac{2.5 C_a I}{R}\right) W = \left(\frac{2.5 * 0.44 * 1.0}{5.5}\right) W = 0.2W \tag{2.19}$$

The total design base shear shall not be less than Equation (2.20).

$$V = 0.11 C_a I W = 0.11(0.44)(1.0) W = 0.048W \tag{2.20}$$

In addition, the 1997 UBC specifies that for Seismic Zone 4, the total base shear shall not be less than specified in Equation (2.21), where R is a factor based on the natural structural system of the building, I is an importance factor, N_v is a near-source factor, and C_a and C_v are seismic coefficients which are determined for a given Seismic Zone and soil profile type.

$$V = \left(\frac{0.8 Z N_v I}{R}\right) W = \left(\frac{0.8 * 0.4 * 1.0 * 1.0}{5.5}\right) W = 0.058W \tag{2.21}$$

Using a value of R=5.5 and an importance factor of I=1.0 for a building of typical use, the total design base shear as predicted by the 1997 UBC is governed by the limiting formula in Equation (2.22).

$$V = \left(\frac{2.5 C_a I}{R}\right) W = \left(\frac{2.5 * 0.44 * 1.0}{5.5}\right) W = 0.2W \tag{2.22}$$

Equation (2.22) states that the total lateral force requirement will be 20% of the effective self-weight of the building, W. Estimating W as 2606 kips, the base shear requirement as determined by the 1997 UBC code may be computed as in Equation (2.23).

$$V = 0.2W = 0.2 * 2606.06\ kips = 521.21 kips \tag{2.23}$$

The value of the design base shear calculated using the 1973 UBC requirements is based on allowable (working) stress, whereas the value computed using 1997 UBC formulas is based on the ultimate strength. For purposes of comparison, the value of base shear computed from the 1973 UBC was multiplied by the load factor of 1.4. It should be noted that the values of the base shear calculated using the current 1997 UBC provisions in the N-S and E-W direction are 19.0 % and 30.0% greater than the lateral force requirement used to design the building in 1975. Therefore, the current 1997 UBC is more demanding for calculation of the design base shear compared to the 1973 UBC. It should also be noted that the estimate of the period given by the 1973 UBC gave a close approximation of the actual value as determined from the recorded data and the finite element calculations. The estimate from the 1997 UBC was 50% higher than the actual although the period did not control the determination of the base shear for this building.

2.7 ANALYSES OF BASE SHEARS

Of the accelerations measured during three of the earthquakes recorded at the base of the building, the maximum values of base acceleration in the N-S (Northridge) and E-W (Landers) directions were 0.07g, which is of no surprise being that the location of the three-story building was far from the epicenter of each earthquake. Thus, to study the seismic demands on the building when subjected to more intense ground shaking, four more demanding ground motions were selected. These four additional ground motions are the following: (1) the ground motion recorded at the Newhall Fire Station during the Northridge earthquake, (2) the ground motion recorded in Lucerne during the Landers earthquake that contains a one-sided displacement pulse, (3) the ground motion recorded at Takatori during the Kobe earthquake that contains two-sided displacement pulses and (4) the ground motions recorded at the Los Gatos Presentation Center during the Loma Prieta earthquake that contains multiple-sided displacement pulses. Therefore, seven ground motions were used for the evaluation of the seismic behavior of this building.

2.8 IN-PLANE SHEAR CAPACITY

The nominal shear capacity of a structural wall can be determined using Equation (2.24), where the coefficient C_d depends on the ratio of M/Vd (ICBO 1997).

$$V_n = C_d A_{mv} \sqrt{f'_m} + A_{mv} \rho f_y \tag{2.24}$$

For these walls, the above equation for nominal shear strength can be expressed as shown in Equation (2.25), where the ratio of $\frac{M}{Vd}$ is approximately 0.52, resulting in a value of C_d = 2.

$$V_n = C_d \sqrt{f'_m} hd + \frac{A_{vh} f_y d}{s_2} \tag{2.25}$$

For the four walls in the N-S direction, the length of an individual wall is 567″, the thickness, h, is 12″, the masonry strength is 1,500 psi and the horizontal steel is 1-#4 at 12″. If the effective length of the wall is taken as $0.8xl_w$, the nominal shear capacity of a single wall is 725 kips, and for the four walls this becomes 2900 kips in the N-S direction. Lateral resistance in the E-W direction is provided by six 8″ masonry walls. Each wall has a length of 32 ft and is reinforced with 1- #4 bar at 24 in. in the horizontal direction. As before, if the effective length of the wall is taken as $0.8*l_w$, the nominal shear capacity of a single wall is 293 kips and for the six walls the total shear capacity becomes 1756 kips in the E-W direction.

2.8.1 Whittier Narrows Earthquake

The linear elastic analytical model was used to predict the base shear demands of the three-story building during the Whittier Narrows earthquake. The results were then compared to the design values of base shear specified by the 1973 and 1997 UBC that were calculated in the previous section. The comparison of the predicted base shear in the N-S and E-W directions to the 1973 and 1997 UBC values during the Whittier Narrows earthquake are displayed in Figures 2.27 and 2.28.

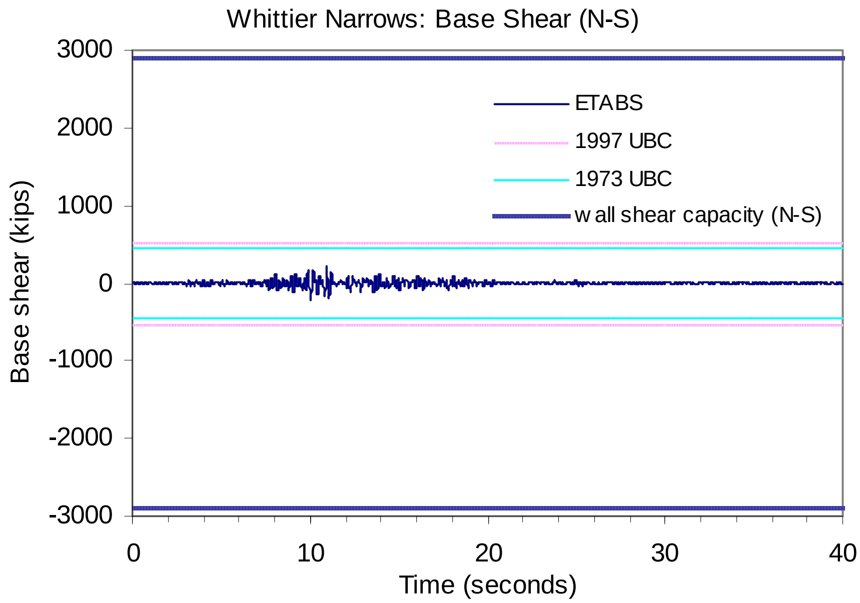

Figure 2.27 N-S design vs. calculated base shear demand, Whittier Narrows, 3-story building.

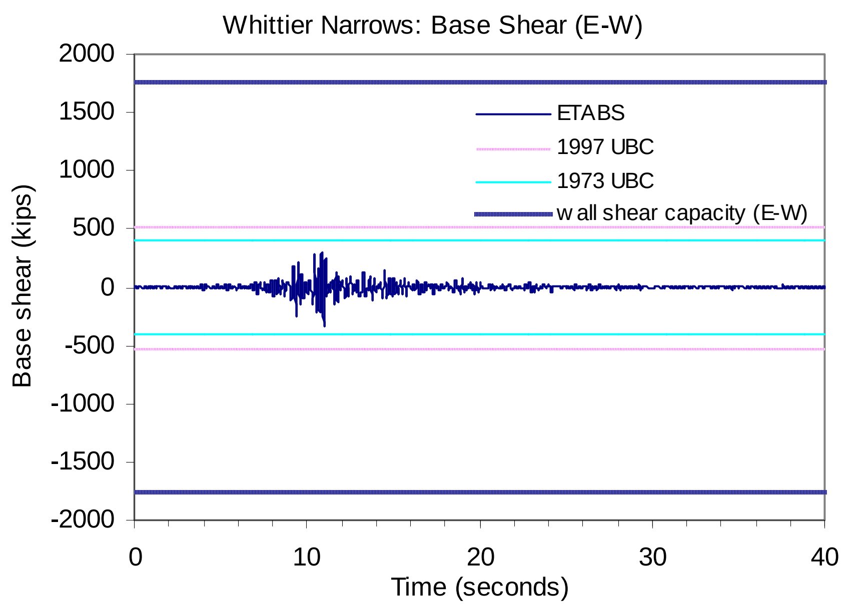

Figure 2.28 E-W design vs. calculated base shear demand, Whittier Narrows, 3-story building.

From these comparisons, it can be seen that the seismic base shear demand on the building is well within the strength limits set by both codes. These results suggest that the three-story building did not suffer any appreciable damage during the Whittier Narrows earthquakes, and consequently it is assumed to have behaved in a linearly elastic manner.

2.8.2 Landers Earthquake

The comparisons of the predicted base shear in the N-S and E-W directions to the 1973 and 1997 UBC values during the Landers earthquake are displayed in Figures 2.29 and 2.30. From inspection of the base shear time histories, it can be seen that the base shear in the E-W direction exceeds the base shear in the N-S direction for much of the time history. This is to be expected, because the transverse ground motion in channel 9 is stronger than the longitudinal motion as measured by channel 13 and may also be affected by increased flexibility of the diaphragm. The base shear demands on the three-story building were below both UBC design values in both directions. Thus, the three-story building performed in a primarily linear manner during the Landers earthquake.

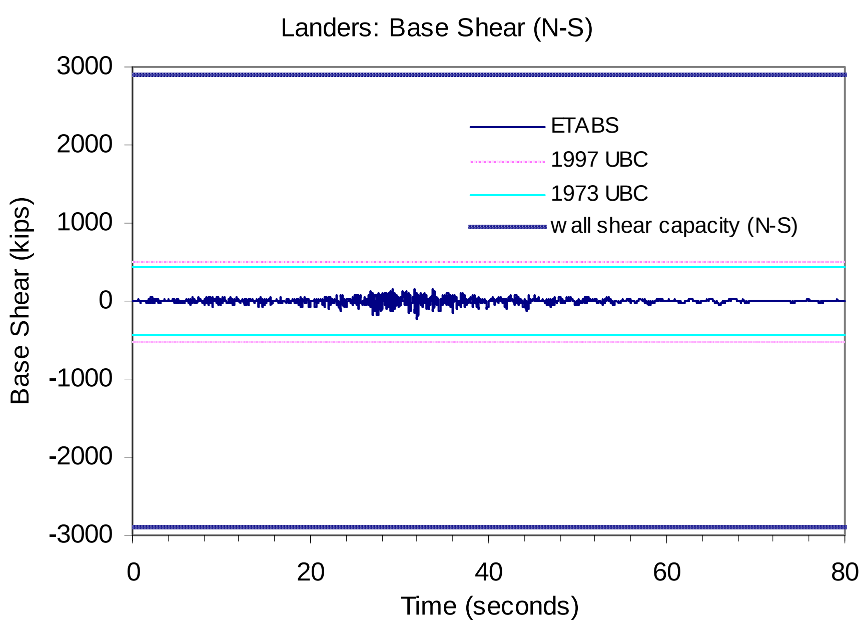

Figure 2.29 N-S design vs. calculated base shear demand, Landers, 3-story building.

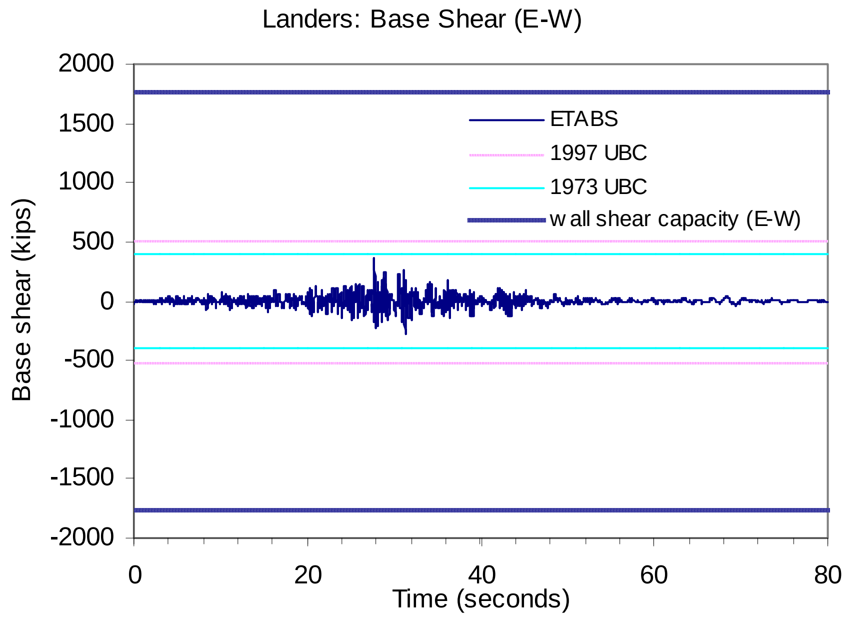

Figure 2.30 E-W design vs. calculated base shear demand, Landers, 3-story building.

2.8.3 Northridge Earthquake

Base shear comparisons of the analytical time history results and for the 1973 and 1997 UBC lateral force requirements in the N-S and E-W directions during the Northridge earthquake are displayed in Figures 2.31 and 2.32. From these comparisons, we can see that the seismic performance of the building was well within both UBC design criteria in both building directions, which is indicative of the linear elastic behavior of the three-story building during the Northridge earthquake.

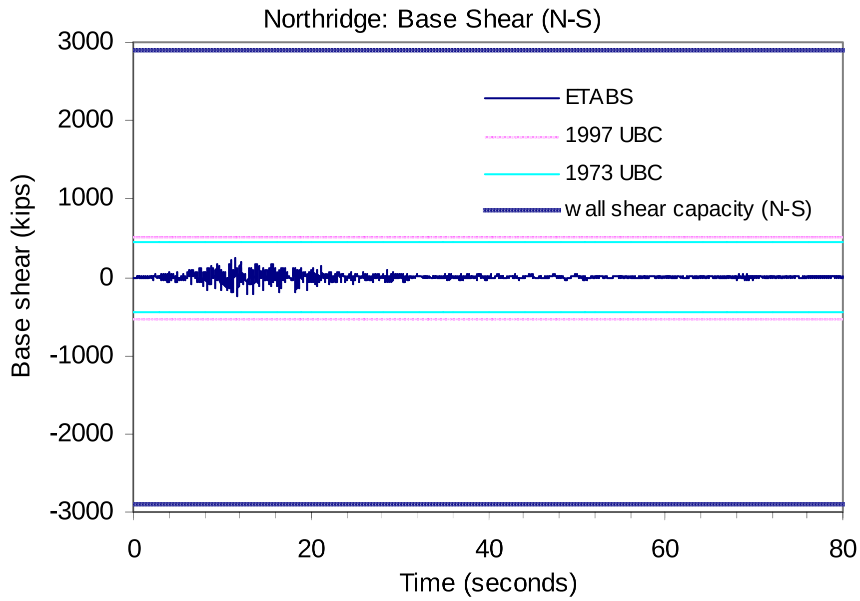

Figure 2.31 N-S design vs. calculated base shear demand, Northridge, 3-story building.

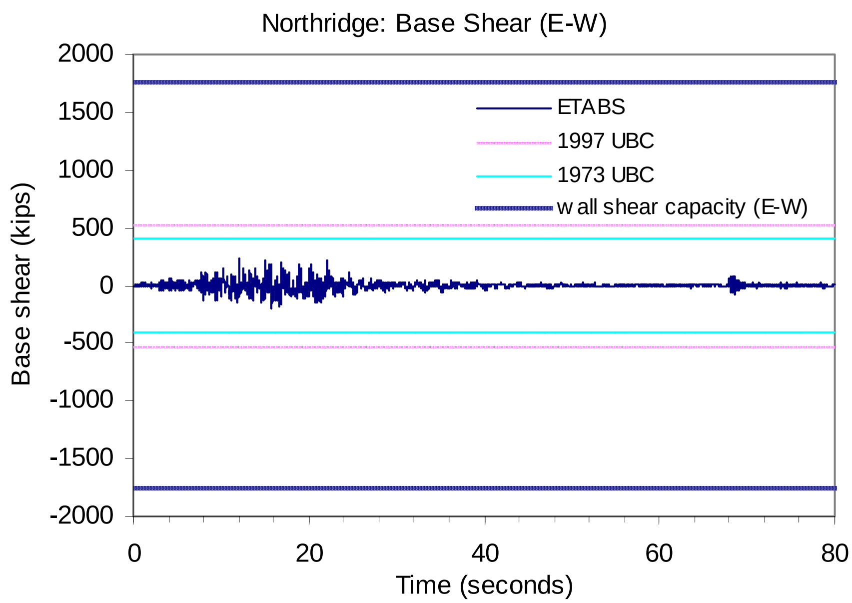

Figure 2.32 E-W design vs. calculated base shear demand, Northridge, 3-story building.

2.8.4 Newhall Fire Station (Northridge Earthquake)

The acceleration recorded at the Newhall Fire Station during the Landers earthquake was used to study seismic response and behavior of the three-story building to strong motion. The N-S and E-W components of this recorded base motion are shown in Figures 2.33 and 2.34. The peak recorded base acceleration values in the N-S and E-W directions were both 0.60g. Elastic response spectra for 5% critical damping were generated for this ground motion and are shown in Figure 2.35.

The calculated base shears in the N-S and E-W directions due to the strong motion recorded at Newhall are compared with the 1973 and 1997 UBC requirements in Figures 2.36 and 2.37. From these comparisons, it can be seen that the base shear demand of this record exceeded both UBC values during the significant portion of the strong motion, thus indicating that inelastic behavior could occur if the strength capacity is the minimum value required by code. Due to demand vs. strength this most likely would have occurred in the E-W direction. Such a result should be expected, since the code specifies the design for a reduced elastic base shear using the system-specific R factor, so that the building will be excited into the inelastic range and become vulnerable to damage under strong ground motion.

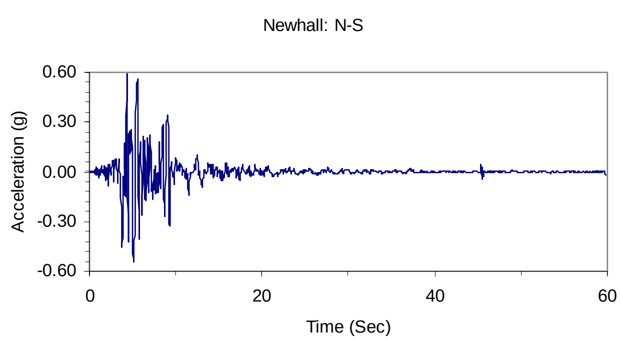

Figure 2.33 N-S acceleration time history, Newhall.

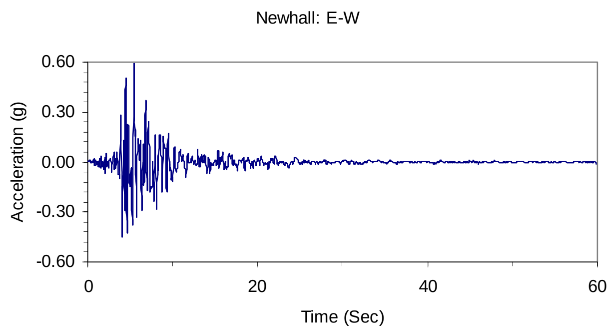

Figure 2.34 E-W acceleration time history, Newhall.

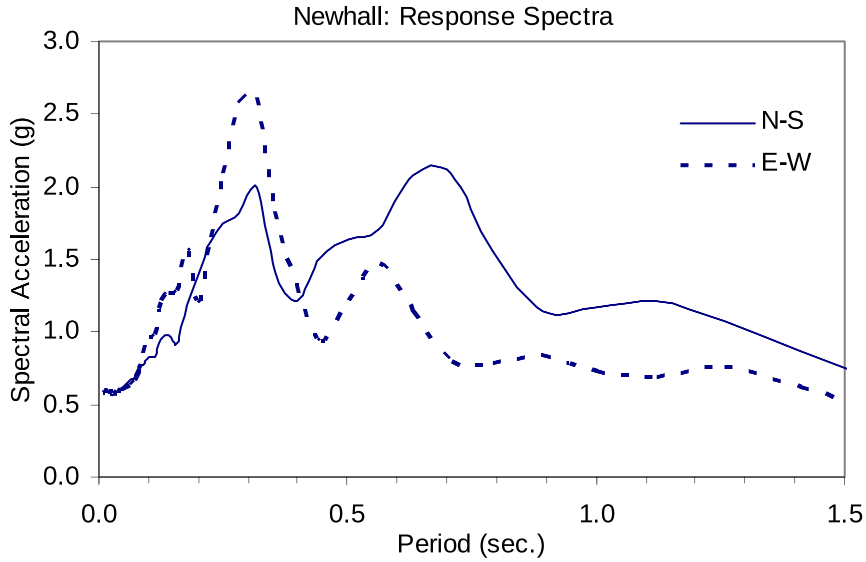

Figure 2.35 N-S and E-W response spectra, Newhall.

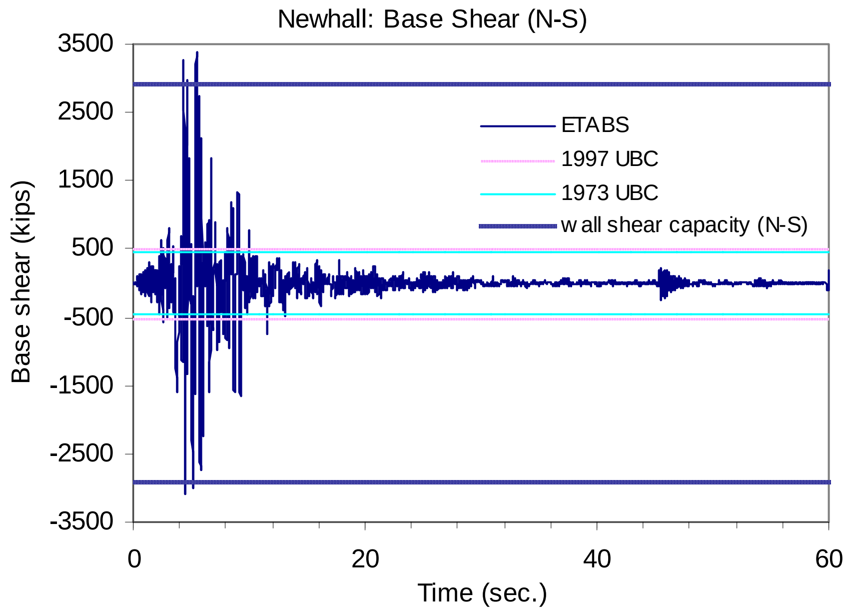

Figure 2.36 N-S design vs. calculated base shear demand, Newhall, 3-story building.

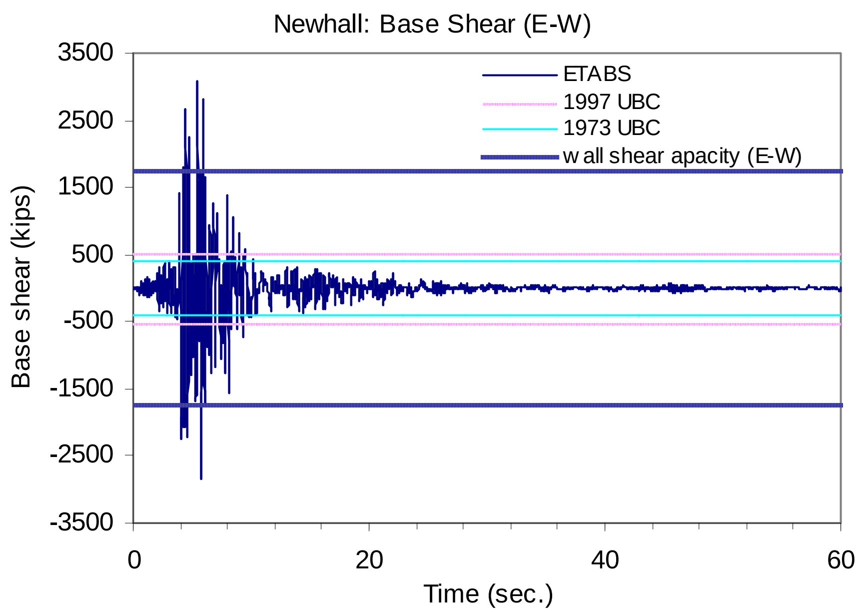

Figure 2.37 E-W design vs. calculated base shear demand, Newhall, 3-story building.

2.8.5 Lucerne (Landers Earthquake)

The recorded ground accelerations at Lucerne during the Landers earthquake in the N-S and E-W directions are shown in Figures 2.38 and 2.39. The recorded peak accelerations in the N-S and E-W directions during this motion are 0.72g and 0.44g. Elastic response spectra for 5% of critical damping were generated using the N-S and E-W ground motions recorded at Lucerne and are shown in Figure 2.40.

Predicted base shear in the N-S and E-W directions during the strong motion recorded at Lucerne are compared with the strength requirements of the 1973 and 1997 UBC in Figures 2.41 and 2.42. These comparisons indicate that the base shear demand on the three-story building exceeded both UBC values for much of the duration of strong ground motion. From Table 2.6 it can be seen that the maximum base shear demand in the N-S direction during this motion was 2,401 kips, which is 443% greater than the 1973 UBC code values of 442.4 kips for which the building was assumed to have originally been designed. The maximum base shear demand in the E-W direction was 2,578 kips, which is 543% greater than the 1973 UBC value of 401.2 kips. In both cases the code values have been scaled by 1.4 to represent ultimate strength. Thus, from this strong motion analyses, it can be concluded that the three-story building would have performed in a nonlinear manner and suffered considerable damage if subjected to a ground motion similar to that recorded at Lucerne and if the actual shear strength is close to the code requirement. However, computed in-plane shear capacities of the walls significantly exceeded the code strength requirements.

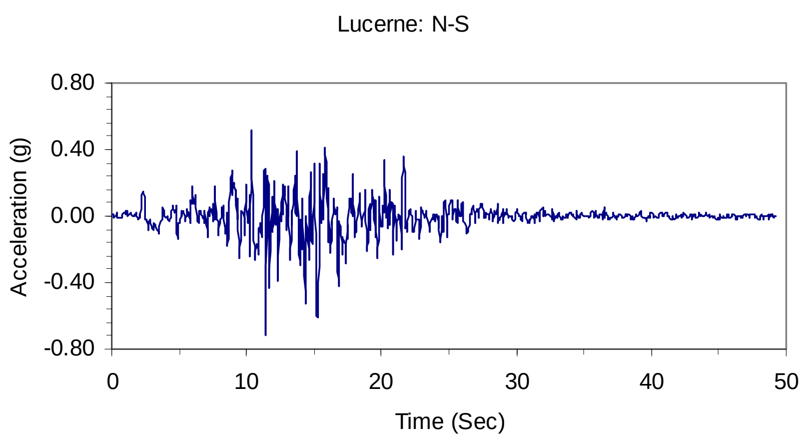

Figure 2.38 N-S acceleration time history, Lucerne.

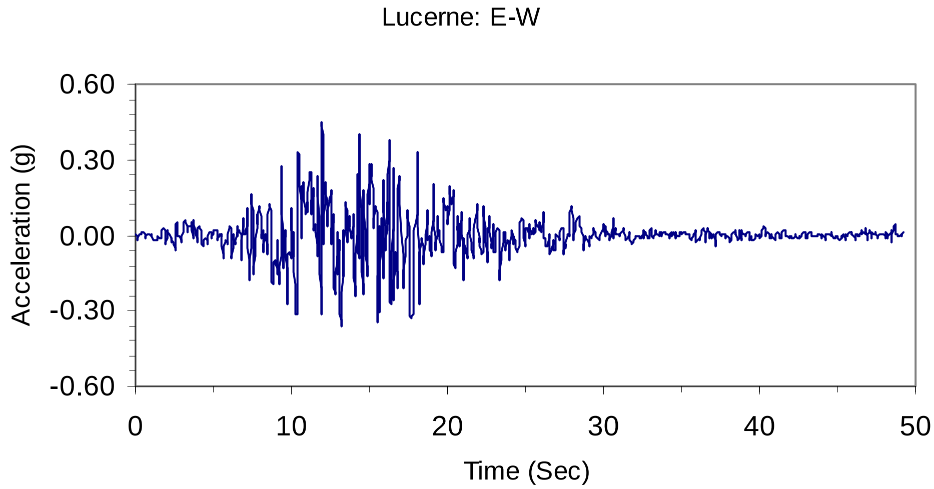

Figure 2.39 E-W acceleration time history, Lucerne.

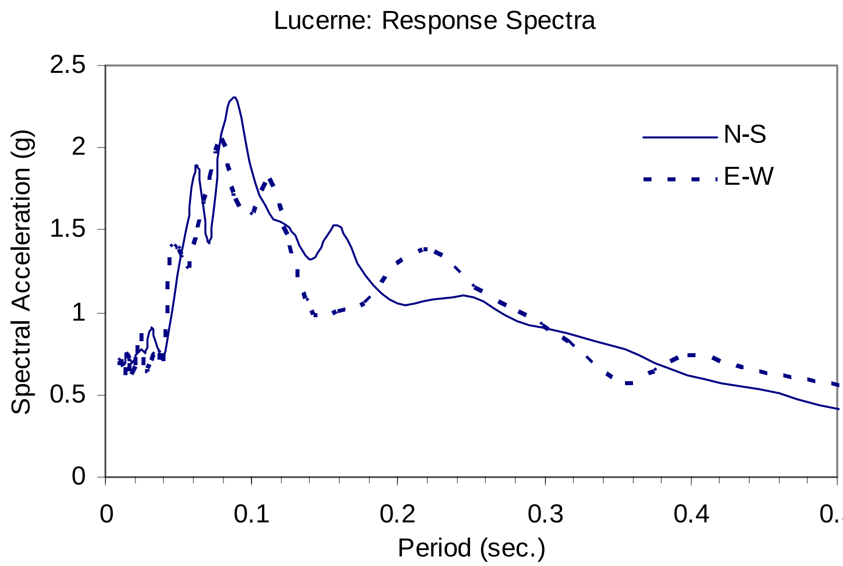

Figure 2.40 N-S and E-W response spectra, Lucerne.

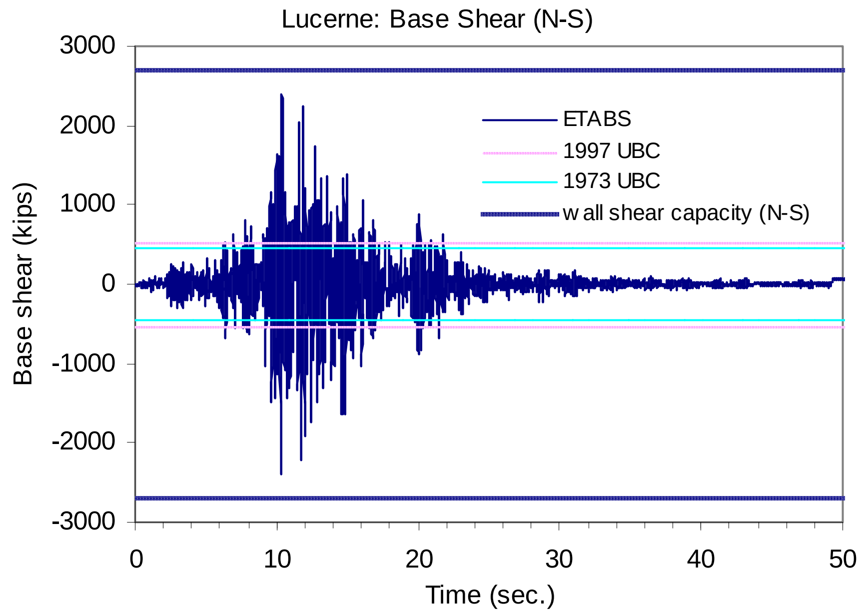

Figure 2.41 N-S design vs. calculated base shear demand, Lucerne, N-S, 3-story building.

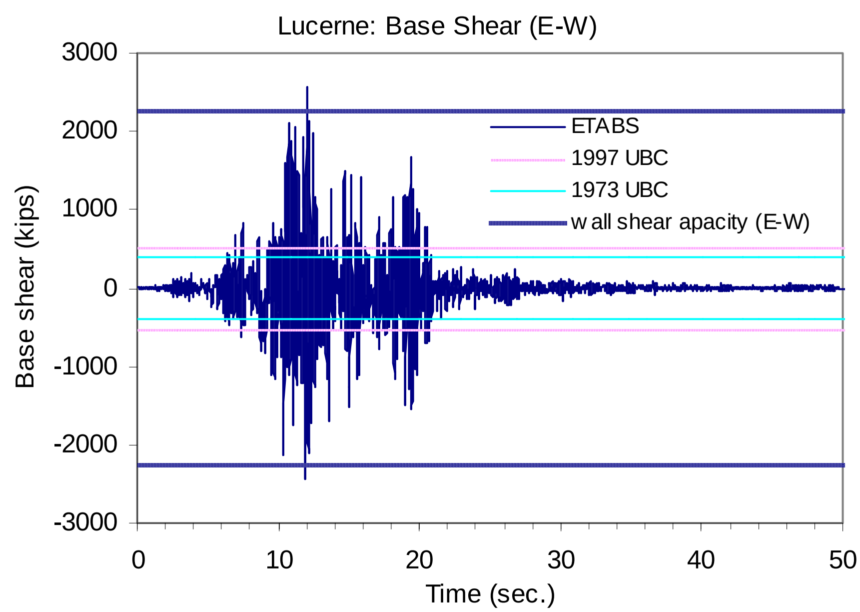

Figure 2.42 E-W design vs. calculated base shear demand, Lucerne, 3-story building.

2.8.6 Takatori (Kobe Earthquake)

The recorded base accelerations at Takatori, Japan during the Kobe earthquake, used to conduct strong motion analyses of the three-story building, are shown in Figures 2.43 and 2.44. The peak recorded accelerations in the N-S and E-W directions during this motion are 0.61g and 0.62g. Elastic response spectra for 5% of critical damping were generated using the N-S and E-W ground motions recorded at Takatori are shown in Figure 2.45.

The comparisons of the predicted base shear in the N-S and E-W directions to the 1973 and 1997 UBC design base shears are presented in Figures 2.46 and 2.47. From these comparisons, it can be seen that the base shear demand of the three-story building exceeded both the 1973 and 1997 UBC criteria for nearly the entire duration of the significant strong motion. From Table 2.6 we can see that the maximum base shear demand in the N-S direction during this motion was 3337 kips, which is 754% greater than the 1973 UBC code values of 442.3 kips for which the building was assumed to have been originally designed. The maximum base shear demand in the E-W direction was 3903 kips, which is 973% greater than the 1973 UBC value of 401.2 kips. Thus, this strong motion analyses, indicates that the three-story building may have performed in a nonlinear manner and suffered considerable damage if subjected to an equivalent base motion.

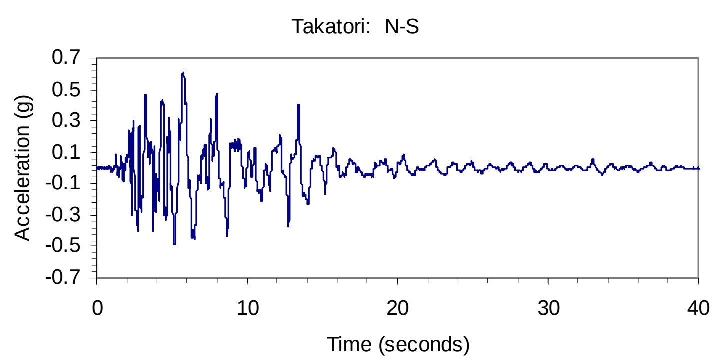

Figure 2.43 N-S acceleration time history, Takatori.

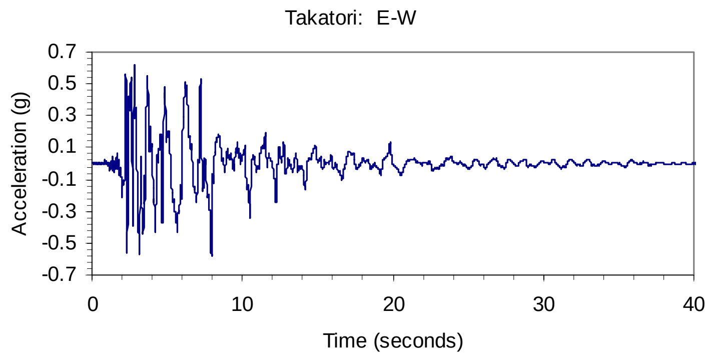

Figure 2.44 E-W acceleration time history, Takatori.

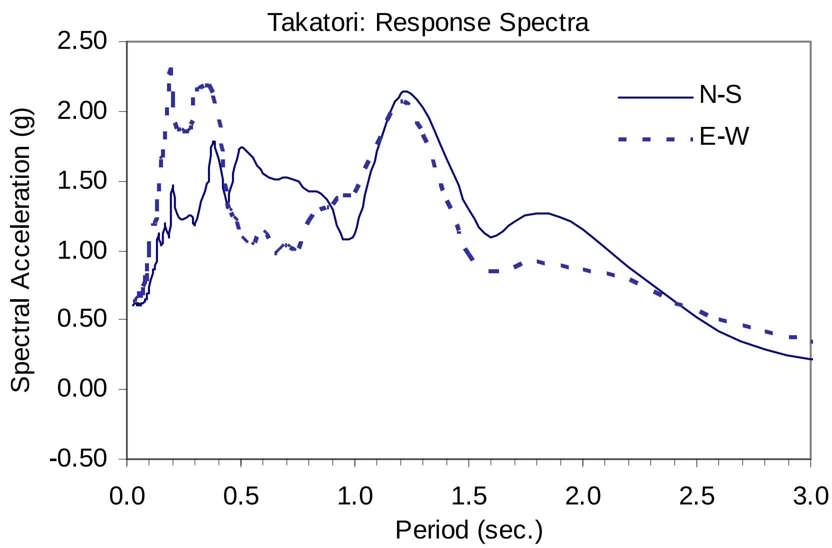

Figure 2.45 N-S and E-W response spectra, Takatori.

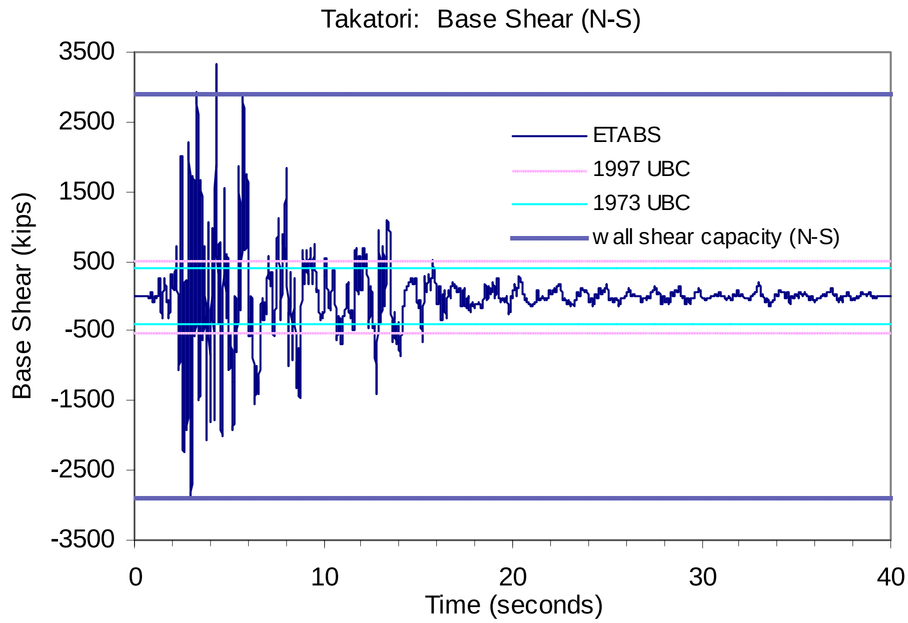

Figure 2.46 N-S design vs. calculated base shear demand, Takatori, 3-story building.

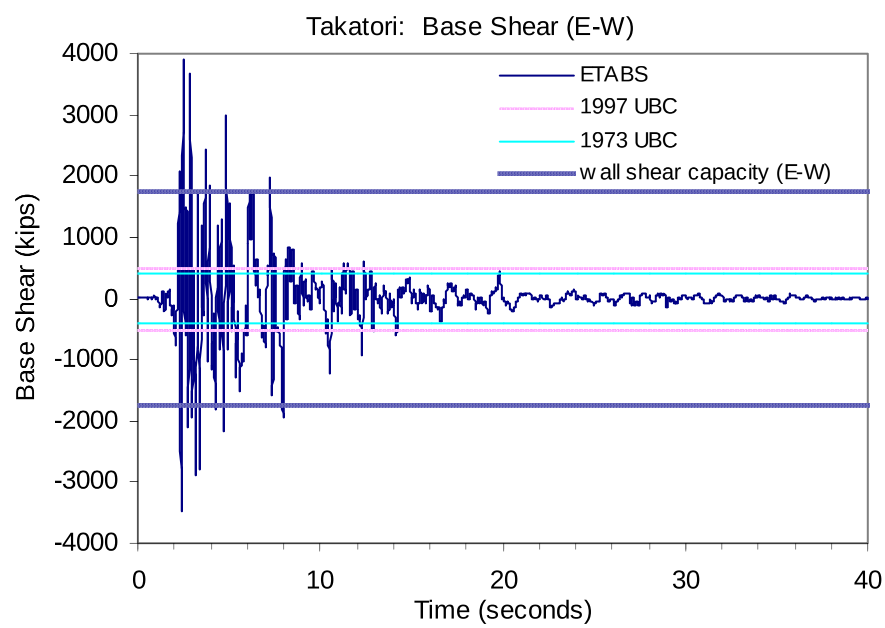

Figure 2.47 E-W design vs. calculated base shear demand, Takatori, 3-story building.

2.8.7 Los Gatos (Loma Prieta Earthquake)

The ground accelerations at Los Gatos Pres. Center (LGPC) recorded during the Loma Prieta earthquake in the N-S and E-W directions used to conduct strong motion analyses of the three-story building are shown in Figures 2.48 and 2.49. The recorded peak accelerations in the N-S and E-W directions during this motion are 0.563g and 0.605g. Elastic response spectra for 5% of critical damping for these ground motions are shown in Figure 2.50.

The comparison of the predicted base shear in the N-S and E-W directions to the 1973 and 1997 UBC values during the strong motion recorded at LGPC are shown in Figures 2.51 and 2.52. From these comparisons, we can see that the base shear demand of the three-story building exceeded both UBC values for nearly the entire duration of the significant strong motion. From Table 2.6 we can see that the maximum base shear demand in the N-S direction during this motion was 2239 kips, which is 505% greater than the 1973 UBC code design values of 442.4 kips for which the building was assumed to have been originally designed. The maximum base shear demand in the E-W direction was 2069 kips, which is 516% greater than the 1973 UBC design criteria of 401.2 kips. Thus, from this strong motion analyses, we can conclude that the three-story building would have performed in a nonlinear manner and suffered considerable damage if subjected to a ground motion similar to that recorded at LGPC. However, strength capacity of the structural walls is estimated to be considerably higher than the minimum code requirement, which may limit the amount of damage in the E-W direction.

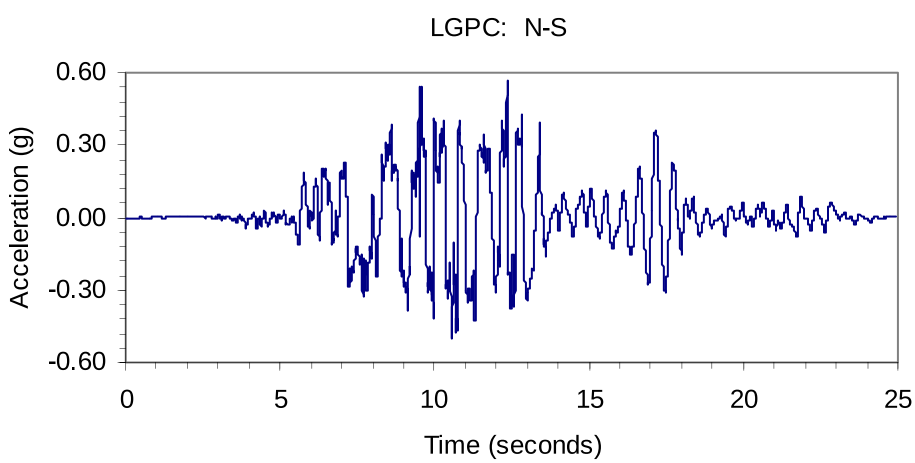

Figure 2.48 N-S acceleration time history, LGPC.

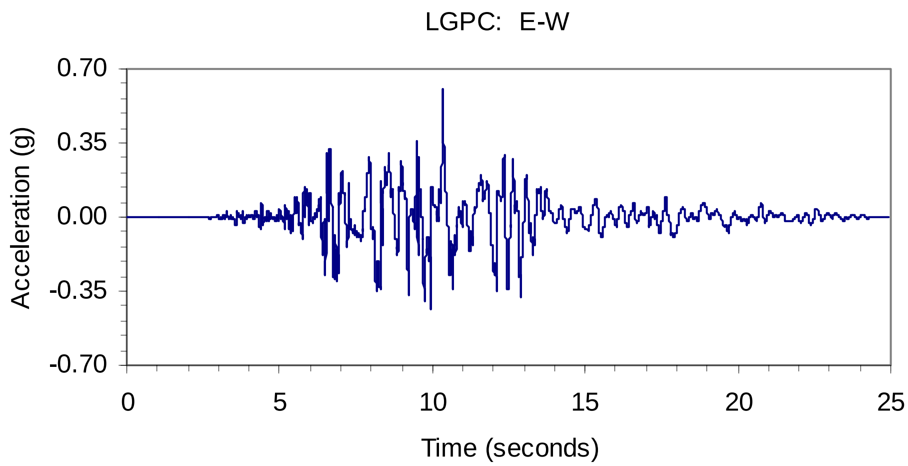

Figure 2.49 E-W acceleration time history, LGPC.

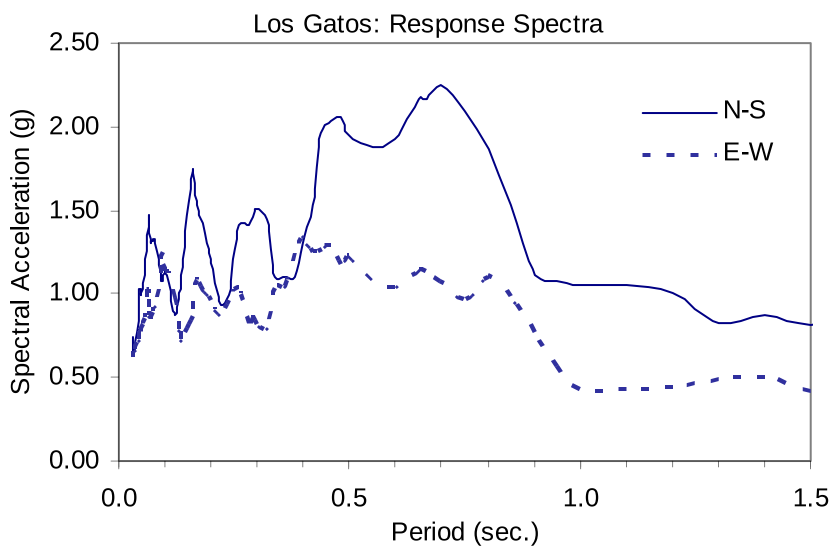

Figure 2.50 N-S and E-W response spectra, LGPC.

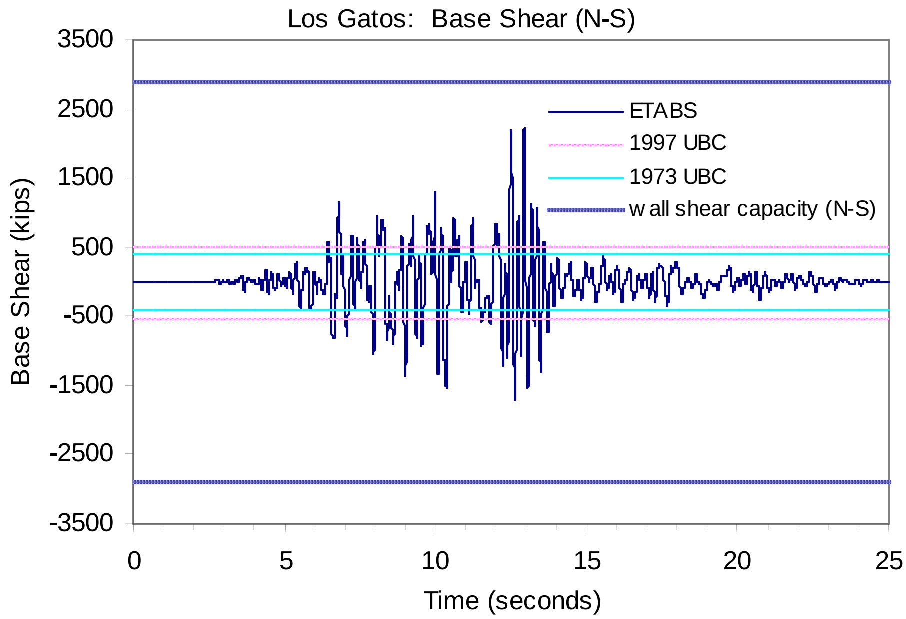

Figure 2.51 N-S design vs. calculated base shear demand, LGPC, 3-story building.

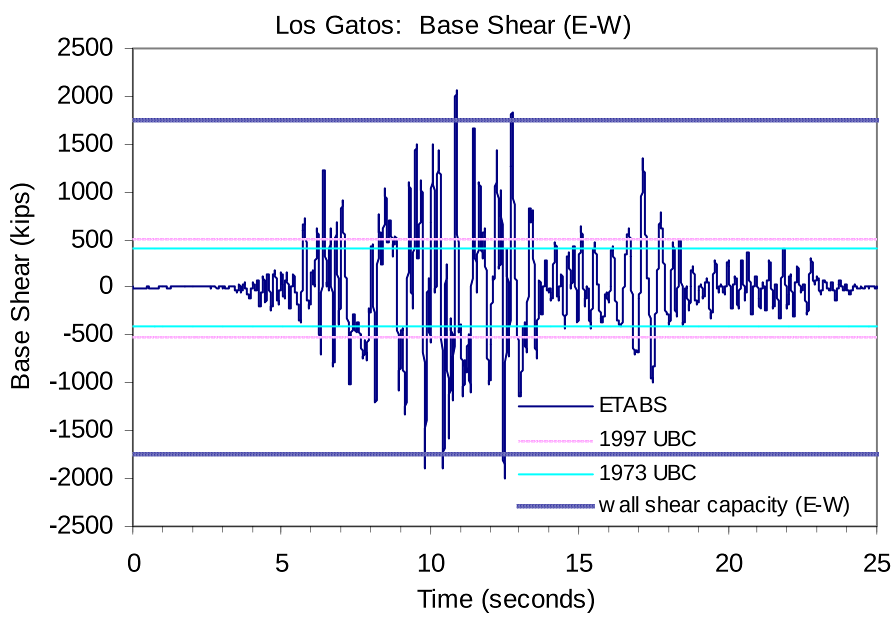

Figure 2.52 E-W design vs. calculated base shear demand, LGPC, 3-story building.

Table 2.6 Summary of N-S and E-W peak absolute base shear demand, 3-story building.

Earthquake		Transverse (E-W) Max. Abs. Base Shear $V_{b,max}$ (kips)	Transverse (E-W) Percent of E-W capacity $\frac{V_{b,\max}}{V_{b,cap}} * 100$ (percent)	Transverse (E-W) Percent of 1973 UBC design strength $\frac{V_{b,\max}}{V_{b,1973}} * 100$ (percent)	Transverse (E-W) Percent of 1997 UBC design strength $\frac{V_{b,\max}}{V_{b,1997}} * 100$ (percent)	Longitudinal (N-S) Max. Abs. Base Shear $V_{b,max}$ (kips)	Longitudinal (N-S) Percent of E-W capacity $\frac{V_{b,\max}}{V_{b,cap}} * 100$ (percent)	Longitudinal (N-S) Percent of 1973 UBC design strength $\frac{V_{b,\max}}{V_{b,1973}} * 100$ (percent)	Longitudinal (N-S) Percent of 1997 UBC design strength $\frac{V_{b,\max}}{V_{b,1997}} * 100$ (percent)
Recorded Motions	Whittier Narrows	334.6	19.1	83.4	64.2	221.8	7.6	50.1	42.5
	Landers	365.9	20.8	91.2	70.2	236.1	8.1	53.4	45.3
	Northridge	241.6	13.8	60.2	46.4	247.3	8.5	55.9	47.4
Strong Motion Analyses	Newhall	3092.1	176.1	770.5	593.2	3395.5	117.1	767.7	651.5
	Lucerne	2578.2	146.8	642.5	494.6	2401.0	82.8	542.9	460.7
	Takatori	3903.6	222.3	972.7	748.9	3336.6	115.1	754.4	640.2
	Los Gatos	2068.5	117.8	515.4	396.9	2239.2	77.2	506.3	429.6

2.9 DIAPHRAGM SHEAR

Perhaps the most critical component of a building with rigid walls and flexible diaphragm is the timber diaphragm. In-plane shear forces due to the deflection of the diaphragm can be significant and under more severe earthquake ground motions can readily exceed allowable stresses specified in current building codes. Under the three ground motions recorded at the building site, the shear demand varies up to 0.24 kips/in. for the roof and up to 0.11 kips/in. for both floors. These values compare with strength capacity of 0.18 kips/in. for the roof and 0.27 kips/in. for the floors. The shear contours due to the recorded Northridge ground motion are representative of this response and are shown in Figure 2.53 for the roof, Figure 2.54 for the third floor and Figure 2.55 for the second floor.

Considering the effect of the more severe ground motions on the diaphragm, the ground motion recorded at the Newhall Fire Station (Northridge), is representative. The diaphragm shear varies from 0.0 to 0.6 kips/inch at the roof and second floor levels and varies from 0.0 to 0.70 kips/inch at the second floor level. In-plane shear contours are shown in Figure 2.56 for the roof, Figure 2.57 for the third floor and Figure 2.58 for the second floor.

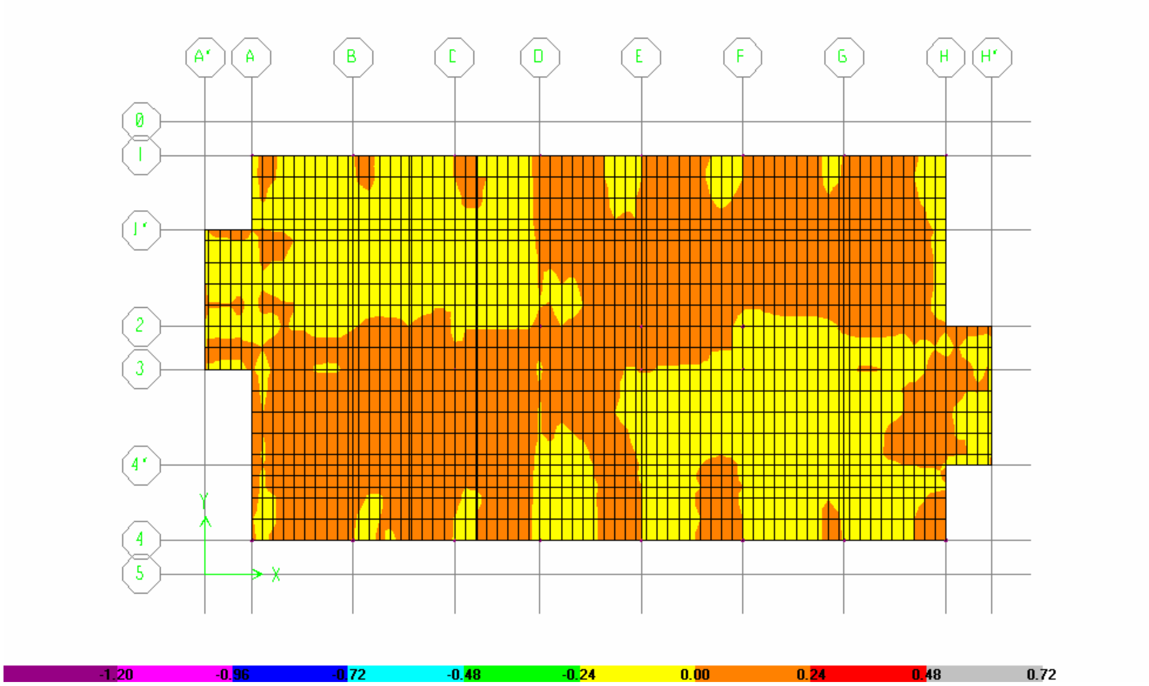

Figure 2.53 In-plane shear force contour, roof, Northridge, 3-story building.

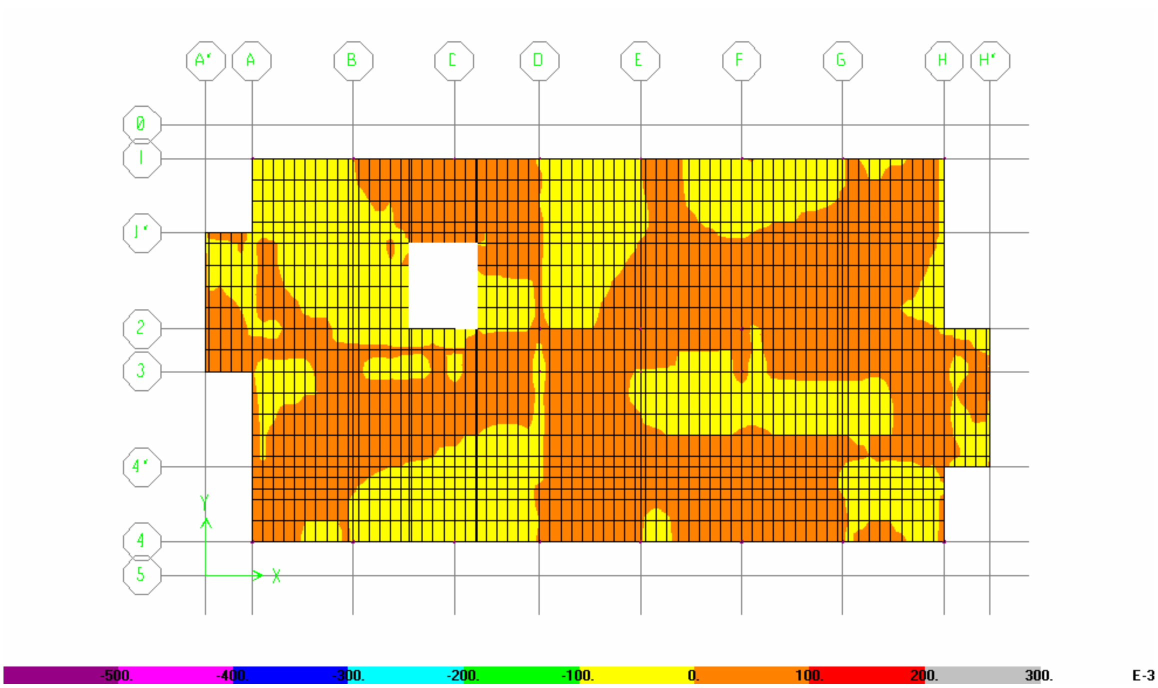

Figure 2.54 In-plane shear force contour, 3rd floor, Northridge, 3-story building.

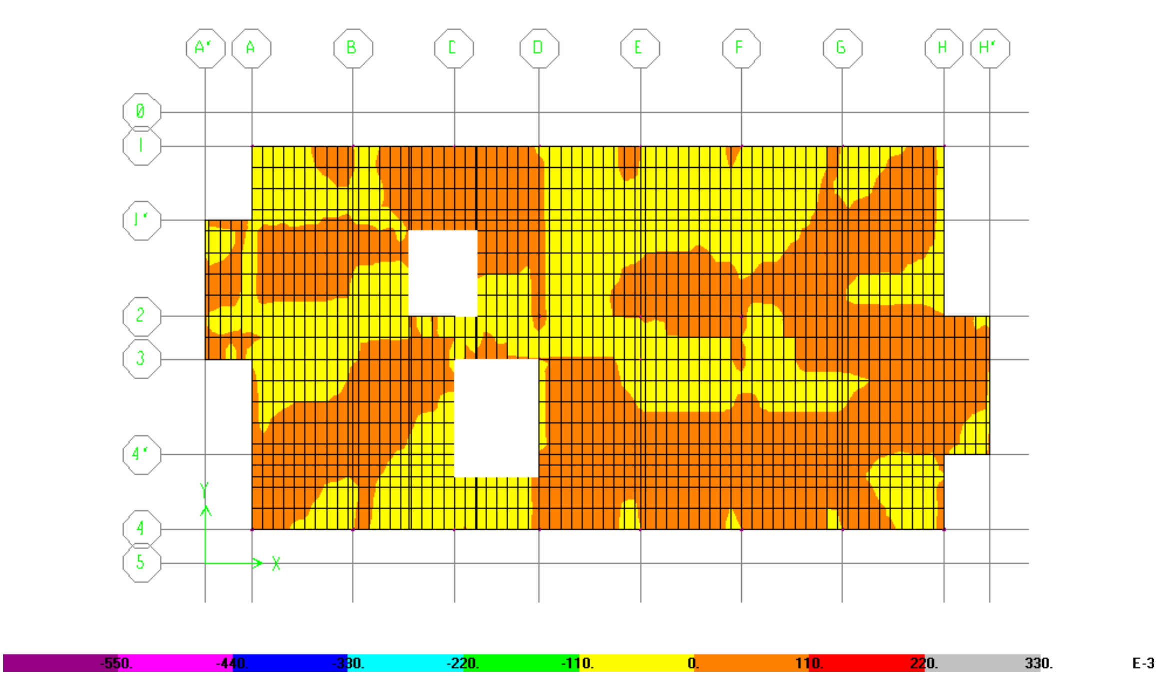

Figure 2.55 In-plane shear force contour, 2nd floor, Northridge, 3-story building.

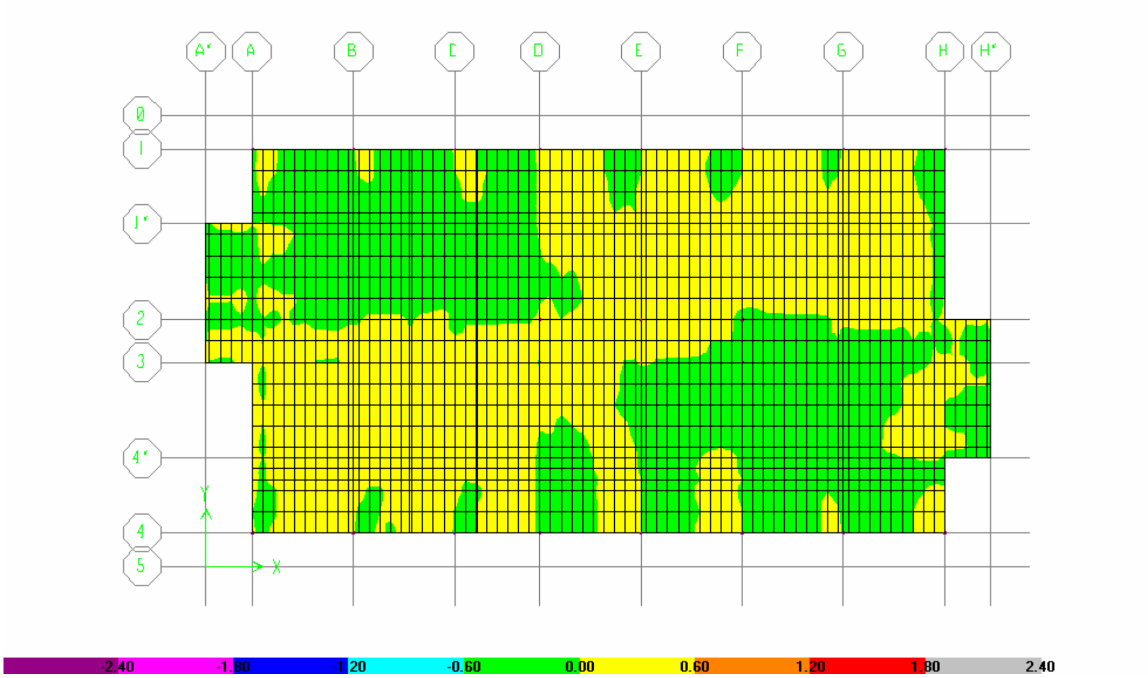

Figure 2.56 In-plane shear force contour, roof, Newhall, 3-story building.

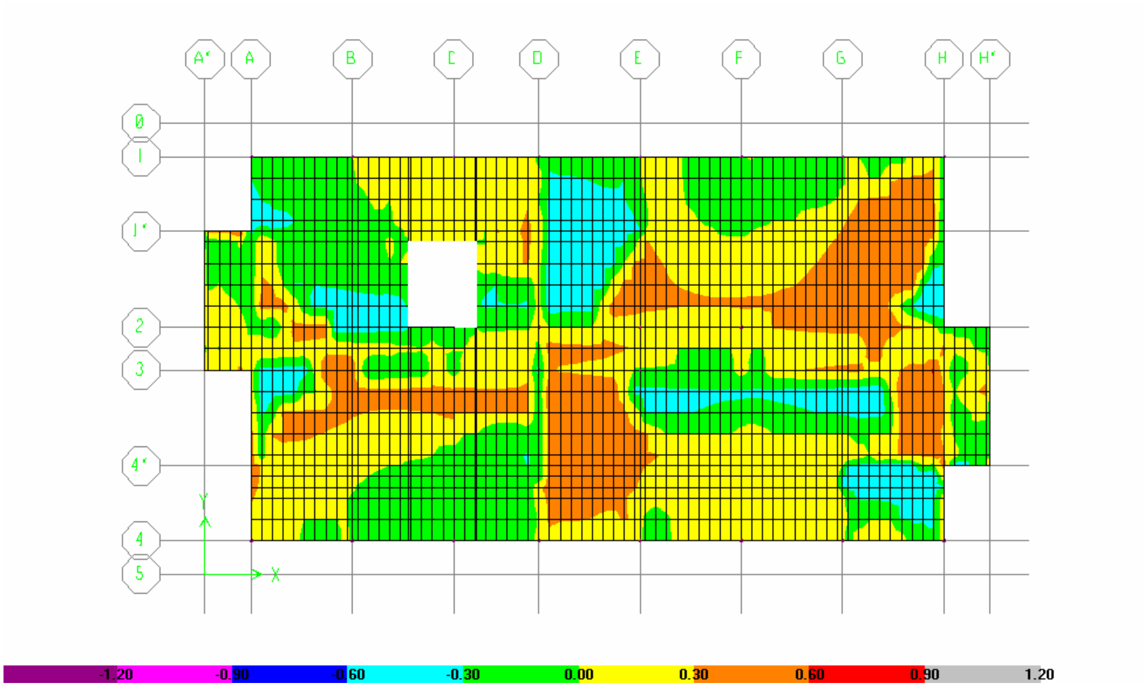

Figure 2.57 In-plane shear force contour, 3rd floor, Newhall, 3-story building.

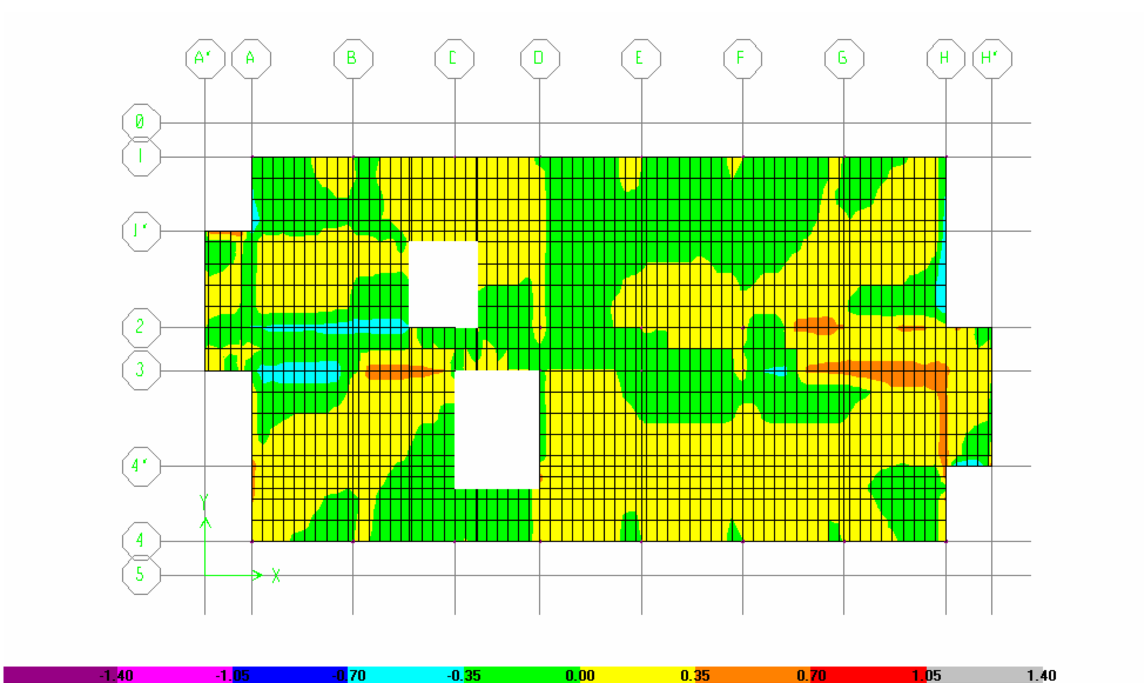

Figure 2.58 In-plane shear force contour, 3rd floor, Newhall, 3-story building.

2.10 MODIFICATION OF ELASTIC RESPONSE: THREE-STORY BUILDING

From Table 2.6 it can seen that the maximum base shear demands from the four ground motions recorded at the site are all less than the 1973 UBC allowable design requirement. However, the maximum base shear demand in the N-S direction due to the Newhall ground motion has a value of 3,396 kips. This is 675% greater than the 1973 UBC code strength design level of 438 kips that is obtained by multiplying the allowable design level of 313 kips by 1.4 to scale it to the strength design level. In a similar manner, the maximum value of base shear in the E-W direction for this record was calculated to be 3,092 kips. This value is 671% greater than the 1973 UBC code allowable design base shear scaled to a strength design level of 401 kips. Therefore, it appears likely that the three-story building would have suffered a significant amount of damage if it had experienced base motion of this magnitude and if the actual yield strengths of the masonry walls were similar to the base shear requirements of the codes. However, it has been shown that the walls of this building, with minimum reinforcing, have substantial overstrength with respect to the code design base shear. This will be discussed in the following paragraphs.

It has been suggested (Bertero 1986) that formulation for the response modification factor, R, can be divided into factors related to reserve strength (overstrength), ductility and redundancy. This is the approach taken in more recent studies (ATC 1995) that resulted in Equation (2.26) for the response modification factor.

$$R = R_s R_\mu R_R \tag{2.26}$$

In Equation (2.26) R_s is a strength factor, R_μ is a ductility factor and R_R is a redundancy factor. It is further suggested in this publication that buildings with as many as four lines of seismic framing be assigned a redundancy factor of unity. Since the building under consideration has six walls in the E-W direction and four walls in the N-S direction, it is concluded that for the purposes of this study the redundancy factor can be considered as 1.0. The value of R given in the code for a bearing wall system having masonry shear walls is 4.5 and the corresponding strength factor is given as 2.8. This implies a ductility factor of $R_\mu = 4.5/2.8 = 1.6$. Considering the response to the Newhall ground motions discussed previously, the reduction factors for strength and ductility are calculated as shown in Table 2.7.

Table 2.7 Base shear response modification factors, 3-story building.

Newhall Fire Station (Northridge, 1994) Ground Motion		
Building Direction	**Transverse (E-W)**	**Longitudinal (N-S)**
Design Strength (V_d) UBC '97, $R = 4.5$	637 Kips	637 Kips
Maximum Strength ($R_s V_d$) (In-plane shear strength, Sec. 2.7)	1756 Kips	2900 Kips
R_s	2.8	4.6
Required Elastic Strength (Table 6)	3092 Kips	3396 Kips
R_μ	1.76	1.17
Design Strength (V_d) UBC '73 x 1.4	401 Kips	438 Kips
Maximum Strength ($R_s V_d$)	1756 Kips	2900 Kips
R_s	4.38	6.62
Required Elastic Strength (Table 6)	3092 Kips	3396 Kips
R_μ	1.76	1.17

These components are computed using the 1997 UBC code with R = 4.5 and the 1973 UBC code that was assumed to have been used to design the three-story building. Although the 1973 design base shear scaled to strength level is between 63% and 69% of the 1997 strength design base shear, the minimum reinforcing requirements for the structural walls cause the amount of reinforcing steel in the walls to be the same for both codes. Therefore, the lateral resistance is the same and the ductility factor remains the same for both codes. The main difference is the overstrength factors that are 2.8 and 4.6 for the ′97 UBC compared to 4.38 and 6.62 for the ′73 UBC in the E-W and N-S directions respectively. Using the minimum steel percentage also means that the lateral resistance depends primarily on the length and width of the walls and can lead to substantial overstrengths in some cases depending on the structural configuration. This can result in a substantial variation in the strength factor. In some cases, it may have prevented serious damage to buildings of this type during strong earthquakes; however, in other cases, it may have induced forces in the connections or diaphragms that were well above their strength capacity. Similarly, increased loads transmitted from the walls into the timber diaphragm may have exceeded the diaphragm capacity and have led to premature failure. It can be seen that as the overstrength factor is reduced, the ductility factor will have to be increased and vice versa. The ductility factors calculated in Table 2.7 have values of 1.76 and 1.17 that are close to the value of 1.6 used for this type of building in the 1997 UBC. It should be emphasized that this example is based on the in-plane shear strength of the structural walls. The performance of the building may be controlled by some other failure mechanism such as diaphragm shear, out-of-plane wall flexure, or diaphragm connection to the walls. The strength of the overall structural system can be evaluated by using a nonlinear pushover analysis that considers the interaction of the strengths of the various components.

2.11 DIAPHRAGM FLEXIBILITY

It is of interest to investigate the UBC 1997 requirements for diaphragm flexibility as applied to the three-story building. The UBC 1997 code requirement will be computed for the three-story building using both static and dynamic loading cases, and the suitability of these requirements will be discussed.

2.11.1 1997 UBC Flexible Diaphragm Requirement

Section 1630.6 of the 1997 Uniform Building Code states that "*Diaphragms shall be considered flexible for the purposes of distribution of story shear and torsional moment when the maximum lateral deformation of the diaphragm is more than two times the average story drift of the associated story*." Thus, the code condition may be expressed using Equation (2.27).

$$1997\,\mathrm{UBC}: \quad \frac{\text{maximum lateral deformation of diaphragm.}}{\text{average associated story drift}} > 2 \tag{2.27}$$

This ratio can be determined as the lateral in-plane displacement of the diaphragm itself under lateral load relative to the story drift of adjoining vertical-resisting elements (walls) under equivalent tributary lateral load. It should also be noted that "story drift" is the lateral displacement of one level relative to the level above or below.

2.11.2 1997 UBC Flexible Diaphragm Verification

Verification of diaphragm flexibility was conducted by comparison of the midspan relative deflection and corresponding support displacement of the roof and third-floor diaphragms of the three-story building in the N-S and E-W building directions. Displacement time history results for the desired locations along the diaphragm were obtained using the ETABS linear elastic mathematical model subjected to the recorded base motions during the Landers earthquake. As previously mentioned, the maximum base acceleration recorded during the three earthquakes for which there are recorded data was 0.07g (Landers); thus it was deemed appropriate to limit this part of the study to characterize the flexibility of the roof and third-floor diaphragms based on the displacement response of the building during the Landers earthquake.

Separate flexibility analyses were conducted using both static equivalent lateral loads as per 1997 UBC, and using dynamic time history analysis results. It should be noted that the 1997 UBC requirement for considering a diaphragm as flexible is for analysis and design using the static procedure and loading the structure independently in each of the two principal directions.

The steps taken to compute the ratio for this study will be discussed in this section. The calculations performed for the 1997 UBC displacement ratio for flexible diaphragm verification are illustrated in Figure 2.59. Note that this figure is not meant to represent the actual configuration of any of the buildings considered in this study. Also, for the sake of simplicity, the drawings shown represent the case where no torsion is present. The gray lines in the diagram represent the undeformed configuration, and the black lines represent the assumed deformed configuration resulting from seismic loading. The steps required to compute the numerator of the 1997 UBC ratio (level i) for this example building are illustrated in Figure 2.59 (a). The maximum diaphragm deformation is the displacement at midspan (relative to the base) for the level of the building under consideration (i.e., level i) minus the average displacements (relative to the base) at the vertical supports. Computation of the denominator for the 1997 UBC displacement ratio is illustrated in Figure 2.59 (b). The denominator requires computation of the interstory drift, which considers the displacement of the story below the level of interest (i.e., $j = i - 1$). The interstory drift for story j is computed for each vertical support and these two values of interstory drift are averaged to obtain the resulting denominator for the 1997 UBC displacement ratio for story j. Hence the displacement ratio becomes $\Delta_{i,d} / \delta_i$.

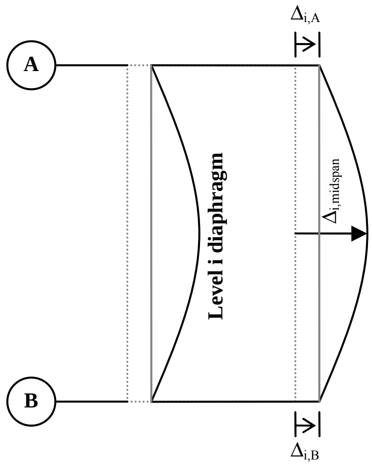

$$
\begin{aligned}
\Delta_{max} &= \text{1997 UBC (numerator), level } i \\
&= \text{maximum diaphragm deformation} \\
&= \Delta_{\text{i,midspan}} - \Delta_{\text{avg, frames}} \\
&= \Delta_{\text{i,midspan}} - \left(\frac{\Delta_{\text{i,A}} + \Delta_{\text{i,B}}}{2} \right)
\end{aligned}
$$

(a) Numerator

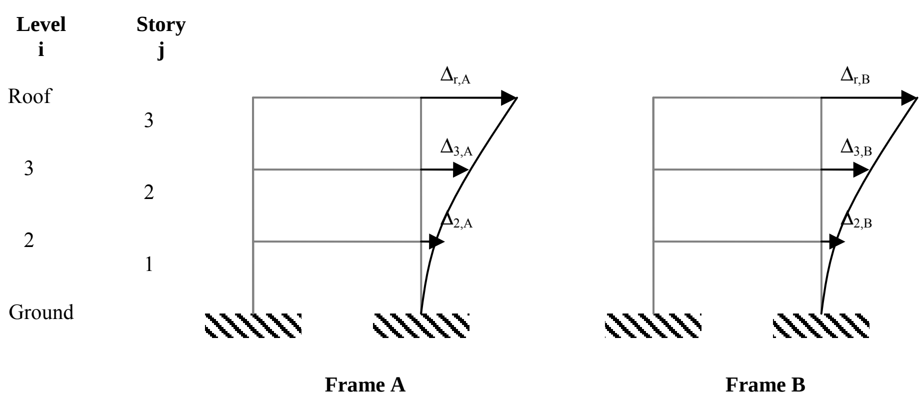

Define for story j, interstory drift δ_j,

$$
\begin{aligned}
\delta_{j,\text{A}} &= \Delta_{j+1,\text{A}} - \Delta_{j,\text{A}} \\
\delta_{j,\text{B}} &= \Delta_{j+1,\text{B}} - \Delta_{j,\text{B}}
\end{aligned}
$$

Δ_0 = 1997 UBC (denominator), story j

corresponding average associated story drift

$$= \frac{\delta_{j,\text{A}} + \delta_{j,\text{B}}}{2}$$

(b) Numerator

Figure 2.59 Example calculation of numerator and denominator, 1997 UBC ratio.

2.11.2.1 Static Loading

Diaphragm flexibility under static loading was studied by considering the behavior of the three-story building under the 1997 UBC inverted triangular static equivalent lateral load pattern in the N-S and E-W building direction separately. The load patterns used were generated with the ETABS 1997 UBC automatic lateral-load-generating option, and were applied to the building through its center of mass parallel to the N-S and E-W building directions. The deflected shape of the third-floor diaphragm of the three-story building subjected to inverted triangular lateral loading in the N-S and E-W directions is displayed in Figures 2.60 and 2.61, respectively. Similarly, Figures 2.62 and 2.63 depict the deflected shape of the roof diaphragm when loaded with the inverted triangular lateral load distribution. Comparing Figure 2.60 with Figure 2.62, it can be seen that in the N-S direction, the diaphragm deforms as a cantilever off the two interior walls with the larger relative deformation occurring at the edge of the diaphragm at the roof level. Comparing Figures 2.61 and 2.63 indicates that the larger relative deformation in the E-W direction is also at the roof level and occurs near the center of each of the two subdiaphragms.

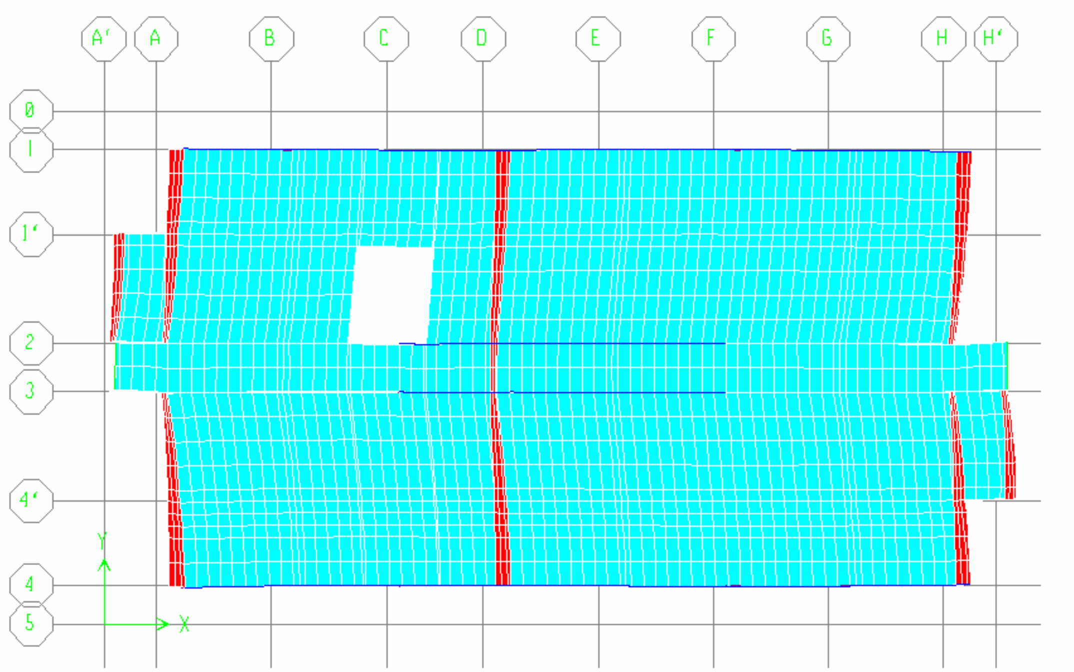

Figure 2.60 N-S deformed shape, '97 UBC static loads, 3rd floor, 3-story building.

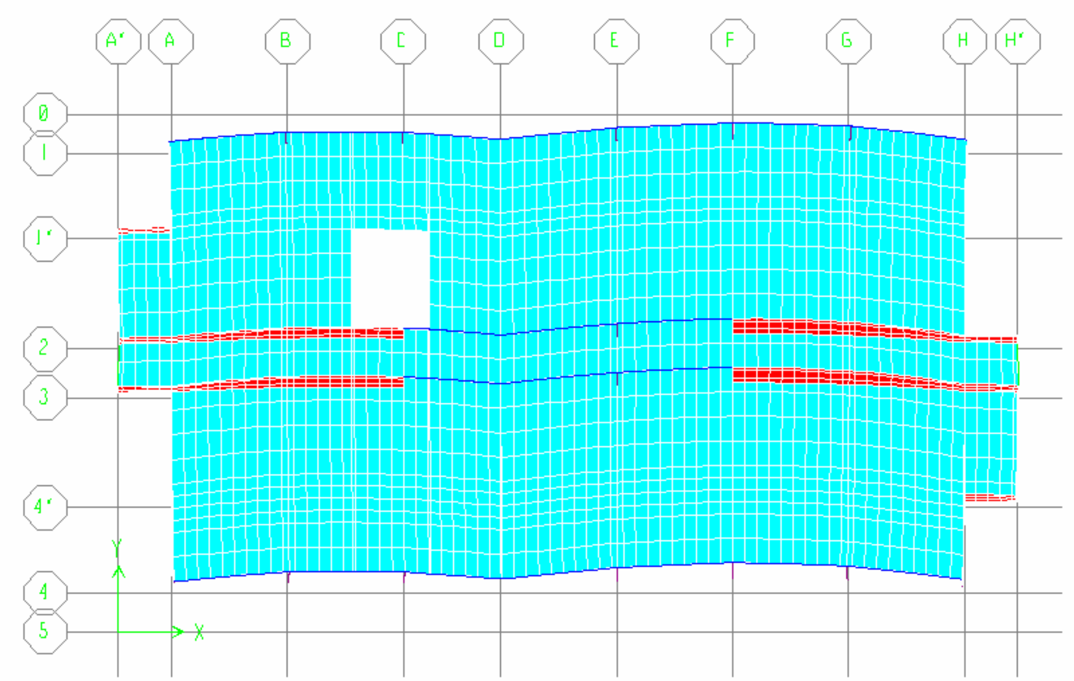

Figure 2.61 E-W deformed shape, ’97 UBC static loads, 3rd floor, 3-story building.

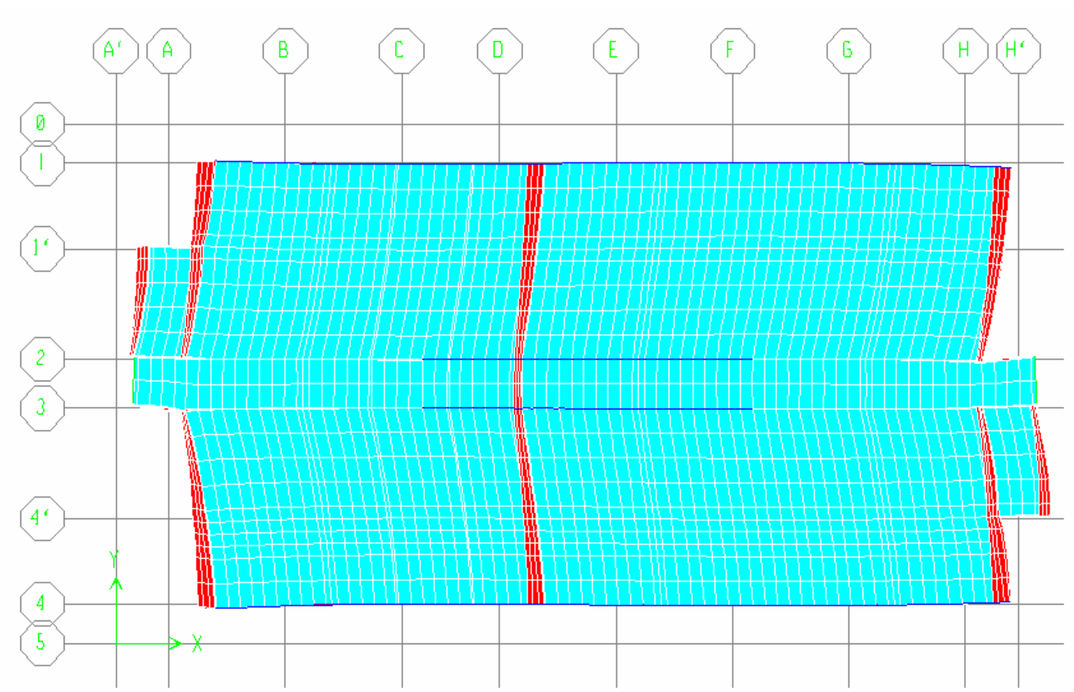

Figure 2.62 N-S deformed shape, ’97 UBC static loads, roof, 3-story building.

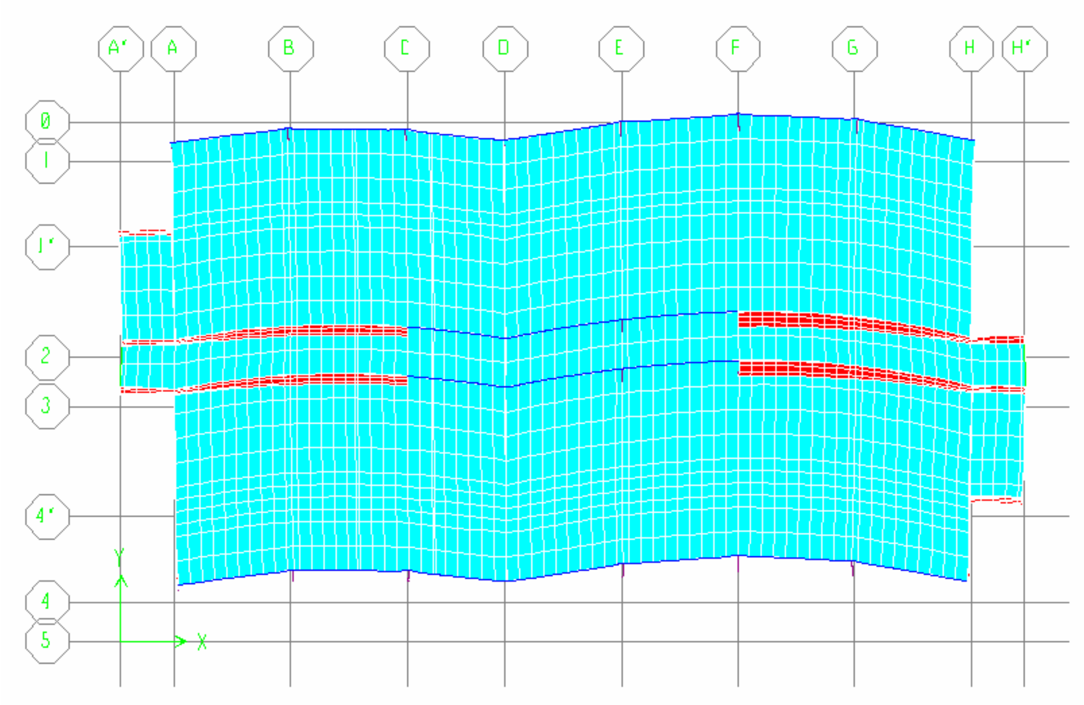

Figure 2.63 E-W deformed shape, ’97 UBC static loads, roof, 3-story building.

Diaphragm flexibility was considered for both directions. To compute the displacement ratio to be compared to the 1997 UBC code criteria for the E-W direction, the maximum lateral deformation of the subdiaphragm was taken to be the difference between the maximum displacement along the subdiaphragm between the adjacent supports and the average displacement of the two adjacent supports. For the N-S direction, maximum lateral deformation in the diaphragm was the difference between the deformation at the “unsupported” edge of the subdiaphragm and the deformation of the supporting walls. Additionally, for either direction, the “average associated story drift” was taken as the average interstory drift of the vertical resisting elements (walls) associated with the subdiaphragm.

To calculate numeric ratios for comparison using the ETABS analytical results, it was necessary to compute the ratios using defined points along the wall and diaphragm near the instrument locations. The points for ratio calculation are shown as a schematic diagram of the plan views of the roof and third floors of the building in Figure 2.64. For convenience, the walls of the building oriented in the E-W direction are labeled from left to right as W1, W2, and W3, respectively.

To compute the diaphragm flexibility ratio for the E-W direction, the maximum lateral deformation was assumed to occur near midspan (sensor 3) between the supported ends of the subdiaphragm at the north end (Figures 2.61 and 2.63). Therefore, taking the difference in displacement between sensor 3 and the average displacement at sensors 2 and 4 produced the maximum absolute displacement of the subdiaphragm at the roof level. The drift of the vertical supporting elements was obtained by taking the difference between the drifts at the roof (sensor 2) minus the drift at the third floor (sensor 5). A similar procedure was used for the third floor taking the difference in displacement between sensor 6 and the average displacement at sensors 5 and 7 to obtain the maximum absolute displacement of the subdiaphragm at the third level. The drift of the vertical supporting elements was obtained by taking the difference between the drifts at the third level (sensor 5) minus the drift at the second level sensor 8. It will be shown that the displacement response at sensor 4 is similar to sensor 2 and that sensor 7 is similar to sensor 5.

In the N-S direction, the sensors were located at the interior walls at the roof (10), third floor (11) and second floor (12) levels; corresponding instrumentation on the diaphragms was not available. Therefore locations directly opposite of locations 10 (Point A) at roof level and 11 (Point B) at the third floor were used to calculate the relative displacement at the edge of the diaphragm. A procedure similar to that just discussed for the E-W direction was used to calculate the code displacement ratio.

Table 2.8 E-W and N-S diaphragm flexibility verification, '97 UBC static loading, roof and 3rd floor diaphragms, 3-story building.

Static Loading				
Floor	**Diaphragm orientation**	**Maximum diaphragm deformation** Δ_{max} (inches)	**Corresponding average associated story drift** Δ_0 (inches)	**1997 UBC Code Ratio** Δ_{max}/Δ_0 (inch/inch)
Roof	E-W	0.1283	0.0255	**5.03**
	N-S	0.1384	0.0288	**4.81**
3rd	E-W	0.0788	0.0684	**1.15**
	N-S	0.0774	0.0576	**1.34**

**Note: Static loading in N-S and E-W directions applied separately

The calculated code displacement ratios for diaphragm flexibility in the N-S and E-W directions under static loading in the N-S and E-W directions are shown in Table 2.8, where values above 2.0 are representative of a flexible diaphragm. The results of these comparisons indicate that according to the aforementioned criteria, the roof diaphragm in both directions may be considered a flexible diaphragm. However, the third floor ratios are below 2.0 for both directions and may be considered as a rigid diaphragm.

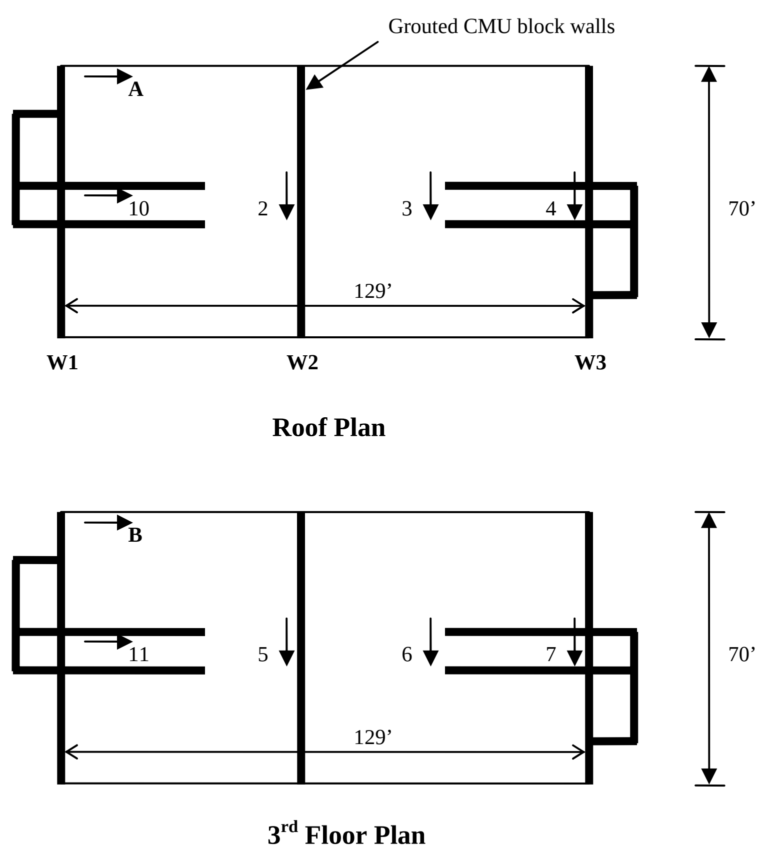

Figure 2.64 Locations for diaphragm flexibility verification, 3rd floor and roof diaphragms, 3-story building.

2.11.2.2 Dynamic Loading

The predicted displacement response of the three-story building during the Landers earthquake was used to compute the flexible diaphragm code criteria again at the roof and third floor levels and in the N-S and E-W directions. In contrast to the static loading case, the dynamic loads were applied simultaneously to the structure as two acceleration time histories at the base in the N-S and E-W directions. Since the displacements varied with time, the displacement ratio was computed at the instant of maximum midspan displacement in the diaphragm. After this initial calculation, the computations were identical to those performed for the static loading case.

Time history plots of the displacements relative to the base of the structure at the midspan and support locations for the roof and third-floor diaphragms in the E-W direction as obtained using the ETABS mathematical model, are shown in Figures 2.65 and 2.66, and corresponding magnified views of the comparison for both diaphragms are shown in Figures 2.67 and 2.68. The magnified view showcasing the comparison of the midspan diaphragm displacement to the corresponding support relative displacements in the E-W direction show that the period of the oscillation of the displacement response is approximately 0.2 sec, and is therefore in agreement with the fundamental period in the E-W direction obtained from the dynamic modal analyses. From Figures 2.65 and 2.66, it is evident that the roof and third-floor diaphragms in the E-W direction do not behave in a rigid manner, as the center of the diaphragm displaces substantially more than the supporting wall. Additionally, Figures 2.69 and 2.70 show the variation of support displacement at walls W2 and W3, the supporting walls of the E-W diaphragm under consideration for the roof and third-floor diaphragms. From this figure it is clear that the two supporting walls undergo very similar displacements (which cause the graph to appear as if there is only one time history) for both the roof and third floors.

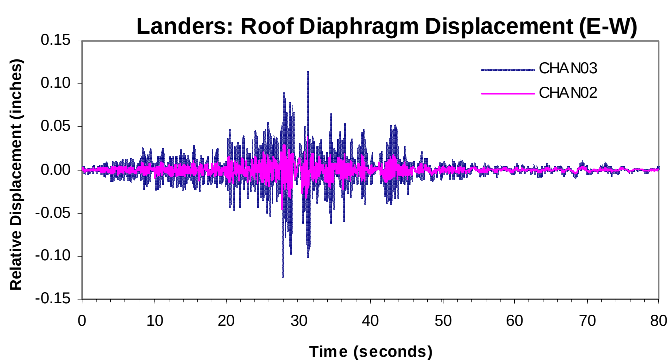

Figure 2.65 E-W midspan vs. support relative displacements, roof, 3-story building.

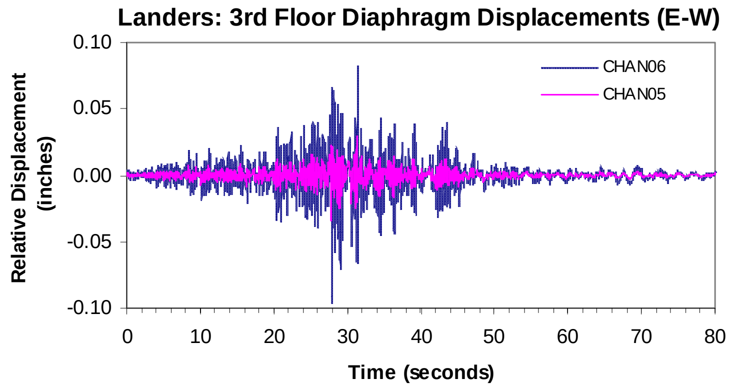

Figure 2.66 E-W midspan vs. support relative displacements, 3rd floor, 3-story building.

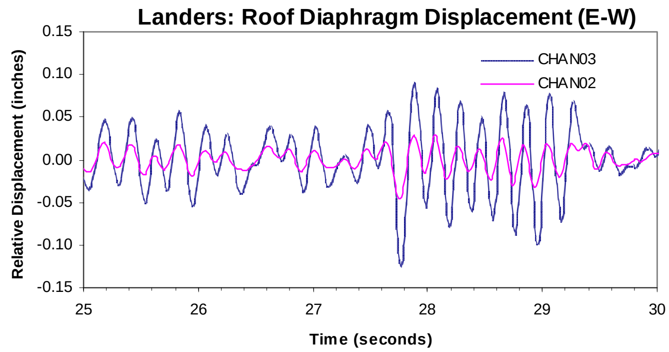

Figure 2.67 E-W midspan vs. support relative displacements (magnified), roof, 3-story building.

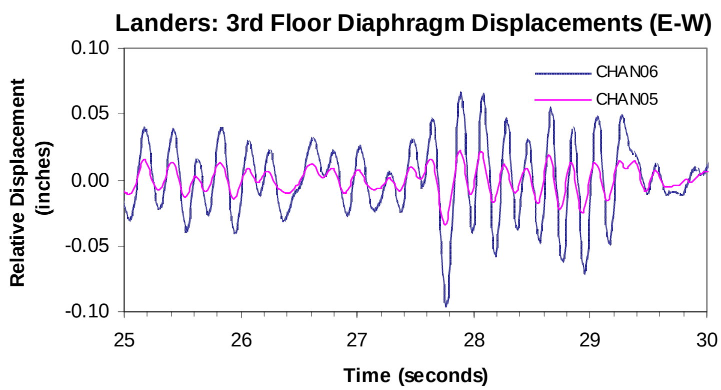

Figure 2.68 E-W midspan vs. support relative displacements (magnified), 3rd floor, 3-story building.

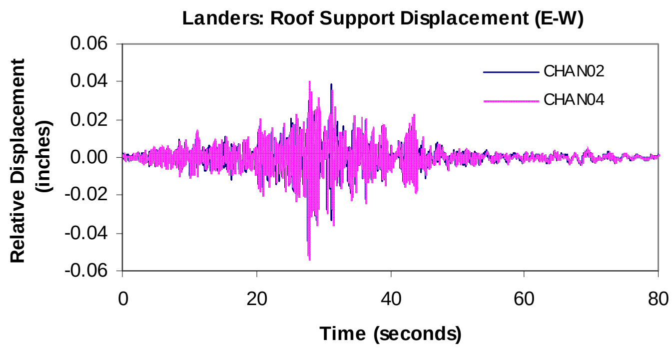

Figure 2.69 E-W supporting walls relative displacements, roof, 3-story building.

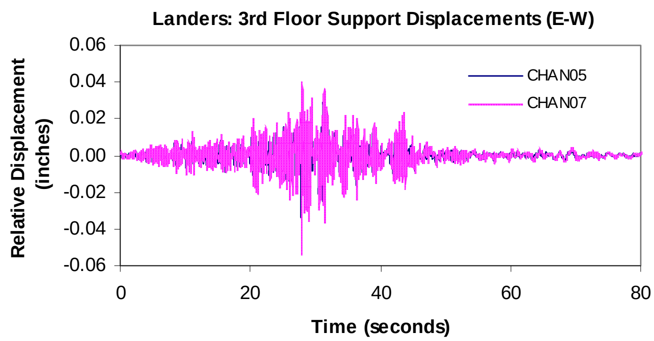

Figure 2.70 E-W supporting walls relative displacements, 3rd floor level, 3-story building.

The time history comparison of the relative displacement at sensor location 10 and point A on the roof diaphragm in the N-S direction are shown in Figure 2.71. A similar comparison for location 11 and point B for the third-floor diaphragm is displayed in Figure 2.72, and the corresponding magnified views for the roof and third-floor diaphragms are shown in Figures 2.73 and 2.74, respectively. As for the E-W direction, the magnified view of the diaphragm displacement time history comparison verify that the period of the building in the N-S direction is approximately 0.2 sec, as computed using modal analyses. Again, we see that even in the N-S direction, both the roof and third-floor diaphragms do not behave rigidly, as the “free” end displaces more than the supported end.

The results of the calculated flexibility ratios for the dynamic loading case are summarized in Table 2.9 and indicate that the relative displacement ratios for both the roof and third-floor diaphragms all exceed 2, thus implying that all the diaphragms in this building meet the 1997 UBC criteria for consideration as flexible diaphragms in both principal building directions. For the roof diaphragm, the results of the static and dynamic loading cases are similar, though the calculated ratios using dynamic loading were higher. However, the results for the third-floor diaphragm under dynamic loading are contradictory to those computed using static loads. The ratios for the third-floor diaphragm in both the N-S and E-W directions for the dynamic load case exceeded 2, indicating that this diaphragm also behaves in a flexible manner, in contrast to the result obtained under static load. More complete instrumentation is needed to evaluate the behavior of the diaphragm.

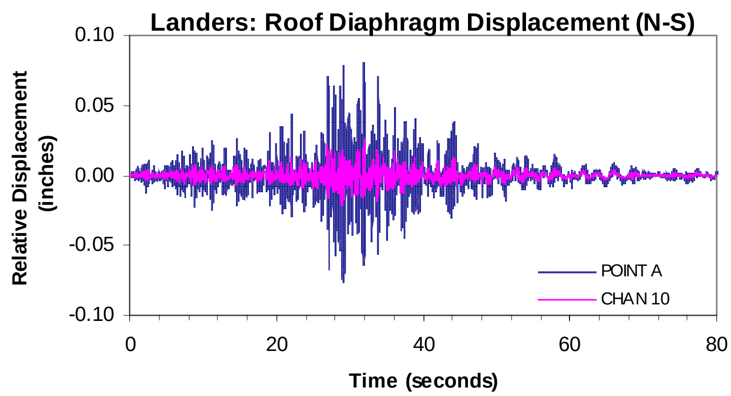

Figure 2.71 N-S midspan vs. support relative displacements, roof, 3-story building.

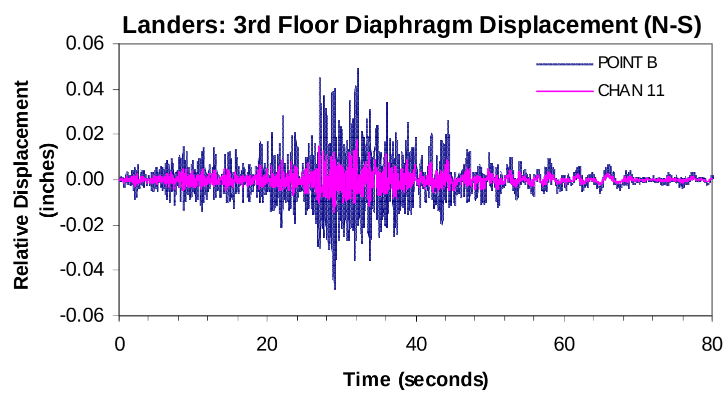

Figure 2.72 N-S midspan vs. support relative displacements, 3rd floor, 3-story building.

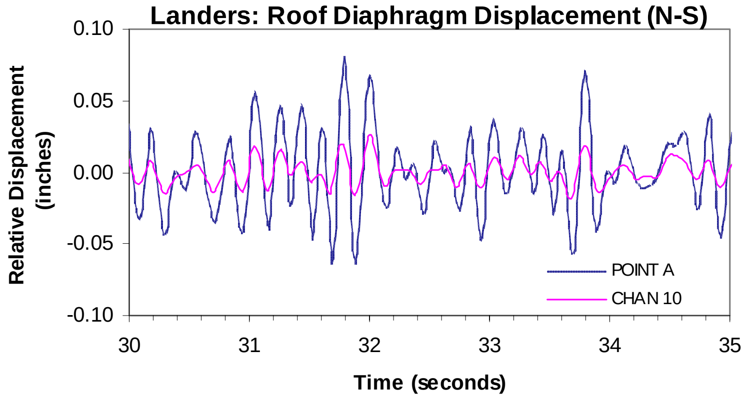

Figure 2.73 N-S midspan vs. support relative displacements (magnified), roof, 3-story building.

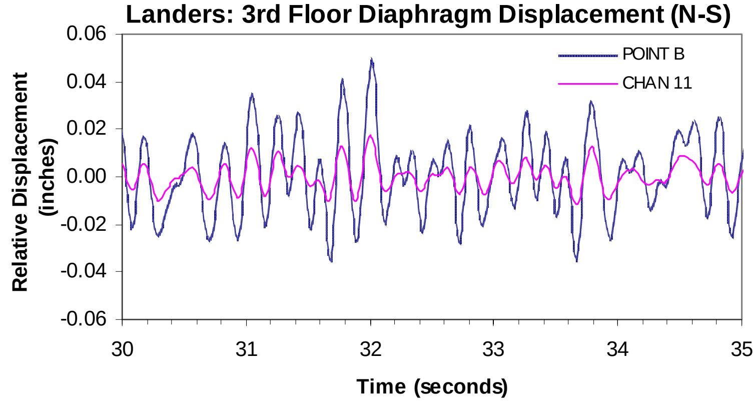

Figure 2.74 N-S midspan vs. support relative displacements (magnified), 3rd floor, 3-story building.

Table 2.9 E-W and N-S diaphragm flexibility verification, dynamic loading, roof and 3rd floor diaphragms, 3-story building.

Dynamic Loading					
Floor	**Diaphragm orientation**	**Maximum diaphragm deformation** Δ_{max} (inches)	**Time of maximum deformation** t_{max} (seconds)	**Corresponding average associated story drift** Δ_0 (inches)	**1997 UBC Code Ratio** Δ_{max}/Δ_0 (inch/inch)
Roof	E-W	0.0807	31.28	0.0093	**8.65**
	N-S	0.0613	31.78	0.0071	**8.66**
3rd	E-W	-0.0619	27.76	-0.0159	**3.90**
	N-S	-0.0361	28.90	-0.0069	**5.24**

**Note: Dynamic loading in N-S and E-W directions applied simultaneously

2.11.3 Base Shear Distribution for E-W Shear Walls (Landers Earthquake)

To add further insight into the behavior of the diaphragms of the three-story building, dynamic time history results for the base shear were studied. It is well known that lateral load is distributed to vertical resisting elements in different ways, depending on the behavior of the diaphragm. If a diaphragm is perfectly rigid, the lateral resisting units (e.g., walls) will resist the lateral load in proportion to relative rigidities of the walls. In contrast, if the diaphragm is flexible, the lateral load is distributed in proportion to tributary area adjacent to the wall.

A plot of the base shear in the supporting walls, W2 and W3, of the E-W diaphragm is shown in Figure 2.75. This figure indicates that for generally all of the earthquake motion, the shear at the base of wall W2 is larger than for wall W3. At the time of maximum shear at the base of the middle wall, (27.76 sec), the shear in wall W2 is 144 kips and the shear in end wall W3 at that time is 114 kips. Therefore, at this instant, the ratio of the shear in W2 to that in W3 is 1.27. Such a result suggests that the diaphragm in the E-W direction is behaving in a flexible manner. Likewise a comparison of the shear in walls W2 and W1 of the E-W diaphragm, Figure 2.76, clearly indicates that wall W2 resists more shear than wall W1. At the point of maximum shear in wall W2 (144 kips), the corresponding shear in wall W1 is 71 kips, and thus the ratio of shear in wall W2 to wall W1 at this point is 2.0. Since the shear resisted by wall W2 is twice as much as the shear resisted in walls W1, it is likely that the E-W diaphragm behaves in a flexible manner. It is also interesting to note that the ratio of tributary areas W2/W1 is 2.33 and W2/W3 is 1.75. It should also be noted that part of this unbalance is due to the built-in eccentricity in the E-W direction. The effect of this eccentricity can also be seen in Figure 2.77, which shows a comparison of the shear in walls W1 and W3.

The results determined from the study of base shear distribution are in general agreement with the results obtained using the code verification ratio for the dynamic loading case, where the behavior of both the roof and third-floor diaphragms in the E-W direction were found to be flexible. This result is also in agreement with the finding that under static loading in the E-W direction, the roof diaphragm behaves in a flexible manner, but this is not true for the third-floor diaphragm under similar loading.

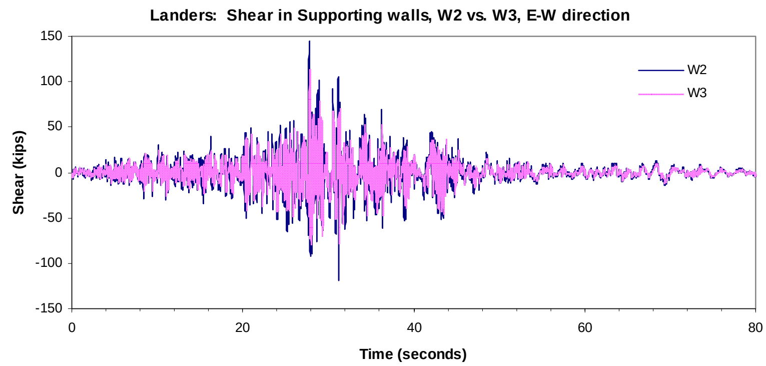

Figure 2.75 Base shear in E-W supporting walls, W2 and W3, Landers.

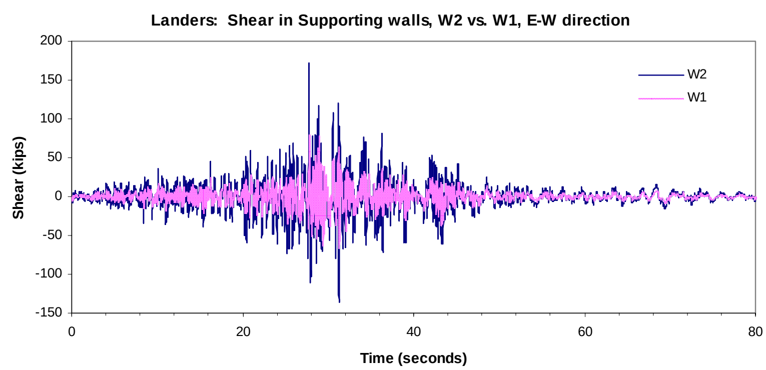

Figure 2.76 Base shear in E-W supporting walls, W2 and W1, Landers.

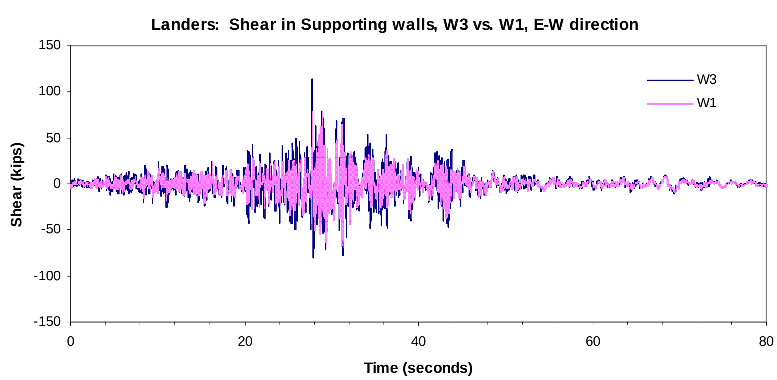

Figure 2.77 Base shear in E-W supporting walls W1 and W3, Landers.

The base shears in the three main walls in the E-W direction under the Landers earthquake base motion are compared in Figures 2.78–2.80 considering the actual flexibility of the diaphragms versus the use of a rigid diaphragm. The base shears in the wall (W1) at the south end of the building are shown in Figure 2.78. These results indicate that the maximum shears are about the same, having values of 85 kips rigid vs. 80 kips flexible. At the middle wall (W2) the shear due to the actual diaphragm is 33% larger than that of the rigid diaphragm (143 kips vs. 107 kips) as shown in Figure 2.79. For wall W3 at the north end of the building, the base shears are almost the same, reaching 114 kips for the actual diaphragm compared to 108 kips for the rigid diaphragm as shown in Figure 2.80.

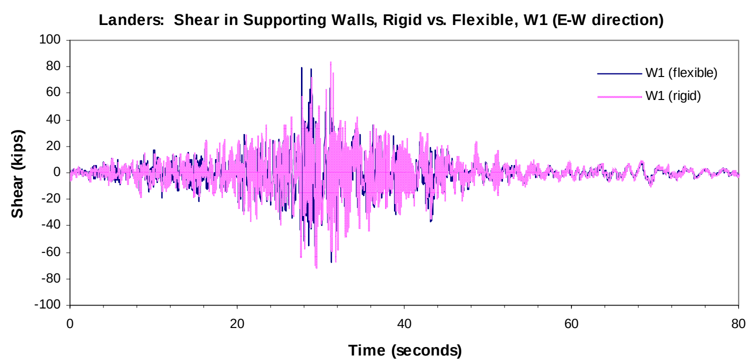

Figure 2.78 Base shear in supporting wall W1 (E-W), rigid vs. flexible, Landers.

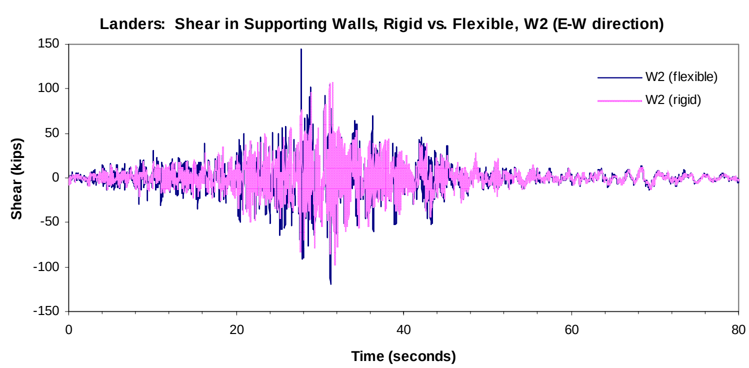

Figure 2.79 Base shear in supporting wall W2 (E-W), rigid vs. flexible, Landers.

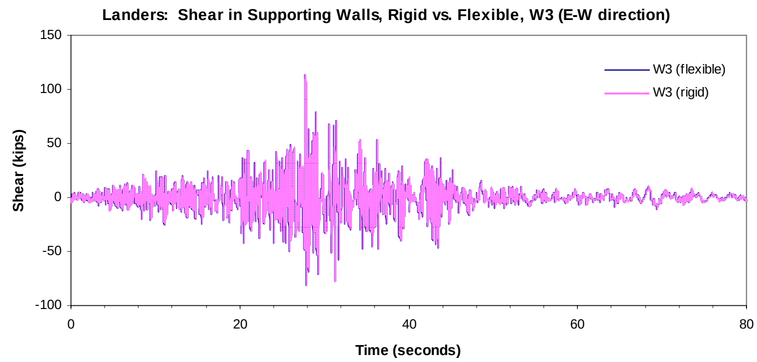

Figure 2.80 Base shear in supporting wall W3 (E-W), rigid vs. flexible, Landers.

2.12 SUMMARY AND CONCLUSIONS FOR THE THREE-STORY BUILDING

2.12.1 Summary

The three-story masonry building has recorded the response from three major earthquakes. However, due to the distance from the building to the epicenter of the earthquake, the base accelerations recorded at the building are relatively low with peak ground accelerations of between 4% and 7% of gravity. Spectral analyses of the recorded data indicate that the period of the fundamental translation modes in each direction are approximately 0.2 sec. A similar result was obtained from the three-dimensional ETABS model of the building. Moving window analyses of the recorded data indicate changes in period due to cracking but no permanent deformation.

Comparison of the recorded response at all instrument locations shows a good correlation with the time history response calculated using the computer model and the idealizations discussed previously. Comparison of the time history of the calculated base shear with the building code design base shear indicates that the response was less than the minimum code design requirements for the three recorded earthquakes. However, using acceleration records obtained at stations closer to the epicenter of two recently recorded earthquakes, the results of the analyses indicate base shear values that far exceed the code minimums. Fortunately, the in-plane shear capacities of the designed walls in each principal direction have considerably higher strength than the code minimum requirements. These capacities are exceeded by the inertial forces developed in the walls under these stronger ground motions for only a limited number of cycles. This significantly higher capacity is due to the minimum steel requirements for structural walls and what appears to be architectural considerations.

2.12.2 Conclusions

The main conclusions that can be reached from the results obtained from study of the three-story building are the following:

1. Careful modeling of geometry, element properties, and material properties along with the use of a three-dimensional model that includes the diaphragm stiffness, can accurately simulate the elastic seismic response of masonry buildings. This was verified by critical comparison with the response measured in an instrumented building.
2. For purposes of comparison, the demanded base shear has been compared with the in-plane shear capacity of the structural walls, which has been estimated according to code. However, it has to be noted that the actual capacity of the building may be controlled by other system components such as the in-plane shear capacity of the diaphragm, the strength of the connections between the diaphragm and the walls, or the out-of–plane moment capacity of the walls that do not have as much overstrength.
3. The in-plane shear capacity of the walls in each principal direction has considerably higher strength than the code minimum requirements and these capacities are exceeded for only a limited number of cycles when the building is subjected to earthquake ground motions recorded at a free-field site nearer the epicenter. This higher strength appears to be due to the length of the walls used in the framing system and the minimum steel requirements for structural walls.
4. The criteria used in the building code for classifying a diaphragm as rigid or flexible contains considerable uncertainty. The value of the code displacement ratio depends upon the method used for the calculation (i.e., static vs. dynamic loading). Significant differences were observed between the measured response obtained using static vs. dynamic loading. Calculated code displacement ratios ranged between 0.73 and 2.55 for static loading, and between 2.1 and 3.8 for dynamic loading. Thus, when using dynamic loading, the code criteria classifies the roof and third-floor diaphragms in the N-S and E-W directions as flexible. However, using static loading, the resulting displacement ratios suggest that not all of the diaphragms may be classified as flexible.

3 Two-Story Office Building: Palo Alto

3.1 BUILDING DESCRIPTION

3.1.1 General

A two-story office building in Palo Alto, California, is the second subject building considered in this study. The structure was constructed in 1974. Plan views of the structural framing elements are presented in Figure 3.1. The building is rectangular in shape, with a lateral-force-resisting system composed of two-way grouted reinforced masonry brick walls at the north and south ends, and a plywood floor system supported by Trus Joists. Vertical loads are carried by interior tubular steel columns and exterior glulam columns, which are twice as numerous at the first story of the building. The building foundation is continuous reinforced concrete footings connected by grade beams under the glulam columns on the exterior, the structural walls at the two ends and the two rows of tube columns down the center of the building length (N-S). Views of the N-S and E-W exterior elevations of the two-story building are shown in Figures 3.2 and 3.3.

3.1.2 Diaphragms

The second-floor diaphragm of the two-story office building consists of 1.5 in. thick lightweight concrete over ¾ in. thick plywood mounted on 36 in. deep open truss joists running in the E-W (transverse) direction every 2 ft. Two interior 5-1/8″ x 15″ glulam beams running in the N-S direction and four 5-1/8″ x 16-½″ glulam beams running around the perimeter complete the floor system. The specified compressive strength of the lightweight concrete, f'_c, is 2500 psi. Douglas fir (DF) plywood sheathing and glulam beams are used. The roof diaphragm consists of ½″ thick DF plywood together with deep interior and exterior glulam DF beams running in both directions. The roof diaphragm is considerably more flexible than the first-floor diaphragm. The aspect ratio of the diaphragm (length/width) is 1.87.

3.1.3 Grouted Walls

The lateral-force-resisting system is composed of four L-shaped two-way grouted brick walls. Two are located at each end of the building to form a channel shape. All grouted masonry shear walls are 12 in. thick. The joining grout is 7 in. thick. Bricks are grade MW (moderate weathering) conforming to ASTM C-62. The bricks were joined with a mortar mix corresponding to a type-S mortar according to ASTM C-270 specifications. Bricks were pre-wetted to have an initial rate of absorption not in excess of 0.25 oz/in.^{2}/min, according to ASTM C-67 provisions. The grout was mixed according to ASTM C-476-63 Table 3.1, course grout, with a specified compressive strength f'_c of 2000 psi and a slump of 10 in.

The grouted walls were reinforced with 1-#4 at 12″ in both horizontal and vertical directions. Additional #8 bars were provided in the vertical direction at the corners of the L-shaped walls. All reinforcing steel is grade 40 and is continuous with 50 diameter laps at splices in the grouted brick walls. Splices are staggered in adjacent bars and special inspection was used during the construction of the walls.

3.1.4 Connection between Diaphragms and Walls

Ledgers for the diaphragms are connected to the grouted walls by ¾ in. "J" bolts anchored to the horizontal steel in the grouted walls. These ledgers are nominally placed every 24″ in both directions and the plywood is connected to them by 10d nails at 3 in.

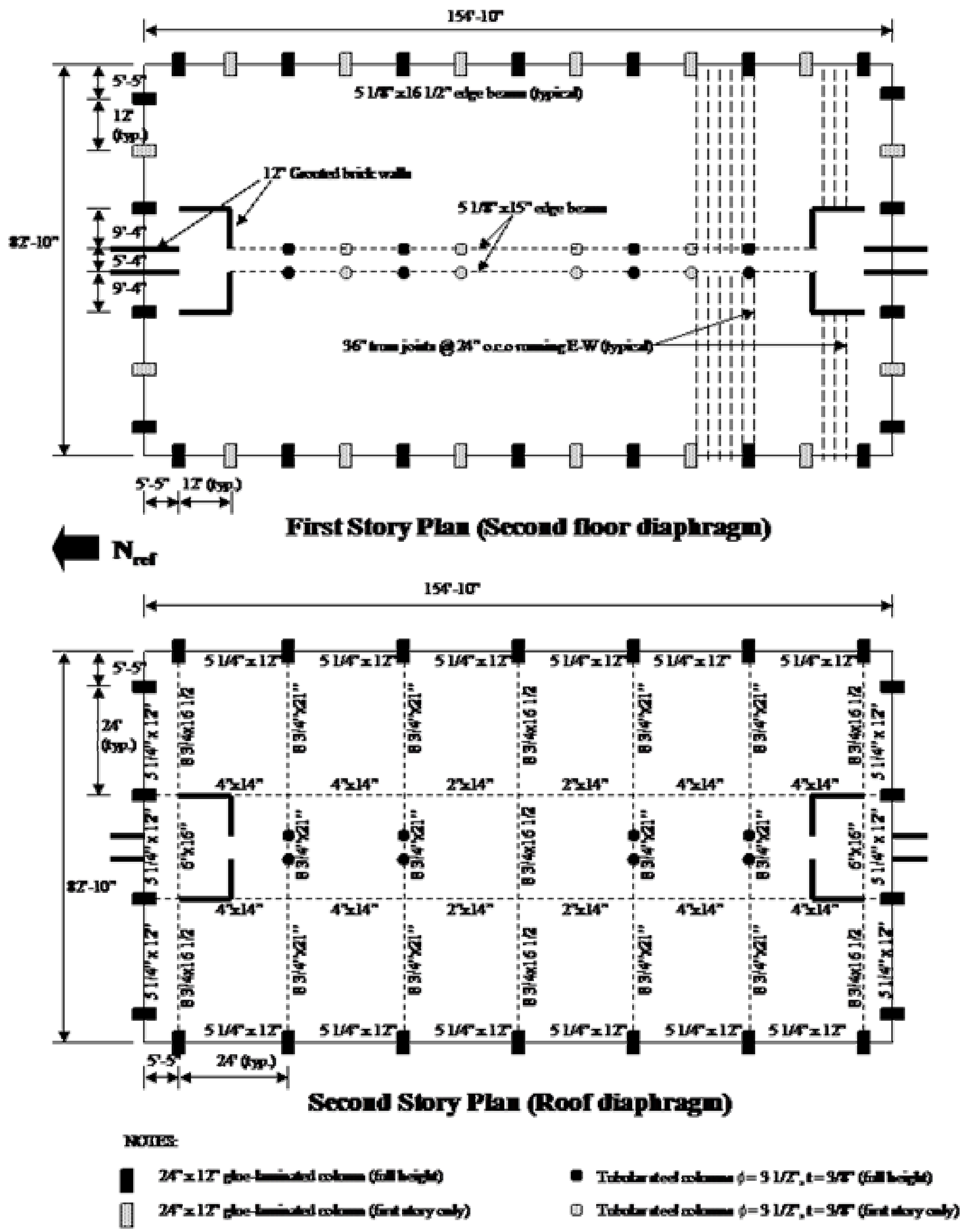

Figure 3.1 Building plan views, 2-story building.

Figure 3.2 N-S exterior view, 2-story building.

Figure 3.3 E-W exterior view, 2-story building.

3.1.5 Foundation System

The slab on grade is a 4″ thick reinforced concrete slab. The foundation consists of continuous, reinforced footings (grade beams) for the grouted brick walls, the exterior glulam columns, and the interior steel columns. Between the slab and foundations there is an engineered fill consisting of 1 in. thick sand, a 6 mm thick polyethylene film lapped every 6 in., and 4″ of pea gravel. The footings are built over sandy clay fill with a capacity of 2000 psf, according to a soil-mechanics study (Tena-Colunga and Abrams 1992). The walls are founded on footings that are 3 ft wide, and have a depth of the 1′6″ for the N-S walls, and 2′6″ for the E-W walls. The width of the footings for the exterior and interior columns is 8″ and their depth is 1′6″.

3.2 THE LOMA PRIETA EARTHQUAKE (1989)

The Loma Prieta earthquake occurred at 5:04 pm (PDT) October 17, 1989. The earthquake had a surface-wave magnitude of 7.1 and its epicenter was located about 10 miles northeast of Santa Cruz and 60 miles southeast of San Francisco. The hypocenter was about 11 miles beneath the earth's surface. The earthquake ruptured a 25-mile segment of the San Andreas fault and was felt from Los Angeles in the south, to the Oregon border to the north, and Nevada to the east. The strong shaking during the earthquake lasted less than 15 sec.

3.3 INSTRUMENTATION AND RECORDED RESPONSE

3.3.1 Observed Damage

Specific information regarding the level of damage that the building suffered after the Loma Prieta earthquake is not available.

3.3.2 Recorded Motions during the Loma Prieta Earthquake (1989)

The two-story office building was instrumented as part of the California Strong Motion Instrumentation Program (CSMIP) with seven sensors. Sensors 1 and 3 recorded horizontal base accelerations in the N-S and E-W directions, while sensor 2 recorded the vertical base acceleration. Sensors 4, 5, and 6 recorded roof accelerations in the E-W direction while sensor 7 recorded accelerations in the N-S direction. The location of each sensor is shown schematically in Figure 3.4. The time histories of the recorded accelerations and corresponding displacements at each of the 7 sensor locations are shown in Appendices B-1 and B-2. The sensors recorded a total of 60 sec of acceleration data; however, only 10 sec can be considered as significant base motion (Tena-Colunga and Abrams 1992). Peak values for this acceleration and computed displacement data are summarized in Tables 3.1 and 3.2, respectively. It should be noted that the peak absolute and relative displacements listed in Table 3.2 refer to the peak values over the duration of the corresponding time history record. In particular the peak relative displacements in Table 3.2 were computed as the maximum value over the corresponding relative displacement time history and thus do not occur at the same time as the peak absolute displacement. From preliminary inspection of the variation with time of the recorded acceleration response of the two-story building, it is apparent that the frequency at each sensor appears to be relatively constant even after the strongest portion of the motion. Such an occurrence suggests that the building remained essentially elastic.

The recorded data for the two-story building indicate that considerable amplification of peak acceleration between the ground and the roof occurred in the E-W direction. The north and south walls experienced peak accelerations at the roof level of 0.34g measured at sensor 4, and 0.32g measured by sensor 6. At the center of the diaphragm a peak acceleration of 0.53g was recorded by sensor 5. The peak base acceleration was recorded as 0.21g in the E-W direction and 0.2g in the N-S direction. The increased acceleration at the center of the diaphragm in the E-W direction is due to the flexibility of the diaphragm in that direction. In the N-S direction, the acceleration at the center of the diaphragm was measured to be 0.36g.

Peak vertical ground acceleration at the base is 0.08g. Vertical accelerations are sometimes a concern in masonry structures, since they may adversely affect the stresses due to gravity loads, especially if these accelerations are high. It is shown in Table 3.1 that the peak recorded vertical ground acceleration was only 0.08g.

The peak computed displacement at the center of the roof diaphragm in the N-S direction obtained from the acceleration data is 5.4 in. compared with 5.38 in. at the base indicating no differential displacement. In the E-W direction, the computed peak ground displacement was 7.0 in. at the base. Displacements calculated from the recorded accelerations at the roof were 7.29 in. and 6.9 in. at the walls and 7.25 in. at the center of the diaphragm. The peak absolute and relative displacements in Table 3.2 refer to the peak values over the duration of the corresponding time history record. Therefore, the peak relative displacement and any associated peak absolute displacement do not occur at the same instant.

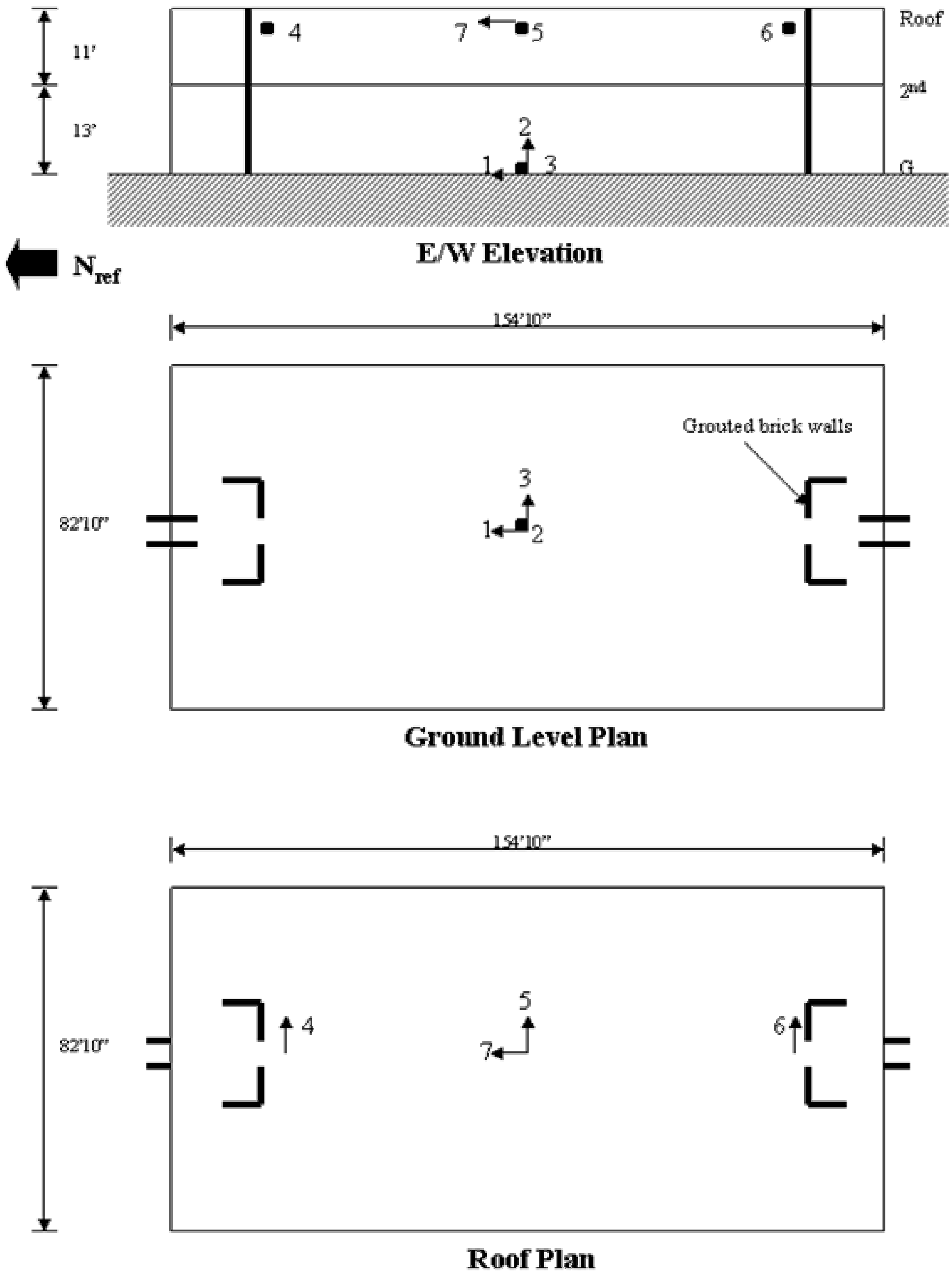

Figure 3.4 Strong motion instrumentation, 2-story building.

Table 3.1 Peak recorded accelerations, Loma Prieta, 2-story building.

Sensor I.D.	Location	Peak Absolute Acceleration (g)
1	Ground (N-S)	0.20
2	Ground (UP)	0.08
3	Ground (E-W)	0.21
4	Roof (E-W)	0.34
5	Roof (E-W)	0.53
6	Roof (E-W)	0.32
7	Roof (N-S)	0.36

Table 3.2 Peak absolute and relative computed displacements, Loma Prieta, 2-story building.

Sensor I.D.	Location	Peak Absolute Displacement (Inches)	Peak Relative Displacement (Inches)
1	Ground (N-S)	4.73	
2	Ground (UP)	1.06	
3	Ground (E-W)	6.31	
4	Roof (E-W)	6.47	0.40
5	Roof (E-W)	6.70	0.80
6	Roof (E-W)	6.19	0.46
7	Roof (N-S)	4.73	0.00

3.4 SPECTRAL ANALYSES

3.4.1 Linear Elastic Response Spectra (LERS)

In order to obtain a better evaluation of the recorded response, LERS for 5% damping for all modes were generated and plotted for selected recorded building motions. Passing the recorded accelerations through a single-degree-of-freedom oscillator having 5% of critical damping generates the spectra. LERS for the base in the N-S and E-W directions were developed using the base motions recorded on channels 1 and 3, respectively, and are displayed in Figure 3.5.

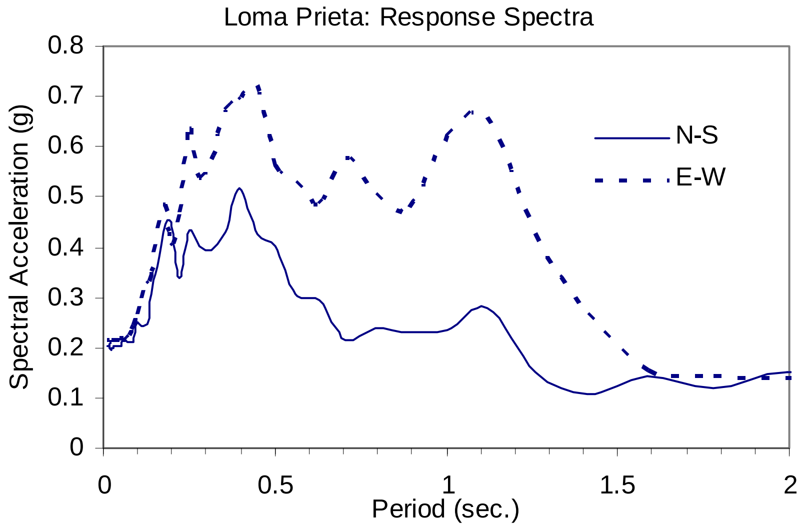

Figure 3.5 N-S and E-W response spectra, Loma Prieta, 2-story building.

3.4.2 Fourier Analyses

Moving window Fourier transfer function analyses were performed using the recorded base and roof motions in the N-S and E-W directions of the building during the Loma Prieta earthquake. Sensors 1 and 7 in the N-S and sensors 3 and 5 in the E-W direction were used to conduct the Moving window Fourier transfer function analyses. In these analyses, the Fourier transfer functions have been calculated for 10-second window lengths with five-second window shifts resulting in 10 windows. In the analysis of the two-story building in the E-W direction, the individual window graphs in the E-W direction indicated that the first peak (or group of peaks) occurred at a frequency of approximately 4 Hz, and a second group of peaks occurred at approximately 6 Hz. However, the recurrent peaks at about 4 Hz during the windowing process indicated that the first mode response of the two-story building occurred somewhere in the lower frequency range. Therefore, the moving window plot was constructed by considering the first mode response to occur at approximately at 4 Hz. The moving window results for the building in the N-S, and E-W are shown in Figure 3.6. From the resulting moving window diagrams for the E-W direction, it can be seen that the period of the two-story building remained essentially constant at a value of approximately 0.28 sec during the entire duration of the earthquake record. Similarly, in the N-S direction, the period of the building remained generally constant at a value of 0.22 sec. This lack of a significant change in the first mode translation period in the N-S and

E-W directions obtained from the moving window analyses suggests that the building did not suffer appreciable structural damage. Therefore, it can be concluded that the two-story building remained essentially elastic during the Loma Prieta earthquake.

Tena-Colunga and Abrams have obtained a period of 0.4 and 0.367 sec in the E-W and N-S directions, respectively, for the two-story Palo Alto building (Tena-Colunga and Abrams 1992). However, Figure 3.6 shows that from the moving window Fourier transfer function analyses of the building, the period of the two-story building is approximately 0.28 sec and 0.22 sec in the E-W and N-S directions, respectively. Such a significant difference in the period obtained for the two-story building from the previous work of Tena-Colunga and Abrams appears to be related to a difference in the interpretation of the peak where the first mode response occurs.

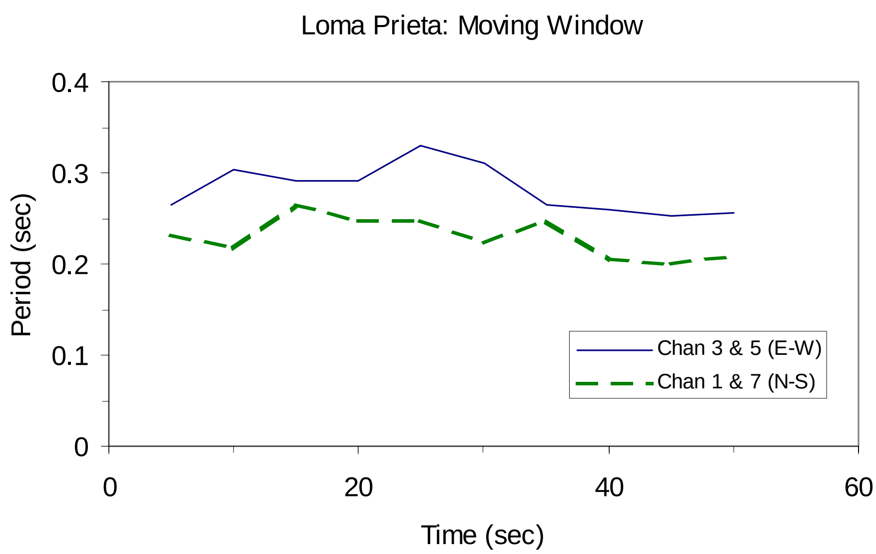

Figure 3.6 Temporal period variation, Loma Prieta, 2-story building.

Tena-Colunga and Abrams used Normalized Fourier Amplitude Spectra as well as Linear Elastic Response Spectra to determine the period of the two-story building. The first mode period occurred in the normalized Fourier amplitude spectra at 0.4 and 0.367 sec for the E-W and N-S directions when choosing the second peak in the normalized spectra to be designated as the first mode response of the building (Tena-Colunga and Abrams 1992). However, by inspection of the same normalized spectra, one may see that there is a spike in the spectra of sensors 3 and 5 at about 0.23 sec, and in the spectra of sensors 1 and 7 at about 0.28 sec, which may be interpreted as the first mode response. Such an assumption may be deemed reasonable, as the E-W and N-S direction periods of the two-story building appear to be close to the values in the normalized Fourier amplitude spectra according to the peak in the E-W direction sensors (3 and 5) and the N-S direction sensors (1 and 7). Therefore, for the analyses of the two-story building, the period will be taken as 0.28 sec, and 0.22 sec, in the E-W and N-S directions, respectively.

3.5 ELASTIC DYNAMIC ANALYSES

3.5.1 Mathematical Model

A three-dimensional linear elastic finite element model using ETABS (Version 7) computer software was developed for the two-story building because the preliminary spectral analyses on the base motions revealed that the building had remained essentially elastic during the Loma Prieta earthquake. This program was used, although it is recognized that several alternative programs could have been used for this phase of the response analysis. The reasons for selecting the ETABS program were discussed previously. An isometric view of the building model used in the ETABS program is shown in Figure 3.7. There are four L-shaped, two-way grouted brick shear walls for the primary lateral-force-resisting system. Two smaller shear walls at each end provide additional lateral resistance, primarily in the N-S direction. The model consists of a total of 7,264 nodal points, 7,676 shell elements, and 1,156 frame elements.

3.5.1.1 Modeling of Plywood Diaphragms

Thick shell elements were employed to model the roof and floor diaphragms. These elements were necessary to adequately capture both the translational and flexural movement of the diaphragms. The thick plate option was selected so that the shear deformation of the diaphragm would also be considered. The roof and second-floor diaphragms of the two-story building utilized structural plywood panels. At the roof level, the ½″ plywood panels are mounted on 2x14 DF joists at 2 ft on center running in the N-S direction. The second-floor diaphragm of the building consists of ¾″ plywood panels mounted on 36″ TJM truss joists running in the E-W direction. An equivalent diaphragm thickness was calculated for membrane behavior and another equivalent thickness was calculated to represent flexural behavior. These properties were used in each principal orthogonal direction of the building for the shell elements at each floor level. Such equivalent, uniform shell element thickness was calculated by determining the equivalent thickness for which either the area or moment of inertia was the same as for the actual diaphragm in each direction. For simplicity, the stiffness of the diaphragms in the E-W and N-S directions was taken to be uncoupled, and therefore two-way action is neglected.

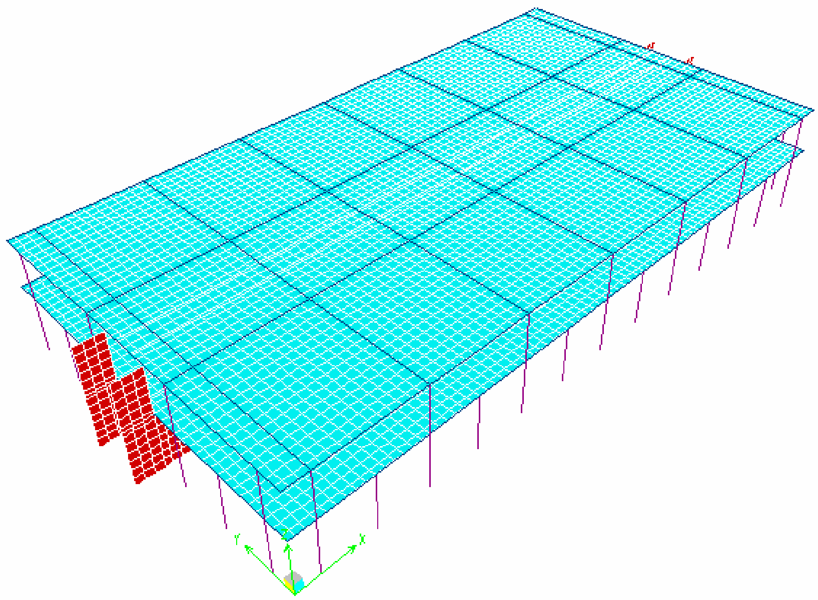

Figure 3.7 3-D linear elastic ETABS model, isometric view, 2-story building.

At the roof level in the E-W direction, equivalent shell element thickness was determined based on the ½″ plywood mounted on 2x4 DF blocking at the plywood edges. In the N-S direction the thickness was based on the ½″ plywood panels and the 2x14 DF joists. At the second-floor level, the E-W direction equivalent thickness was based on ¾″ plywood on top of the 36″ TJM open web trusses at 2 ft on center. The equivalent thickness in the N-S direction was based on 3/4″ plywood with 2x4 DF flat blocking at every 4 ft at the plywood edges. The 1-½″ lightweight concrete fill (110 pcf) on top of the plywood was ignored in the equivalent shell element thickness calculations. Such a decision may be considered reasonable, since the concrete strength is 2,000 psi, with no reinforcing nor any actual connection to the diaphragm. Therefore, in this study the contribution to the effective stiffness of the second-floor diaphragm is neglected.

The calculated equivalent membrane thickness for the roof diaphragm in the E-W and N-S building directions was 0.61 in., and 1.34 in., respectively. The calculated bending thickness for the roof diaphragm in the E-W and N-S directions was 1.13 in. and 6.97 in. At the second-floor level, the membrane thickness used in the E-W and N-S directions was 0.61 in., and 1.63 in., respectively. Equivalent bending thickness for the second-floor diaphragm in the E-W and N-S directions was calculated as 1.79 in., and 16.41 in., respectively. It should be noted that the large value of bending thickness for the second-floor diaphragm in the N-S direction is due to the open web Trus Joist spanning along the N-S dimension of the two-story building.

Orthotropic material behavior was essential to model the difference in diaphragm material properties between the E-W and N-S directions. Effective material properties were calculated for the roof and floor diaphragms, in order to include the interaction of the TJM trusses and the plywood. The average modulus of elasticity of plywood was taken to be 1,700 ksi. The average modulus of elasticity of the 36″ TJM trusses at the second-floor level was taken to be 1,905 ksi. Equation (3.1) was used to calculate equivalent EI value for open-web TJM trusses (truss only), where E is the effective modulus of elasticity, I is the actual moment of inertia of the truss section, and d is average depth of truss minus 3.5 in.

$$EI = 10.06x10^6 d^2 \tag{3.1}$$

The direction of the grain of the plywood was also considered in the calculations of the effective modulus of elasticity of the diaphragms (i.e., E_{weak}=1/35*$E_{strong} \approx$ 50ksi) (Breyer, et al. 1999). The equivalent elastic modulus of each diaphragm in each direction was taken as the average of each of the respective components used in the equivalent thickness calculations. With such considerations in mind, the effective moduli of elasticity used at the roof level were 875 ksi (plywood-weak-direction, beams) in the N-S direction, and 1,700 ksi (plywood-strong-direction, beams) in the E-W direction. For the floor diaphragm shell elements, an effective modulus of elasticity was taken as 1,700 ksi (plywood-strong-direction) in the N-S direction, and 975 ksi (plywood-weak-direction, TJM trusses) in the E-W direction.

Since no data were readily available regarding the shear modulus of TJI and TJM truss joists, the equivalent shear modulus value of each of the diaphragms was simply taken as the average shear modulus of plywood. Thus, a value of 90 ksi for the shear modulus was used for the shell elements modeling each diaphragm and for both principal directions of the building.

3.5.1.2 Modeling of Masonry Shear Walls

Thick plate shell elements were used to model the 12″ grouted brick shear walls. For calculation of the equivalent shell element thickness for flexural behavior and membrane action of the masonry shear walls, cracking of the wall section was assumed and was computed based on the effective cracked section thickness for a rectangular section under bending. In doing so, application of the effective cracked section thickness for a reinforced concrete section was assumed even though the section was reinforced masonry (i.e., $t_{eff} = 0.35t_{orig}$). Thus, the membrane and bending thickness for the shell elements used to model the shear wall was taken to be 4.2″ for the 12″ walls. However, the weight of the walls used in the model is based on the original dimensions of the walls.

Isotropic material behavior is assumed for the masonry shear walls and the modulus of elasticity for masonry is calculated using Equation (3.2), where f'_m is taken as 1,500 ksi.

$$E = 750 f'_m \tag{3.2}$$

Poisson's ratio for masonry was assumed to be 0.2, and the shear modulus was calculated internally by ETABS to be G=468.75 ksi based on the dependence relation in Equation (3.3) for an isotropic material.

$$G = \frac{E}{2(1+\upsilon)} \tag{3.3}$$

3.5.1.3 Other Modeling Considerations

The connection of the interior and exterior glulam beams to the glulam columns and steel tube columns was assumed to be simple shear type. Therefore, end moments about the strong axis of the frame elements used to model these beams are released at the second floor of the two-story building. Exterior columns were idealized with pinned connections, as the actual connection consists of a steel saddle housing the glulam column and cannot transfer a large moment into the soil. Additional line masses are added on framing elements (beams, columns) whose locations are coincident with the nonstructural elements of the building that provide additional mass.

3.5.1.4 Weight (Mass) Determination

The weight (mass) of the second-floor level and roof was estimated based on the reduced set of structural blueprints obtained from CSMIP. However, it was necessary to estimate the weights of some of the finish materials of each building. In the weight estimations, the self weight of the grouted brick masonry walls was assumed to be 120 pcf. The unit weight of glulam was taken as 30 pcf, and the weight of exterior glass was taken as 8 psf. Each nominal dimension of the lumber was reduced by ½ inch to reflect the true dimension. All weight calculations based on plan-view area unit weights were based on the outer dimensions of the building. Estimations of the total weight (mass) of each floor level of the building were based on the heights tributary to each level. The details of the roof weight (mass) calculations for the two-story building are displayed in Table 3.3.

Table 3.3 Roof weight (mass) calculations, 2-story building.

Component	Assumed Unit Weight (psf)	Weight (k)
Roof Framing	x	77
Roofing	6	77
Hung Ceiling	8	103
Exterior Glass	8	19
Mechanical Equipment	50	14
Exterior Stud Wall	x	12
Exterior GLB Columns	x	6
Interior Steel Columns	x	0
Edge Beams	x	5
Interior Beams	x	14
Shear Wall	x	62
Total Roof Weight		388
Roof Translational Mass		1.00k-s^2/in

An average lineal weight of the 36″ TJM trusses was obtained from the Trus Joist McMillan Product Specifications Manual. The lineal weight was taken to be 8.5 lb/ft for a 36″ TJM open-web truss. The estimations made for the weight (mass) at the second-floor level of the building are detailed in Table 3.4. The total weight of the building used for dynamic analyses is 1,227.68 kips (3.18 k-s^2/in.).

Table 3.4 2nd floor weight (mass) calculations, 2-story building.

Component	Assumed Unit Weight (psf)	Weight (k)
Roof Framing	x	130
Concrete Slab (Lt. Wt.)	x	217
Flooring	2	26
Hung Ceiling	8	103
Exterior Glass	8	43
Exterior Stud Wall	x	3
Exterior GLB Columns	x	20
Interior Steel Columns	x	1
Edge Beams	x	7
Interior Beams	x	3
Partitions	10	129
Shear Wall	x	157
Total 2nd Floor Weight		839
2nd Floor Translational Mass		$2.17 k\text{-}s^2/in$

3.5.2 Modal Period Analyses

The mode shapes and frequencies for the first 27 modes were evaluated by using the three-dimensional finite element ETABS model of the two-story building. The translation mode shapes in the N-S and E-W directions obtained from the ETABS model are shown in Figures 3.8 and 3.9. A torsional mode shape is displayed in Figure 3.10. The periods of vibration corresponding to the N-S and E-W mode shapes are 0.23 and 0.35 sec, respectively. The torsion period of vibration was calculated to be 0.34 sec.

The translation mode in the E-W direction captures the in-plane bending of the diaphragm with the E-W direction shear walls acting as supports in the horizontal plane. The linear elastic analytical model gave a close approximation to the modal periods obtained from the spectral analyses of 0.22 and 0.32 sec in the N-S and E-W directions, respectively. In running the dynamic analysis of the model, the code recommended minimum value for the participating mass in each principal orthogonal direction of the building was exceeded. Using 27 modes of vibration in the ETABS model represented 98.7% of the participating mass, which exceeds the 90% requirement in the 1997 UBC.

3.5.3 Calculated and Recorded Response Comparisons

3.5.3.1 Loma Prieta Displacement and Acceleration Comparisons

In order to study the dynamic time history response of the two-story Palo Alto office building when subjected to the recorded motions at its base, the 3-D linear elastic model was subjected to simultaneous base accelerations recorded in the N-S and E-W directions.

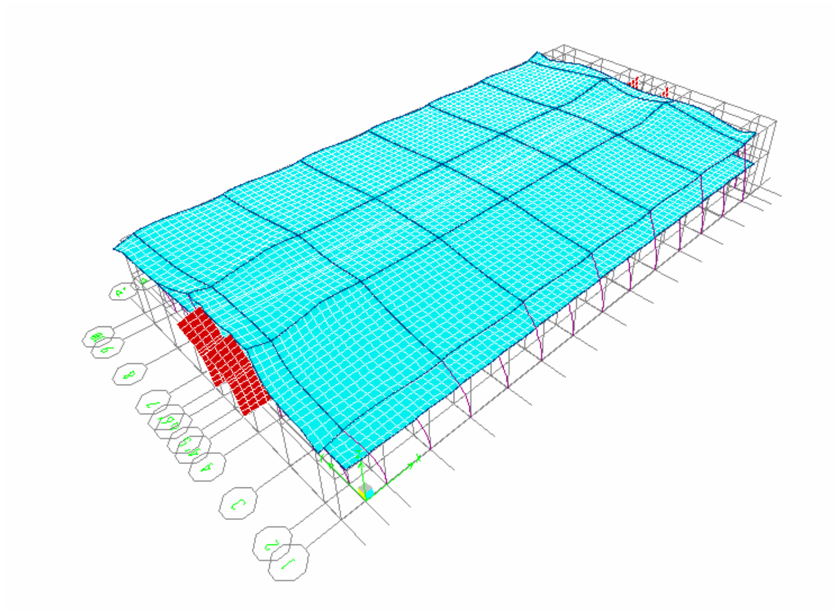

Figure 3.8 N-S translational mode shape, 2-story building.

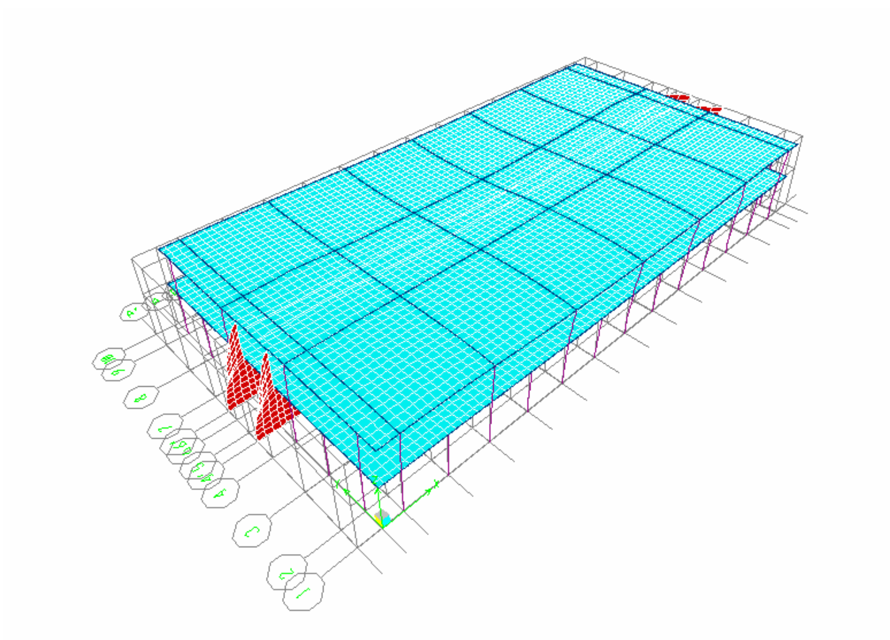

Figure 3.9 E-W translational mode shape, 2-story building.

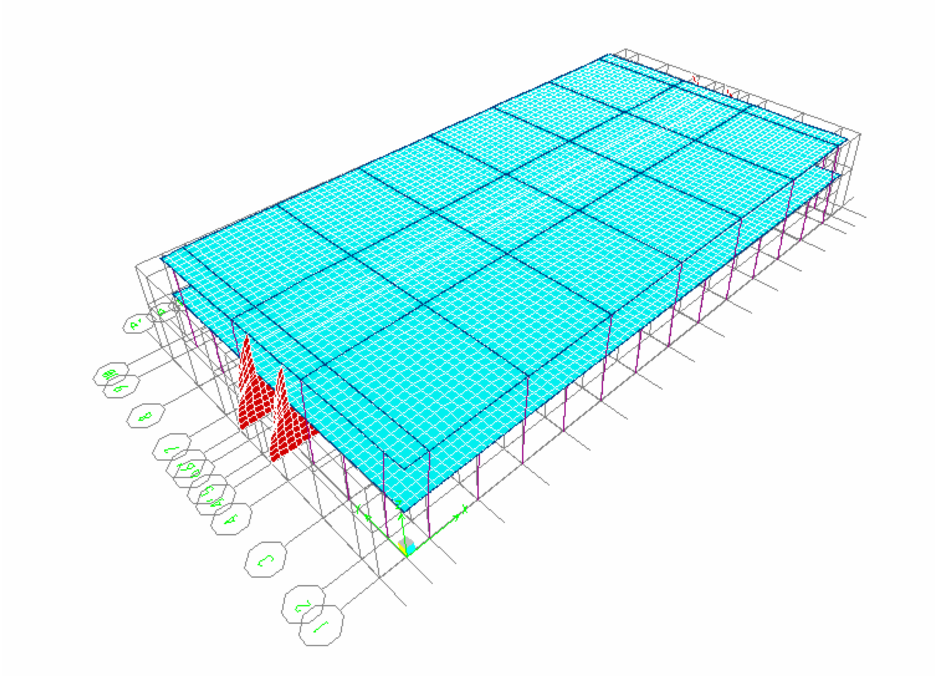

Figure 3.10 Torsion mode shape, 2-story building.

Time history comparisons of the calculated response with that recorded for the two-story building are presented for the ground motion recorded at the base during the Loma Prieta earthquake. A value of 5% critical damping value for all 27 modes was used in the dynamic response analyses.

The three-dimensional analytical model was also used to compute the dynamic displacement time history responses at each sensor location above ground level. The ETABS acceleration time history results were computed and integrated to obtain the corresponding displacement response of the building.

Acceleration and displacement comparisons between the predicted values from the analytical model and from the actual recorded response for sensor 5 of the two-story building during the Loma Prieta earthquake are shown in Figures 3.11 and 3.12. From these figures, it can be seen that a close correlation between the recorded and predicted displacements was obtained. Although the calculated accelerations tended to overestimate the magnitude of acceleration spikes, the model was still able to sufficiently reproduce the general acceleration characteristics of the recorded motion. Such an occurrence may be due in part to the fact that the exact location of the recording instrument is unknown and hence, the recorded values may be influenced by the torsional response of the building. This also makes it hard to know if the calculated results represent the exact location of the sensor in the building. The acceleration and displacement time history comparisons for the remaining three roof-level sensors are given by Tokoro (Tokoro 2001).

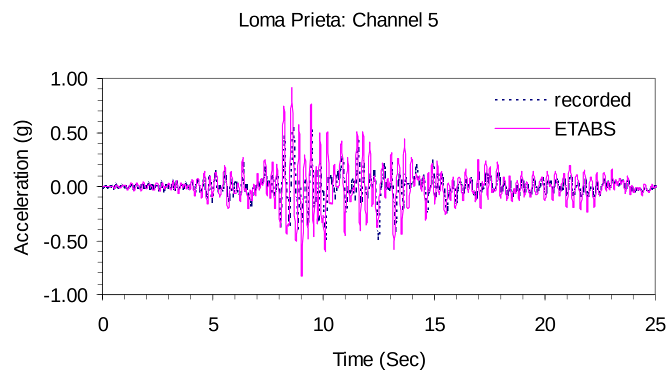

Figure 3.11 Calculated vs. recorded accelerations (ch. 5), Loma Prieta, 2-story building.

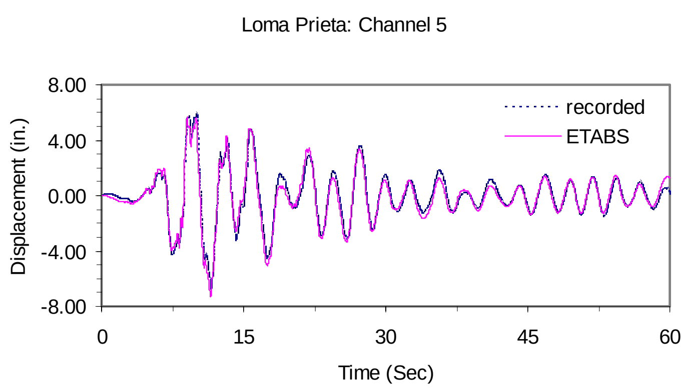

Figure 3.12 Calculated vs. recorded displacements (ch. 5), Loma Prieta, 2-story building.

3.6 UNIFORM BUILDING CODE COMPARISON

3.6.1 Code Seismic Force Requirement (UBC 1973)

The two-story building was designed in 1974, according to the governing building code at that time. Therefore, the 1973 UBC was used to estimate the nominal shear strength of the building.

The UBC 1973 code specifies that separate base shear design values be calculated along each principal dimension of the building. The base shear, V, in the longitudinal or transverse direction of the building may be calculated using Equation (3.4).

$$V = KCWZ \tag{3.4}$$

The seismic coefficient, C, is specified by Equation (3.5), and the period, T, can be estimated using Equation (3.6), where H is the total height of the building in feet, and D is the plan dimension of the building in the direction of seismic loading parallel to a principal building dimension.

$$C = \frac{0.05}{\sqrt[3]{T}} \tag{3.5}$$

$$T = \frac{0.05H}{\sqrt{D}} \tag{3.6}$$

Due to the difference in longitudinal and transverse dimensions of the two-story building, the period, and hence the base shear had to be computed for loading along both directions. Using the empirical formula for estimating the period in the N-S and E-W directions of the two-story building the periods are calculated as shown in Equations (3.7) and (3.8).

$$T_{NS} = \frac{0.05H}{\sqrt{D_{NS}}} = \frac{0.05(22.83\,ft)}{\sqrt{154.5\,ft}} = 0.092 \text{ sec} \tag{3.7}$$

$$T_{EW} = \frac{0.05H}{\sqrt{D_{EW}}} = \frac{0.05(22.83\,ft)}{\sqrt{83\,ft}} = 0.13 \text{ sec} \tag{3.8}$$

Similarly, the seismic coefficients in the N-S and E-W directions are as shown in Equations (3.9) and (3.10), respectively.

$$C_{NS} = \frac{0.05}{\sqrt[3]{T_{NS}}} = \frac{0.05}{\sqrt[3]{0.092 \sec}} = 0.11 \tag{3.9}$$

$$C_{EW} = \frac{0.05}{\sqrt[3]{T_{EW}}} \frac{0.05}{\sqrt[3]{0.13 \sec}} = 0.10 \tag{3.10}$$

Using K=1.33 and Z=1.0, the resulting design seismic resistance coefficients are shown in Equations (3.11) and (3.12).

$$V_{NS} = (ZKC_{NS})W = (1.0)(1.33)(0.11)W = 0.15W \tag{3.11}$$

$$V_{EW} = KC_{EW}WZ = (1.0)(1.33)(0.10)W = 0.13W \tag{3.12}$$

Equations (3.13) and (3.14) show the design base shears in the N-S and E-W directions as a result of taking W to be the effective dead load of the building.

$$V_{NS} = 0.15W = 0.15(1228\,kips) = 184.20\,kips \tag{3.13}$$

$$V_{EW} = 0.13W = 0.13(1228\,kips) = 159.64\,kips \tag{3.14}$$

3.6.2 Code Design Requirements (UBC 1997)

The period of the two-story building was calculated according to Method A of the 1997 UBC provisions, with the value of C_t equal to 0.020. According to the 1997 UBC, the period of the two-story building may be approximated by "Method A," as given by Equation (3.15).

$$T = 0.020(h_n)^{3/4} = 0.02(22.83\,ft)^{3/4} = 0.21\sec \tag{3.15}$$

The actual soil profile at the location of the building is unknown, which made using the default soil profile S_D necessary in the code analysis calculations. Since the two-story building is located in California, it was necessary to use the seismic zone factor Z=0.4 for buildings in Zone 4 according to the code. Near-source factors were chosen based on a generating seismic source A and a distance to source exceeding 15km, where N_a and N_v were each taken to be 1.0. The seismic coefficients C_a and C_v for a building in seismic zone 4 and sited on a soil of profile S_D is to be calculated using the 1997 UBC formulas depicted in Equations (3.16).

$$\begin{aligned} C_a &= 0.44N_a = 0.44(1.0) = 0.44 \\ C_v &= 0.64N_v = 0.64(1.0) = 0.64 \end{aligned} \tag{3.16}$$

The building was considered to be a masonry shear wall frame building and therefore a structural system factor of R=5.5 was used in the base shear calculations. The 1997 UBC defines that the design base shear V in a given direction of a building should be determined from Equation (3.17**)**. However, the total design base shear need not exceed Equation (3.18). And the total design base shear shall not be less than Equation (3.19**)**.

$$V = \left(\frac{C_v I}{RT}\right)W = \left(\frac{0.64*1.0}{5.5*0.21\sec}\right)W = 0.56W \tag{3.17}$$

$$V \le \left(\frac{2.5C_a I}{R}\right)W = \left(\frac{2.5*0.44*1.0}{5.5}\right)W = 0.2W \tag{3.18}$$

$$V = 0.11C_a IW = 0.11(0.44)(1.0)W = 0.048W \tag{3.19}$$

In addition, the 1997 UBC specifies that for Seismic Zone 4, the total base shear shall not be less than Equation (3.20**)**, where R is a factor based on the type of structural system of the building, I is an importance factor, N_v is a near-source factor, and C_a and C_v are seismic coefficients which are determined for a given Seismic Zone and soil profile type.

$$V = \left(\frac{0.8ZN_v I}{R}\right)W = \left(\frac{0.8*0.4*1.0*1.0}{5.5}\right)W = 0.058W \tag{3.20}$$

For a masonry shear wall building frame system, a structural system factor of R=5.5 is specified. Due to the perimeter and interior framing this value was used in the base shear calculations. Using this value of R and an importance factor of I=1.0 for a building enduring typical usage, in the 1997 UBC formulas to calculate the base shear, the total design base shear is predicted by the 1997 UBC as governed by Equation (3.21).

$$V = \left(\frac{2.5C_a I}{R}\right)W = \left(\frac{2.5*0.44*1.0}{5.5}\right)W = 0.2W \tag{3.21}$$

The above expression states that the total lateral force requirement will be 20% of the effective self-weight of the building, W. Estimating W as 1228 kips, Equation (3.22) is the calculated base shear requirement as determined by the 1997 UBC code.

$$V = 0.2W = 0.2*1228\ kips = 245.6\ kips \tag{3.22}$$

The value of the design base shear calculated using the 1997 UBC requirements is based on ultimate strength, whereas the value computed using 1993 UBC formulas is based on the allowable stress design. For purposes of comparison, the value of base shear computed from the 1973 UBC was multiplied by the load conversion factor for masonry of 1.4 to increase the base shear to the strength design level. It should be noted that the values of the base shear calculated using the current 1997 UBC provisions are 3.0% less than the lateral force requirement for the N-S direction and 7.2% greater than the lateral force requirement in the E-W direction used in the 1973 UBC that was assumed to have been the basis for the design of the building in 1974.

3.7 ANALYSES OF BASE SHEAR

The elastic response of the structure is evaluated considering the time history demands of the ground motions recorded at the base of the two-story building during the Loma Prieta earthquake. Four additional ground motions were used to evaluate the performance of the two-story building to stronger, more demanding ground motions as well as to study the response to records characterized as having significant displacement pulses. The four additional ground motions used in the study to represent stronger ground motions are the following: (1) the ground motion recorded at the Newhall Fire Station during the Northridge earthquake, (2) the ground motion recorded at Lucerne during the Landers earthquake that contains a one-sided displacement pulse, (3) the ground motion recorded at Takatori during the Kobe earthquake that contains two-sided displacement pulses, and (4) the ground motions recorded at the Los Gatos Presentation Center during the Loma Prieta earthquake.

The recorded ground accelerations at the base of the two-story building were quite small, which is characteristic of a location far from the epicenter or fault trace of the earthquake. Therefore, the addition of the four strong ground motion records brought the total ground motions used in the study of this building to five. The details of these additional recorded motions were discussed in a previous section.

3.7.1 In-Plane Shear Capacity

The nominal shear capacity of a structural wall can be calculated using Equation (3.23), where the coefficient C_d depends on the ratio of $\frac{M}{Vd}$.

$$V_n = C_d \sqrt{f'_m} hd + \frac{A_{vh} f_y d}{s_2} \tag{3.23}$$

For these walls, the ratio of $\frac{M}{Vd}$ is greater than unity and therefore C_d = 1.2. For all structural walls, the thickness, h, is 12″, the masonry strength is 1,500 psi and the horizontal steel reinforcement is 1-#4@12″. The four main walls in the N-S direction are 144″ in length. If the effective length of the wall is taken as $0.8l_w$, the nominal shear capacity of a single wall is 141 kips and for the four walls this becomes 564 kips. In addition there are four other walls at the first-floor level that are 114″ in length in the N-S direction. These walls add an additional 445 kips of lateral resistance for a total of 1009 kips in the N-S direction. In the E-W direction there are four walls with each wall having a length of 112″. When $0.8l_w$ is used for the effective length of the wall, the nominal shear capacity of the four walls is only 437 kips, which is less than half of the capacity in the other direction.

3.7.2 Loma Prieta Earthquake

The linear elastic analytical model was used to predict the base shear demands of the two-story building during the Loma Prieta earthquake. The results were then compared to the design values of base shear specified by the 1973 and 1997 editions of the UBC that were calculated in the previous section. The comparisons of the predicted base shear in the N-S and E-W directions as compared to the 1973 and 1997 UBC values during the Loma Prieta earthquake are displayed in Figures 3.13 and 3.14. From these comparisons, the base shear in the N-S direction exceeds the design criteria by approximately 35%, although the base shear is approximately 33% of the calculated shear capacity of the N-S walls. In the E-W direction, the base shear exceeds the design criteria by more than 100% and in addition one excursion in the base shear reaches the calculated capacity of the E-W walls indicating the potential for damage to these elements.

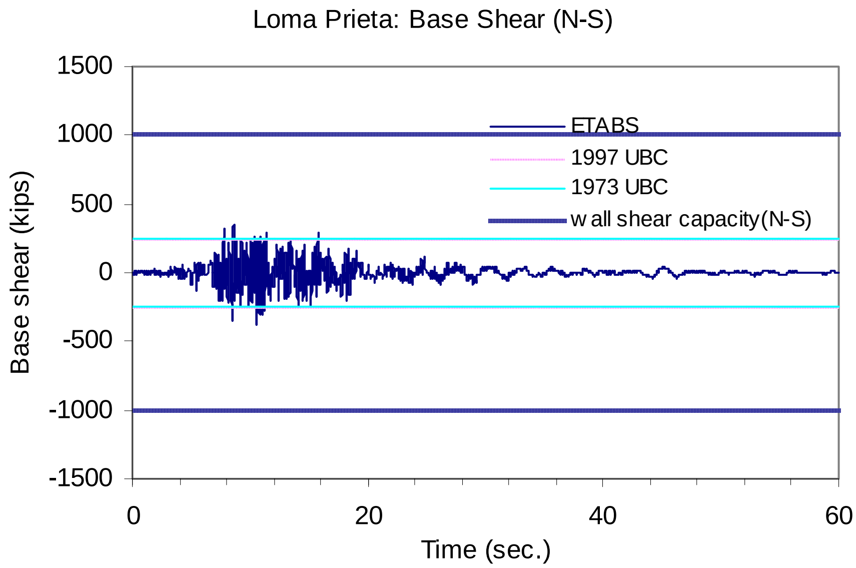

Figure 3.13 N-S design vs. calculated base shear demand, Loma Prieta, 2-story building.

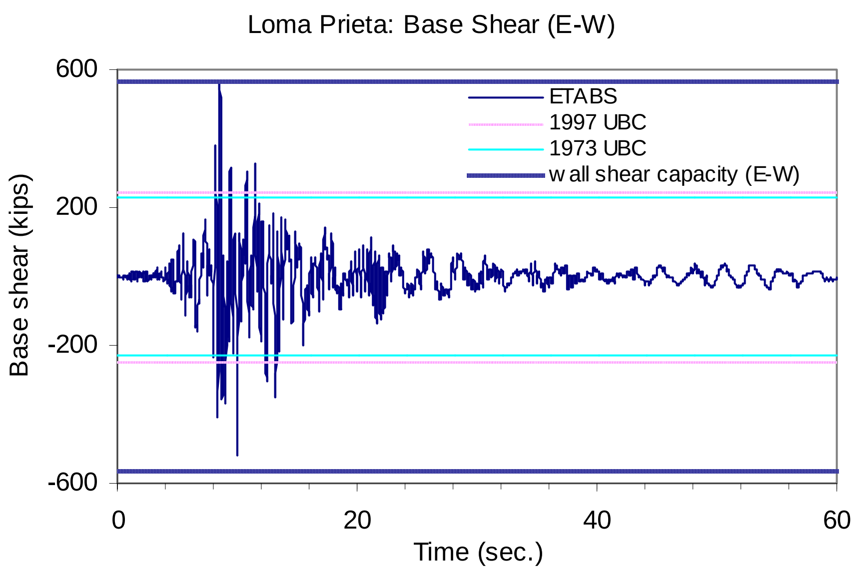

Figure 3.14 E-W design vs. calculated base shear demand, Loma Prieta, 2-story building.

3.7.3 Newhall (Northridge Earthquake)

The acceleration recorded at the Newhall Fire Station during the Landers earthquake was used to study the seismic response and behavior of the two-story building to more demanding ground motion. The comparison of the predicted base shear in the N-S and E-W directions with the 1973 and 1997 UBC values under this ground motion is shown in Figures 3.15 and 3.16. From these comparisons, it can be seen that the base shear demand of the two-story building exceeded both UBC values for the significant strong motion duration. From Table 3.6 we can see that the maximum base shear demand during this motion was 1,690 kips in the N-S direction, which is 934% greater than the 1973 UBC code values of 184 kips for which the building was assumed to have originally been designed. It can also be seen that the calculated shear capacity is exceeded by approximately six peak excursions of the base shear. The maximum value of base shear in the E-W direction was calculated to be 1,932 kips, or 1185% greater than the 1973 UBC design value of 163 kip. The base shear time history also exceeds the calculated shear capacity by as much as 342% with numerous excursions above the capacity limit during almost six seconds of the time history. Therefore, it is very likely that the two-story building would have suffered significant damage if it were to experience base motion of this magnitude.

Table 3.5 shows a comparison of the design base shear for the two-story building as per the 1997 UBC and 1973 UBC codes.

3.7.4 Lucerne (Landers Earthquake)

Calculated base shear in the N-S and E-W directions under the ground motion recorded at Lucerne are compared to the 1973 and 1997 UBC values in Figures 3.17 and 3.18. From these comparisons, it can be seen that the base shear demand of the two-story building exceeded both UBC values for nearly the entire duration of the significant strong motion. Response data summarized in Table 3.6 indicate that the maximum base shear demand in the N-S direction during this motion was 1,367 kips, which is 755% greater than the 1973 UBC code values of 184 kips (ASD) for which the building was assumed to have been originally designed. However, only one cycle of the base shear just reaches the calculated capacity of the walls in this direction. The maximum base shear demand in the E-W direction was 710 kips, which is 336% greater than the 1973 UBC value of 160 kips (ASD). The maximum base shear is also 62% larger than the calculated shear capacity. Comparing the time history base shear with the calculated capacity indicates that the capacity is exceeded on as many as nine occasions. Thus, from this strong motion analyses, we can conclude that the building most likely would have suffered considerable damage to the E-W walls if subjected to an equivalent base motion.

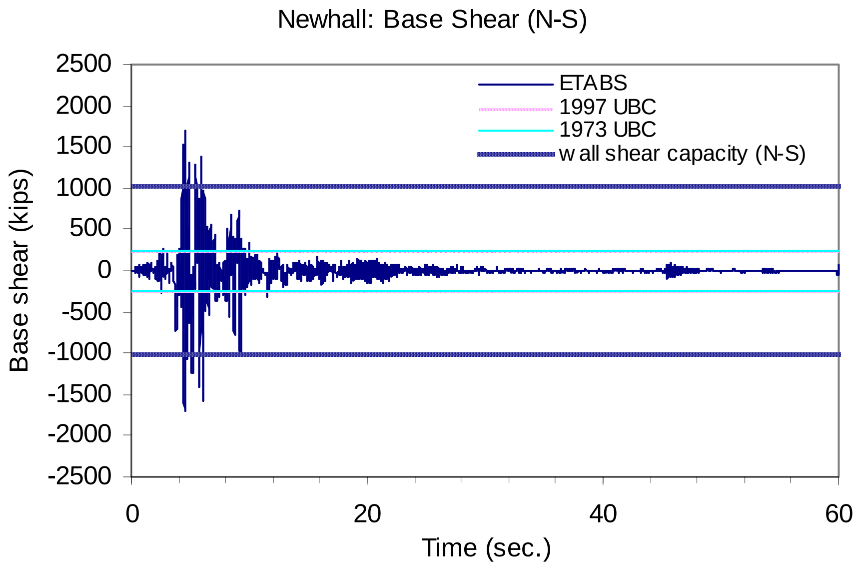

Figure 3.15 N-S design vs. calculated base shear demand, Newhall, 2-story building.

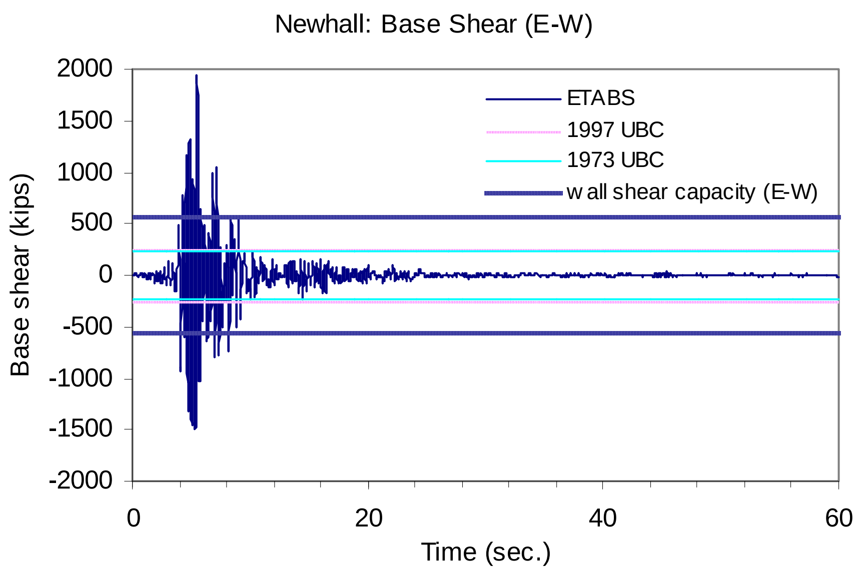

Figure 3.16 E-W design vs. calculated base shear demand, Newhall, 2-story building.

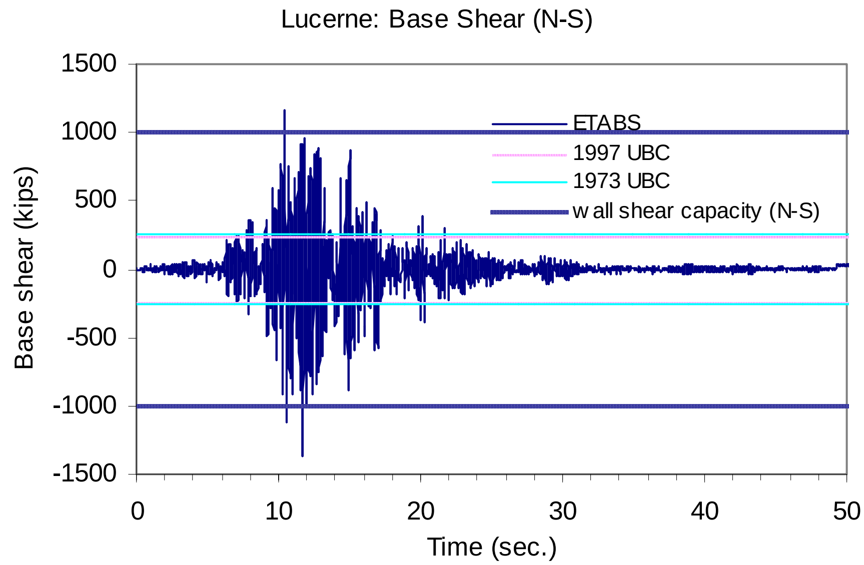

Figure 3.17 N-S design vs. calculated base shear demand, Lucerne, 2-story building.

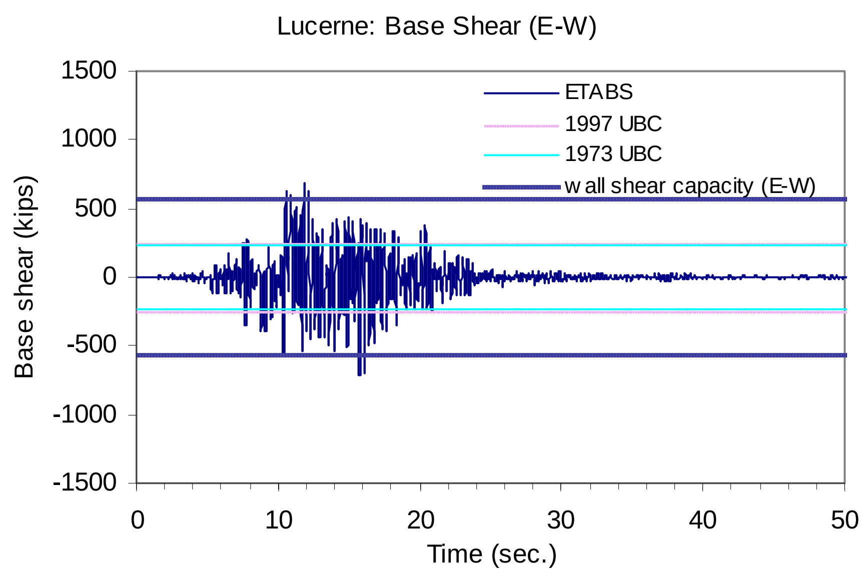

Figure 3.18 E-W design vs. calculated base shear demand, Lucerne, 2-story building.

3.7.5 Takatori (Kobe Earthquake)

Calculated base shear in the N-S and E-W directions under the ground motions recorded at Takatori during the Kobe earthquake are compared to the 1973 and 1997 UBC values in Figures 3.19 and 3.20. From these comparisons, it can be seen that the base shear demand of the two-story building exceeded both UBC values for nearly the entire duration of the significant strong motion. Data presented in Table 3.6 indicate that the maximum base shear demand in the N-S direction during this motion was 1,369 kips, which is 756% greater than the 1973 UBC code values of 184 kips for which the building was assumed to have originally been designed. The maximum base shear demand in the E-W direction was 2,179 kips, which is 1,337% greater than the 1973 UBC value of 160 kips. Thus, from this strong motion analyses, it is likely that the two-story building would have suffered significant damage if subjected to an equivalent base motion.

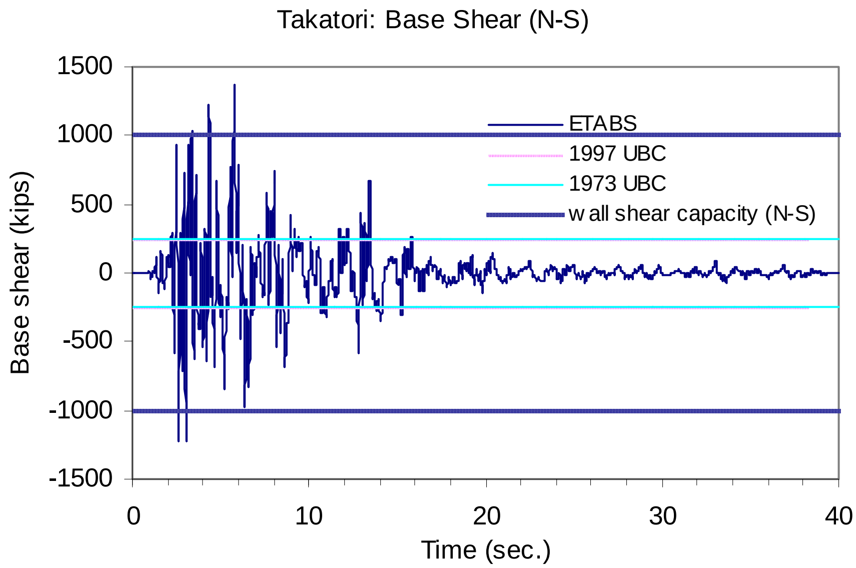

Figure 3.19 N-S design vs. calculated base shear demand, Takatori, 2-story building.

Table 3.5 Wall shear capacity/design strength summary, 2-story building.

Building Direction	Wall Shear Capacity	Design Base Shear		Design vs. capacity values	
		1973 UBC	1997 UBC	$V_{b,cap}$ vs. $V_{b,1973}$	$V_{b,cap}$ vs. $V_{b,1997}$
	$V_{b,cap}$ (kips)	$V_{b,1973}$ (kips)	$V_{b,1997}$ (kips)	$\frac{V_{b,cap}}{V_{b,1973}} * 100$ (percent)	$\frac{V_{b,cap}}{V_{b,1997}} * 100$ (percent)
Transverse (E-W)	564.0	159.6	245.6	353.4	229.6
Longitudinal (N-S)	1009.0	184.2	245.6	547.8	410.8

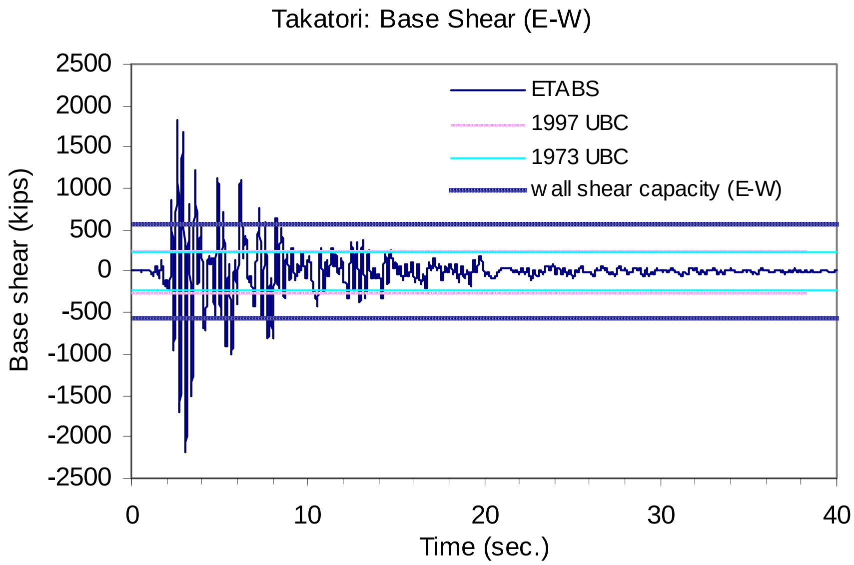

Figure 3.20 E-W design vs. calculated base shear demand, Takatori, 2-story building.

3.7.6 Los Gatos Presentation Center (Loma Prieta Earthquake)

Comparisons of the predicted base shear in the N-S and E-W directions under the ground motions recorded at the Los Gatos Presentation Center during the Loma Prieta earthquake to the 1973 and 1997 UBC values are shown in Figures 3.21 and 3.22. These comparisons indicate that the base shear demand exceeded both UBC values for nearly the entire duration of the significant strong motion. Data summarized in Table 3.6 indicate that the maximum base shear demand in the N-S direction during this motion was 1,000 kips, which is 543% greater than the 1973 UBC code values of 184 kips for which the building was assumed to have originally been designed. The maximum base shear demand in the E-W direction was 1,543 kips, which is 947% greater than the 1973 UBC value of 160 kips. Thus, from this strong motion analysis, significant building damage is suggested if the building were subjected to a similar base motion.

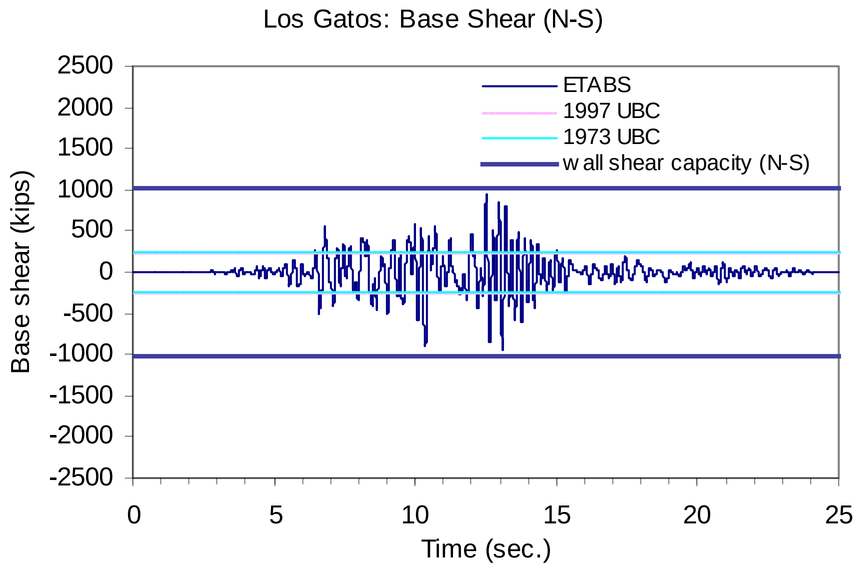

Figure 3.21 N-S design vs. calculated base shear demand, LGPC, 2-story building.

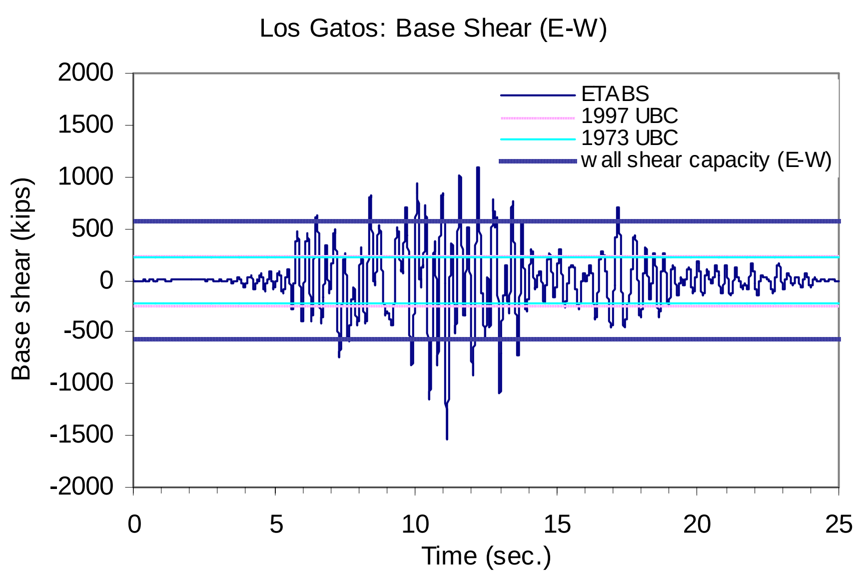

Figure 3.22 E-W design vs. calculated base shear demand, LGPC, 2-story building.

3.8 DIAPHRAGM SHEAR

Shear contours for the ground motion recorded at the base of the building during the Loma Prieta earthquake are shown in Figure 3.23 for the roof diaphragm and Figure 3.24 for the second-floor diaphragm. The maximum value at the roof level is less than 0.5 kips/in. and the maximum value at the second floor is less than 0.65 kips/in. These values compare with a strength value of

0.18 kips/in. at the roof and 0.42 kips/in. at the second floor. It should be noted that the second-floor value includes the effect of 1.5 in. of lightweight concrete, which is placed on top of the plywood.

Shear contours under the ground motion recorded at the Newhall Fire Station are representative of more severe ground motions, and are shown in Figures 3.25 and 3.26 for the roof and second floor, respectively. These indicate a maximum demand at the roof of 0.6 kips/in. and a maximum demand at the second floor of 0.7 kips/in.

Table 3.6 Summary of N-S and E-W design vs. calculated peak absolute base shear demand, 2-story building.

Flexible Diaphragm Analyses									
Earthquake		Buildling Dimension							
		Transverse (E-W)				Longitudinal (N-S)			
		Max. Abs. Base Shear $V_{b,max}$ (kips)	Percent of E-W capacity $\frac{V_{b,\max}}{V_{b,cap}} * 100$ (percent)	Percent of 1973 UBC design strength $\frac{V_{b,\max}}{V_{b,1973}} * 100$ (percent)	Percent of 1997 UBC design strength $\frac{V_{b,\max}}{V_{b,1997}} * 100$ (percent)	Max. Abs. Base Shear $V_{b,max}$ (kips)	Percent of N-S capacity $\frac{V_{b,\max}}{V_{b,cap}} * 100$ (percent)	Percent of 1973 UBC design strength $\frac{V_{b,\max}}{V_{b,1973}} * 100$ (percent)	Percent of 1997 UBC design strength $\frac{V_{b,\max}}{V_{b,1997}} * 100$ (percent)
Recorded Motions	Loma Prieta	559.1	99.1	244.8	227.7	382.7	37.9	151.0	155.9
Strong Motion Analyses	Newhall	1932.1	342.6	845.9	786.9	1690.0	167.5	666.8	688.3
	Lucerne	709.9	125.9	310.8	289.1	1367.0	135.5	539.4	556.7
	Takatori	2179.0	386.3	954.0	887.4	1369.1	135.7	540.2	557.6
	Los Gatos	1543.0	273.6	675.5	628.4	952.7	94.4	375.9	388.0

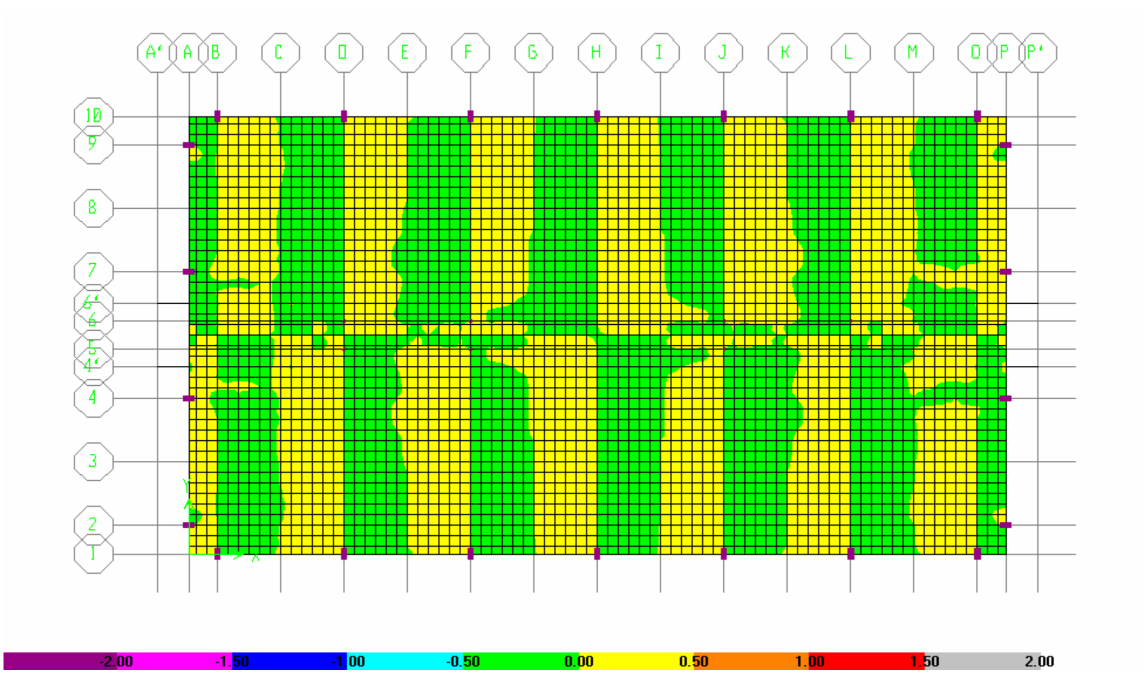

Figure 3.23 In-plane shear contour, roof, Loma Prieta, 2-story building.

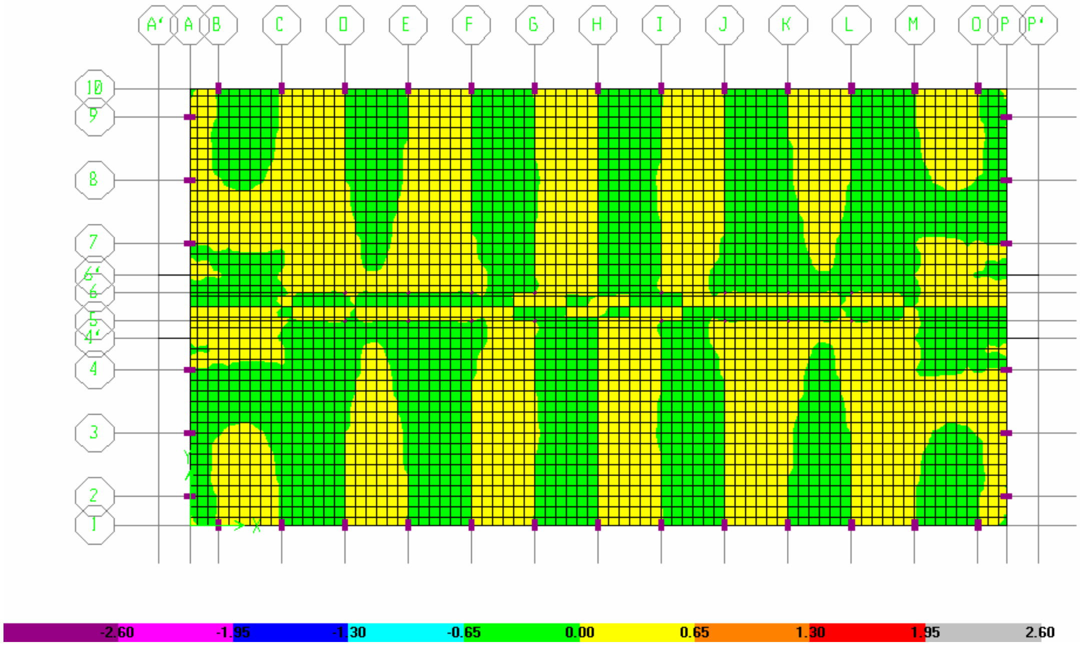

Figure 3.24 In-plane shear force contour, 2nd floor, Loma Prieta, 2-story building.

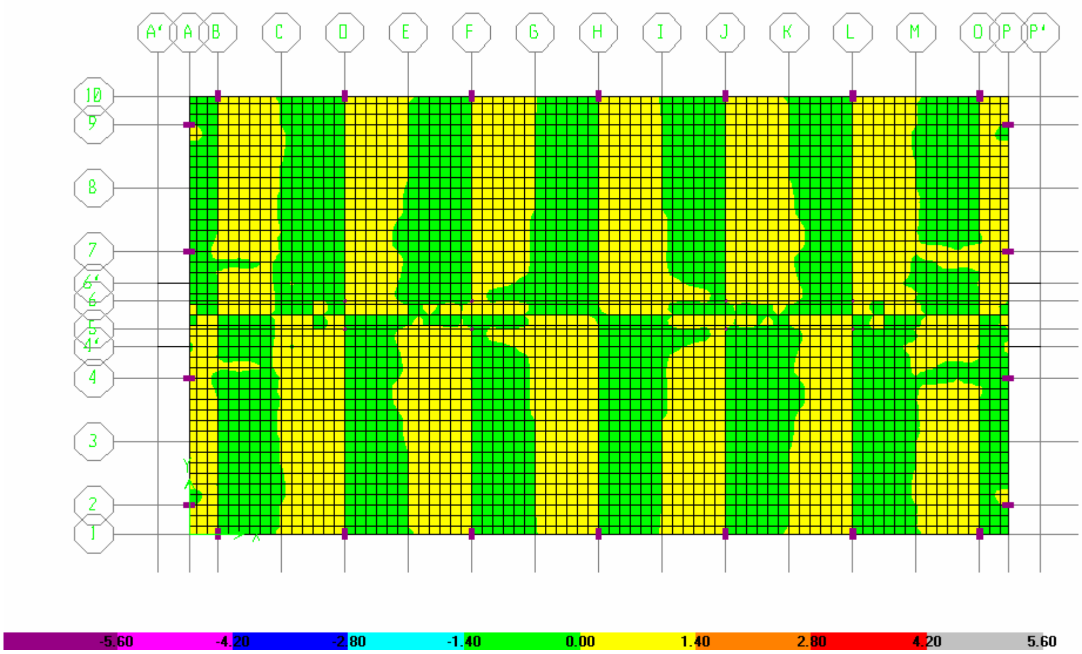

Figure 3.25 In-plane shear force contour, roof, Newhall, 2-story building.

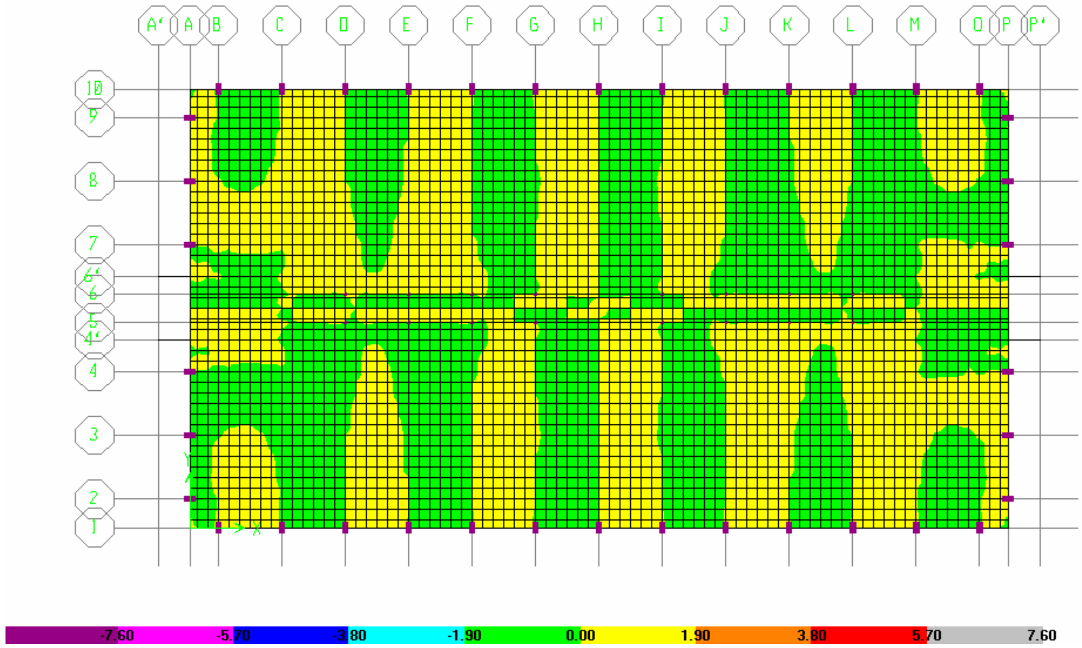

Figure 3.26 In-plane shear force contour, 2nd floor, Newhall, 2-story building.

3.9 MODIFICATION OF ELASTIC RESPONSE: TWO-STORY BUILDING

From Figure 3.14 it was shown that due to the ground motion recorded at the building during the Loma Prieta earthquake, the maximum base shear, while exceeding the 1973 UBC design requirement, just reached the wall shear capacity (564 kips) on one cycle in the E-W direction (559 kips). In the N-S direction the capacity is larger (1009 kips) and the base shear demand was less (383 kips). The maximum base shears developed by the Loma Prieta earthquake ground motions and the four more severe earthquake ground motions are summarized in Table 3.6.

The maximum base shear demand in the N-S direction due to the Newhall ground motion has a value of 1,690 kips. This is 655% greater than the 1973 UBC code value of 184 kips multiplied by 1.4 to scale it to the strength design level (258 kips). In a similar manner, the maximum value of base shear in the E-W direction for this record was calculated to be 1,932 kips. This value is 866% greater than the 1973 UBC code design base shear scaled to a strength design level of 223 kips. From these calculations, it appears likely that the two-story building would have suffered a significant amount of damage if it had experienced base motion of this magnitude and if the actual yield strengths of the masonry walls were similar to the base shear requirements of the codes. However, it has been shown that the walls of this building, with minimum reinforcing, have substantial overstrength with respect to the code design base shear. This will be evaluated in the following paragraphs.

The building can be considered as having four walls in both the N-S and E-W directions. Therefore, for the purposes of this study, the redundancy factor was taken as unity. The value of R given in the code for a building frame system having masonry shear walls is 5.5 and the corresponding strength factor is given as 2.8. This implies a ductility factor of $R_\mu = 5.5/2.8 = 2.0$. Considering the response to the Newhall ground motions discussed previously, the response reduction factors for strength and ductility are calculated as shown in Table 3.7.

Table 3.7 Base shear modification factors, 2-story building.

Newhall Fire Station (Northridge, 1994) Ground Motion		
Building Direction	**Transverse (E-W)**	**Longitudinal (N-S)**
Design Strength (V_d) UBC '97, $R = 5.5$	246 Kips	246 Kips
Maximum Strength ($R_s V_d$) (In-plane shear strength)	564 Kips	1,009 Kips
R_s	2.3	4.1
Required Elastic Strength ($R_\mu R_s V_d$)	1,932 Kips	1,690 Kips
R_μ	3.4	1.7
Design Strength (V_d) UBC '73	223 Kips	258 Kips
Maximum Strength ($R_s V_d$)	564 Kips	1,009 Kips
R_s	2.53	3.91
Required Elastic Strength ($R_\mu R_s V_d$)	1,932 Kips	1,690 Kips
R_μ	3.4	1.7

As mentioned previously for the three-story building, the lateral resistance is a function of the length of the structural walls used in each direction and may be more of an architectural consideration than a strength consideration. This can result in a substantial variation in the over-strength factor. It can be seen that as the overstrength factor is reduced, the ductility factor will have to be increased and visa-versa. The ductility factors calculated in Table 3.7 have values of 1.7 and 3.4, respectively. It should be noted that this example is based on the in-plane shear strength of the structural walls that has the same value for both building codes, since minimum steel reinforcement was used in both cases. Hence the maximum base shear strengths and the ductility factors are the same; however, the overstrength factors depend upon the code requirement considered. The performance of the building may be controlled by some other failure mechanism such as diaphragm shear, wall flexure, or diaphragm connection to the walls. The strength of the structure can be evaluated by using a nonlinear pushover analysis that considers all possible failure mechanisms.

3.10 DIAPHRAGM FLEXIBILITY

3.10.1 UBC 1997 Flexible Diaphragm Requirement

Paragraph 1630.6 of the 1997 Uniform Building Code indicates that, *"Diaphragms shall be considered flexible for the purposes of distribution of story shear and torsional moment when the maximum lateral deformation of the diaphragm is more than two times the average story drift of the associated story."* Equation (3.24) is an expression of this code condition.

$$1997\,\text{UBC}: \quad \frac{\text{maximum lateral deformation of diaphragm.}}{\text{average associated story drift}} > 2 \tag{3.24}$$

This ratio can be determined as the difference between the maximum lateral in-plane displacement of the diaphragm relative to the average story drift of the adjoining vertical resisting elements (walls).

3.10.2 UBC 1997 Flexible Diaphragm Verification

Verification of diaphragm flexibility was conducted by comparison of the midspan and corresponding support displacement of the roof and second-floor diaphragms in the N-S and E-W building directions. Displacement time history results for the desired locations along the diaphragm were obtained using the ETABS linear elastic mathematical model subjected to the recorded base motions during the Loma Prieta earthquake. This ground motion has a recorded peak base acceleration of 0.20g. Separate flexibility analyses were conducted using both static equivalent lateral loads as per 1997 UBC, and using dynamic time history analysis results. As mentioned previously for the three-story building, the 1997 UBC criteria for considering a diaphragm as flexible or rigid is based on a static analysis with lateral loading applied independently in each of the two principal directions.

3.10.2.1 Static Loading

Diaphragm flexibility under static loading was studied by considering the behavior of the two-story building under the 1997 UBC inverted triangular static equivalent lateral load pattern in the N-S and E-W building direction separately. The load patterns used were generated with the ETABS 1997 UBC automatic lateral-load-generating option, and were applied to the building through its center of mass parallel to the N-S and E-W building directions**.** Figures 3.27 and 3.28 show the deflected shapes of the roof diaphragm of the two-story building when subjected to this static loading in the E-W and N-S directions, and Figures 3.29 and 3.30 show the deflected shapes of the second-floor diaphragm when loaded in the E-W and N-S directions. It is clear from these diagrams that the roof diaphragm appears to exhibit larger deformation toward the center as compared to its counterpart for the second floor.

Diaphragm flexibility was evaluated in both directions. To compute the displacement ratio for comparison with the 1997 UBC code criteria for the E-W direction, the maximum lateral deformation of the diaphragm was taken to be the difference between the displacement at the middle of the diaphragm and its vertical supporting elements (i.e., the average displacement of the supporting walls in the E-W direction). For the N-S direction, maximum lateral deformation was the difference between the "unsupported" edge of the diaphragm and the average displacement of the supporting walls in the N-S direction. Additionally, for either direction, the "average associated story drift" was taken as the average interstory drift of the vertical walls in the direction under consideration.

In order to calculate numeric ratios for comparison using the ETABS analytical results, it was necessary to compute the ratios at defined points along the wall and diaphragm. The points used for ratio calculation are shown schematically in plan views of the roof and second floor of the building in Figure 3.31.

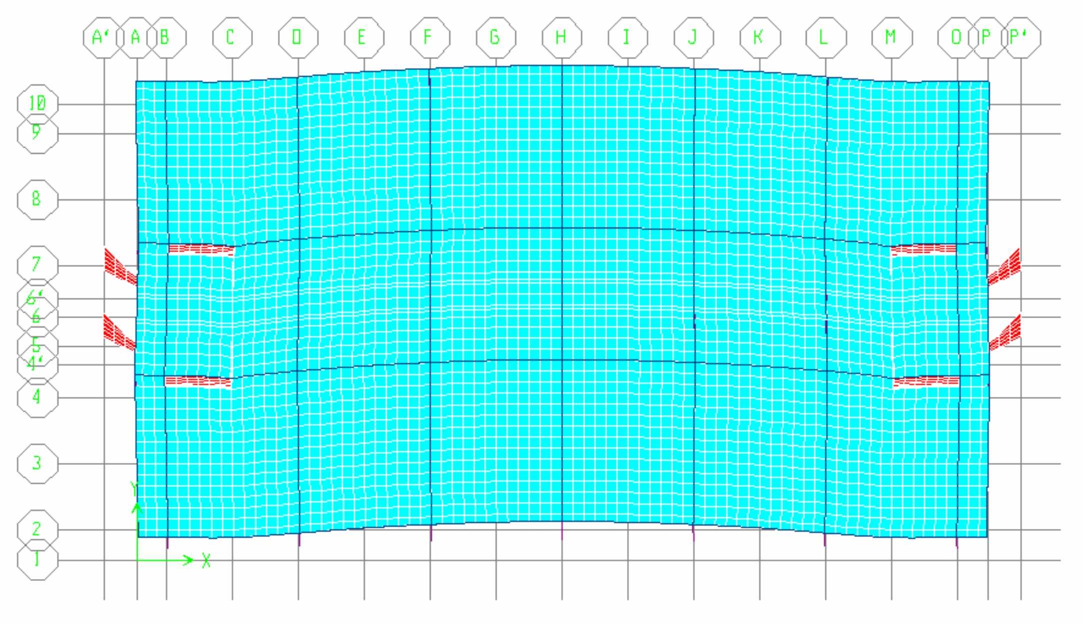

Figure 3.27 E-W deformed shape, '97 UBC static loads, roof, 2-story building.

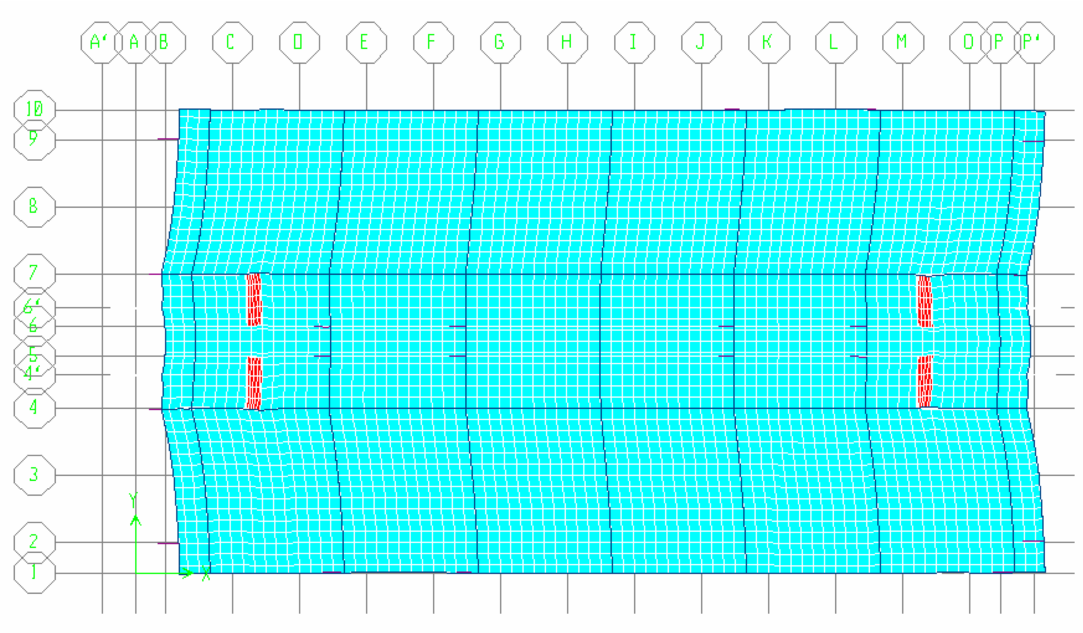

Figure 3.28 N-S deformed shape, '97 UBC static loads, roof, 2-story building.

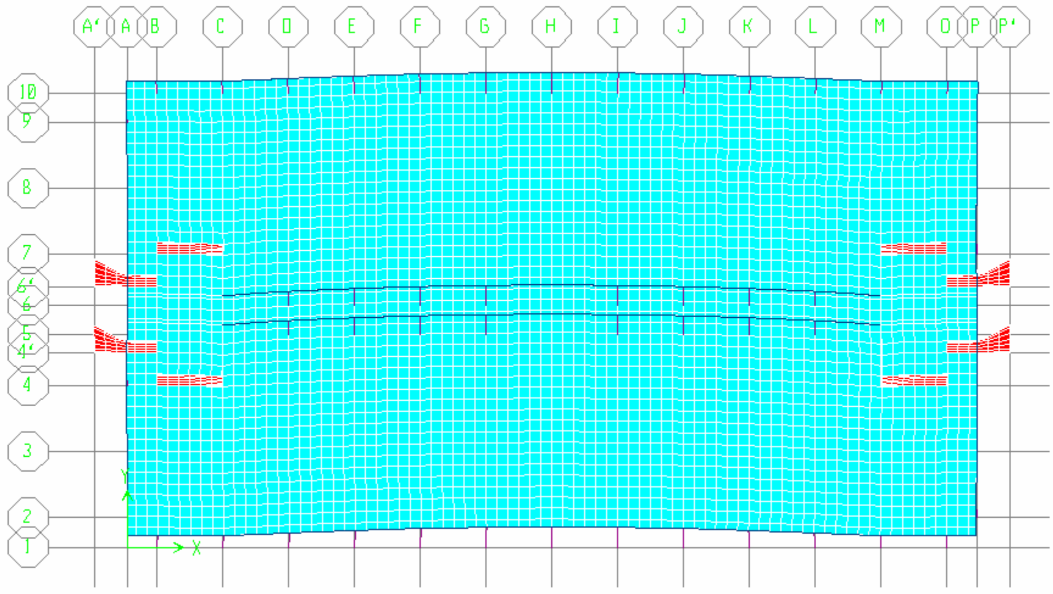

Figure 3.29 E-W deformed shape, '97 UBC static loads, 2^{nd} floor, 2-story building.

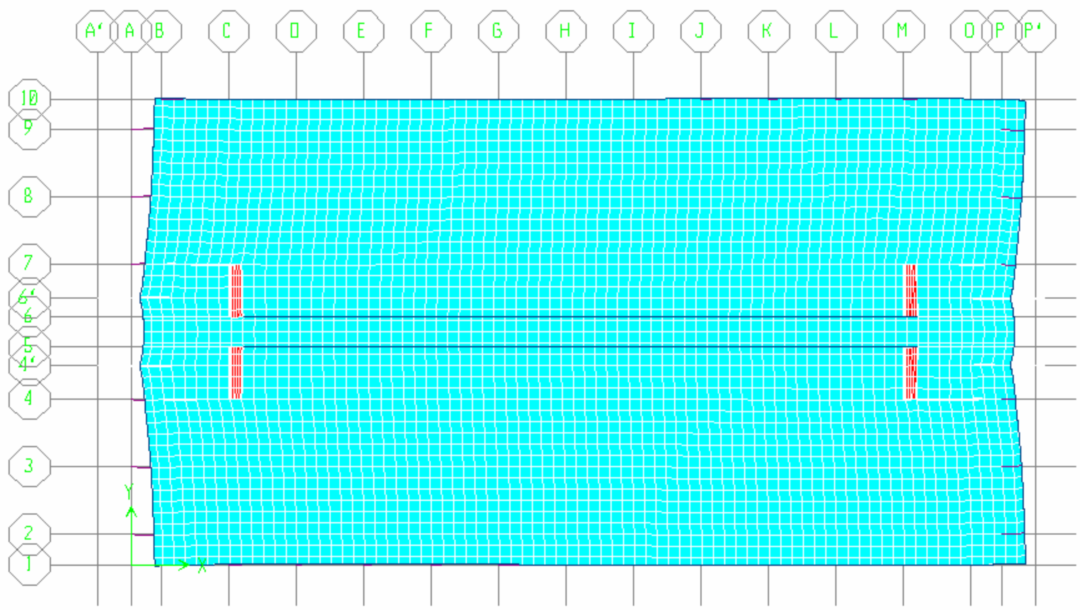

Figure 3.30 N-S deformed shape, '97 UBC static loads, 2^{nd} floor, 2-story building.

To compute the displacement ratio for the code criteria for the roof diaphragm in the E-W direction, which has wall supports at each end, the maximum lateral deformation was assumed to occur at midspan between the two end supports. The maximum absolute displacement of the diaphragm, relative to the base, was obtained from sensor 5 at the roof level. Since there were no instruments on the second-floor level, it was necessary to use predicted displacement data from the time history analysis at the location corresponding to sensor 4 on the roof. This point is shown as Y in Figure 3.31. Taking the difference in displacement between sensor 5 and the average displacement at sensors 4 and 6 produced the maximum displacement of the roof diaphragm. The drift of the vertical supporting elements was obtained by taking the drift at the roof (sensor 4) minus the drift at the second floor (point Y). A similar procedure was followed for the second floor using data points A and Y.

In the N-S direction, only one sensor (7) was located at the center of the roof in this direction. In this case, calculated data points at the second level, B and X, corresponding to locations W and Z at the roof level were required as shown in Figure 3.31. These data points were used to calculate the displacement ratios in the N-S direction for the roof and second-floor levels following the procedure discussed for the E-W direction.

The displacement ratios representing the code criteria for diaphragm flexibility for the roof and second-floor diaphragms are shown in Table 3.8 for static loading in the N-S and E-W directions. These results indicate that the code displacement ratios for the roof and second-floor diaphragms in both the N-S and E-W are less than 2, indicating a rigid diaphragm by 1997 UBC criteria.

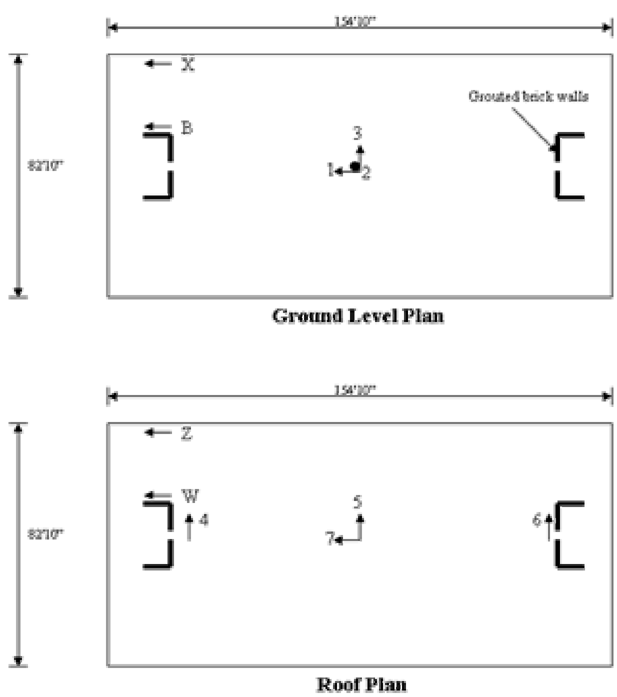

Figure 3.31 Diaphragm flexibility verification locations, 2nd floor and roof diaphragms, 2-story building.

Table 3.8 Diaphragm flexibility verification, '97 UBC static loading, 2-story building.

Static Displacements				
Floor	**Diaphragm orientation**	**Maximum diaphragm deformation** Δ_{max} (inches)	**Corresponding average associated story drift** Δ_0 (inches)	**1997 UBC Code Ratio** Δ_{max}/Δ_0 (inch/inch)
Roof	E-W	0.1909	0.1144	**1.67**
	N-S	0.0779	0.0588	**1.32**
2nd	E-W	0.1101	0.1143	**0.96**
	N-S	0.0470	0.0538	**0.87**

**Note: Static loading in N-S and E-W directions applied separately.

3.10.2.2 Dynamic Loading

The predicted displacement response of the two-story building during the Landers earthquake was used to compute the flexible diaphragm criteria again at the roof and second-floor levels in the N-S and E-W directions. In contrast to the static loading case, the dynamic loads were applied simultaneously to the structure as two acceleration time histories at the base in the N-S and E-W directions. Since the displacements at a data point varied with time, the ratio representing the code criteria was computed at the instant of maximum midspan displacement determined from the time history analyses. After this preliminary, the computations were identical to those performed for the static loading case.

Time history plots of the displacements relative to the base of the structure at the midspan and support locations of the roof and second-floor diaphragms in the E-W direction, obtained using the ETABS mathematical model, are shown in Figures 3.32 and 3.33. Magnified views of the comparison for both diaphragms are shown in Figures 3.34 and 3.35. The magnified view of the diaphragm to support relative displacements in the E-W direction shows that the period of oscillation of the displacement response is approximately 0.32 sec, which is in agreement with the E-W translational period obtained from the dynamic modal analyses. These time histories clearly show that the roof and second-floor diaphragms in the E-W direction behave in a flexible manner, as the center of the diaphragm displaces substantially more than the supporting wall.

The time history comparison of the relative displacement at data point W and point Z on the roof diaphragm in the N-S direction is shown in Figure 3.36. A similar comparison for location B and point X for the second-floor diaphragm is displayed in Figure 3.37. Magnified views for both cases are subsequently shown in Figures 3.38 and 3.39. The magnified view of the diaphragm displacement time history comparison verifies that the period of the building in the N-S direction is approximately 0.2 sec, as computed using modal analyses. It can be seen that even in the N-S direction, both the roof and second-floor diaphragms do not behave rigidly, as the "free" end displaces significantly more than the supported end.

The results of the calculated flexibility ratios for the dynamic loading case are summarized in Table 3.9 and indicate that the relative displacement ratios for both the roof and second-floor diaphragms are all under 2, thus implying that all the diaphragms in this building may not be classified as flexible according to the 1997 UBC criteria.

For the two-story building, the results obtained using both static and dynamic analyses indicate that the diaphragms at the second floor and roof should not be considered as flexible according to the code displacement criteria.

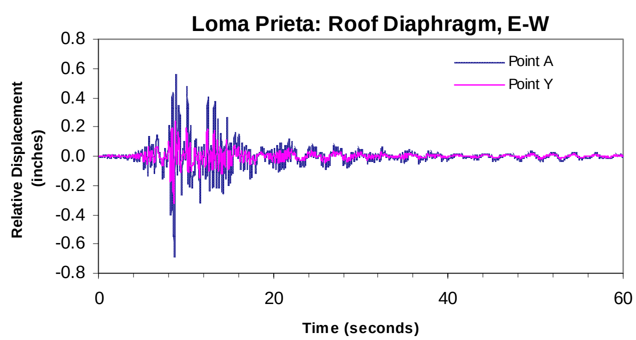

Figure 3.32 E-W midspan vs. support relative displacements, roof, 2-story building.

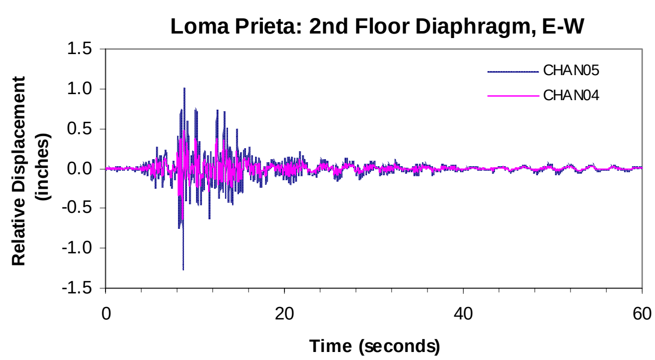

Figure 3.33 E-W midspan vs. support relative displacements, 2nd floor, 2-story building.

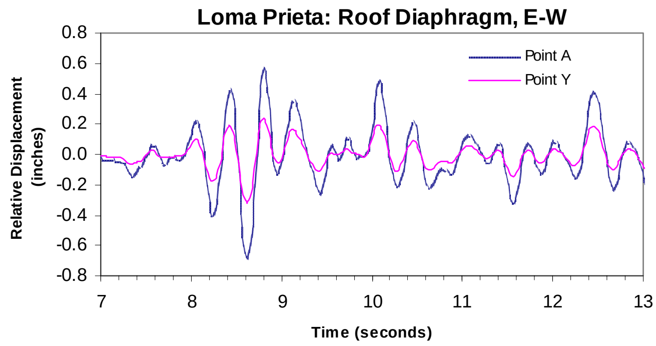

Figure 3.34 E-W midspan vs. support relative displacements (magnified), roof, 2-story building.

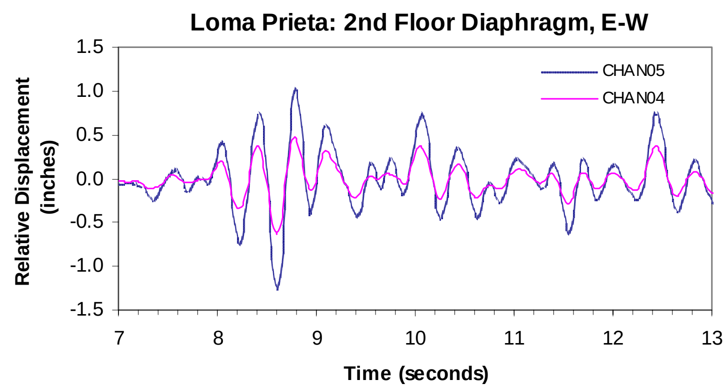

Figure 3.35 E-W midspan vs. support relative displacements (magnified), 2nd floor, 2-story building.

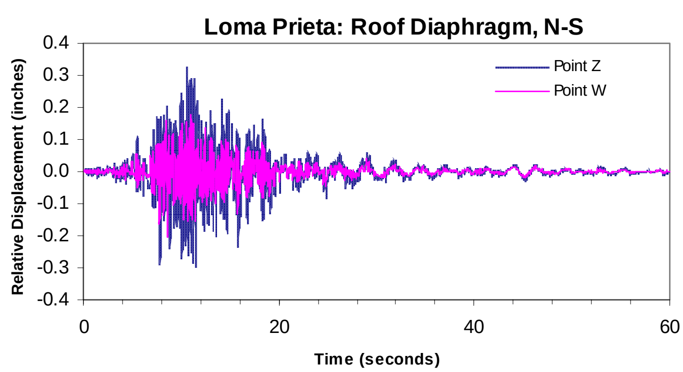

Figure 3.36 N-S midspan vs. support relative displacements, roof, 2-story building.

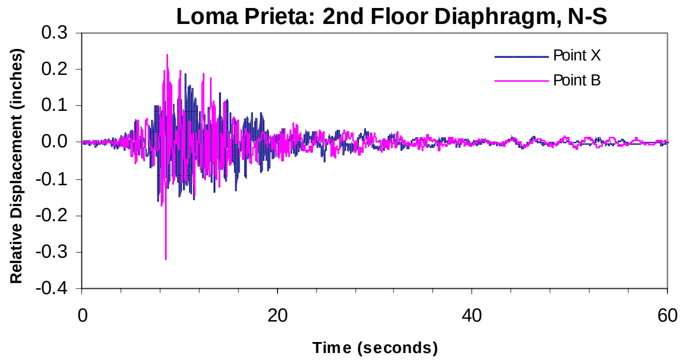

Figure 3.37 N-S midspan vs. support relative displacements, 2^{nd} floor, 2-story building.

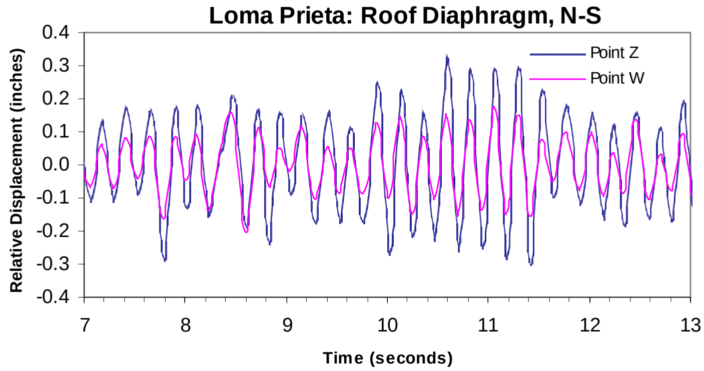

Figure 3.38 N-S midspan vs. support relative displacements (magnified), roof, 2-story building.

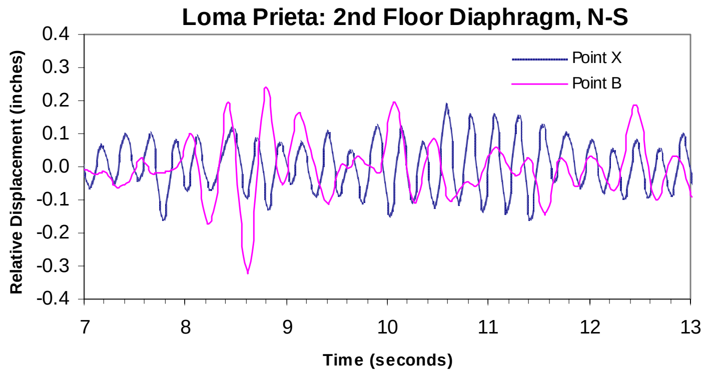

Figure 3.39 N-S midspan vs. support relative displacements (magnified), 2^{nd} floor, 2-story building.

Table 3.9 Diaphragm flexibility verification, dynamic loading, roof and 2nd floor diaphragms, 2-story building.

Dynamic Loading					
Floor	Diaphragm orientation	Maximum diaphragm deformation Δ_{max} (inches)	Time of maximum deformation t_{max} (seconds)	Corresponding average associated story drift Δ_0 (inches)	1997 UBC Code Ratio Δ_{max}/Δ_0 (inch/inch)
Roof	E-W	-0.6446	8.60	-0.3122	**2.06**
	N-S	0.1801	10.60	0.0704	**2.56**
2nd	E-W	-0.3701	8.58	-0.3063	**1.21**
	N-S	0.1112	10.58	0.0785	**1.42**

**Note: Dynamic loading in N-S and E-W directions applied simultaneously.

3.10.3 Maximum Absolute Column Shears (Lucerne Record)

Due to the small size of the shear walls relative to the outside building dimensions, it is suspected that the columns will take a large portion of the shear demand imposed on them during an earthquake. Thus, the column shear demands in the two-story building were studied for one of the stronger ground motion records, the Lucerne record. From the linear dynamic time history results from the two-story building for the Lucerne record, the maximum absolute column shears were found for all first-story exterior and interior columns. Figure 3.40 shows the column callout of all exterior and interior columns in the two-story building. Table 3.10 is a summary of the maximum absolute first-story column shears using the two components of the Lucerne ground motion.

The maximum absolute value of total base shear demand for the two-story building for the Lucerne record in the N-S and E-W directions, obtained from linear elastic analysis, was 1367.0 kips and 709.9 kips, respectively. Table 3.10 shows that the total of the maximum absolute interior column shears is 3.18 kips and 5.32 kips in the N-S and E-W directions, respectively. Likewise, the total of the absolute maximum for the exterior columns are 31.84 kips and 94.14 kips for the exterior columns in the N-S and E-W directions. Therefore, the percentage of the maximum base shear resisted by the interior columns is 0.23% and 0.75% in the N-S and E-W directions. Similarly, the exterior columns resist 2.3% and 13.3% in the N-S and E-W directions. Thus, it may be concluded that the shear walls resist the majority of the total base shear in both the N-S and E-W directions. Also, it is recognized that adding the maximum absolute values of the column shears may exhibit excessive overconservatism, considering that the maximum may not occur at the exact same time in the time history record.

Table 3.10 N-S and E-W maximum absolute column shears, Lucerne, 2-story building.

Summary of Exterior Column Shears (LUCERNE record)		
Exterior Column Designation	V_{NS} (kips)	V_{EW} (kips)
C1	0.38	4.71
C2	0.52	6.71
C3	0.40	7.93
C4	0.63	7.93
C5	0.52	6.71
C6	0.54	4.71
C7	0.82	4.09
C8	0.84	5.62
C9	0.79	8.95
C10	0.76	5.62
C11	0.80	4.09
C12	0.87	2.61
C13	0.72	2.61
C14	0.72	1.29
C15	0.38	0.68
C16	0.82	0.38
C17	0.52	0.53
C18	0.84	1.83
C19	0.40	0.34
C20	0.79	0.29
C21	0.63	0.34
C22	0.76	1.83
C23	0.52	0.53
C24	0.80	0.38
C25	0.54	0.68
C26	0.87	1.29
C27	2.51	0.68
C28	0.23	1.18
C29	0.65	0.96
C30	0.65	0.92
C31	0.23	1.14
C32	2.51	0.85
C33	2.53	0.68
C34	0.82	1.18
C35	0.59	0.96
C36	0.59	0.92
C37	0.82	1.14
C38	2.53	0.85
TOTALS	31.84	94.14

Summary of Interior Column Shears (LUCERNE record)		
Interior Column Designation	V_{NS} (kips)	V_{EW} (kips)
C40	0.16	0.38
C41	0.24	0.42
C42	0.14	0.47
C43	0.51	0.47
C44	0.10	0.42
C45	0.19	0.38
C46	0.18	0.30
C47	0.14	0.23
C48	0.16	0.29
C49	0.24	0.35
C50	0.14	0.37
C51	0.51	0.37
C52	0.10	0.35
C53	0.18	0.23
C54	0.19	0.29
TOTALS	3.18	5.32

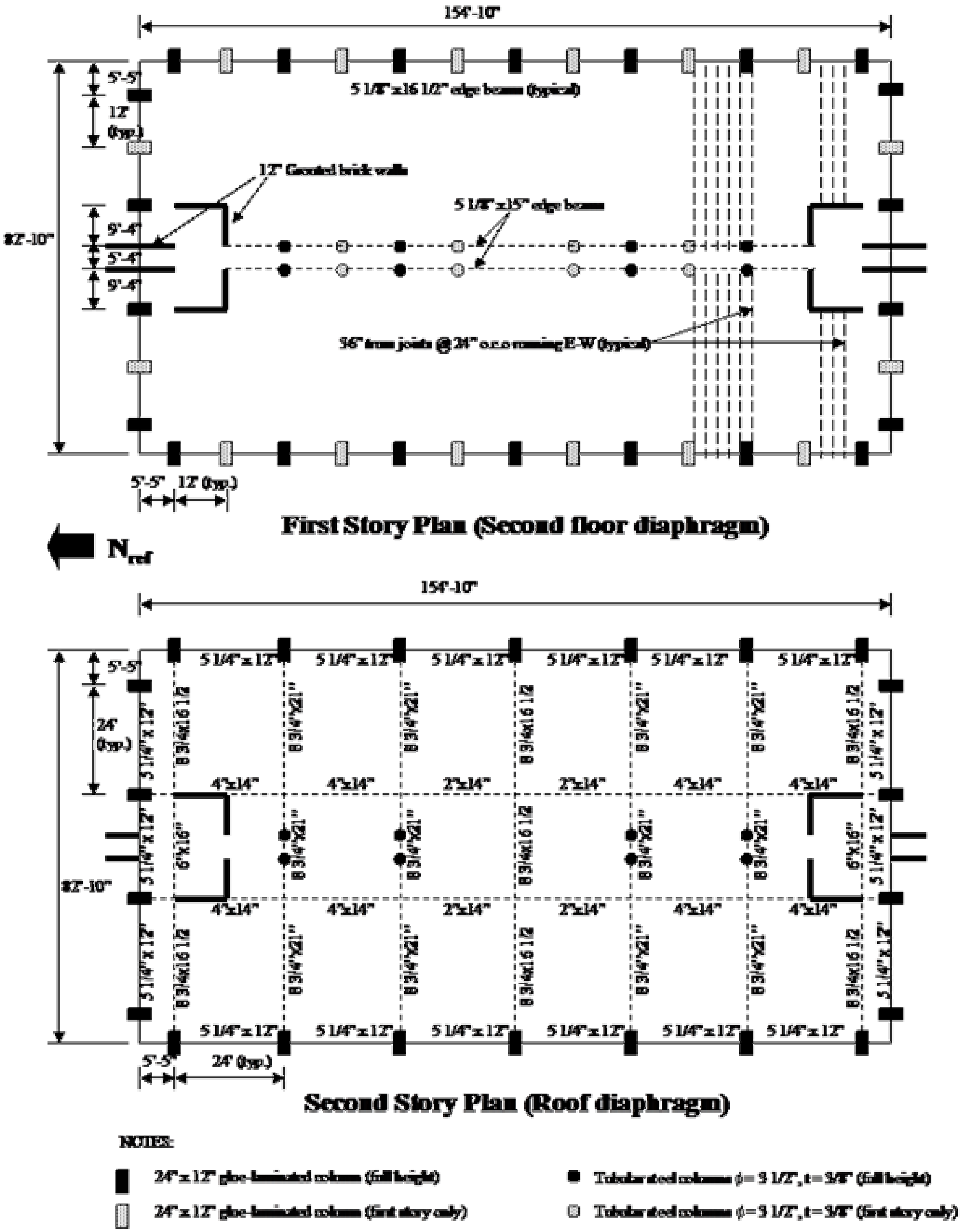

Figure 3.40 Column designations, 2-story building.

3.11 SUMMARY AND CONCLUSIONS FOR THE TWO-STORY BUILDING ANALYSES

3.11.1 Summary

The two-story masonry building has recorded the response from one major earthquake. Spectral analyses of the recorded data indicate that the period of the fundamental translation modes in the N-S and E-W directions are 0.22 sec and 0.28 sec, respectively. The results obtained from the three-dimensional ETABS model of the building indicated corresponding values of 0.23 sec and 0.35 sec. Comparison of the recorded response at all instrument locations shows a good correlation with the time history response calculated using the computer model and the idealizations discussed previously. Comparison of the time history of the calculated base shear with the base shear requirements of the building code indicates that the response was less than the minimum code requirements for the recorded earthquake. Strong motion analyses using an additional 4 ground motion records show that the wall capacity values are greatly exceeded for a limited number of cycles, which could potentially result in nonlinear behavior of the structure.

3.11.2 Conclusions

The main conclusions that can be reached from the results obtained for the two-story building are the following:

1. Careful modeling of geometry, element properties and material properties along with the use of a three-dimensional model that includes the orthotropic stiffness properties of the diaphragm, can accurately simulate the elastic seismic response of masonry buildings. This was verified by critical comparison with the response measured in an instrumented building.
2. For purposes of comparison, the in-plane shear capacity of the structural walls has been used as an indication of capacity. However, the actual capacity of the building may be controlled by the in-plane shear capacity of the diaphragm, the connections of the diaphragm to the walls, or the out-of-plane moment capacity of the walls. This aspect will require further study.
3. For the two-story building, the value of the code displacement criteria for evaluating diaphragm flexibility did not depend on the loading method (i.e., static vs. dynamic). All calculated displacement ratios using both static and dynamic loading were less than 2 and

yielded the result that the roof and second-floor diaphragms may not be considered to be flexible. This result was different for that observed for the three-story building.

4. The strength capacity in the E-W direction is approximately half of that in the N-S direction, making the building more vulnerable to E-W ground motion. This is not the intent of the code requirements.

4 One-Story Building: San Francisco

4.1 BUILDING DESCRIPTION

4.1.1 General

The third building under investigation in this study is a one-story substation building designed in 1971 in San Francisco. Plan and elevation views giving the overall dimensions of the structural framing elements are shown in Figure 4.1. Details of the diaphragm to wall connections are shown in Figures 4.2–4.5. Locations of various connection details, relative to the plan view of the one-story building are shown in Figure 4.2. Figures 4.3 and 4.4 show the connection details of the lower and upper E-W (longitudinal) walls to the roof diaphragm, respectively (i.e., sections 1 and 2). Similarly, Figure 4.5 is the connection detail of a N-S (transverse) wall to the roof diaphragm (section 3). The transverse dimension of the building is oriented in the N-S direction, and the longitudinal dimension of the building is oriented in the E-W direction. The building is rectangular in shape, with four exterior concrete masonry shear walls, which are designed to carry both lateral and gravity loads. Horizontal loads are carried in the floor system by means of a flexible steel T-deck diaphragm, connected to the concrete walls by means of a series of steel plates and welds. The building foundation consists of continuous reinforced footings that extend under the structural walls at the two ends of the building.

4.1.2 Diaphragms

The roof diaphragm of the one-story substation building consists of a 6″-18 ga. "Inland T Deck" with a yield stress of f_y = 36 ksi. The ribs of the deck span in the transverse (N-S) dimension of the building. The aspect ratio of the diaphragm (length/width) is approximately 32′-8″/22′ = 1.48.

4.1.3 Grouted Walls

The one-story building has 8″ thick concrete block walls on all four sides, which comprise the lateral-force-resisting system of the building in both orthogonal directions. All reinforcing was ASTM A-615 grade 40 steel (f_y = 40 ksi). Typical flexural vertical reinforcing in the block walls is 1-#4 at 16″ o.c., and typical horizontal shear reinforcing is 2-#4 at 16″ o.c. The minimum concrete compressive strength of the concrete block walls is f'_c = 2,500 psi at 28 days. The concrete block was open-end grade "A" units in common bond construction with solid grout. Concrete blocks were jointed with a mortar of type "S" with minimum compressive strength of 2,000 psi at 28 days.

4.1.4 Connection between Diaphragms and Walls

The roof diaphragm in the N-S direction has a gentle slope with one end of the deck raised 4″ above the level of the deck at the opposite end. At the higher end of the deck (north wall) the ribs of the T-deck are cradled inside and fillet welded to a 3 x 3 ½ x ¼″ angle that is welded to the top leg of a 3 x 3 x ¼″ angle as shown in Figure 4.4 (sect. 2). The 3 x 3 x ¼″ angle is connected to a 2″ corbel cut into the 8″ masonry wall using ¾″ of grout and ½″ ϕ steel bolts at 32″ on center. At the lower end of the deck along the south wall, the ribs of the deck sit inside a 3 x 3 x ¼″ angle running parallel to the length of the wall as shown in Figure 4.3 (section 1). The horizontally oriented leg of the angle is connected to the wall by ¾″ of grout sitting on a 2″ corbel in the wall, with the vertical leg of the angle bolted to the wall with ½″ ϕ steel bolts at 32″ on center. In the N-S direction, the ribs of the deck run parallel to the length of the walls at the east and west ends of the building. At each of these walls, the bottom of a single deck rib sits on a 6 x ¼″ plate with ½″ ϕ x 12″ anchors at 32″ o.c. as shown in Figure 4.5 (section 3).

4.1.5 Foundation System

The slab on grade is a 6″ thick reinforced concrete slab utilizing a typical reinforcing schedule of 1-#4 at 12″ o.c. in the E-W (longitudinal) direction. The foundation consists of continuous reinforced footings (grade beams) on which the structural masonry shear walls are supported.

The depth of the grade beams is 18″ with a width of 10″, with #3 stirrups at 12″ o.c. and 4-#4 rebars placed in a rectangular formation in the cross section. Engineered fill was used between the slab and foundation of the building.

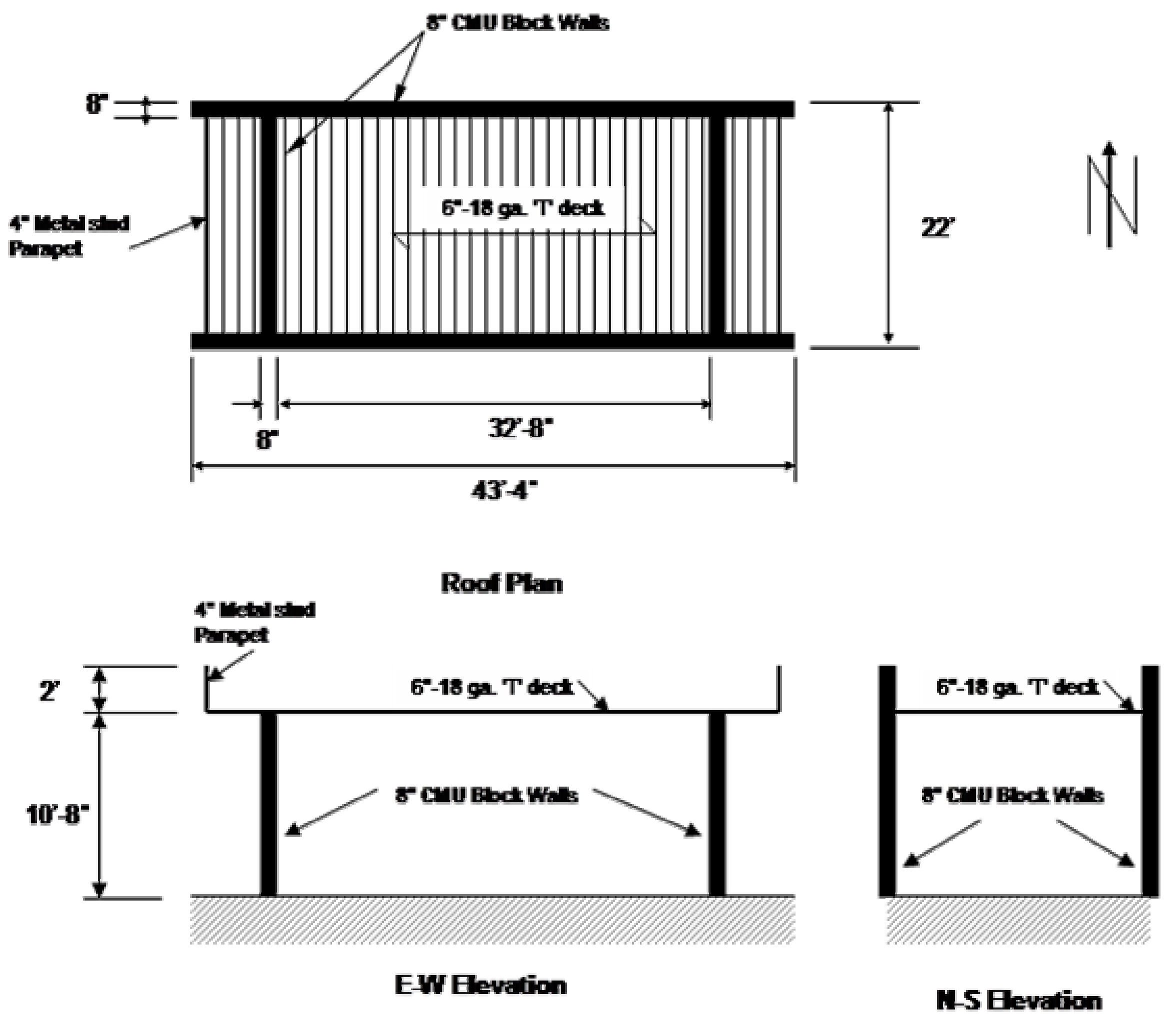

Figure 4.1 Plan and elevation views, 1-story building.

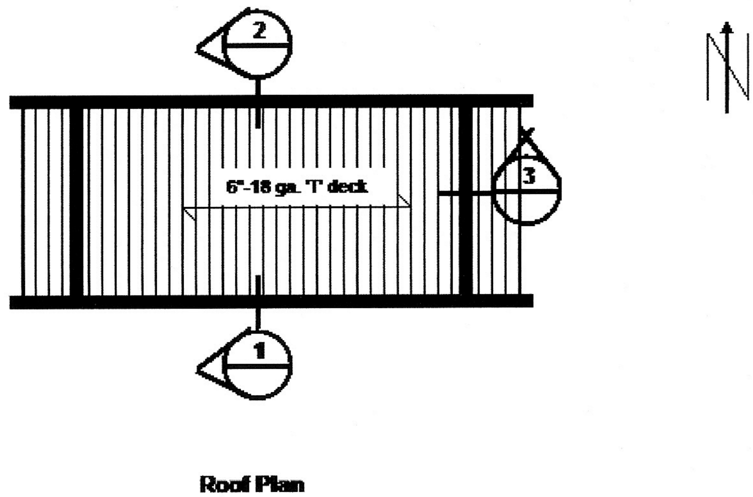

Figure 4.2 Section locations, 1-story building.

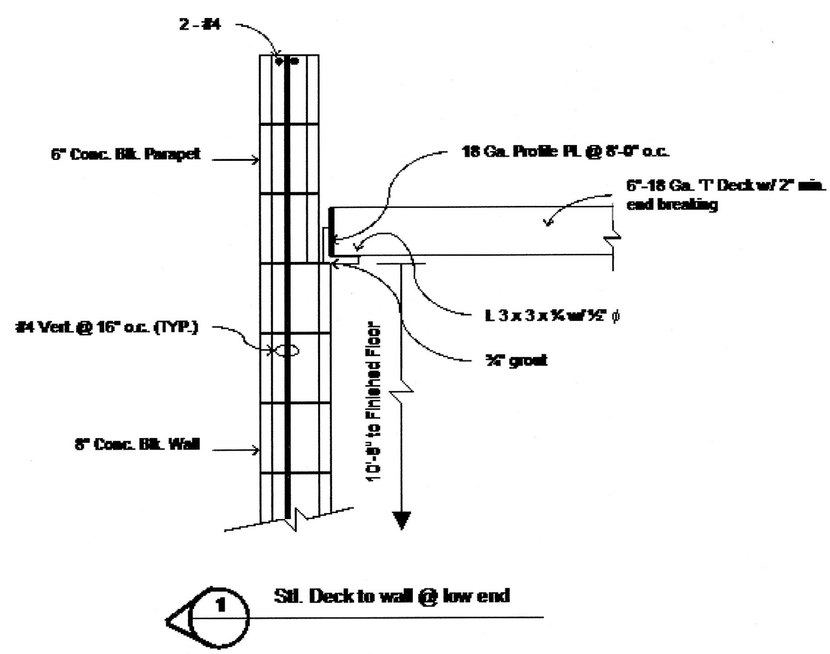

Figure 4.3 Connection details, section 1, 1-story building.

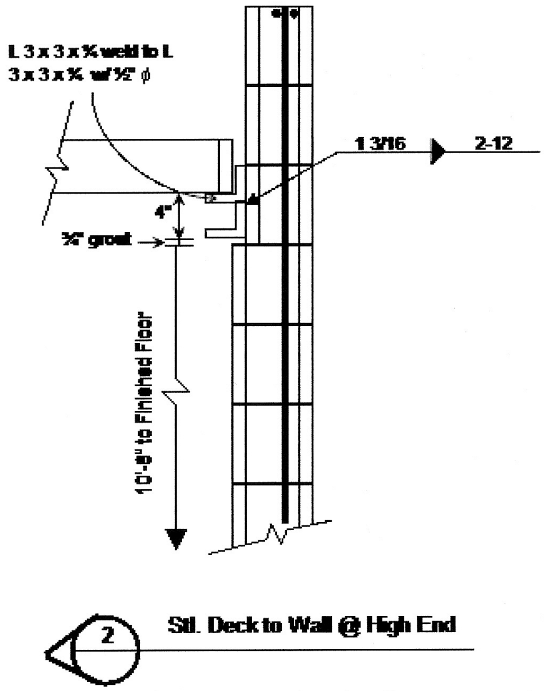

Figure 4.4 Connection details, section 2, 1-story building.

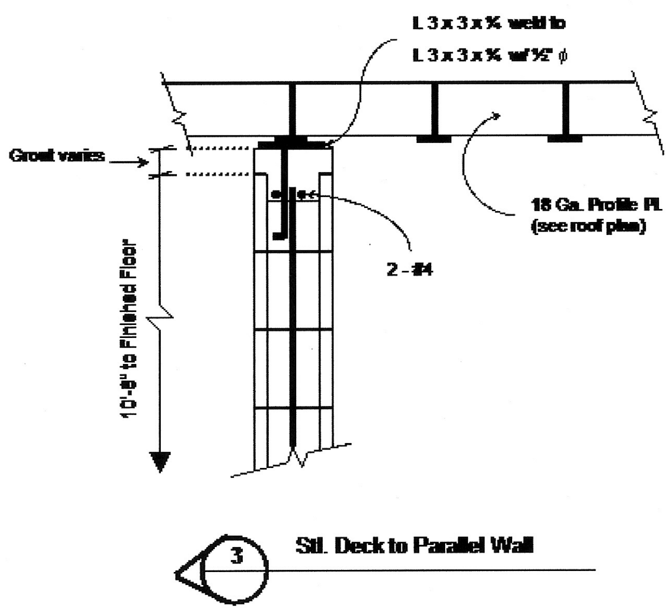

Figure 4.5 Connection details, section 3, 1-story building.

4.2 INSTRUMENTATION AND RECORDED RESPONSE

The one-story building is not instrumented.

4.3 ELASTIC DYNAMIC ANALYSES

4.3.1 Mathematical Model

A three-dimensional linear elastic finite element model using ETABS (version 7) computer software was developed for the one-story substation building. An isometric view of the building model used in the ETABS program is shown in Figure 4.6. The model consists of a total of 274 nodal points and 444 shell elements.

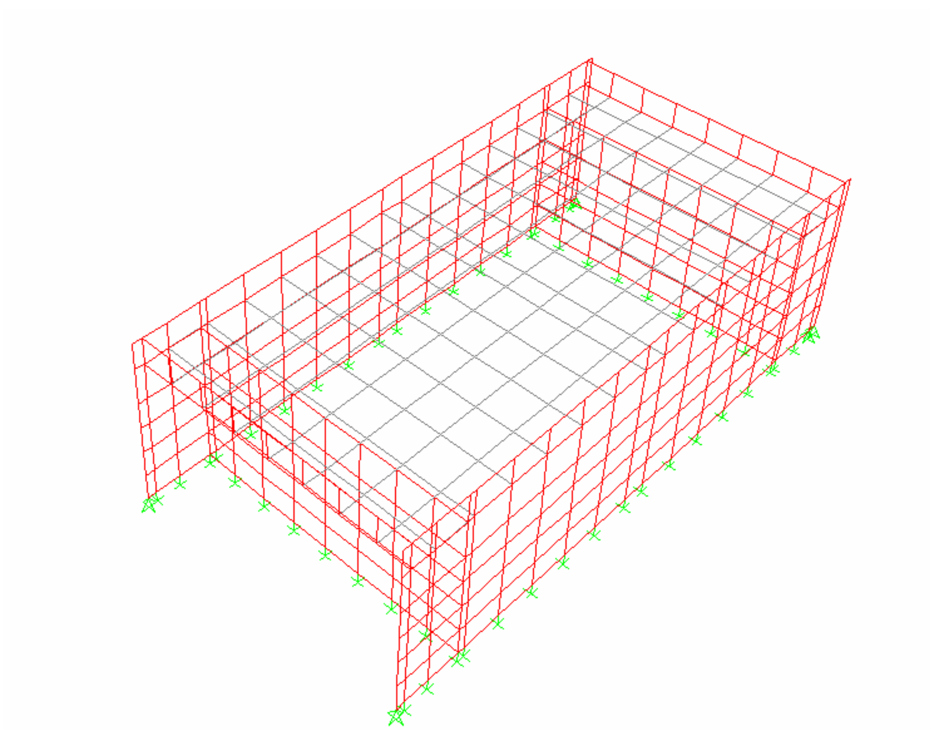

Figure 4.6 3-D linear elastic ETABS model, isometric view, 1-story building.

4.3.1.1 Modeling of Steel Diaphragms

Thick shell elements were used to model the roof diaphragm. These elements were necessary to adequately capture both the translational and flexural movement of the diaphragms. The thick plate option was selected so that the shear deformation of the diaphragm would also be considered. The roof diaphragm is a 18 ga 6″ T-deck. An equivalent diaphragm thickness was calculated for membrane behavior and a similar thickness was calculated to represent flexural behavior, which were the thickness of rectangular sections whose width, area, and moment of inertia were identical to that of the original section. These properties were used in each principal orthogonal direction of the building. For simplicity, the stiffness of the diaphragms in the E-W and N-S directions was taken to be uncoupled.

At the roof level in the N-S (transverse) direction, equivalent shell element thickness was determined based on the 18 ga. 6″ T-deck, with a thickness of 0.05 in. (based on 18 ga. steel). In the E-W (longitudinal) direction, both equivalent bending and membrane thickness were taken as the thickness of the horizontal component of the deck equal to 0.05 in. The calculated equivalent membrane thickness for the roof diaphragm in the E-W and N-S building directions was 0.05 in., and 0.0748 in., respectively. The calculated bending thickness for the roof diaphragm in the E-W and N-S directions was 0.05 in. and 1.27 in., respectively.

For analysis, isotropic material behavior of the steel was assumed. Material properties for the steel material weight and shear modulus were assumed to be $\nu=0.3$ and $\gamma=2.83 \times 10^{-4}$ k/in^3. Additionally, a modulus of elasticity of 29,000 ksi was used in the analysis.

4.3.1.2 Modeling of Masonry Shear Walls

Thick plate shell elements were used to model the 8″ concrete block shear walls. For calculation of the equivalent shell element thickness for flexural behavior and membrane action of the masonry shear walls, cracking of the wall section was assumed and was computed based on the effective cracked section thickness for a rectangular section under bending. In doing so, application of the effective cracked section thickness for a reinforced concrete section was assumed even though the section was reinforced masonry (i.e., $t_{eff} = 0.35t_{orig}$ as discussed previously). Thus, the membrane and bending thickness for the shell elements used to model the shear wall was taken to be 2.8″ for the 8″ walls. However, the weights of the walls used in the model were based on the original dimensions of the walls.

Isotropic material behavior was assumed for the concrete shear walls. The compressive strength of the concrete was specified as $f'_c = 2500\,\text{psi}$. Therefore, the modulus of elasticity for the concrete walls was calculated using Equation (4.1), and computed to be equal to 2850 ksi.

$$E = 57\sqrt{f'_c} \qquad (4.1)$$

Poisson's Ratio for masonry was assumed to be 0.2, and the shear modulus was calculated internally by ETABS to be G = 1188 ksi, using Equation (4.2) for an isotropic material.

$$G = \frac{E}{2(1+\upsilon)} \tag{4.2}$$

4.3.1.3 Other Modeling Considerations

The effect of the foundation was not considered in this study, and hence the support conditions for the vertical elements in the model are considered as fully fixed. Also, the finite element mesh used for the roof diaphragm was such that the nodal points common to the walls and the diaphragm were at the centerline of the weld along a particular dimension. The additional mass of the metal stud parapet was not added to the model for simplicity. In addition, all dimensions in the model were considered centerline-to-centerline distances.

4.3.1.4 Weight (Mass) Determination

The weight (mass) at the roof level was estimated, and was needed for future use in computing the design base shear. In the weight estimations, the self-weight of the grouted concrete block masonry walls was assumed to be 120 pcf. All weight calculations were based on plan-view area unit weights and on the outer dimensions of the building. The details of the roof weight (mass) calculations for the one-story building are displayed in Table 4.1.

Table 4.1 Roof weight (mass) calculations, 1-story building.

Component	Assumed Unit Weight	Weight (k)
Roof Steel Decking	7 psf	6
Shear Wall	120 pcf	113
Metal Stud Parapet	7 psf	x
Total Roof Weight		126
Roof Translational Mass		0.326 k-s^2/in

4.3.2 Modal Period Analyses

Using the three-dimensional finite element ETABS model of the one-story building, the mode shapes and frequencies for the first 15 modes were evaluated. The building exhibits double symmetry about both building axes. Accidental torsion is neglected and the torsional mode shape is not shown. The translation mode shapes in the N-S direction obtained from the ETABS model are shown in Figure 4.7 and those obtained in the E-W direction shown in Figure 4.8. The periods of vibration corresponding to the N-S and E-W mode shapes are 0.0501 and 0.0322 sec, respectively.

The translation mode in the N-S direction captures the in-plane bending of the diaphragm with the N-S shear walls acting as fixed diaphragm supports in the horizontal plane. There is little deformation of the diaphragm and the masonry walls in the E-W direction due to the rigidity of the longitudinal walls and the relatively short length of the N-S walls. This is reflected in the mass participation factors, which were calculated to be 58% in the N-S direction and only 16% in the E-W direction. Note that the roof is very lightweight and nearly all of the mass for the building is in the walls. In the E-W direction, the longitudinal walls contain most of the building mass but due to their stiffness, do not participate in the dynamic response. This is reflected in the low mass participation factor in this direction. Possible additional flexibility at the foundation was not considered in this study.

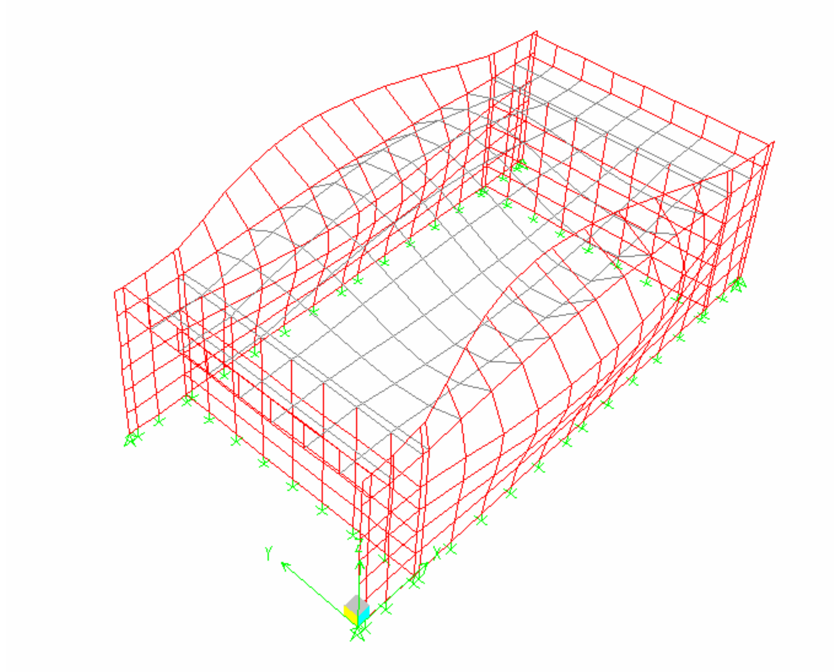

Figure 4.7 Translational mode shape, N-S direction, 1-story building.

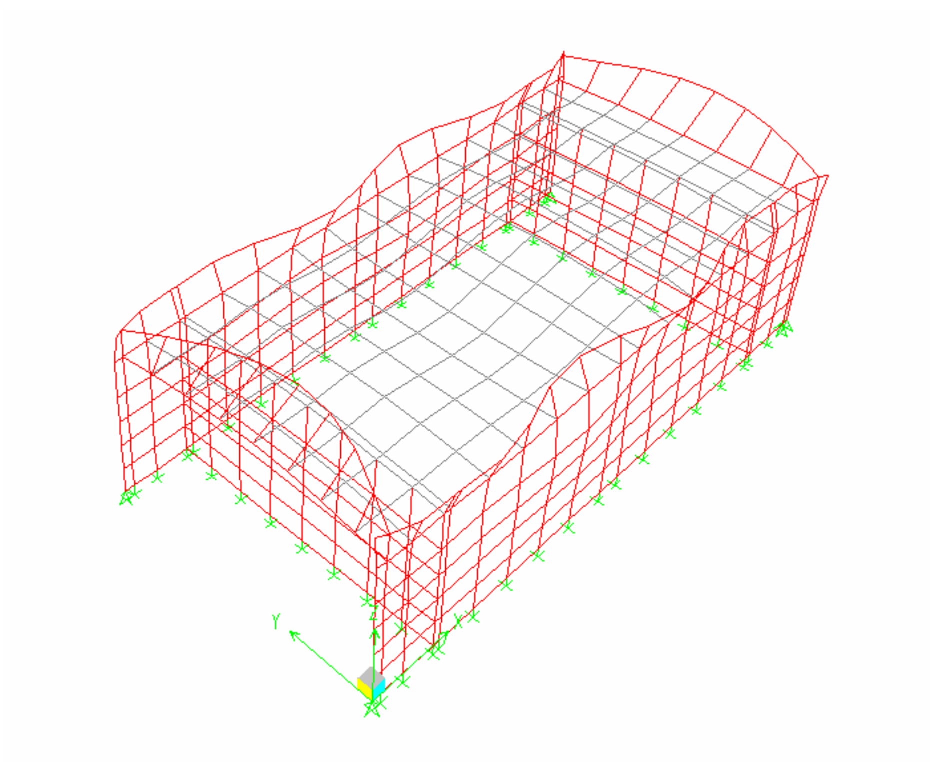

Figure 4.8 Translational mode shape, E-W direction, 1-story building.

4.3.3 Calculated Time History Displacement Response

As previously discussed, there are no recorded data for the one-story building, due to the lack of instrumentation. Thus, no verification of the model using displacement comparisons with recorded data will be presented. However, using the same techniques and modeling assumptions as in the instrumented two- and three-story buildings, the model of the one-story building was developed, and was subjected to an ensemble of earthquake ground motions. The resulting displacement responses are presented. A schematic showing the nodal locations, where the relative displacements will be monitored is shown in a plan view in Figure 4.9. Locations 61 and 68 are on the N-S walls (diaphragm support locations). Locations 28 and 27 are along the E-W walls, and point 221 is at the center of the diaphragm with respect to both directions. Due to the dual symmetry possessed by this building about both principal axes, only the response quantities at points 27 and 61 will be considered. The following sections will summarize the relative displacement time histories (relative to the base) for a support location on the E-W and N-S walls, as well as the relative displacement in the middle of the diaphragm in the N-S and E-W directions.

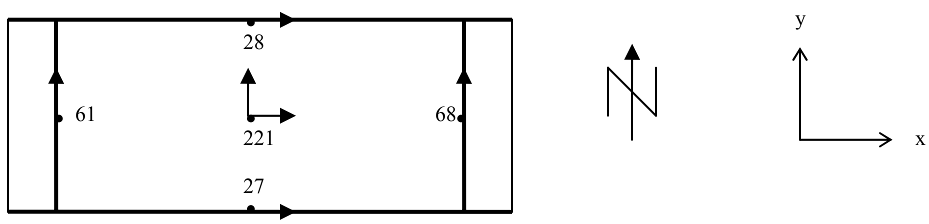

Figure 4.9 Reference points for time history analyses, 1-story building.

Since this building is not instrumented, there is no input base acceleration or recorded response for the building that can be used for analytical investigation. Therefore six ground motions recorded in the free field at other locations were selected for use in this phase of the investigation. The six ground motions used in the study are the following: the two components of ground motion recorded at (1) Lucerne during the 1992 Landers earthquake, (2) Newhall Fire Station during the 1994 Northridge earthquake, (3) Hollywood Storage Lot during the 1952 Kern County earthquake, (4) Hollywood far field (Kern County), (5) Arleta Fire Station record

(Northridge), and (6) Los Gatos Presentation Center (1989 Loma Prieta). The Newhall and Arleta records are two strong motion records obtained during the Northridge earthquake. As mentioned previously for the other buildings, the Lucerne record obtained during the Landers earthquake is considered a one-sided displacement pulse and the Los Gatos Presentation Center record obtained during the Loma Prieta earthquake is considered as having multiple-sided displacement pulses. The two Hollywood records obtained during the Kern County earthquake are minor ground accelerations due to the distance from the epicenter and are considered to be representative of motions in seismic zones of lower risk.

4.3.3.1 Newhall Record (Northridge Earthquake)

Figure 4.9 shows the displacement relative to the base of the structure at the middle of the roof diaphragm (point 221) in the N-S and E-W directions using both components of the Newhall record. Also shown are the relative displacements at the support (wall) locations in the N-S (points 61, 68) and E-W (points 27, 28) directions. Note the changes in the scale due to the small deformations. From Figure 4.10 the maximum E-W displacement in the diaphragm is seen to be only 0.00036 in. compared to a maximum wall displacement of 0.00015 in. In the N-S direction, shown in Figure 4.11, the maximum diaphragm displacement is 0.009 in. and the maximum wall displacement is 0.001 in..

4.3.3.2 Lucerne Record (Landers Earthquake)

Figures 4.12 and 4.13 show the displacement relative to the base of the structure at the middle of the roof diaphragm (point 221) in the E-W and N-S directions using both components of the Lucerne record. Also shown are the relative displacements at the support (wall) locations in the N-S (points 61, 68) and E-W (points 27, 28) directions. From Figure 4.12, the maximum displacement in the diaphragm in the E-W direction is 0.00042 in., whereas the maximum displacement at the wall is 0.00016 in. In the N-S direction, Figure 4.13, the maximum diaphragm displacement is 0.014 in. and the maximum displacement of the wall is only 0.0015 in.

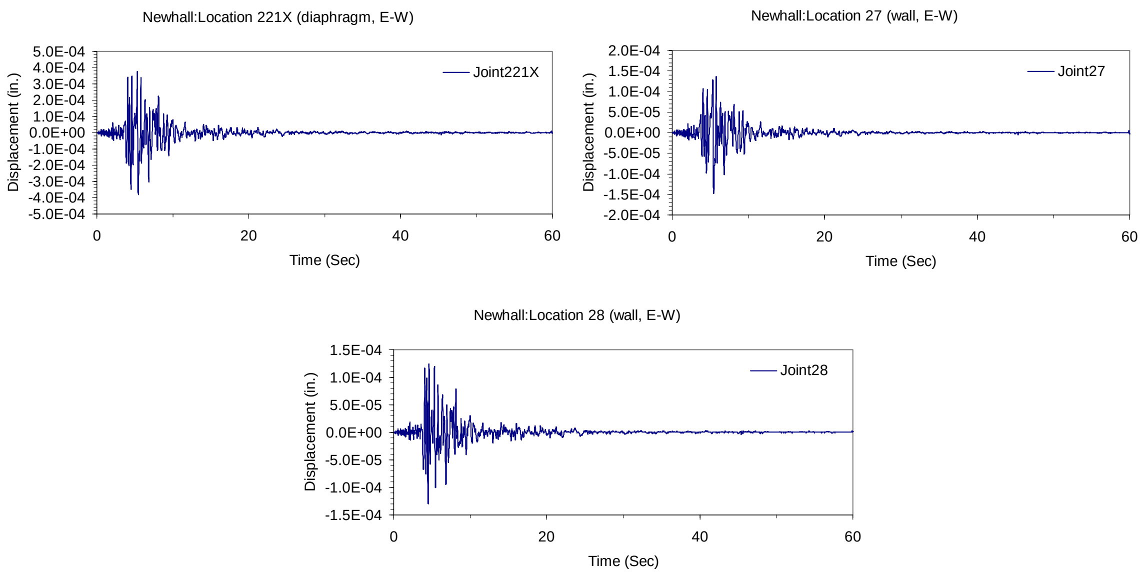

Figure 4.10 E-W diaphragm relative displacement (pt. 221X) and corresponding support displacements (pts. 27, 28), Newhall, 1-story building.

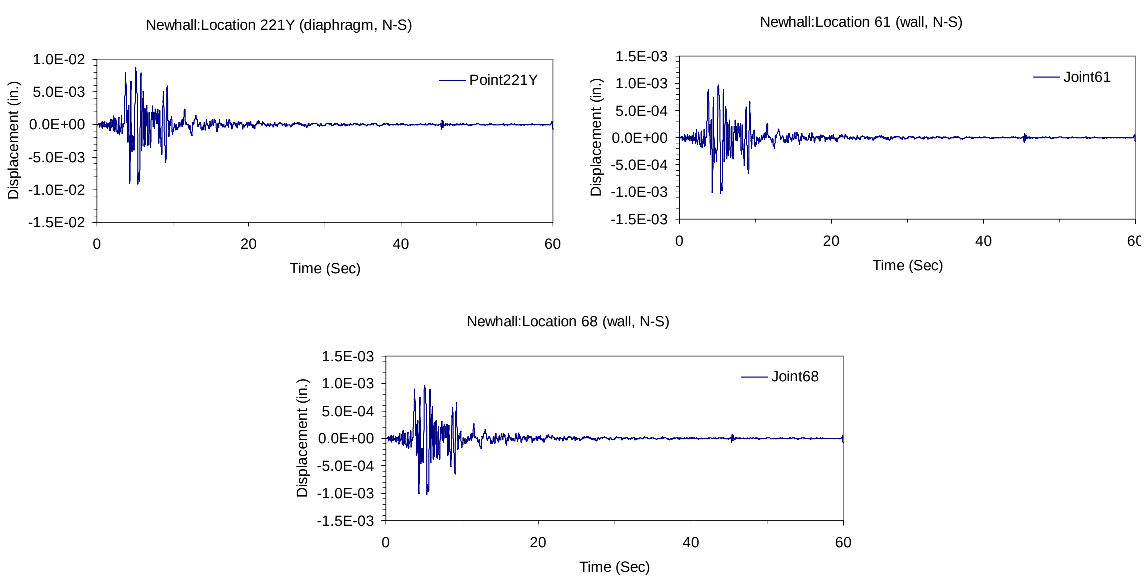

Figure 4.11 N -S diaphragm relative displacement (pt. 221Y) and corresponding support displacements (pts. 61, 68), Newhall, 1-story building.

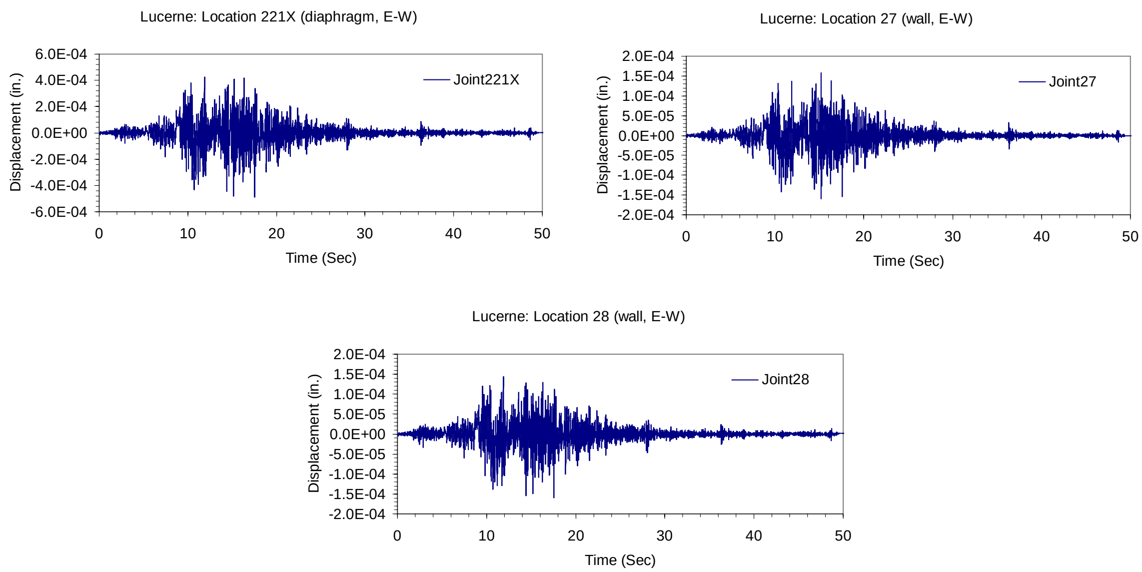

Figure 4.12 E-W diaphragm relative displacement (pt. 221X) and corresponding support displacements (pts. 27, 28), Lucerne, 1-story building.

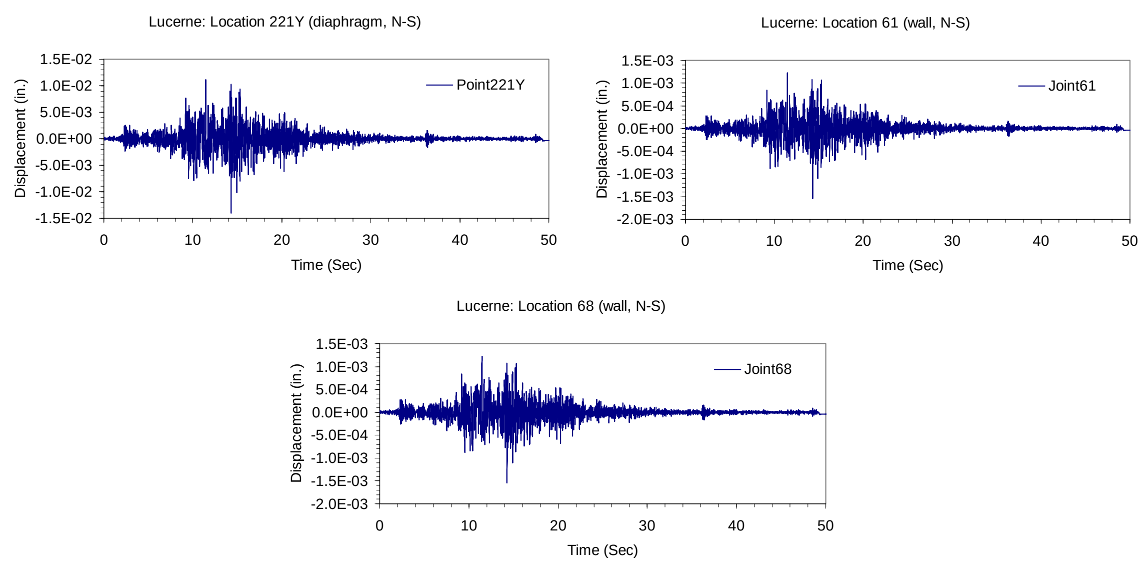

Figure 4.13 N-S diaphragm relative displacement (pt. 221Y) and corresponding support displacements (pts. 61, 68), Lucerne, 1-story building.

4.3.3.3 Arleta Record

The recorded base accelerations at the Arleta Fire Station during the Northridge earthquake in the N-S and E-W directions are shown in Figures 4.14 and Figure 4.15**,** respectively. The peak acceleration N-S is 0.32g and the peak acceleration E-W is 0.36g.

The relative displacement (to the base of the structure) at the middle of the roof diaphragm (point 221) in the N-S and E-W directions using both components of the Arleta record is shown in Figures 4.16 and 4.17. Also shown is the relative displacement at the support (wall) locations in the N-S (points 61, 68) and E-W (points 27, 28) directions. The maximum displacement in the E-W direction (Fig. 4.16) has a value of 0.00023 in. in the diaphragm and 0.000076 in. in the wall. In the N-S direction (Fig. 4.17), the maximum diaphragm displacement is 0.0048 in. compared with a maximum displacement at the wall of 0.00054 in.

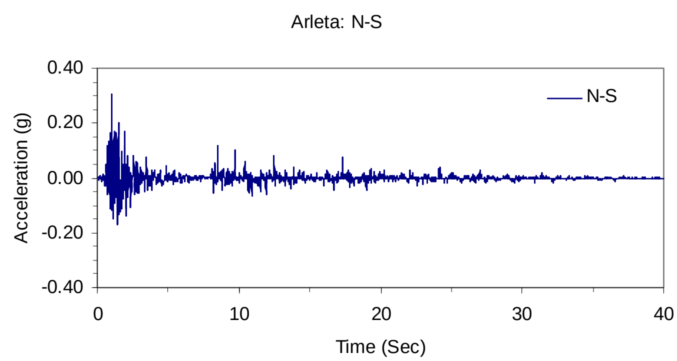

Figure 4.14 N-S acceleration time history, Arleta.

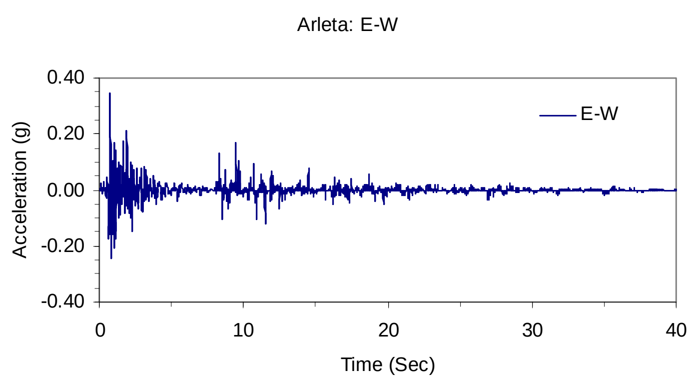

Figure 4.15 E-W acceleration time history, Arleta.

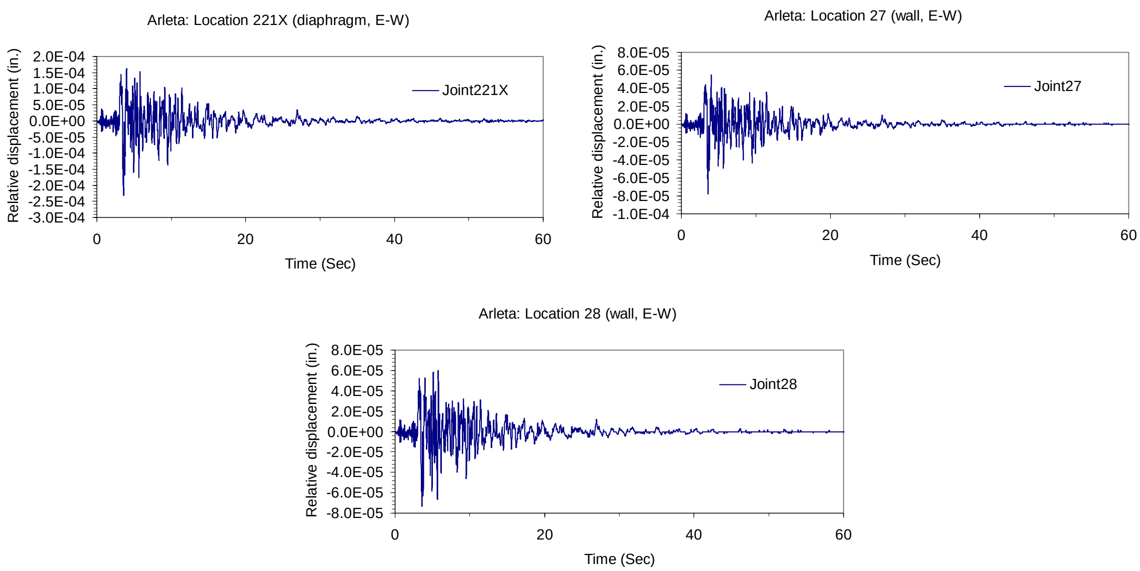

Figure 4.16 E-W diaphragm relative displacement (pt. 221X) and corresponding support displacements (pts. 27, 28), Arleta, 1-story building.

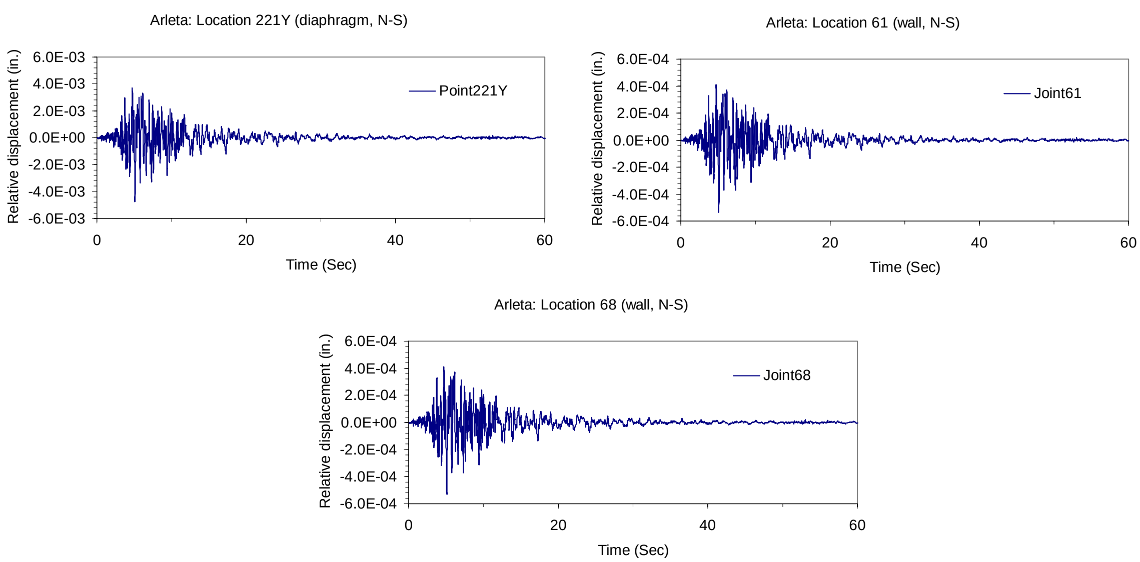

Figure 4.17 N-S diaphragm relative displacement (pt. 221Y) and corresponding support displacements (pts. 61, 68), Arleta, 1-story building.

4.3.3.4 Los Gatos (Loma Prieta Earthquake)

Figures 4.18 and 4.19 show the displacement relative to the base of the structure at the middle of the roof diaphragm (point 221) in the N-S and E-W directions using both components of the Los Gatos record. Also shown are the relative displacements at the support (wall) locations in the N-S (points 61, 68) and E-W (points 27, 28) directions. From Figure 4.18 it can be seen that the maximum displacement in the diaphragm is 0.00044 in. in the E-W direction compared with 0.00013 in. in the wall. In the N-S direction, shown in Figure 4.19, the maximum displacement in the diaphragm is 0.013 in. compared with 0.0014 in. in the wall support.

4.3.3.5 Hollywood Far Field (HOLFF) (1952 Kern County Earthquake)

The ground accelerations recorded at the Hollywood far-field station during the Kern County earthquake (1952) are shown in Figure 4.20 for the N-S component and in Figure 4.21 for the E-W component. The peak recorded acceleration in the N-S direction is 0.058g and the peak value E-W is 0.043g.

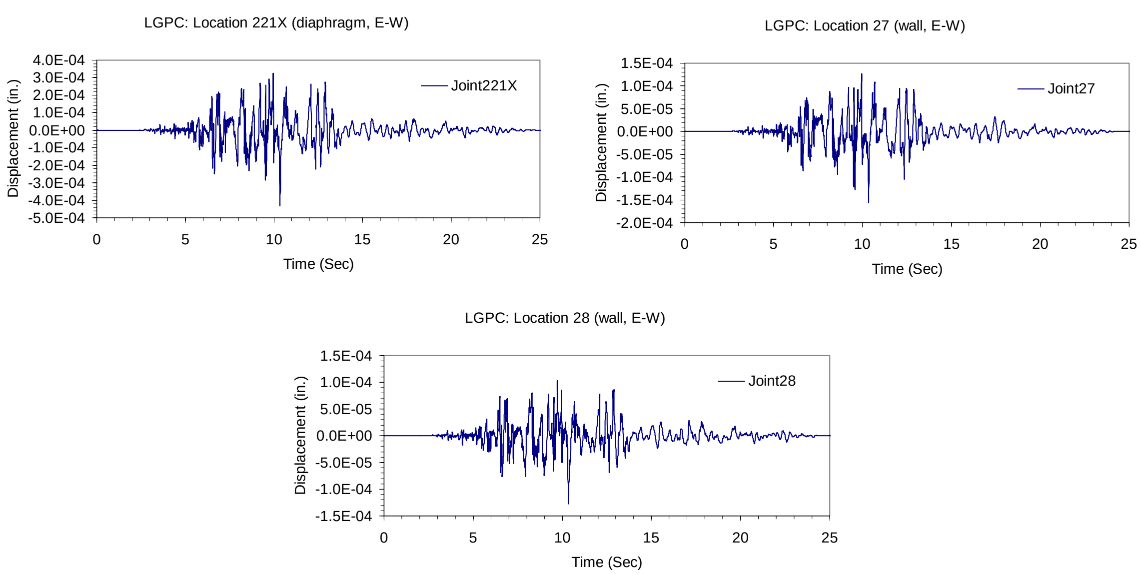

Figure 4.18 E-W diaphragm relative displacement (pt. 221X) and corresponding support displacements (pts. 27, 28), LGPC, 1-story building.

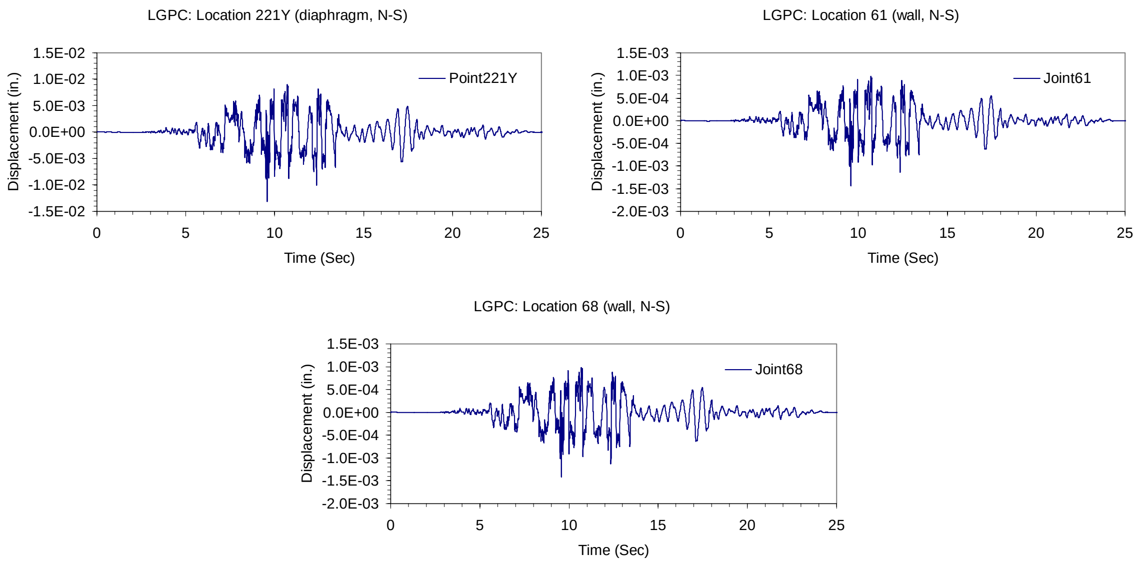

Figure 4.19 N-S diaphragm relative displacement (pt. 221Y) and corresponding support displacements (pts. 61, 68), LGPC, 1-story building.

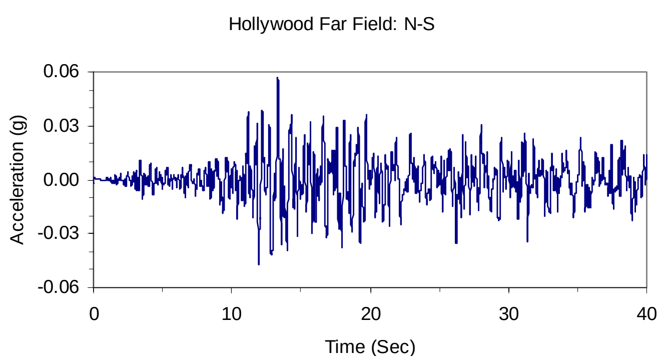

Figure 4.20 N-S acceleration time history, HOLFF.

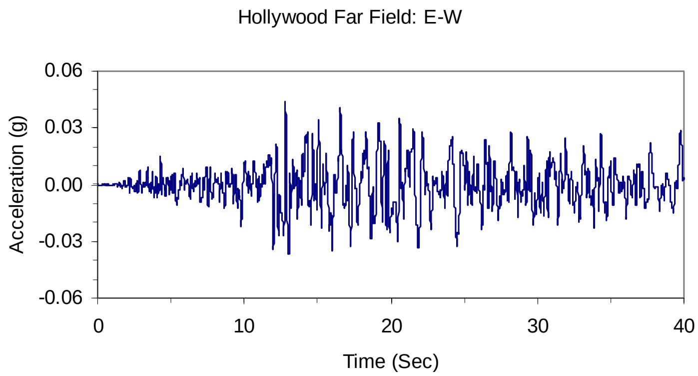

Figure 4.21 E-W acceleration time history, HOLFF.

The displacements relative to the base of the structure at the middle of the roof diaphragm (point 221) in the N-S and E-W directions using both components of the Hollywood far field record are shown in Figures 4.22 and 4.23. Also shown are the relative displacements at the support (wall) locations in the N-S (points 61, 68) and E-W (points 27, 28) directions. The displacements in the N-S direction are shown in Figure 4.22**.** The maximum displacement in the diaphragm is shown to be 0.00072 in. and the maximum displacement at the wall support is 0.00008 in. In the E-W direction, shown in Figure 4.23, the maximum displacement in the diaphragm is 0.000038 in. and the maximum displacement at the wall is 0.000013 in.

4.3.3.6 Hollywood Storage Lot (HSL) (1952 Taft Earthquake)

The accelerations recorded in the N-S and E-W directions in the parking lot of the Hollywood Storage Building during the 1952 Kern County earthquake are shown in Figures 4.24 and 4.25, respectively. The peak acceleration is 0.055g in the N-S direction and 0.04g in the E-W direction.

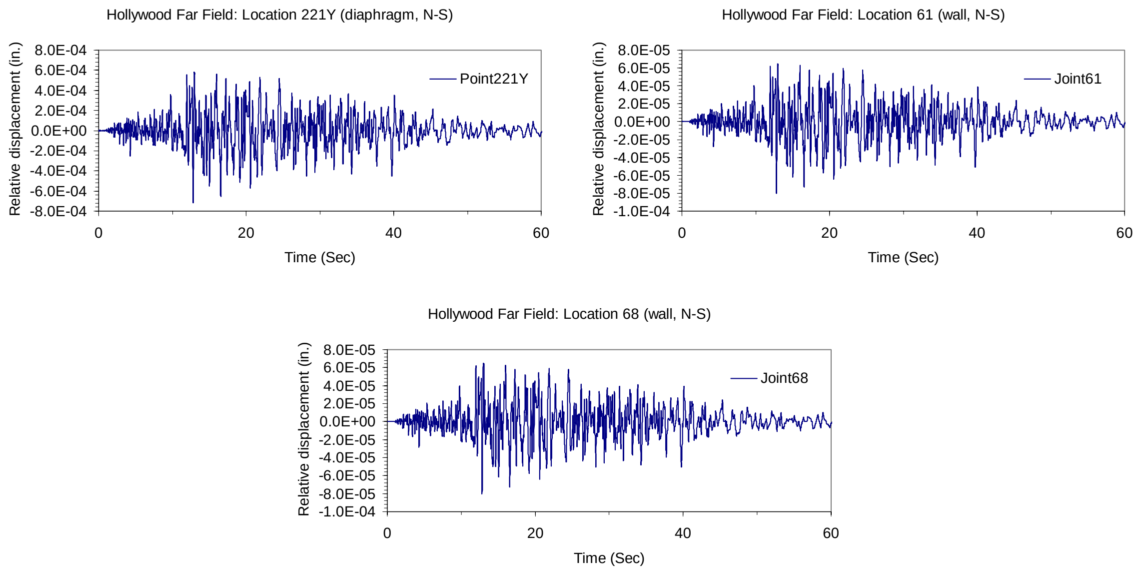

Figure 4.22 N-S diaphragm relative displacement (pt. 221X) and corresponding support displacements (pts. 61, 68), HOLFF, 1-story building.

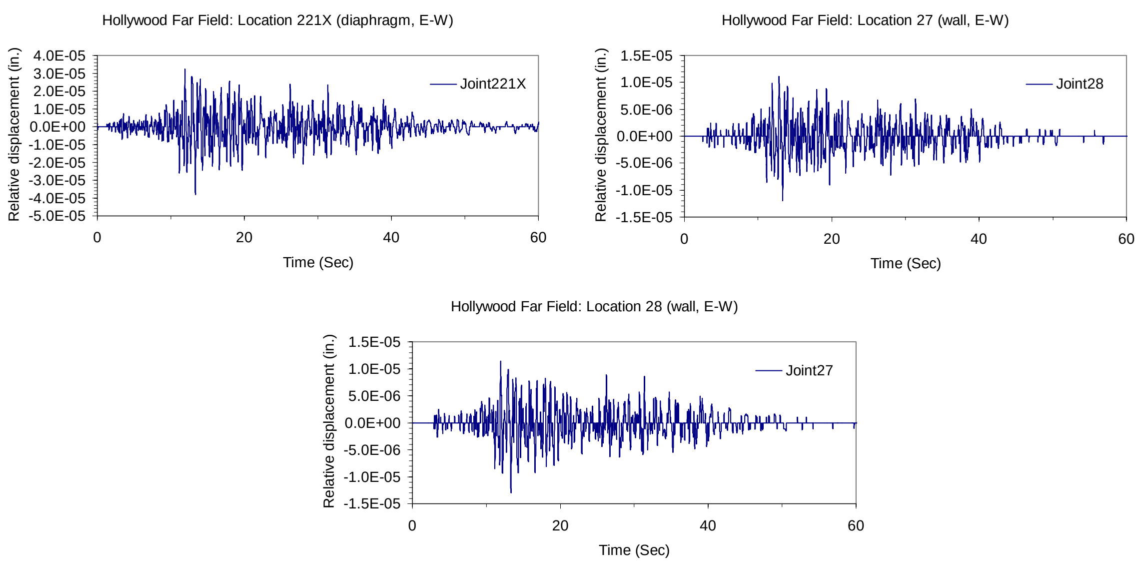

Figure 4.23 E-W diaphragm relative displacement (pt. 221Y) and corresponding support displacements (pts. 27, 28), HOLFF, 1-story building.

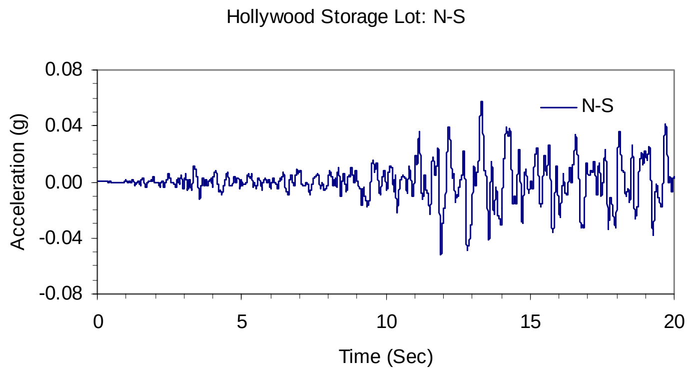

Figure 4.24 N-S acceleration time history, HSL.

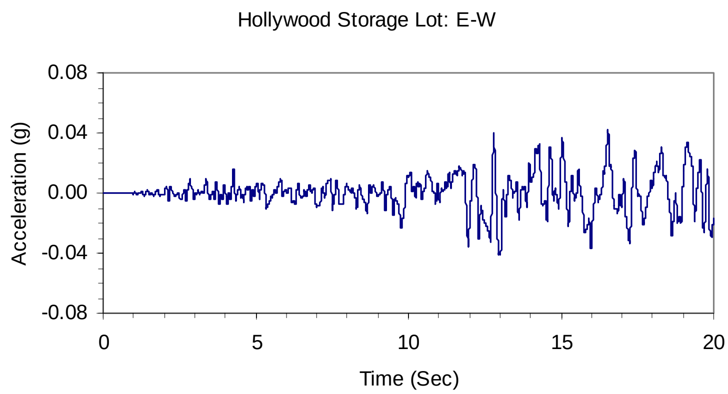

Figure 4.25 E-W acceleration time history, HSL.

Shown in Figures 4.26 and 4.27 are the displacements relative to the base at the middle of the roof diaphragm (point 221) in the N-S and E-W directions using both components of the Hollywood Storage Lot record. Also shown are the relative displacement at the support (wall) locations in the N-S (points 61, 68) and E-W (points 27, 28) directions. The maximum displacement of the diaphragm in the E-W direction obtained from Figure 4.26 is 0.00004 in. compared with 0.000014 in. at the support wall. In the N-S direction, the maximum displacement in the diaphragm is 0.0007 inches compared with 0.000078 in. at the support wall as shown in Figure 4.27.

It is of importance to note that for all but one of these ground motions, the diaphragm would be classified as rigid in the E-W direction according to the current code criteria. This would require that in this direction, accidental torsion should be considered. In the N-S direction, according to the UBC displacement ratio, the diaphragm will be classified as flexible.

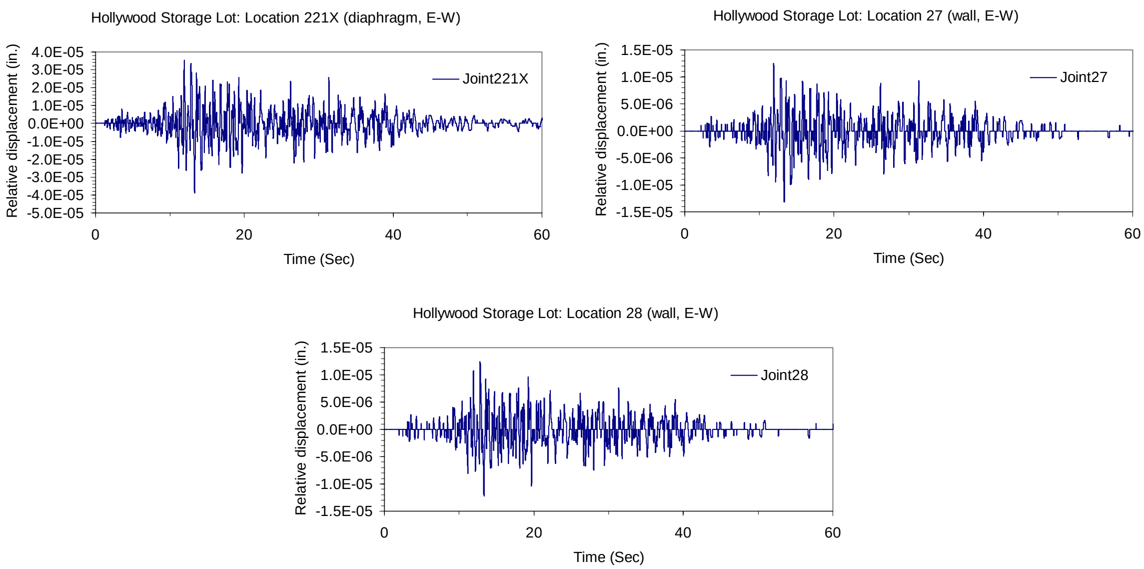

Figure 4.26 E-W diaphragm relative displacement (pt. 221X) and corresponding support displacements (pts. 27, 228), HSL, 1-story building.

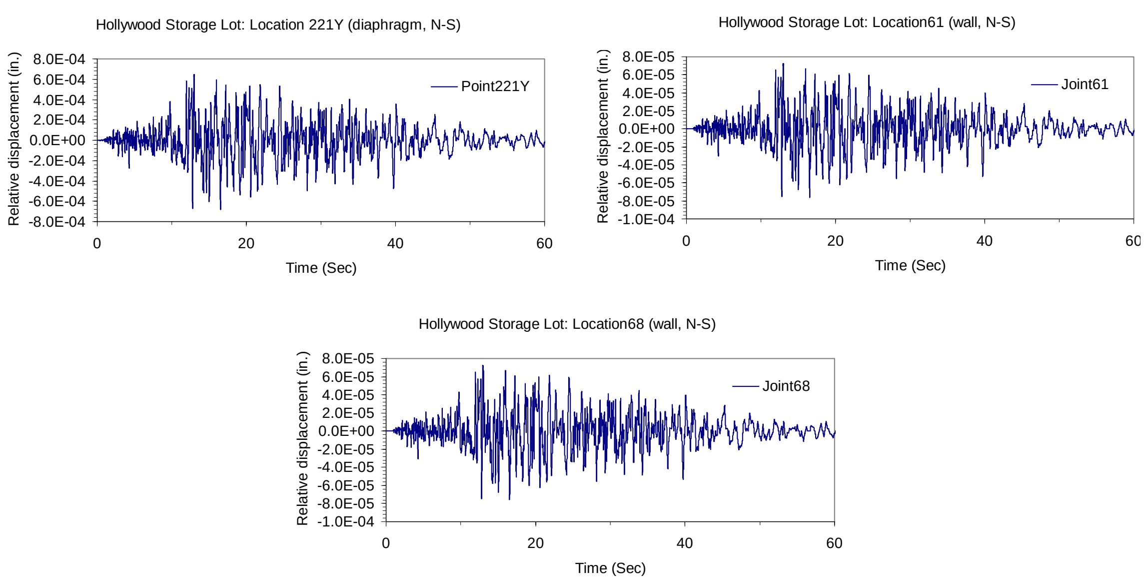

Figure 4.27 N-S diaphragm relative displacement (pt. 221Y) and corresponding support displacements (pts. 61, 68), HSL, 1-story building.

4.4 UNIFORM BUILDING CODE COMPARISON

The one-story substation building located in San Francisco was designed in 1971, and is assumed to be designed for the lateral force requirements of the 1969 City and County of San Francisco Building Code. The lateral force requirements of this code were similar to those of the 1967 UBC. Therefore, for the purposes of this study, it is assumed that the code provisions involving the design base shear are the same as those specified in the 1973 UBC, since major changes to these provisions were made in 1960 and 1976. The design base shear was also calculated using the 1997 UBC in order to assess current code provisions for such a design.

4.4.1 Code Seismic Force Requirement (UBC 1973)

The UBC 1973 code specifies that separate base shear design values be calculated along each principal dimension of the building. The base shear, V, in the longitudinal or transverse direction of the building may be calculated using Equation (4.3).

$$V = KCWZ \tag{4.3}$$

The seismic coefficient, C, is specified using Equation (4.4), and the period, T, can be estimated using the empirical formula in Equation (4.5), where H is the total height of the building in feet, and D is the plan dimension of the building in the direction of seismic loading parallel to a principal building dimension.

$$C = \frac{0.05}{\sqrt[3]{T}} \tag{4.4}$$

$$T = \frac{0.05H}{\sqrt{D}} \tag{4.5}$$

Due to the difference in longitudinal and transverse dimensions of the two-story building, the period, and hence the base shear had to be computed for loading along both directions. The use of Equation (4.5) to estimate the period in the N-S and E-W directions of the one-story building yields Equations (4.6) and (4.7).

$$T_{NS} = \frac{0.05H}{\sqrt{D_{NS}}} = \frac{0.05(10.67\,ft)}{\sqrt{22\,ft}} = 0.11\text{sec} \tag{4.6}$$

$$T_{EW} = \frac{0.05H}{\sqrt{D_{EW}}} = \frac{0.05(10.67\,ft)}{\sqrt{43.33\,ft}} = 0.081\text{sec} \tag{4.7}$$

Using Equation (4.4), the seismic coefficients in the N-S and E-W directions are computed in Equation (4.8) and (4.9).

$$C_{NS} = \frac{0.05}{\sqrt[3]{T_{NS}}} = \frac{0.05}{\sqrt[3]{0.135\sec}} = 0.0975 \tag{4.8}$$

$$C_{EW} = \frac{0.05}{\sqrt[3]{T_{EW}}} \frac{0.05}{\sqrt[3]{0.096\sec}} = 0.109 \tag{4.9}$$

Using K=1.33 and Z=1.0 in Equation (4.3) the calculated design seismic resistance coefficients are as shown in Equation (4.10) and (4.11).

$$V_{NS} = (ZKC_{NS})W = (1.0)(1.33)(0.0975)W = 0.13W \tag{4.10}$$

$$V_{EW} = (ZKC_{EW})W = (1.0)(1.33)(0.109)W = 0.14W \tag{4.11}$$

Equations (4.12) and (4.13) are the result of taking W to be the effective dead load of the building and computing the design base shears in the N-S and E-W directions.

$$V_{NS} = 0.13W = 0.13(126\,kips) = 16.4\,kips \tag{4.12}$$

$$V_{EW} = 0.14W = 0.14(126\,kips) = 17.6\,kips \tag{4.13}$$

4.4.2 Code Design Requirements (UBC 1997)

The period of the one-story building was calculated according to Method A of the 1997 UBC provisions, with the value of C_t equal to 0.020. According to the 1997 UBC, the period of the one-story building may be approximated by "Method A," as given by the following empirical formula in Equation (4.14).

$$T = 0.020(h_n)^{3/4} = 0.02(10.67)^{3/4} = 0.12\sec \tag{4.14}$$

The actual soil profile at the location of the building is unknown, which made using the default soil profile S_D necessary in the code analysis calculations. Since the one-story building is located in California, it was necessary to use the seismic zone factor Z=0.4 for buildings in Zone 4 according to the code. Near-source factors were chosen based on a generating seismic source A and a distance to source exceeding 15 km, where N_a and N_v were each taken to be 1.0. The seismic coefficients C_a and C_v for a building in seismic zone 4 and sited on a soil of profile S_D is to be calculated using Equation (4.15) from the 1997 UBC.

$$\begin{aligned} C_a &= 0.44N_a = 0.44(1.0) = 0.44 \\ C_v &= 0.64N_v = 0.64(1.0) = 0.64 \end{aligned} \tag{4.15}$$

The 1997 UBC defines that the design base shear V in a given direction of a building should be determined from Equation (4.16), though the total design base shear need not exceed Equation (4.17). The total design base shear shall not be less than specified in Equation (4.18).

$$V = \left(\frac{C_v I}{RT}\right) W = \left(\frac{0.64 * 1.0}{4.5 * 0.12}\right) W = 1.19W \tag{4.16}$$

$$V \leq \left(\frac{2.5 C_v I}{R}\right) W = \left(\frac{2.5 * 0.44 * 1.0}{4.5}\right) W = 0.24W \tag{4.17}$$

$$V = 0.11 C_a I W = 0.11(0.44)(1.0)W = 0.048W \tag{4.18}$$

In addition, the 1997 UBC specifies that for Seismic Zone 4, the total base shear shall not be less than Equation (4.19), where R is a response modification factor based on the type of structural system for the building, I is an importance factor, N_v is a near source factor, and C_a and C_v are seismic coefficients which are determined for a given Seismic Zone and soil profile type.

$$V \geq \left(\frac{0.8 Z N_v I}{R}\right) W = \left(\frac{0.8 * 0.4 * 1.0 * 1.0}{4.5}\right) W = 0.058W \tag{4.19}$$

For a concrete shear wall load-bearing system, a structural system factor of R=4.5 was used in the base shear calculations. Using this value of R and an importance factor of I=1.0 for a typical building, the total design base shear as predicted by the 1997 UBC is governed by Equation (4.20).

$$V = \left(\frac{2.5 C_v I}{R}\right) W = \left(\frac{2.5 * 0.44 * 1.0}{4.5}\right) W = 0.24W \tag{4.20}$$

The above expression states that the total lateral force requirement will be 24% of the effective self-weight of the building, W. Estimating W as 126 kips, the base shear requirement as determined by the 1997 UBC is as shown in Equation (4.21).

$$V = 0.24W = 0.24 * 126 kips = 30.24 kips \tag{4.21}$$

The value of the design base shear calculated using the 1973 UBC requirements is for an allowable stress, whereas the value computed using 1997 UBC formulas based on the strength design. For purposes of comparison, the value of base shear computed from the 1973 UBC was multiplied by the load factor for masonry of 1.4. Thus, the value of base shear computed by the 1973 UBC for this building, as expressed in terms of strength design is 22.96 kips and 24.64 kips in the N-S and E-W directions, respectively. It should be noted that the values of the base shear calculated using the current 1997 UBC provisions are 32% greater than the lateral force requirement N-S and 23% greater than the lateral force requirement E-W used to design the building in 1971 (i.e., using the 1973 UBC criteria).

4.5 ANALYSES OF BASE SHEAR

The elastic response of the structure is evaluated considering the time history base shear demands of six recorded earthquake acceleration time histories and the in-plane shear as specified by building code and the in-plane shear capacity as determined from wall thickness and reinforcing.

4.5.1 In-Plane Shear Capacity

The nominal shear capacity of a structural wall can be calculated using Equation (4.22), where the coefficient C_d depends on the ratio of M/Vd.

$$V_n = C_d \sqrt{f'_m} hd + \frac{A_{vh} f_y d}{s_2} \tag{4.22}$$

For these walls, the ratio of M/Vd is greater than unity and therefore C_d = 1.2. For all structural walls, the thickness, h, is 8 in., the masonry strength is 2,500 psi, and the horizontal steel reinforcement is Grade 40 reinforcement consisting of 2-#4@32″. The two walls in the N-S direction have a length, l_w of 248 in.. If the effective length, d, of the wall is taken as $0.8l_w$, the nominal shear capacity of a single wall is 195 kips and for the two walls in the N-S direction this becomes 390 kips. In the E-W direction there are two walls with each wall having a length of 520 in. When $0.8l_w$ is used for the effective length of the wall, the nominal shear capacity of each wall is 408 kips, and for the two walls in the E-W direction, the wall shear capacity becomes 816 kips, which is more than twice the capacity in the N-S direction.

4.5.2 Newhall Record (Northridge Earthquake)

The comparison of the predicted base shear in the N-S and E-W directions to the 1973 and 1997 UBC values during the strong motion recorded at Newhall are compared in Figures 4.28 and 4.29.

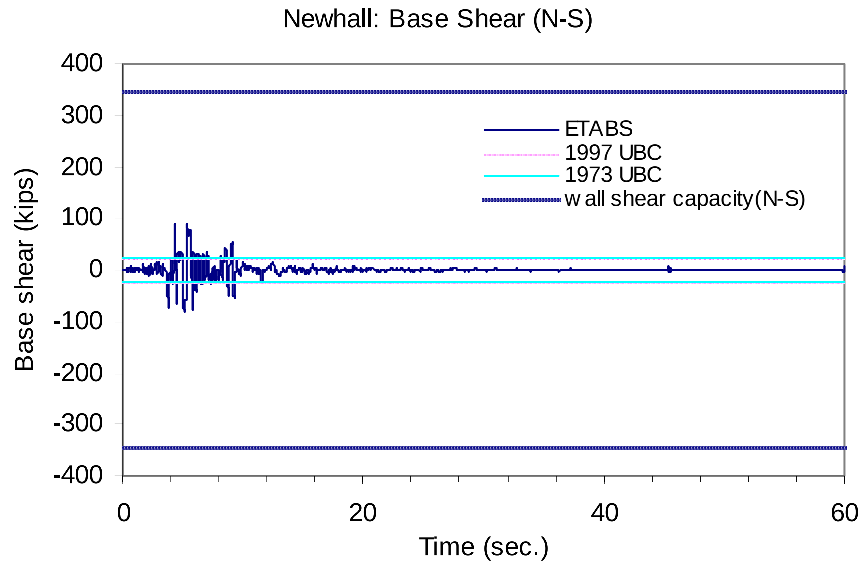

Figure 4.28 N-S design vs. calculated base shear demand, Newhall, 1-story building.

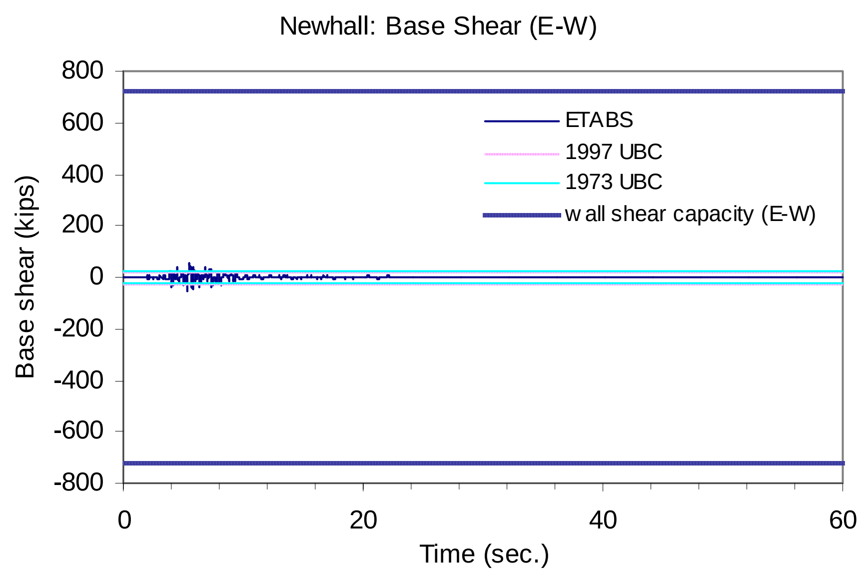

Figure 4.29 E-W design vs. calculated base shear demand, Newhall, 1-story building.

4.5.3 Lucerne Record (Landers Earthquake)

The comparison of the predicted base shear in the N-S and E-W directions to the 1973 and 1997 UBC values during the strong motion recorded at Lucerne are presented in Figures 4.30 and 4.31.

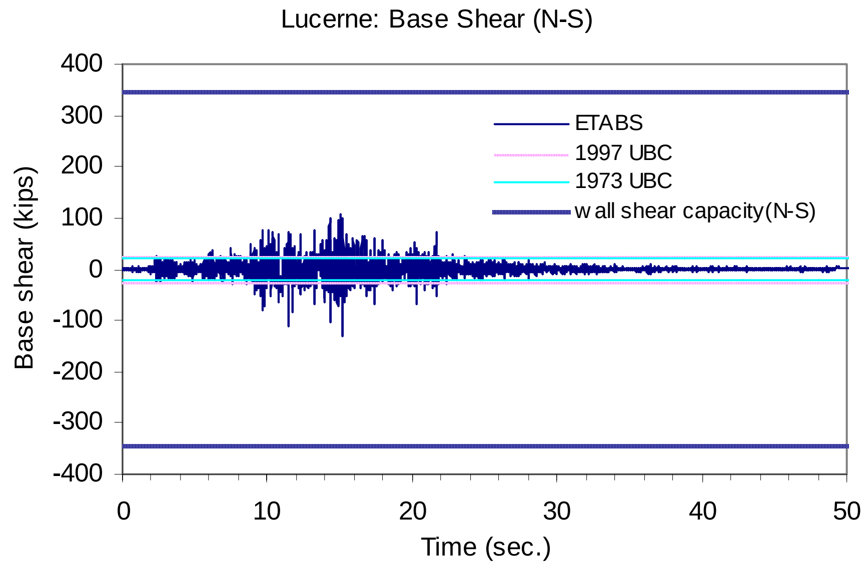

Figure 4.30 N-S design vs. calculated base shear demand, Lucerne, 1-story building.

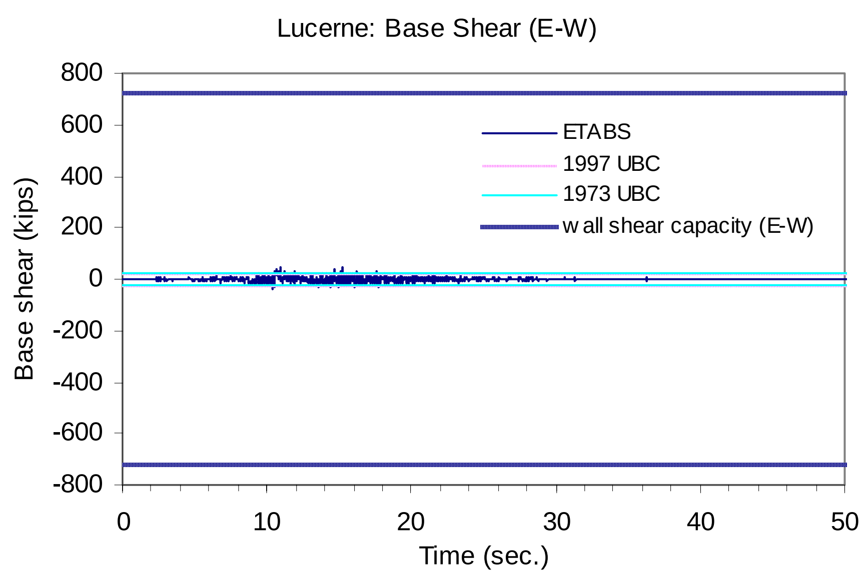

Figure 4.31 E-W design vs. calculated base shear demand, Lucerne, 1-story building.

4.5.4 Arleta Record

The comparison of the predicted base shear in the N-S and E-W directions to the 1973 and 1997 UBC values during the strong motion recorded at Arleta are presented in Figures 4.32 and 4.33, respectively.

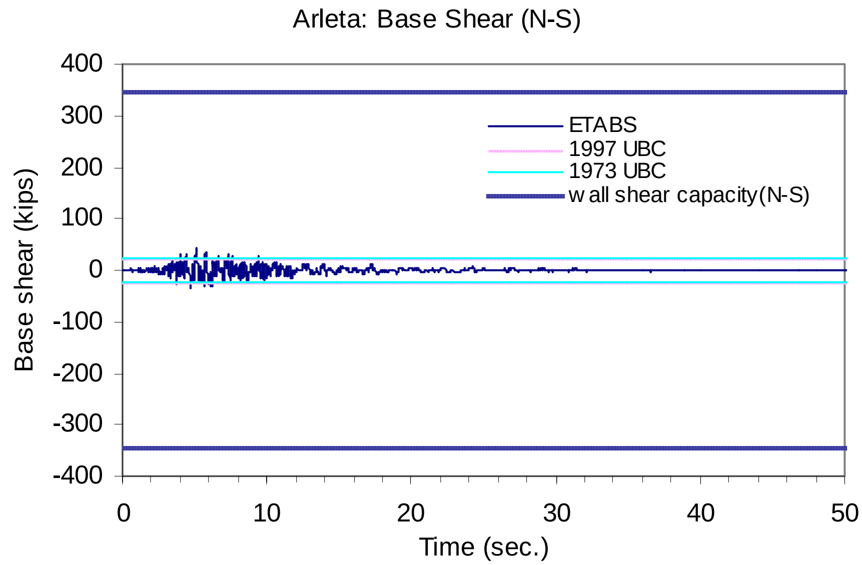

Figure 4.32 N-S design vs. calculated base shear demand, Arleta, 1-story building.

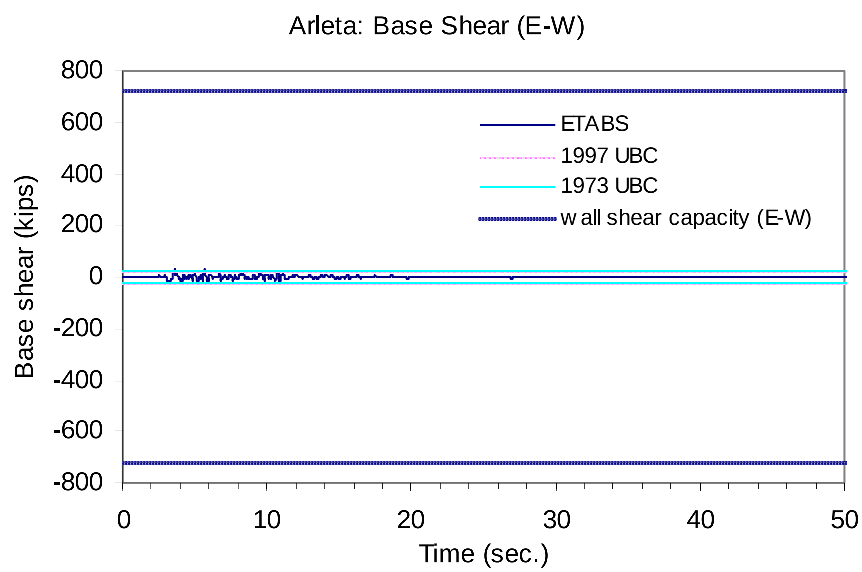

Figure 4.33 E-W design vs. calculated base shear demand, Arleta, 1-story building.

4.5.5 Los Gatos

Comparison of the predicted base shear in the N-S and E-W directions to the 1973 and 1997 UBC values for the strong motion recorded at Los Gatos are presented in Figures 4.34 and 4.35.

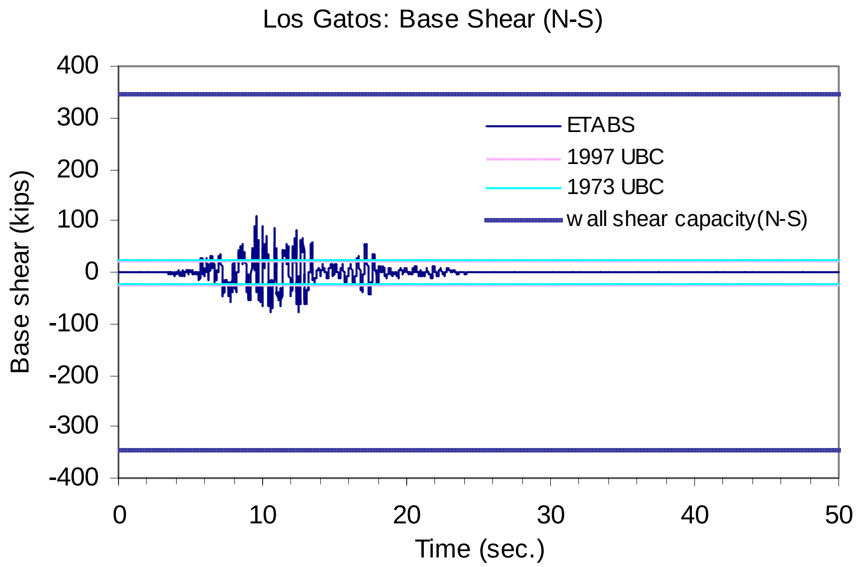

Figure 4.34 N-S design vs. calculated base shear demand, LGPC, 1-story building.

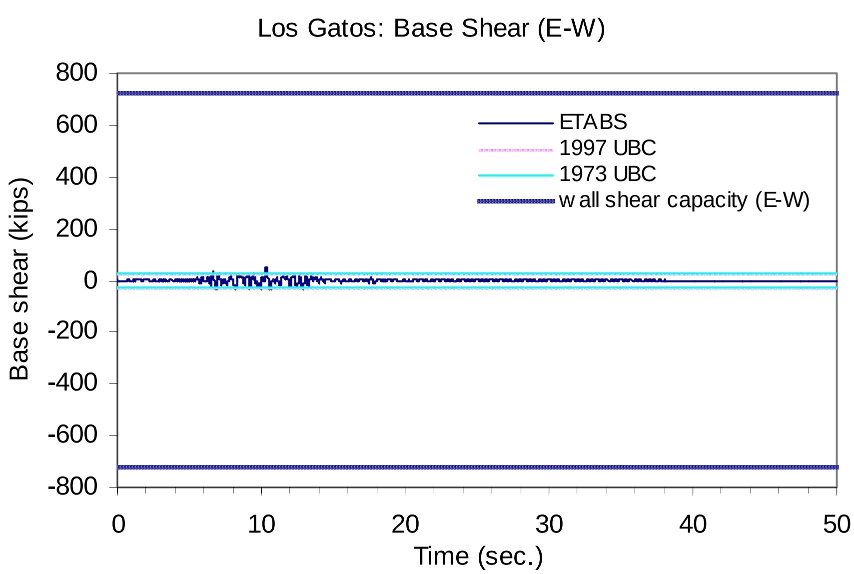

Figure 4.35 E-W design vs. calculated base shear demand, LGPC, 1-story building.

4.5.6 Hollywood Far Field (HOLFF) (1952 Taft Earthquake)

The comparison of the predicted base shear in the N-S and E-W directions to the 1973 and 1997 UBC values during the strong motion recorded at Hollywood far field during the 1952 Taft earthquake are presented in Figures 4.36 and 4.37.

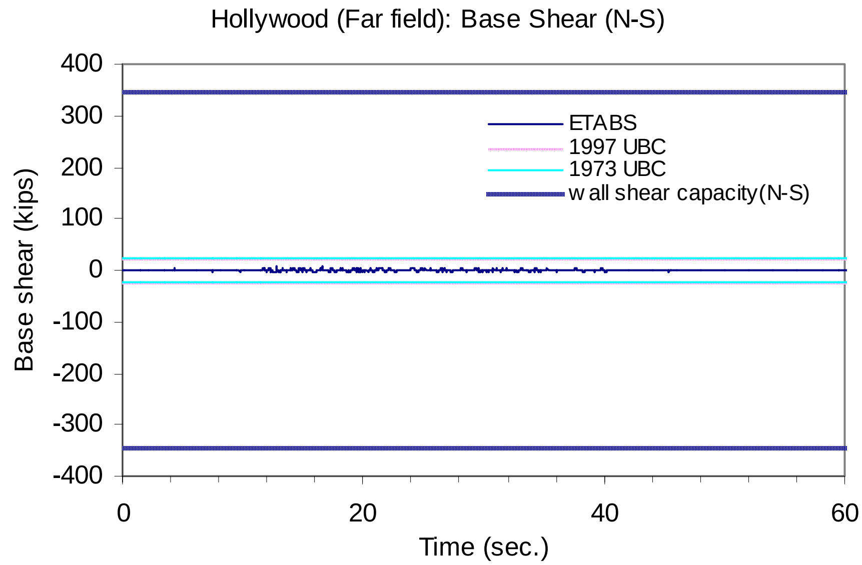

Figure 4.36 N-S design vs. calculated base shear demand, HOLFF, 1-story building.

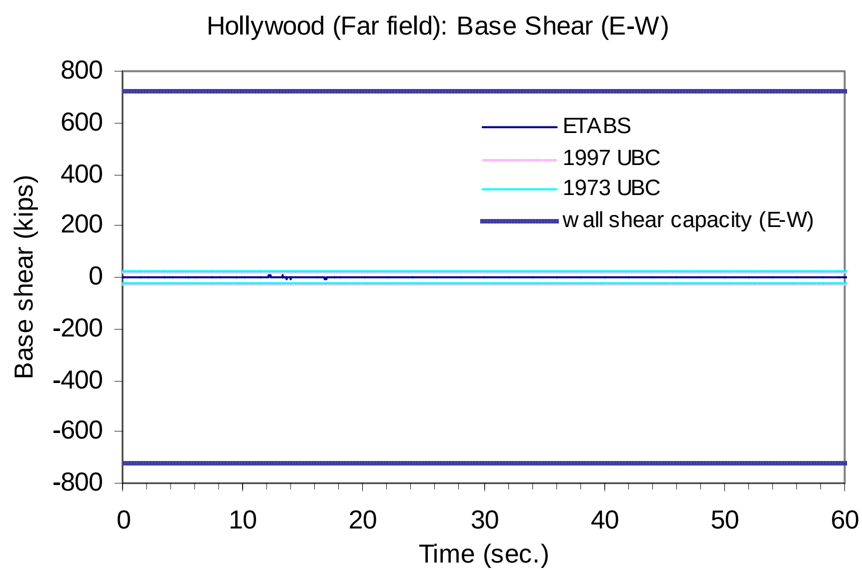

Figure 4.37 E-W design vs. calculated base shear demand, HOLFF, 1-story building.

4.5.7 Hollywood Storage Lot (HSL) (1952 Taft Earthquake)

The comparison of the predicted base shear in the N-S and E-W directions to the 1973 and 1997 UBC values during the strong motion recorded at the Hollywood Storage Lot during the 1952 Taft earthquake are presented in Figures 4.38 and 4.39.

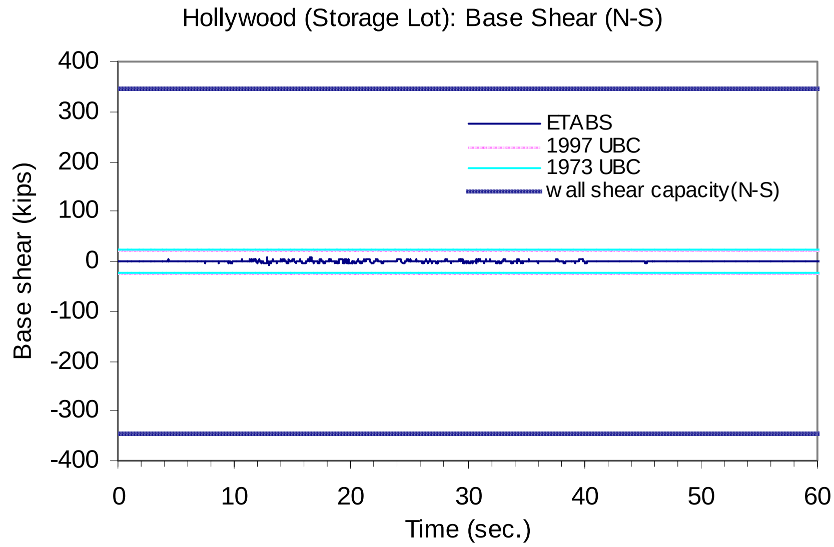

Figure 4.38 N-S design vs. calculated base shear demand, HSL, 1-story building.

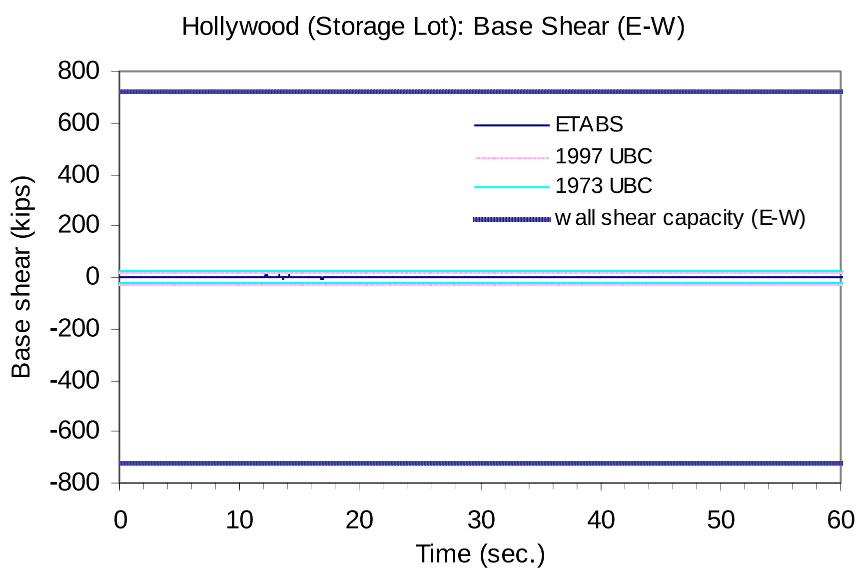

Figure 4.39 E-W design vs. calculated base shear demand, HSL, 1-story building.

4.6 MODIFICATION OF ELASTIC RESPONSE: ONE-STORY BUILDING

The maximum base shears developed by two weak ground motions recorded at the Hollywood Storage building and four additional recorded strong ground motions are summarized in Table 4.2. Considering the weak ground motions, it can be seen that the maximum developed base shear (4.4 kips) is well below the minimum design value of both codes (23 kips). Considering the strong ground motions, it can be seen that the code values are exceeded by as much as 467%. However, as discussed for the previous two buildings, this building also has considerable overstrength based on the minimum reinforcing requirements for the masonry walls. In the E-W direction the capacity is larger (816 kips) and the maximum base shear demand of 58 kips is only 7% of capacity. It can be noted that the shear capacity of the masonry alone is 400 kips which would be more than sufficient for this component of the ground motion.

The maximum base shear demand in the N-S direction, due to the Los Gatos ground motion, has a value of 107 kips and the capacity is 390 kips. Hence in this direction the maximum demand is 27% of capacity. In this direction the masonry walls alone have a capacity of 192 kips which is above the base shear demand. This indicates that the base shear developed by the strong ground motions is also well below the capacity of the resisting walls and implies that the response will be primarily linear elastic. The reduction factors for the elastic response are evaluated in the following paragraphs.

This building has two lines of seismic walls in each direction and due to its small size, the redundancy factor will be taken as 1.0 for purposes of this study. The value of R given in the code for a building frame system having masonry shear walls is 4.5 and the corresponding strength factor is given as 2.8. This implies a ductility factor of $R_\mu = 4.5/2.8 = 2.0$. Considering the response to the Newhall and Los Gatos ground motions discussed previously, the response reduction factors for strength and ductility are calculated as shown in Table 4.3.

Table 4.2 Summary of N-S and E-W design vs. calculated peak absolute base shear demand, 1-story building.

Flexible Diaphragm Analyses										
Earthquake		Building Dimension								
		Transverse (E-W)				Longitudinal (N-S)				
		Max. Abs. Base Shear $V_{b,max}$ (kips)	Percent of E-W capacity $\frac{V_{b,\max}}{V_{b,cap}} * 100$ (percent)	Percent of 1973 UBC design strength $\frac{V_{b,\max}}{V_{b,1973}} * 100$ (percent)	Percent of 1997 UBC design strength $\frac{V_{b,\max}}{V_{b,1997}} * 100$ (percent)	Max. Abs. Base Shear $V_{b,max}$ (kips)	Percent of N-S capacity $\frac{V_{b,\max}}{V_{b,cap}} * 100$ (percent)	Percent of 1973 UBC design strength $\frac{V_{b,\max}}{V_{b,1973}} * 100$ (percent)	Percent of 1997 UBC design strength $\frac{V_{b,\max}}{V_{b,1997}} * 100$ (percent)
Strong Motion Analyses	Newhall	57.8	11.1	234.6	229.4	88.2	25.5	384.4	350.2
	Lucerne	45.9	8.8	186.1	182.0	125.0	36.1	544.5	496.1
	Los Gatos	47.3	9.1	192.2	187.9	107.3	31.0	467.4	425.9
	Arleta	32.1	6.2	130.2	127.3	44.4	12.8	193.4	176.2
Lower Ground Motions	Hollywood (far field)	4.3	0.8	17.5	17.1	6.7	1.9	29.0	26.4
	Hollywood (storage lot)	4.4	0.8	17.8	17.4	6.3	1.8	27.3	24.9

Table 4.3 Base shear modification factors, 1-story building.

Ground Motion	Newhall	Los Gatos
Building Direction	**Transverse (E-W)**	**Longitudinal (N-S)**
Design Strength (V_d) UBC '97, R = 4.5	30.2 Kips	30.2 Kips
Maximum Strength (R_sV_d) (In-plane shear strength)	520 Kips	346 Kips
R_s	17.	11.
Required Elastic Strength ($R_\mu R_s V_d$)	58 Kips	107 Kips
R_μ	.11	.31
Design Strength (V_d) UBC '73	24.6 Kips	23.0 Kips
Maximum Strength (R_sV_d)	520 Kips	346 Kips
R_s	21	15
Required Elastic Strength ($R_\mu R_s V_d$)	58 Kips	107 Kips
R_μ	.11	.31

As mentioned previously for the other two buildings, the lateral resistance is a function of the length of the structural walls used in each direction and may be more of an architectural consideration than a strength consideration. This can result in a substantial variation in the overstrength factor. It can be seen that as the overstrength factor is increased, the required ductility factor is reduced, and the building remains well within the elastic response range. The ductility factors calculated in Table 4.3 have values of 0.11 and 0.31. It should be noted that this example is based on the in-plane shear strength of the structural walls. The performance of the building may be controlled by some other failure mechanism such as diaphragm shear, wall flexure out-of-plane or diaphragm connection to the walls. However, due to the very light weight of the roof diaphragm, these possible failure modes seem less likely for this building. The strength of the structure can be evaluated by using a nonlinear pushover analysis that considers all possible failure mechanisms.

4.7 MOMENT CONTOURS (WALLS)

The moment contours for the four walls of the one-story building computed for the six ground motions used for dynamic time history analyses are shown in this section. Since the building possesses dual symmetry, the moment contours will be shown only for one of the walls in the N-S and one of the walls in the E-W direction. Vertical reinforcing steel consisted of 1-#4 bar spaced at 16 in. Since there was only a single curtain of steel, the reinforcing was assumed as placed in the middle of the concrete wall, resulting in an effective depth of 4 in. Using the material properties f_y = 40 ksi and f'_m = 2.5 ksi, the out of plane moment capacity of the wall was calculated to be 1.75 in.-kips/in. A combination of 1.2D+0.5L+1.0E was used for development of the out-of-plane moment contours shown in the remainder of this section.

4.7.1 Newhall Record (Northridge Earthquake)

The moment contours obtained for the one-story building show the ***out-of-plane moments*** for the N-S and E-W walls using the two orthogonal components of the Newhall record, and are shown in Figures 4.40 and 4.41, respectively. The values shown on the bottom of each moment contour figure are in moment per unit length (e.g., kip-in./in.). The values of moment per unit lengths in the color regions should be taken as the upper bound of the regions (for conservatism), since the values cannot be determined in a more accurate way.

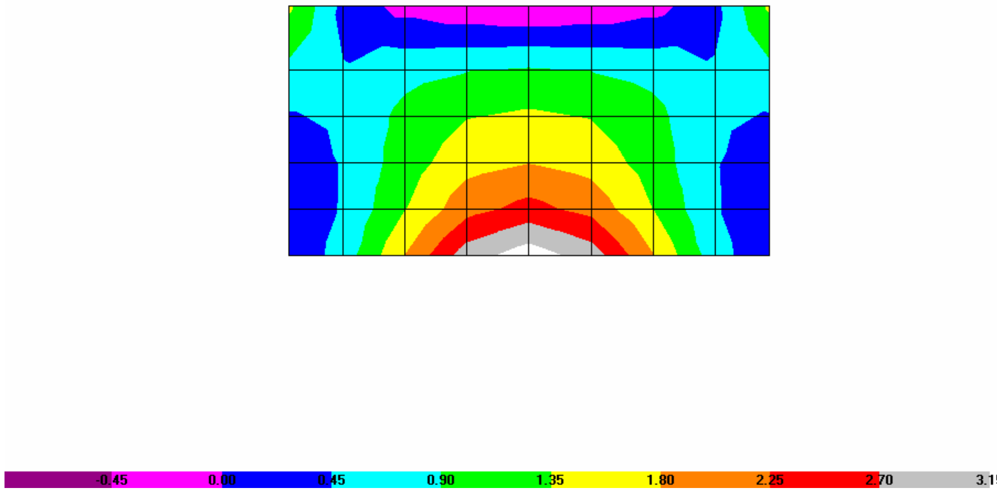

Figure 4.40 Moment contour for a N-S wall, Newhall, 1-story building.

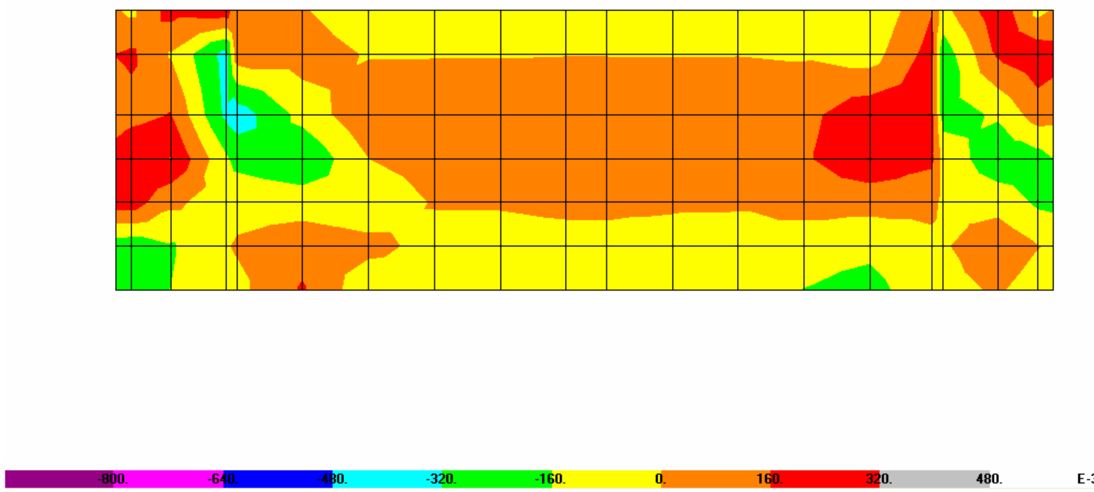

Figure 4.41 Moment contour for an E-W wall, Newhall, 1-story building.

4.7.2 Lucerne Record (Landers Earthquake)

The moment contours for the N-S and E-W walls using the two orthogonal components of the Lucerne record are shown in Figures 4.42 and 4.43, respectively.

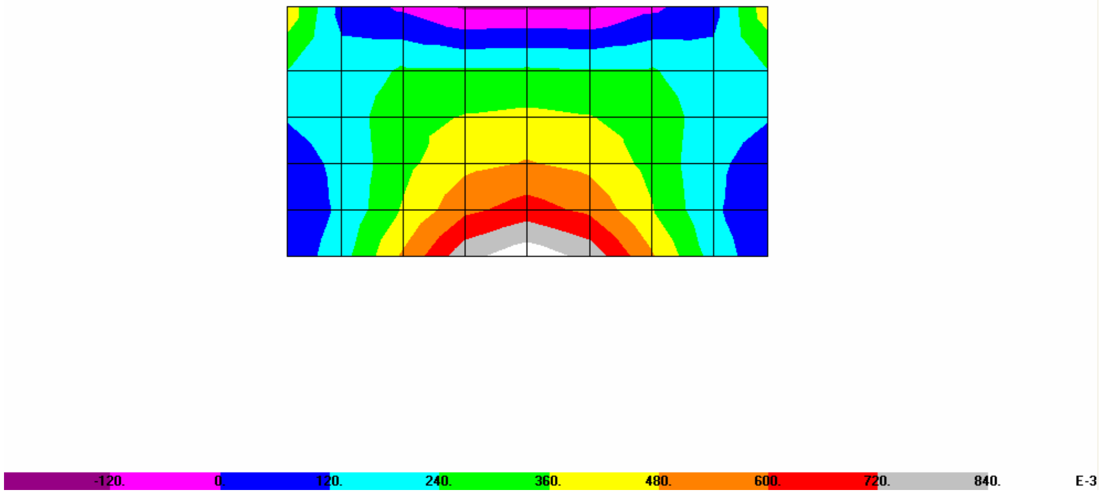

Figure 4.42 Moment contour for a N-S wall, Lucerne, 1-story building.

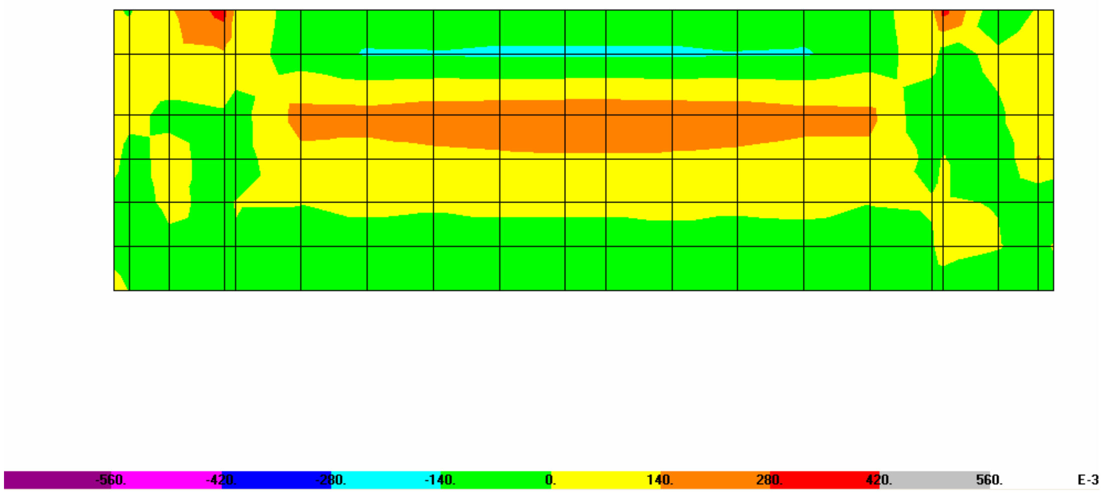

Figure 4.43 Moment contour for an E-W wall, Lucerne, 1-story building.

4.7.3 Arleta Record (Northridge Earthquake)

The moment contours for the N-S and E-W walls using the two orthogonal components of the Arleta record are shown in Figures 4.44 and 4.45, respectively.

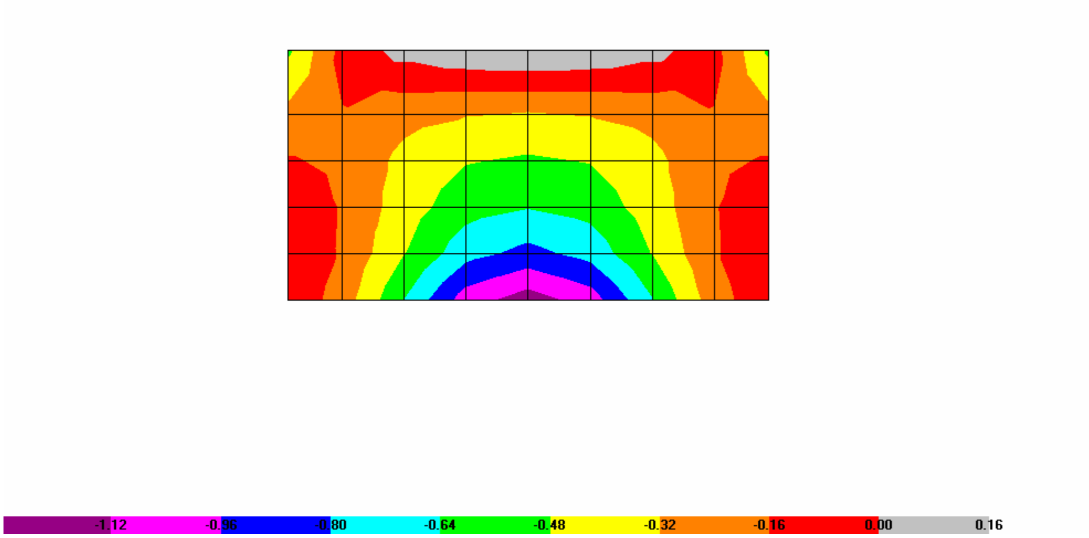

Figure 4.44 Moment contour for a N-S wall, Arleta, 1-story building.

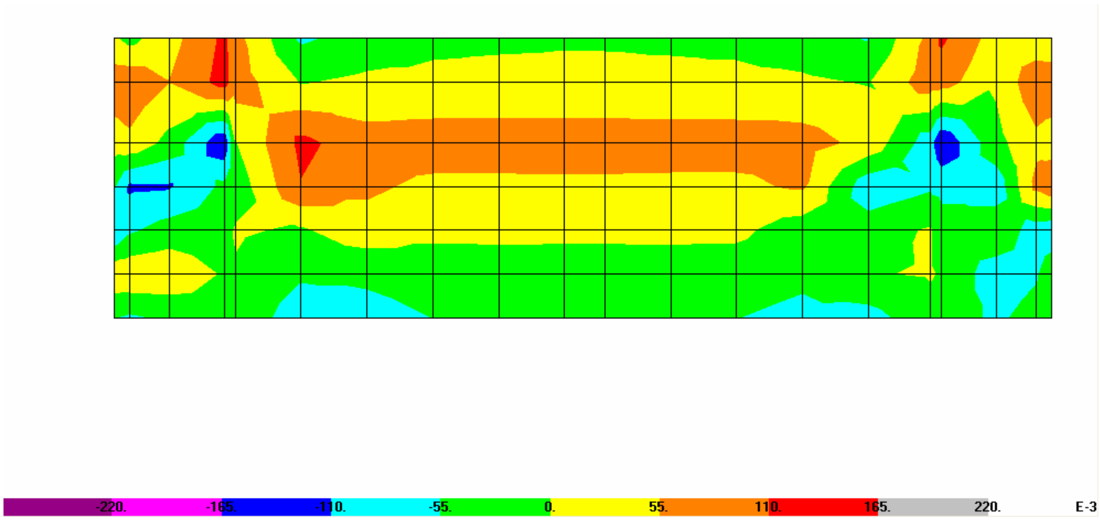

Figure 4.45 Moment contour for an E-W wall, Arleta, 1-story building.

4.7.4 LGPC Record (Loma Prieta Earthquake)

The moment contours for the N-S and E-W walls using the two orthogonal components of the Los Gatos record are shown in Figures 4.46 and 4.47, respectively.

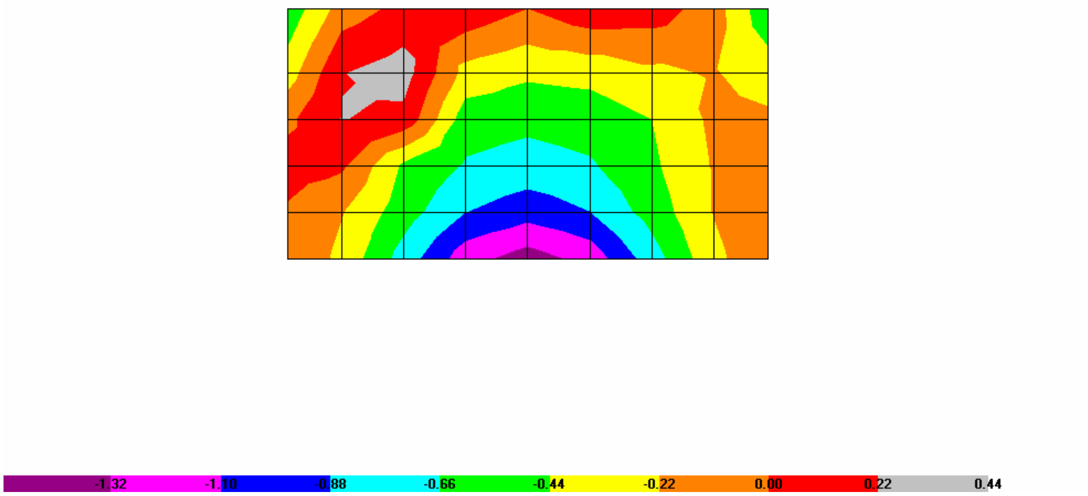

Figure 4.46 Moment contour for a N-S wall, LGPC, 1-story building.

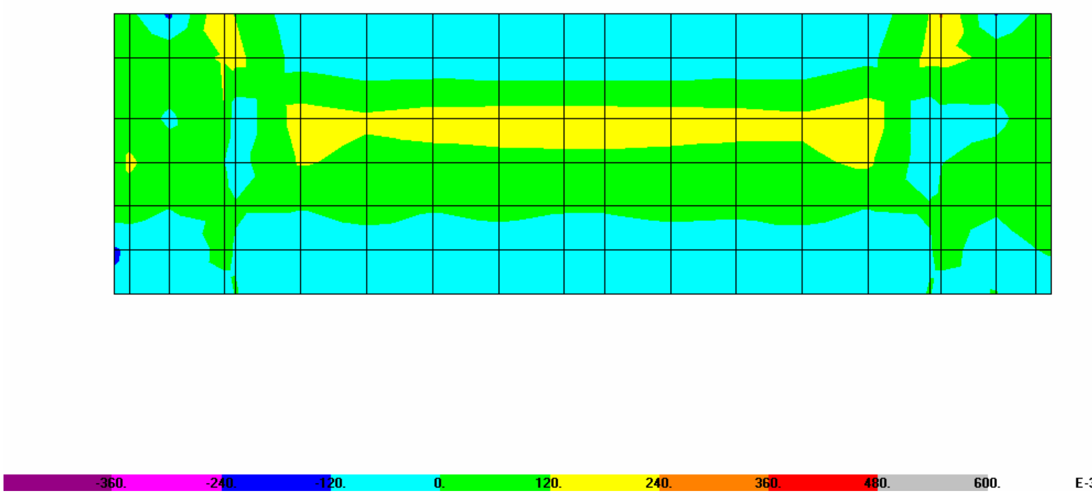

Figure 4.47 Moment contour for an E-W wall, LGPC, 1-story building.

4.7.5 Hollywood Far Field (Kern County Earthquake)

The moment contours for the N-S and E-W walls using the two orthogonal components of the Hollywood far-field record are shown in Figures 4.48 and 4.49, respectively.

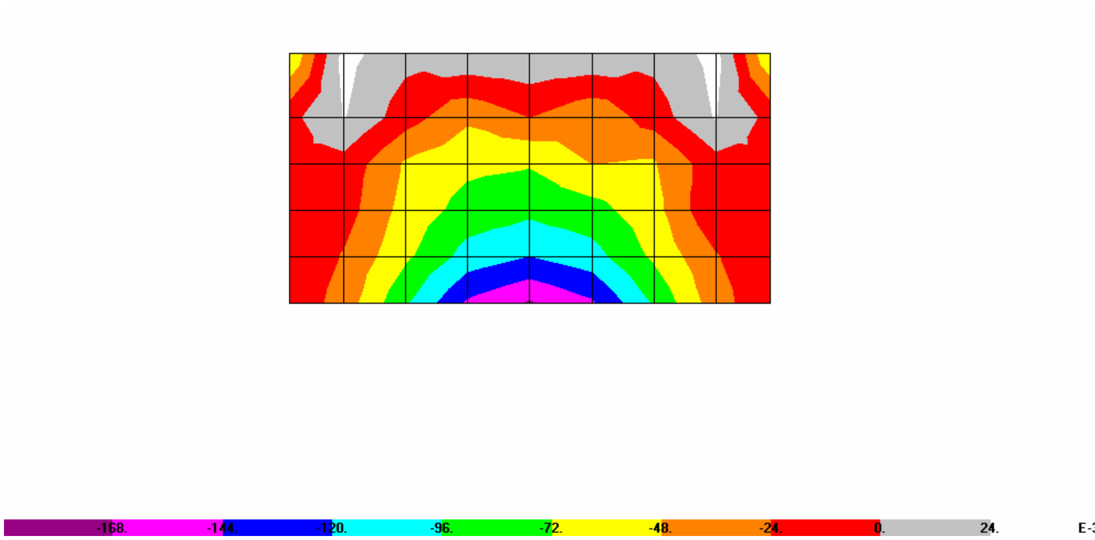

Figure 4.48 Moment contour for a N-S wall, HOLFF, 1-story building.

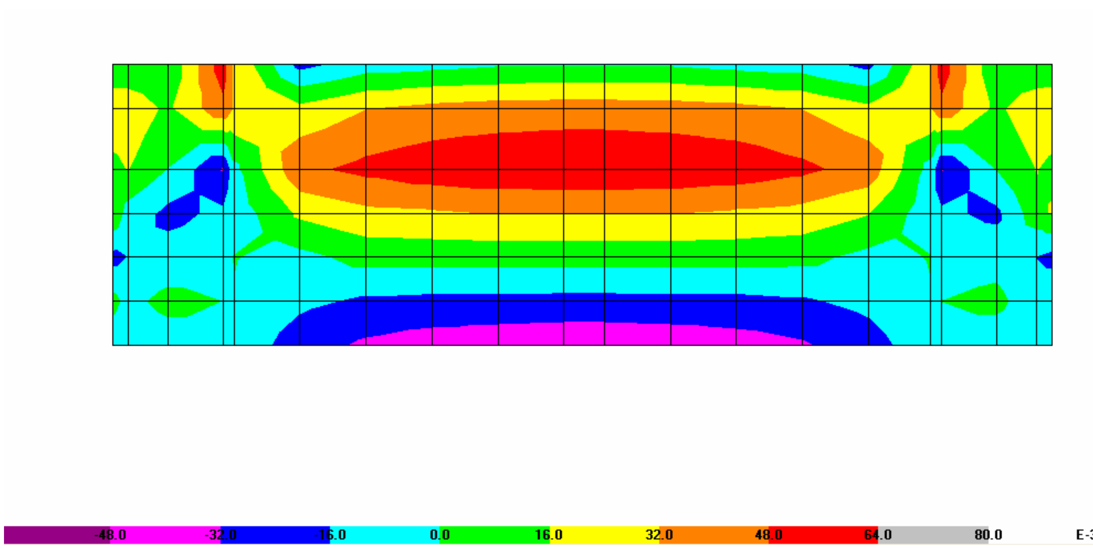

Figure 4.49 Moment contour for an E-W wall, HOLFF, 1-story building.

4.7.6 Hollywood Storage Lot (Kern County Earthquake)

The moment contours for the N-S and E-W walls using the two orthogonal components of the Hollywood Storage Lot record are shown in Figures 4.50 and 4.51, respectively.

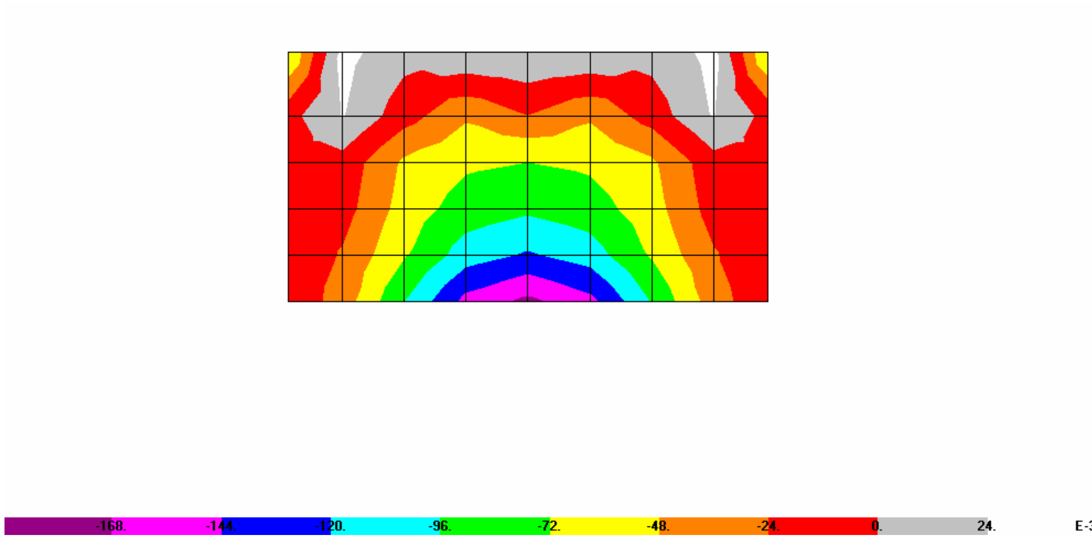

Figure 4.50 Moment contour for a N-S wall, HSL, 1-story building.

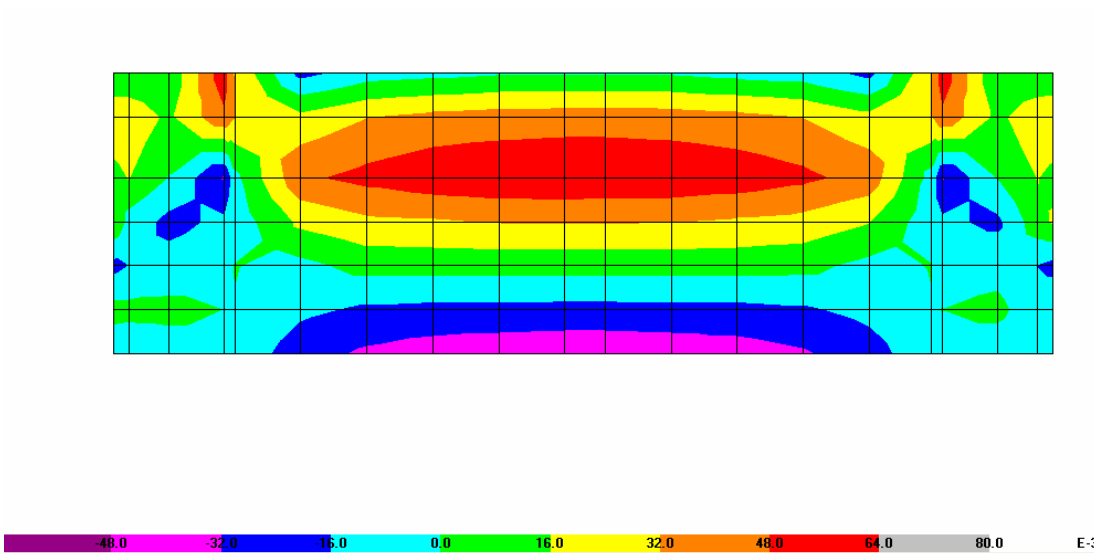

Figure 4.51 Moment contour for an E-W wall, HSL, 1-story building.

The moments calculated in the walls of the one-story building are summarized in Table 4.4. These data indicate that the out-of-plane moment capacity of the wall (1.75 in.-kip/in.) was exceeded under the Newhall ground motion at a localized position at the base of the wall near the mid-length of the wall. The moment demand at this location is influenced by the assumed fixed-boundary condition for the out-of-plane moment. Under the other three strong ground motions considered in this study, no yielding of the reinforcement is predicted although there would undoubtedly be some cracking. Considering the out-of-plane moments developed under the two lower acceleration records, the maximum moments in the walls are approximately one tenth of the moment capacity.

Table 4.4 Maximum out-of-plane wall moment (in.-kips/in.).

Earthquake Ground Motion	Transverse Wall	Longitudinal Wall
Newhall Fire Station	3.15	0.24
Lucerne	0.84	0.21
Arleta Fire Station	1.12	0.11
Los Gatos Presentation Ctr.	1.32	0.18
Hollywood Far Field	0.17	0.56
Hollywood Parking Lot	0.18	0.60

4.8 SUMMARY FOR ONE-STORY BUILDING

The one-story building had no instrumentation, and thus neither model verification nor spectral analyses could be performed. However, the modeling considerations were the same as those employed in the three- and two-story buildings, and it is assumed that the model can predict the behavior of this building in the same manner as observed in the other cases. Linear elastic time history analysis was conducted using a total of 6 sets of ground motion records, four representing severe ground motions with displacement-pulse effects, and two representing minor ground motions. Displacement time histories at the walls and middle of the roof diaphragm in both the N-S and E-W directions were presented, and their significance discussed. The amplitude of the displacement time histories for all cases are near zero, indicating little relative movement of the building during the simulations. This indicates that the building is primarily moving with the ground as a rigid body.

Base shear time history comparisons were shown for all 6 sets of ground motion records and are well below both the design values and wall capacity values as based on in-plane shear. An evaluation of out-of-plane bending moments in the walls indicated that for one ground motion (Newhall) the moment capacity was exceeded in a localized area of the lower portion of the transverse walls. The results also show that the one-story building would not suffer any appreciable damage in the event of earthquakes similar to those used in these simulations.

A recent study (Cohen, et al. 2002) describes shaking table tests on two one-story, half-scale masonry buildings. The size of the prototype building was 18′ x 44′ x 14′ and one had a metal deck roof diaphragm. These dimensions are similar to those of the one-story building considered in this study which has dimensions 22′ x 43′ x 10.7′ with the exception that the test buildings had two 8′ x 8′ openings in one of the longitudinal sides to permit access. The measured periods obtained from the tests were 0.05 sec in the transverse direction and 0.083 sec in the longitudinal direction. The period in the transverse direction is identical to the corresponding period in the study building (0.05 sec). In the longitudinal direction the period in the test building is longer .083 sec versus 0.032 sec in the study building. This is most likely due to the openings in the longitudinal wall of the test building. The following response effects were noted based on the results of the shaking table tests: (a) the cracking patterns observed in the tests suggested that the half-scale specimens remained basically elastic when the input base accelerations were less than 0.50g and (b) the in-plane transverse response of the roof diaphragms and the associated out-of-plane transverse response of the masonry walls played important roles in the seismic response of the test buildings. These results are in general agreement with those of the current study.

5 Summary and General Conclusions

5.1 SUMMARY

The objectives of this study were to (1) assess the applicability of the 3D analytical models presently available for analyzing the elastic seismic performance of reinforced masonry buildings, (2) to estimate through dynamic analyses the response of the two reference buildings and compare the results with corresponding values recorded in the buildings during recent earthquakes, (3) to estimate the lateral strength that will be demanded of the reference study buildings if subjected to critical ground motions during their service life, and (4) to evaluate the implications of the obtained results regarding the reliability of present seismic code regulations for the design of such buildings.

Case studies have been presented describing the seismic response of two instrumented reinforced masonry buildings with plywood diaphragms and a one-story reinforced masonry building with a T-deck (steel) roof diaphragm and no instrumentation. Two existing buildings for which the recorded response to seismic ground motions is available were chosen for analytical investigation. The first building, a three-story office building in Lancaster, California, was analyzed for its behavior during the Whittier Narrows, Landers, and Northridge earthquakes. A second two-story office building in Palo Alto was studied to evaluate its seismic response during the Loma Prieta earthquake. Analysis of the displacement response obtained from the recorded acceleration time histories for each of the two instrumented buildings showed little variation in frequency response, thus suggesting elastic behavior. Spectral analyses were performed to determine the dynamic characteristics of each structure consisting of response spectra and Fourier analyses. Moving window Fourier transfer function analyses conducted on the recorded response of each building showed that both structures remained essentially elastic during each earthquake.

A three-dimensional linear elastic dynamic model was developed using ETABS computer software. For the two instrumented buildings, base shear time histories during each of the recorded ground motions were computed using the analytical model and compared to the design base shear required by the building code for which each building was designed as well as to the design base shear required by the current 1997 UBC code. To study the predicted response of each building to more severe and near-fault motions, additional earthquake accelerations recorded at other sites were used. Base shear demands were computed for these ground motions and compared with the minimum design base shear required by code. The base shear comparisons using the recorded motions at the base of the buildings verified that the behavior of each building during the recorded base motion was essentially elastic. However, analysis of the response of these buildings to the additional severe ground motions recorded at different sites indicated that each building would likely suffer damage.

Spectral analyses were performed on each of the two instrumented buildings to determine the dynamic characteristics of the building using the accelerations recorded in the building during the seismic ground shaking. Three-dimensional, linear-elastic finite element models were developed for use with the ETABS program. Linear elastic analyses were conducted for the ground motions recorded at the base of the buildings and the resulting building response was compared to that measured by the sensors on the building. Base shear demands were also studied by comparing the 1997 UBC design base shear values to the values predicted by the analytical models. In-plane shear forces in the horizontal diaphragms were evaluated in terms of shear-flow contours, and out-of-plane bending moments in the walls were also evaluated in terms of contour plots that were compared to the computed ultimate strengths.

For each of the instrumented buildings, an investigation of the 1997 UBC criteria for flexible diaphragms was conducted. Two sets of relative displacement ratios used by the code were computed based on either static loading (per 1997 UBC) or dynamic loading. For the three-story building, static and dynamic analyses resulted in significantly different values of the diaphragm flexibility ratio and indicated different classifications of the diaphragms. However, for the two-story building, the code ratios computed for the roof and second-floor diaphragms using both static and dynamic loading agreed as to the classification of the diaphragms as not flexible.

The one-story building lacked instrumentation, and thus it was not possible to conduct spectral analyses and model verification. A linear elastic ETABS model was constructed for this building using similar modeling techniques to those used in both instrumented buildings. Dynamic time history analysis was performed specifically for the displacement at the wall and diaphragm midspan, and base shear in the N-S and E-W directions. A total of 6 total sets of recorded ground motions were used in the analyses. These are thought to be representative of (1) severe ground motions, (2) single and multiple displacement-pulse ground motions, and (3) moderate ground motions in seismic zones of reduced risk. The results from these analyses suggest that the one-story building will not suffer appreciable damage in the event of being subjected to any of these ground motions.

5.2 CONCLUSIONS

From the analysis of the results presented in this study, the following conclusions have been reached.

1. The modeling capabilities of the current ETABS (version 7) program, including the use of a three-dimensional model that includes the diaphragm stiffness, can accurately reproduce the elastic response of reinforced masonry buildings considering the actual stiffness characteristics of the diaphragms. This was verified by critical comparison with the response measured in two instrumented masonry buildings.
2. In considering the three-dimensional response, building behavior characteristics such as distribution and participation of mass, orthotropic behavior of the timber diaphragms, interaction of frames and walls, orthogonal reaction components on connections and the interaction of two simultaneous seismic input motions are accounted for directly.
3. Consideration of the effect of cracking on the section properties are necessary to satisfactorily model grouted reinforced masonry shear walls. This is particularly true for structures that have experienced one or more earthquakes.
4. The three-story case study building experienced three earthquake ground motions that produced base shear demands that were smaller than the design base shear required by the 1973 UBC, used in the design, and by the 1997 UBC.
5. The two story case study building experienced ground motions that generated base shears that were as much as 50% above the design base shear. However, the estimated capacity indicated that the building had sufficient overstrength so that any structural damage

would be limited. There may have been some limited cracking of the masonry, though the reinforcing steel appears to have remained elastic.

6. The base shear comparisons for the three-story building indicate that the 1997 UBC lateral force requirements result in a higher design base shear relative to the 1973 UBC provisions. The value of the design base shear in the E-W direction is 30% higher and the value in the N-S direction is 19% higher than the 1973 values.
7. Observation of the recorded acceleration and displacement response, the moving window Fourier transfer function analyses, and the base shear comparisons all provide convincing evidence that the three-story building remained essentially elastic during the three earthquake ground motions recorded at the base.
8. It is likely that some damage would be incurred in each of the structures studied if they were subjected to the severe earthquake ground motions. However, this damage potential is tempered by the existing overstrength of the walls due to the use of minimum reinforcement. This capacity is exceeded for only a limited number of cycles.
9. For purposes of comparison, the in-plane shear capacity of the structural walls has been used as an indication of capacity. However, the actual capacity of the building may be controlled by the in-plane shear capacity of the diaphragm, the connections of the diaphragm to the walls, or the out-of-plane moment capacity of the walls.
10. The in-plane shear capacities of the walls in each principal direction for the 3-story building have considerably higher strength than the code minimum requirement and these capacities are exceeded for only a limited number of displacement cycles. This higher strength appears to be due to the length of the walls used in the framing system and the minimum steel requirements for the structural walls.
11. The value of the code displacement ratio used as a criteria for determining when the roof or floor diaphragms should be considered as flexible does not appear to give consistent results and depends upon the method of calculation (i.e., static vs. dynamic). Significant differences were observed as summarized in Table 5.1.

Table 5.1 Summary of flexibility classifications for diaphragms of 2- and 3-story buildings under static and dynamic loading.

Location	Building			
	Three Story		Two Story	
	Static	Dynamic	Static	Dynamic
Roof	*Flexible*	*Rigid*	*Rigid*	*Flexible*
Story	*Flexible*	*Flexible*	*Rigid*	*Rigid*

12. Differences were observed between the period and design base shear between the 1973 UBC and 1997 UBC. In the 1973 code, the period is a function of the building dimension in the direction of loading, whereas, the period determined in the 1997 code is independent of plan dimensions and uses a single period based on the building height for both directions. Both of these code provisions produce estimates of the building periods that are not consistent with the values computed from the computer model or obtained from the recorded response. This results in an inconsistency in determination of the design base shear.
13. Results of this study indicate that in-plane shear in the timber diaphragms may be the weak part of the building system.
14. The assumption of flexible vs. rigid diaphragm may have a significant effect on the distribution of base shear forces to the resisting elements that are generally shear walls.
15. Results from dynamic time history analyses indicating small demands compared with available capacity suggest that the one-story building will not suffer any appreciable damage in the event of severe earthquake ground motions similar to those used in the analyses conducted for the two- and three-story buildings.
16. The in-plane shear strength capacity of the walls of all three buildings exhibits a significant overstrength relative to code lateral force requirements. This appears to be due to the size and length of the walls and the architectural considerations in the design. This study has shown that the base shear developed by severe ground motions can significantly exceed the minimum base shear specified by building codes. In this case, the additional shear strength of the walls will be advantageous. However, the overstrength of the walls may attract additional inertial forces due to the ground shaking, and, in addition,

may place an increased load on another more critical element such as the roof or floor diaphragm and the connection of these diaphragms to the walls. Therefore, other elements of the structural system should be designed for the increases in seismic forces arising from the overstrength of the walls suggesting the use of a higher overstrength factor in the design of connecting elements.

17. From a design standpoint, defining the diaphragm as “flexible” or “rigid” can have a significant effect on the individual lateral resisting elements. If the diaphragm meets the criteria for a flexible diaphragm, the lateral design forces will be distributed to the elements according to mass of their tributary area. If they are classified as rigid, the distribution of lateral design forces will be according to their lateral stiffness. In addition, a rigid diaphragm will require consideration of accidental torsion.

5.3 RECOMMENDATIONS

1. To date there has been very little testing of subdiaphragms. More recent tests (Pardoen, et al., 1999) have considered parameters interior to the sub-diaphragm (nailing, plywood thickness, and panel orientation) but have not addressed the interaction of the sub-diaphragm with the wall. Also, the use of closely spaced truss joists has not has not been considered nor has the use of different blocking schemes. Some of these tests should be biaxial, since the diaphragm is under a biaxial state of stress with orthotropic material properties. Hence, additional tests of timber diaphragms need to be conducted.

2. This study has shown that the connections between the diaphragm and the supporting walls can experience significant multi-component loading at certain critical locations on the diaphragm. This effect combined with the directional properties of timber, parallel to grain or perpendicular to grain, will have a significant effect on connector performance. Tests to date have consider uniaxial loading that is generally parallel to the grain.

3. The effects of vertical accelerations on diaphragm response should be investigated. If vertical accelerations have a significant effect on the response, this will increase the triaxial state of loading on the connections to the walls.

4. Additional instruments are needed on the diaphragms to evaluate the actual flexibility. For the two-story building the seven instruments were not nearly enough and the recorded data had to be supplemented by calculated data. Since diaphragm flexibility is a function of the interstory displacement, recordings are necessary on two or three consecutive floor levels.

REFERENCES

Abrams, D.P., "Response of Unreinforced Masonry Buildings," Journal of Earthquake Engineering, Vol. 1, No. 1, January 1997, pp 257-273.

Brandow, G. E., Hart, G. and Virdee, A., "Design of Reinforced Masonry Structures," Concrete Masonry Association of California and Nevada (CMACH), Sacramento, California, 1997.

Breyer, D. E., Fridley, K. J. and Cobeen, K. E., "Design of Wood Structures: ASD," McGraw Hill, Fourth Edition, 1999.

Cohen, G.L., Klingner, R.E., Hayes, J.R., and Sweeney, S.C., "Seismic Response of Low-Rise Masonry Buildings with Flexible Roof Diaphragms," Proceedings, Seventh U.S. National Conference on Earthquake Engineering, Boston, MA, July, 2002.

Computers and Structures, Inc., "ETABS Users Manual, Version 7.0", Computers and Structures, Inc., 1999.

"CSMIP Strong-Motion Records from the Northridge, California Earthquake of January 17, 1994, Report No. OSMS 94-07," California Dept of Conservation, Sacramento, CA, February 18, 1994.

International Conference of Building Officials (ICBO), "Uniform Building Code," 1997 Edition, Whittier, CA, 1997.

International Conference of Building Officials (ICBO), "Uniform Building Code," 1973 Edition, Whittier, CA, 1973.

Pardoen, G.C., Del Carlo, D. and Kazanjy, R.P., "Stiffness of Timber Diaphragms and Strength of Timber Connections," Report No. PEER-99, Pacific Earthquake Engineering Research Center, May, 1999.

Raggett, J.D. and Rojahn, C., "Dynamic Amplification of Ground Motions by Low-Rise, Stiff Shear Wall Buildings," SMIP91 Seminar on Seismological and Engineering Implications of Recent Strong-Motion Data, Preprints, California Division of Mines and Geology, Sacramento, 1991, pp 1-11.

Tena-Colunga, A. and Abrams, D.P., "Seismic Behavior of Structures with Flexible Diaphragms," Journal of Structural Engineering, Vol. 122, No. 4, April, 1996, pp 439-445.

Tena-Colunga, A. and Abrams, D.P., “Simplified 3-D Dynamic Analysis of Structures with Flexible Diaphragms,” Earthquake Engineering & Structural Dynamics, Vol. 24, No. 2, February, 1995, pp 221-232.

Tena-Colunga, A. and Abrams, D.P., “Quasi-Dynamic Analysis for the Seismic Evaluation of Structures with Flexible Diaphragms,” Proceedings, 1993 National Earthquake Conference, Central United States Earthquake Consortium, Memphis, 1993, pp 459-468, Vol. II.

Tena-Colunga, A. and Abrams, D.P., “Response of an Instrumented Masonry Shear Wall Building with Flexible Diaphragms During the Loma Prieta Earthquake,” UILU-ENG-92-2025, Civil Engineering Studies, Structural Research Series 577, Dept. of Civil Engineering, Univ. of Illinois at Urbana-Champaign, Urbana, December, 1992.

Tena-Colunga, A., “Seismic Evaluation of Unreinforced Masonry Structures with Flexible Diaphragms,” Earthquake Spectra, Vol. 8, No. 2, May, 1992, pp 305-318.

Trus Joist MacMillan, Commercial Applications Product Manual, 1998.

American Institute of Steel Construction (AISC), “Load & Resistance Factor Design,” Vol. 1, Second Edition, USA, 1998.

APPENDIX A-1

Recorded Acceleration Time Histories, Whittier Narrows, 3-Story Building

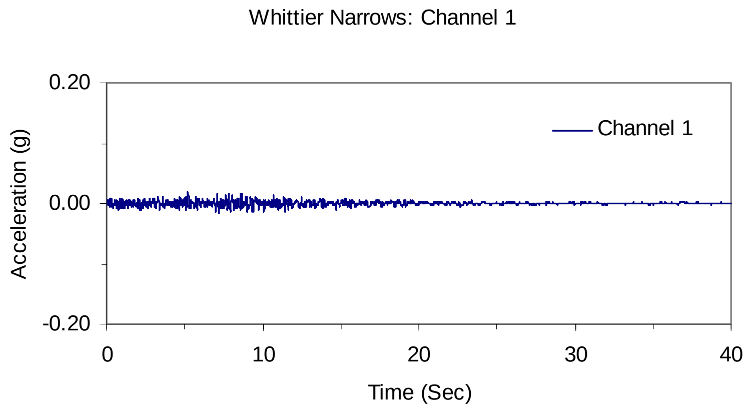

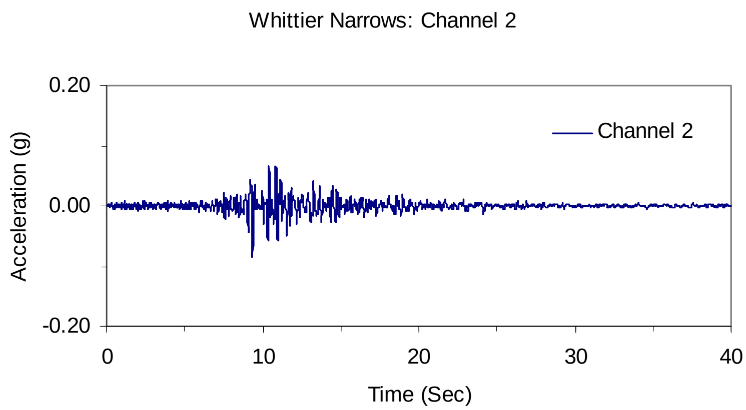

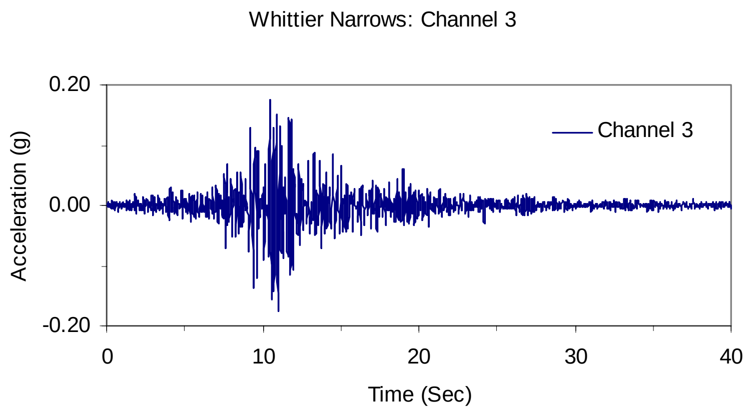

Whittier Narrows: Channel 4

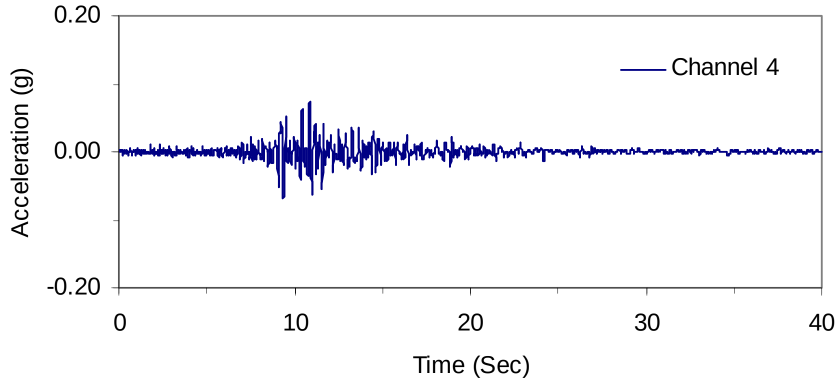

Whittier Narrows: Channel 5

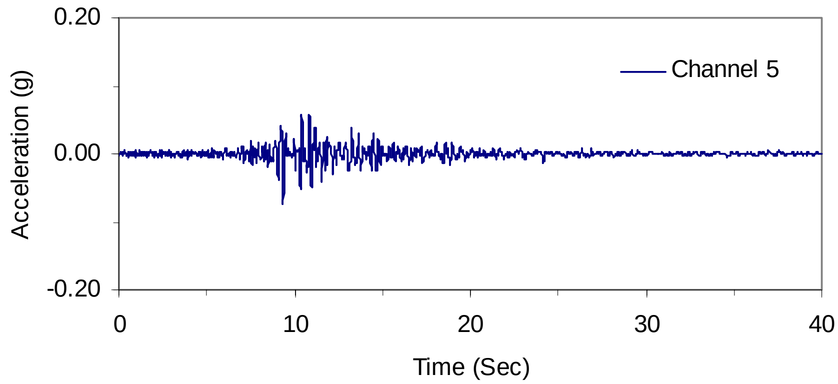

Whittier Narrows: Channel 6

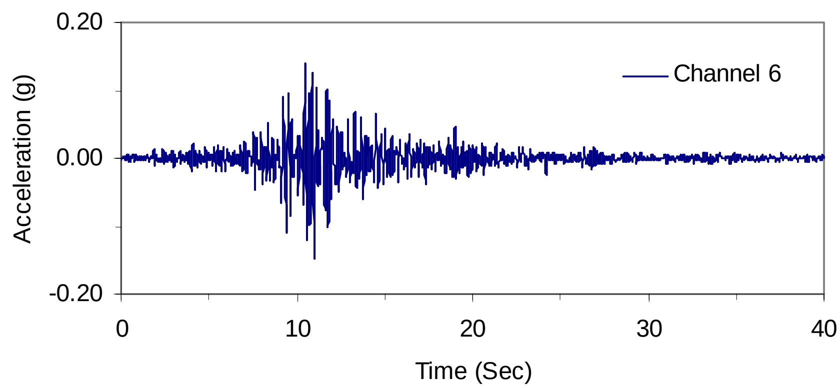

Whittier Narrows: Channel 7

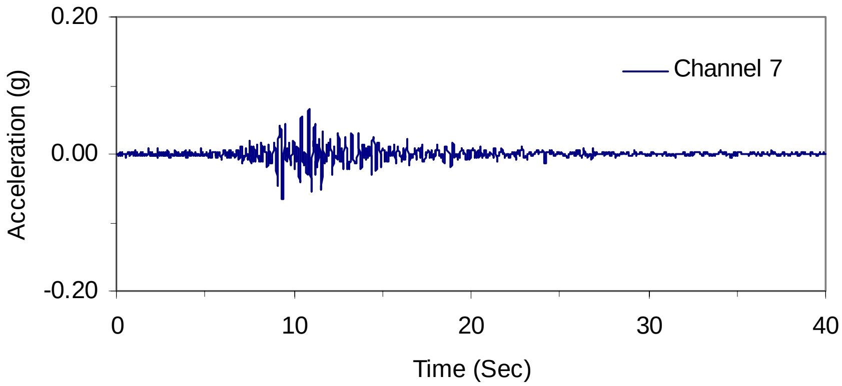

Whittier Narrows: Channel 8

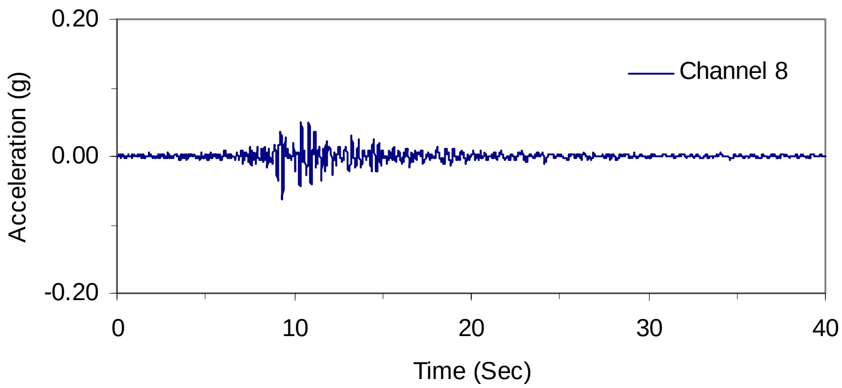

Whittier Narrows: Channel 9

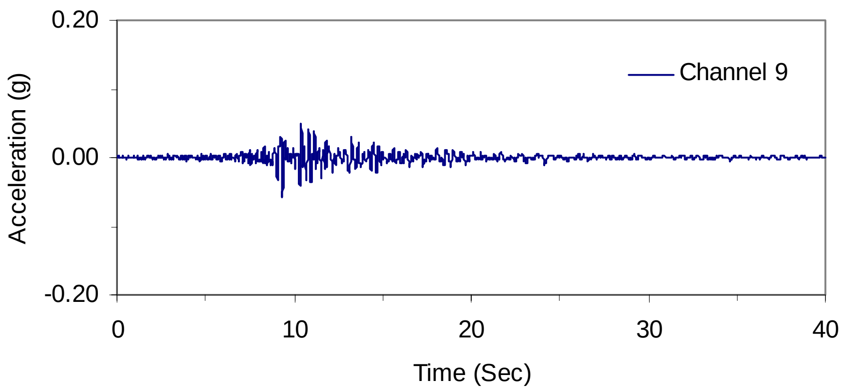

Whittier Narrows: Channel 10

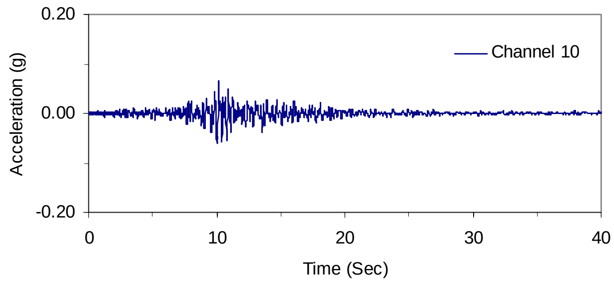

Whittier Narrows: Channel 11

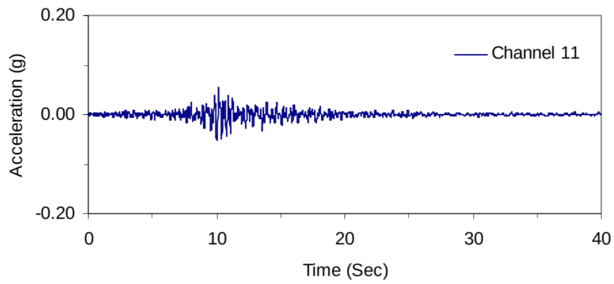

Whittier Narrows: Channel 12

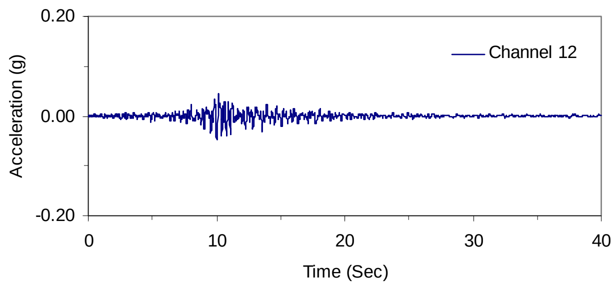

Whittier Narrows: Channel 13

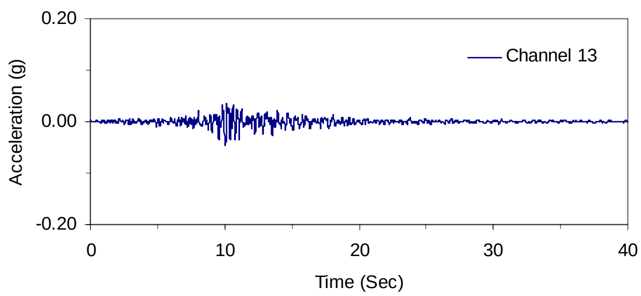

APPENDIX A-2

Recorded Displacement time histories, Whittier Narrows, 3-Story Building

Whittier Narrows: Channel 1

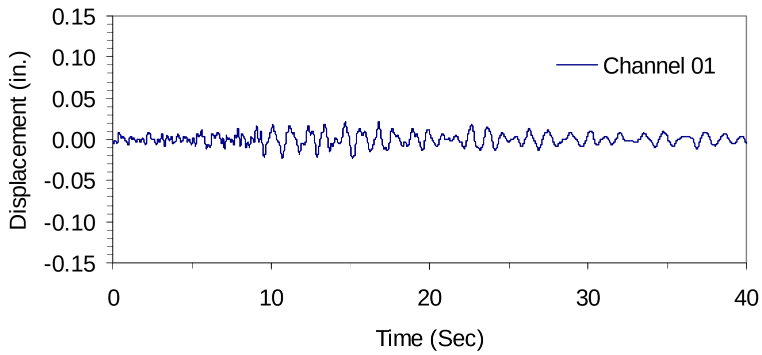

Whittier Narrows: Channel 2

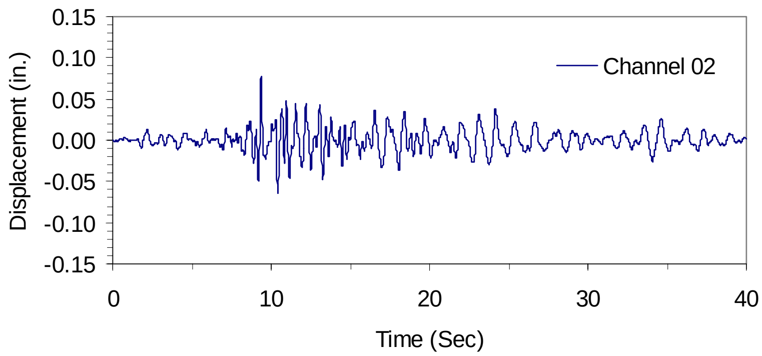

Whittier Narrows: Channel 3

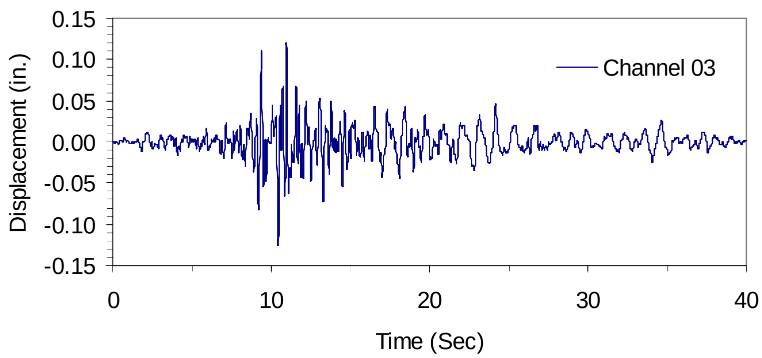

Whittier Narrows: Channel 4

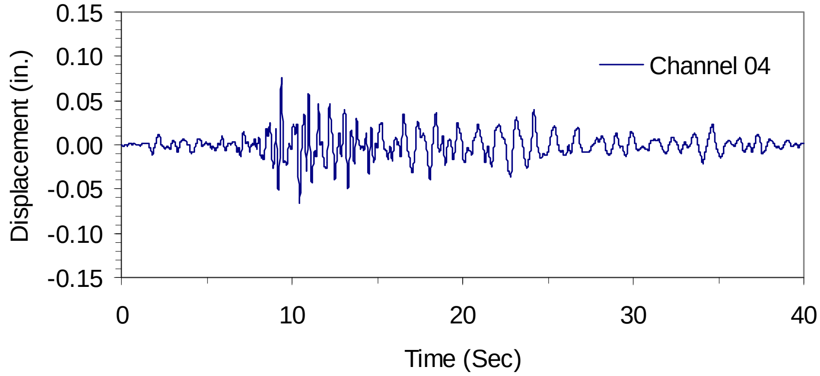

Whittier Narrows: Channel 5

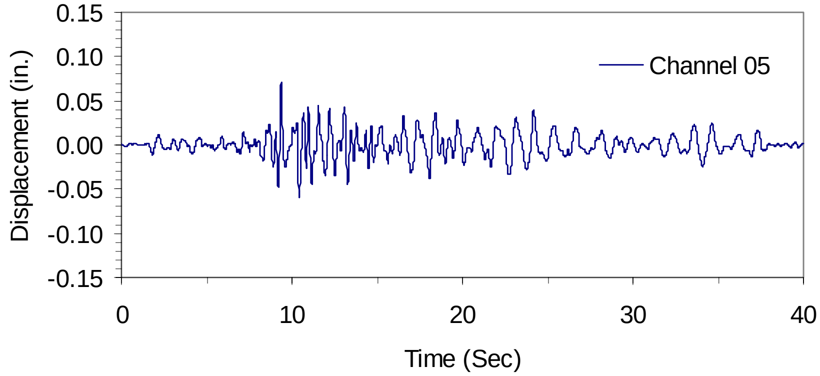

Whittier Narrows: Channel 6

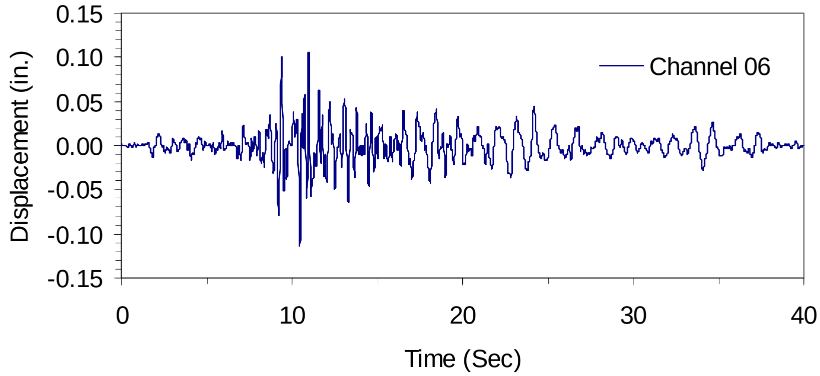

Whittier Narrows: Channel 7

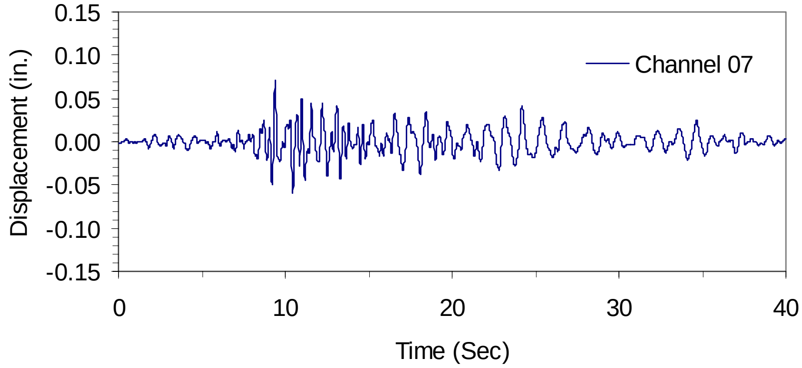

Whittier Narrows: Channel 8

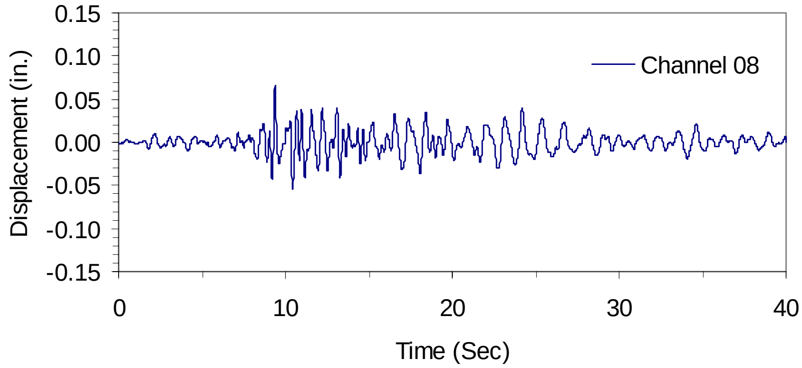

Whittier Narrows: Channel 9

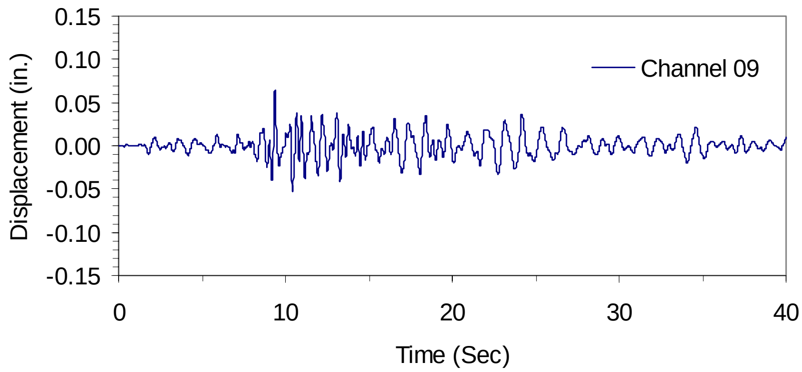

Whittier Narrows: Channel 10

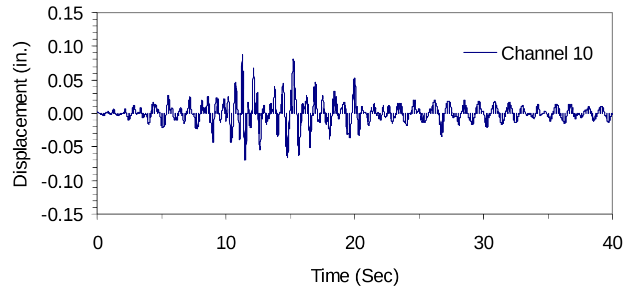

Whittier Narrows: Channel 11

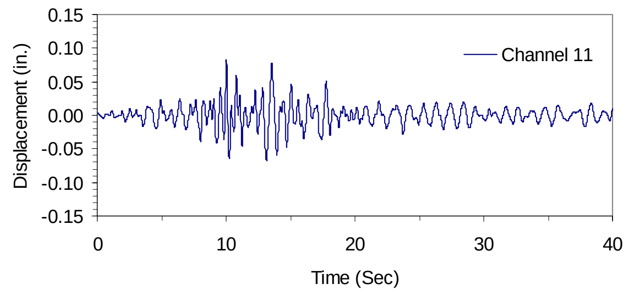

Whittier Narrows: Channel 12

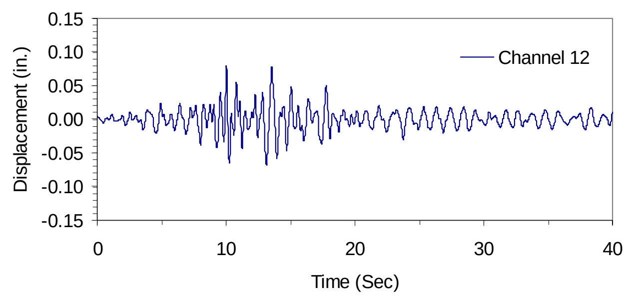

Whittier Narrows: Channel 13

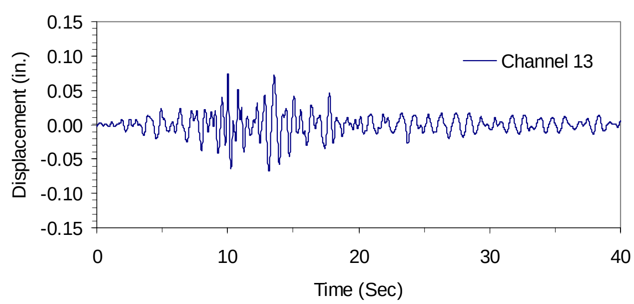

APPENDIX A-3

Recorded Acceleration Time Histories, Landers, 3-Story Building

Landers: Channel 1

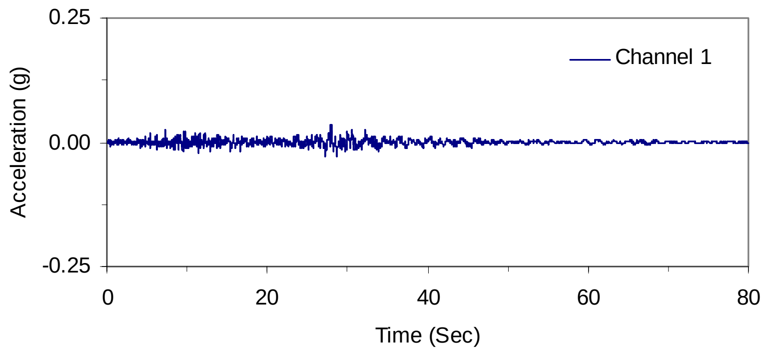

Landers: Channel 2

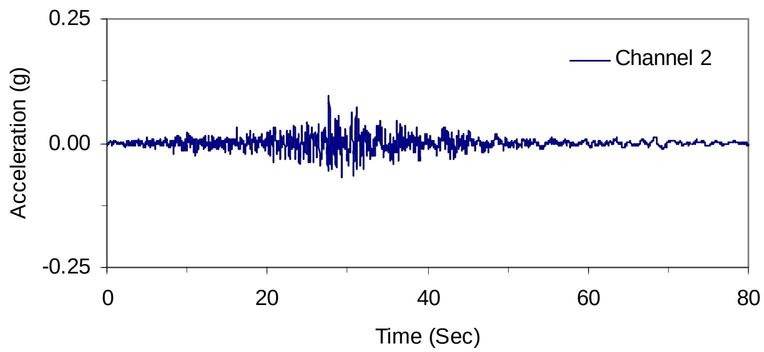

Landers: Channel 3

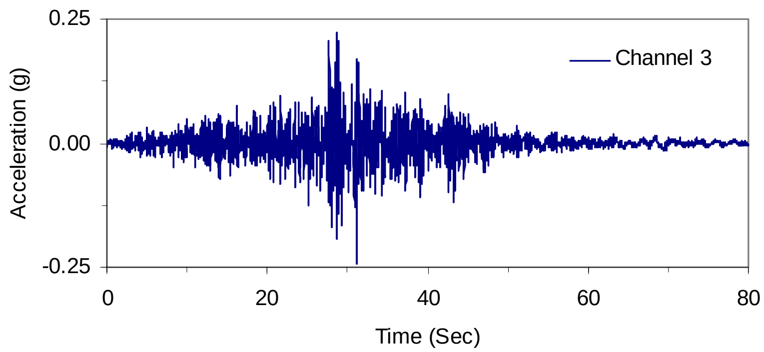

Landers: Channel 4

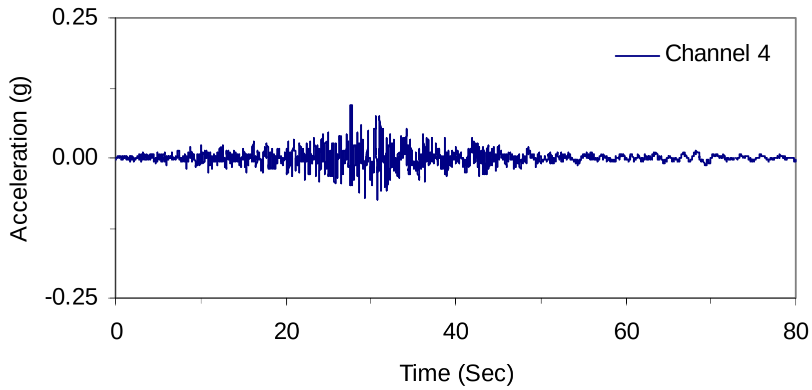

Landers: Channel 5

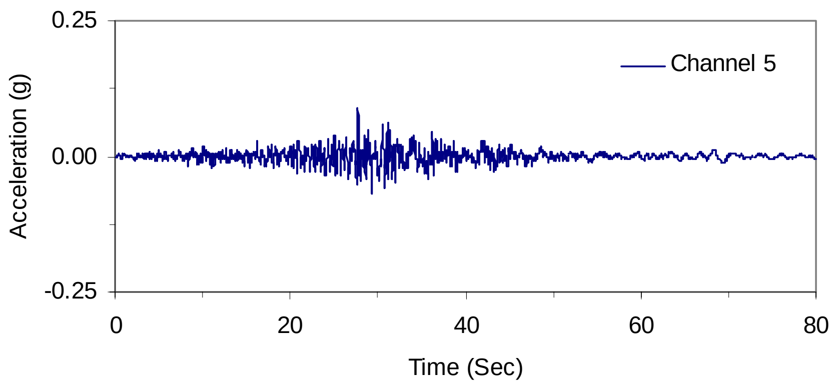

Landers: Channel 6

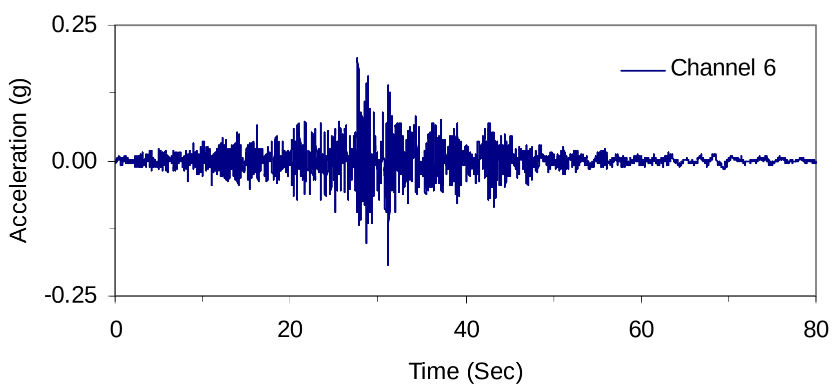

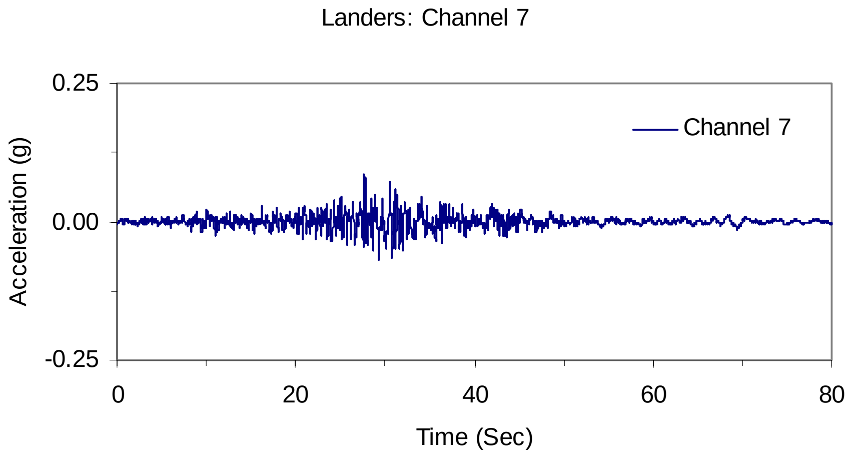
Landers: Channel 7
0.25
0.00
-0.25
Acceleration (g)
Channel 7
0
20
40
60
80
Time (Sec)

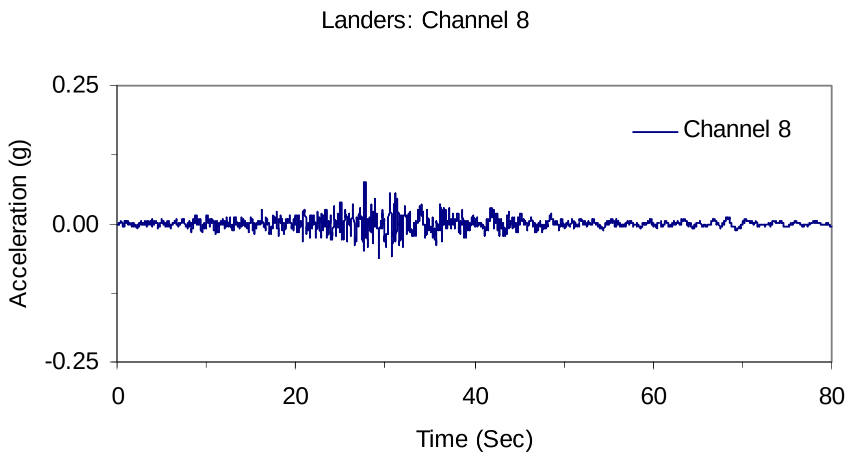
Landers: Channel 8
0.25
0.00
-0.25
Acceleration (g)
Channel 8
0
20
40
60
80
Time (Sec)

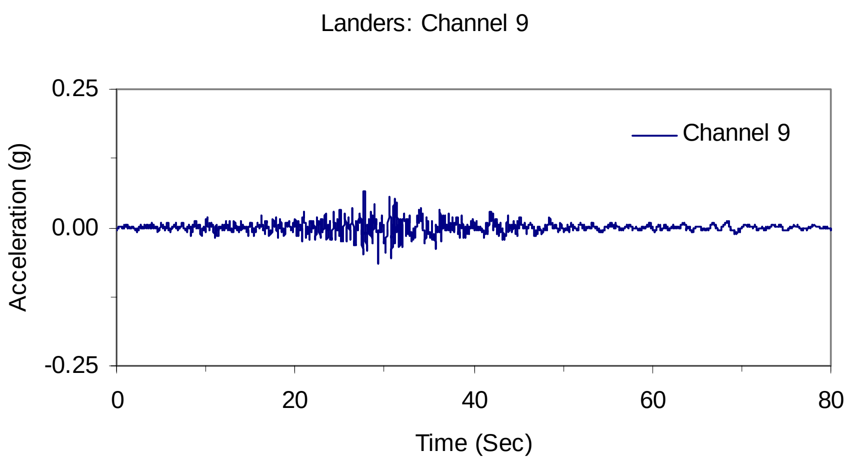
Landers: Channel 9
0.25
0.00
-0.25
Acceleration (g)
Channel 9
0
20
40
60
80
Time (Sec)

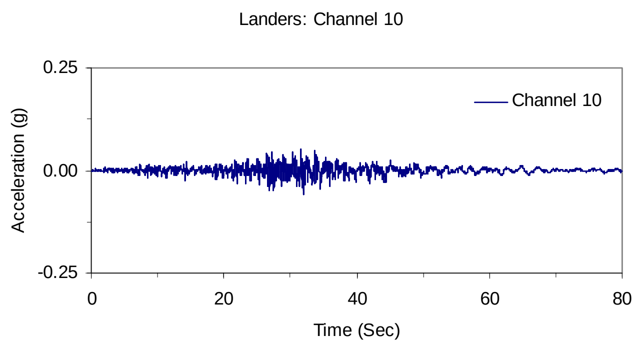
Landers: Channel 10
Channel 10
0.25
0.00
-0.25
Acceleration (g)
0
20
40
60
80
Time (Sec)

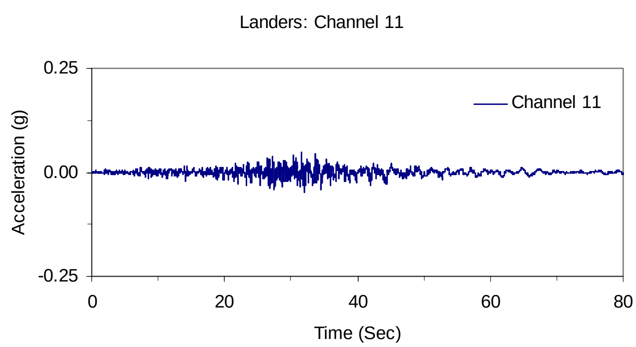
Landers: Channel 11
Channel 11
0.25
0.00
-0.25
Acceleration (g)
0
20
40
60
80
Time (Sec)

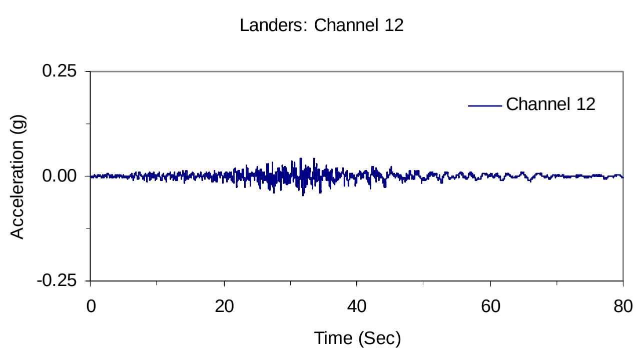
Landers: Channel 12
Channel 12
0.25
0.00
-0.25
Acceleration (g)
0
20
40
60
80
Time (Sec)

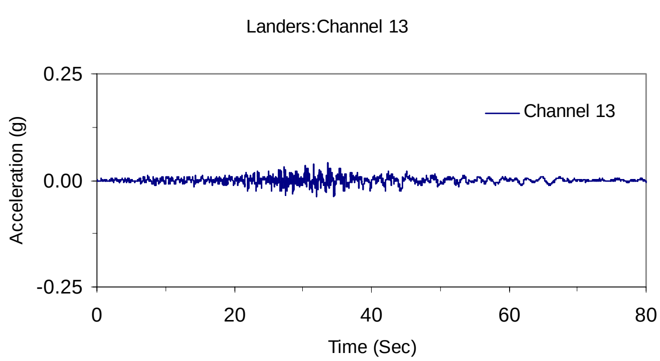
Landers:Channel 13
Channel 13
0.25
0.00
-0.25
Acceleration (g)
0
20
40
60
80
Time (Sec)

APPENDIX A-4

Recorded Displacement Time Histories, Landers, 3-Story Building

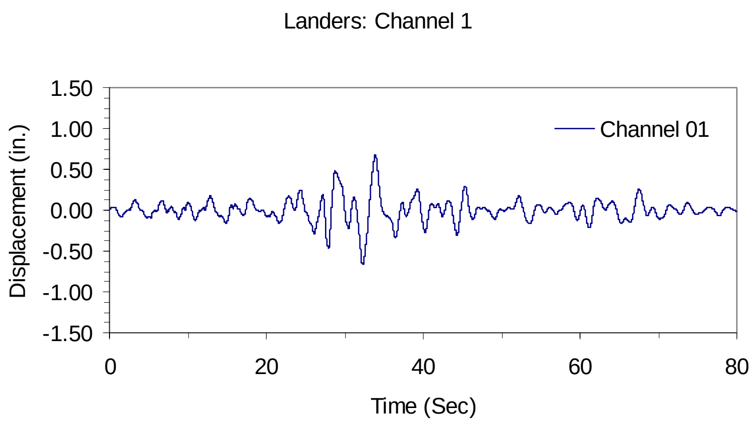

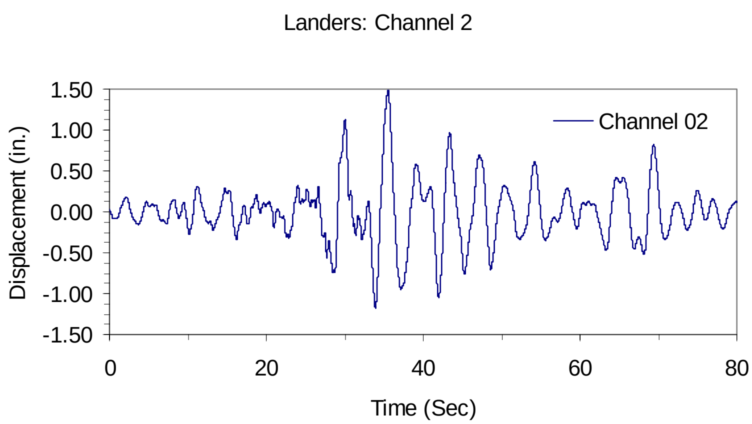

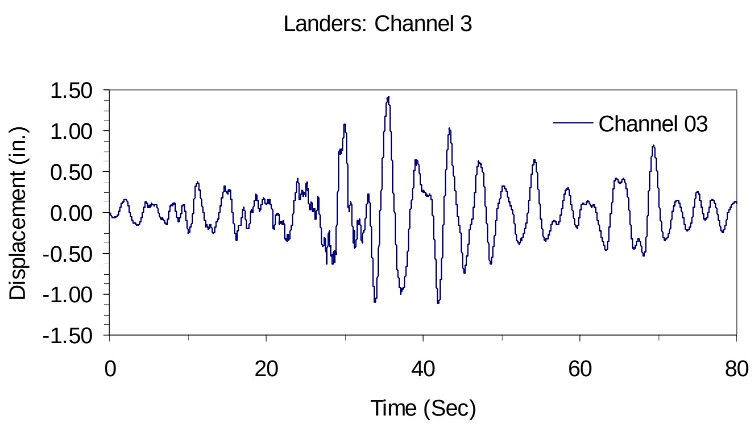

Landers: Channel 4

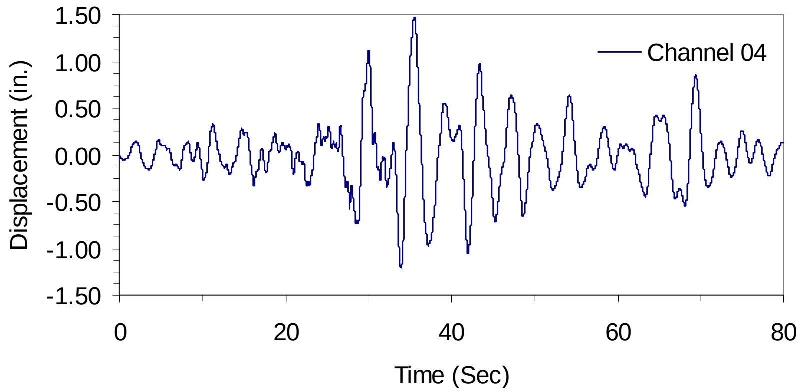

Landers: Channel 5

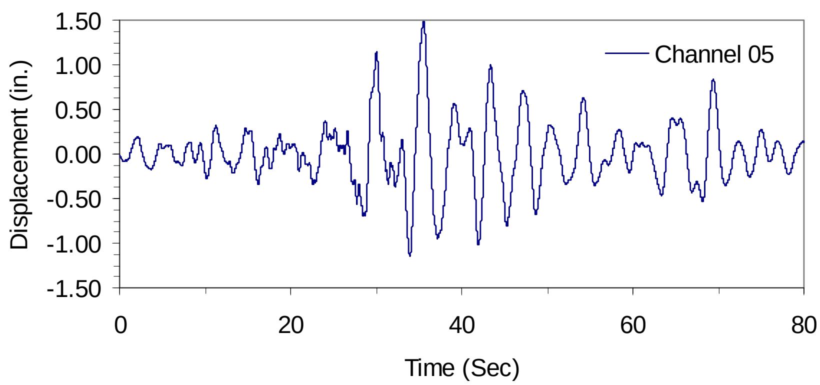

Landers: Channel 6

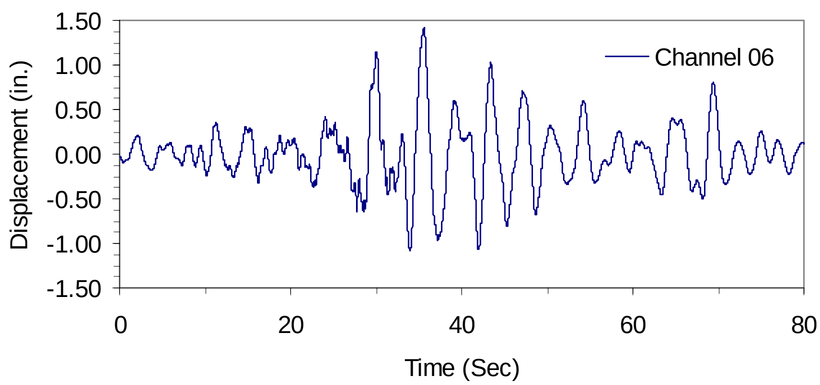

Landers: Channel 7

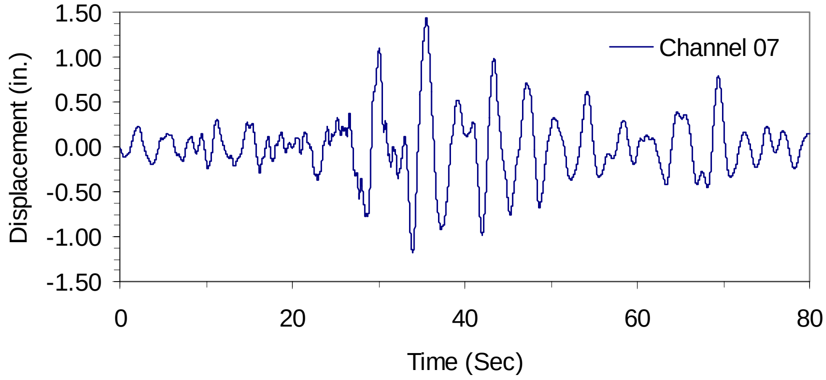

Landers: Channel 8

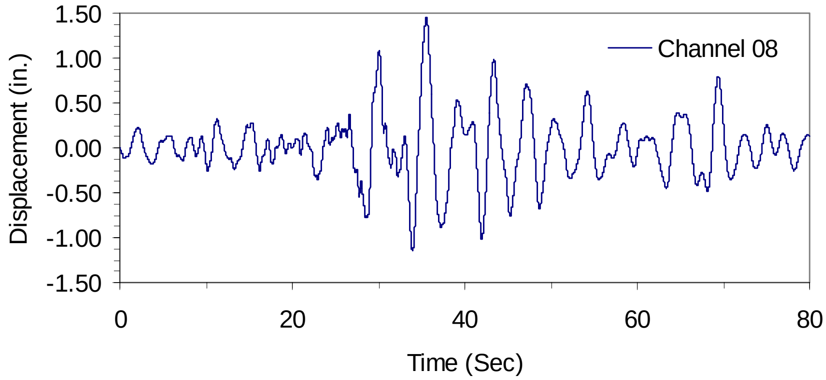

Landers: Channel 9

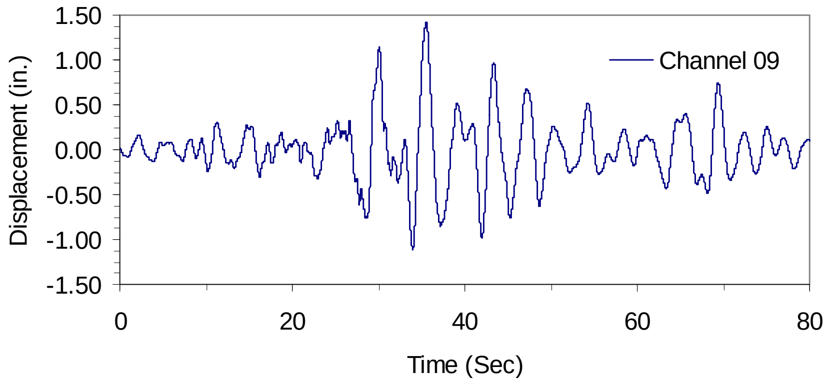

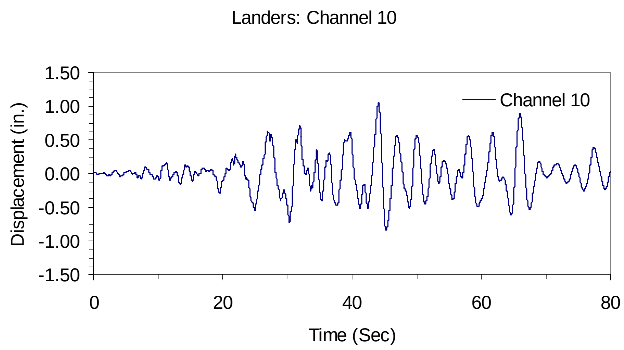
Landers: Channel 10
Channel 10
Displacement (in.)
1.50
1.00
0.50
0.00
-0.50
-1.00
-1.50
0
20
40
60
80
Time (Sec)

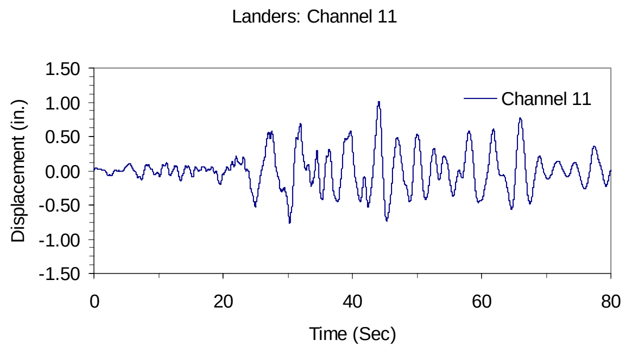
Landers: Channel 11
Channel 11
Displacement (in.)
1.50
1.00
0.50
0.00
-0.50
-1.00
-1.50
0
20
40
60
80
Time (Sec)

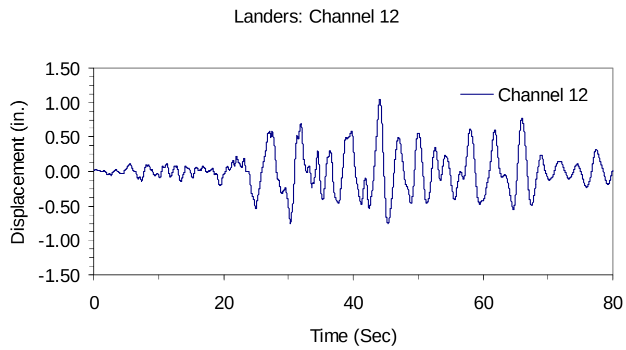
Landers: Channel 12
Channel 12
Displacement (in.)
1.50
1.00
0.50
0.00
-0.50
-1.00
-1.50
0
20
40
60
80
Time (Sec)

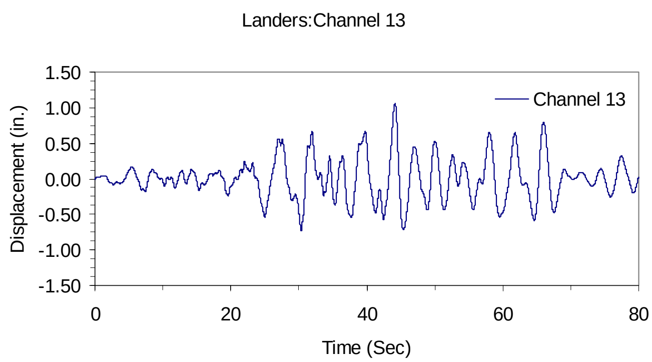
Landers:Channel 13
Channel 13
Displacement (in.)
1.50
1.00
0.50
0.00
-0.50
-1.00
-1.50
0
20
40
60
80
Time (Sec)

APPENDIX A-5

Recorded Acceleration Time Histories, Northridge, 3-Story Building

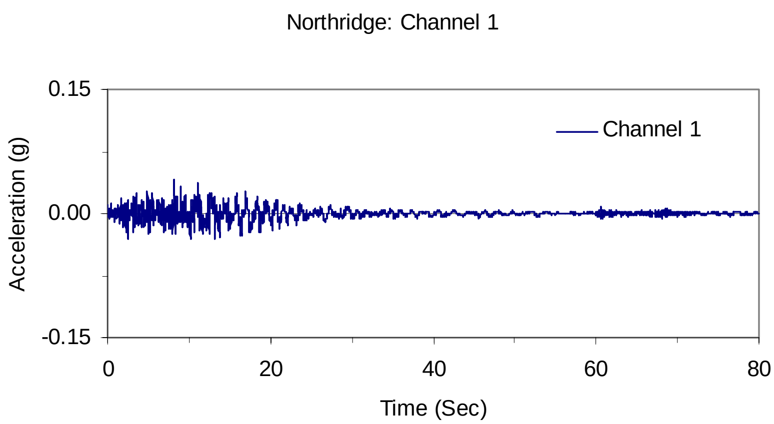

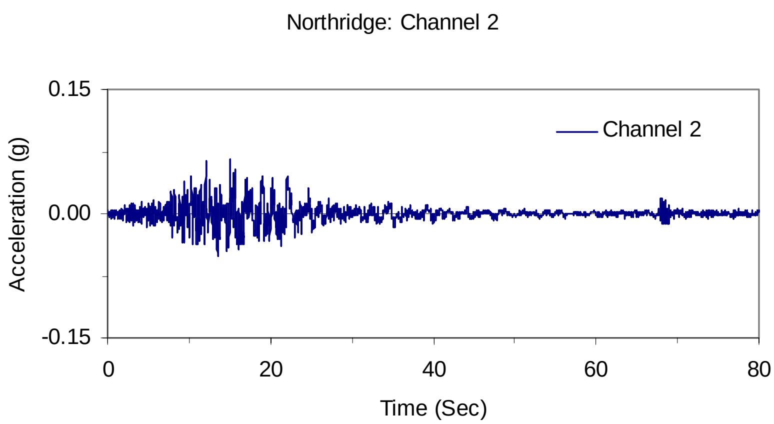

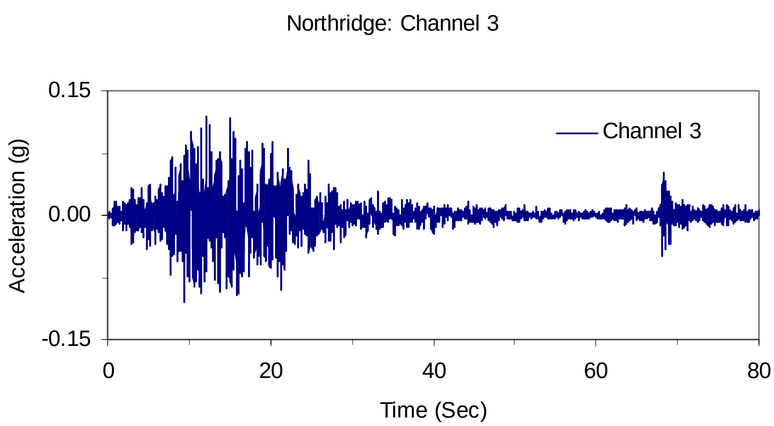

Northridge: Channel 4

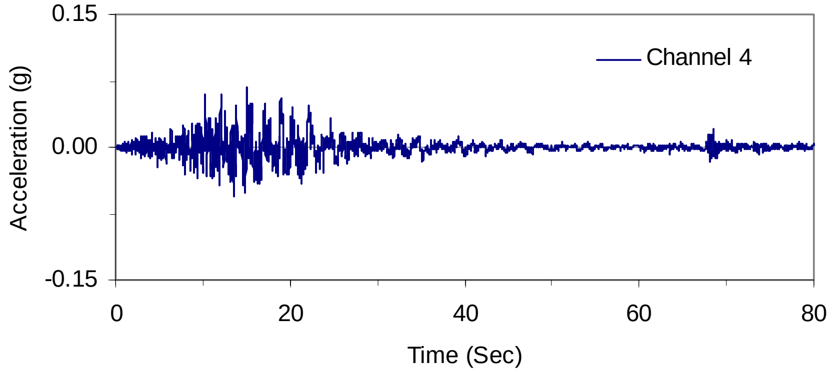

Northridge: Channel 5

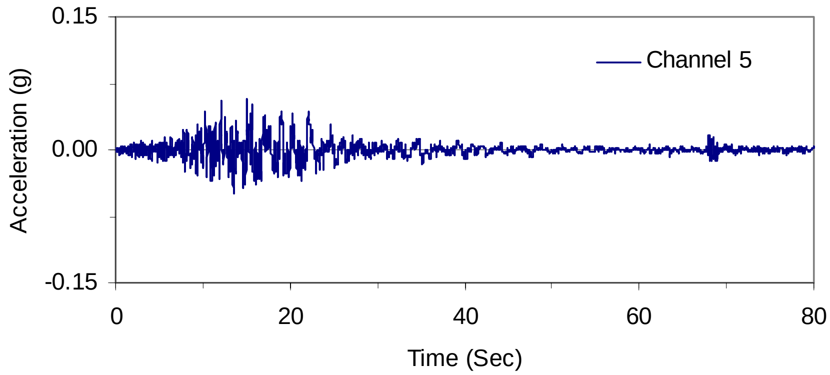

Northridge: Channel 6

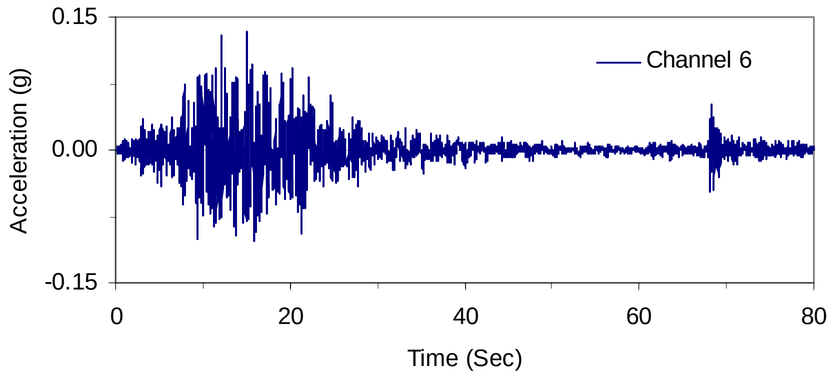

Northridge: Channel 7

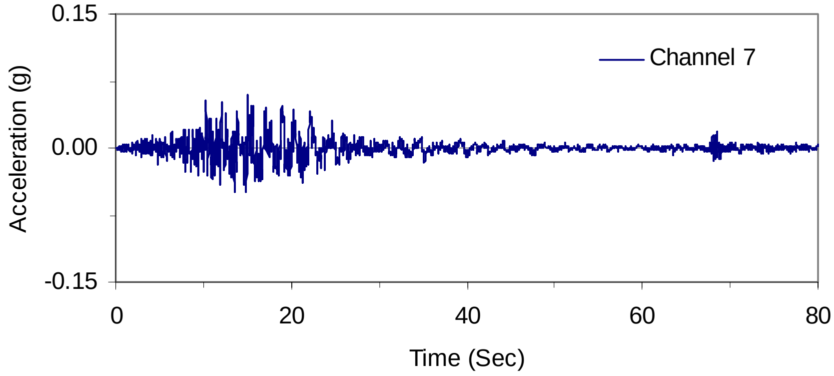

Northridge: Channel 8

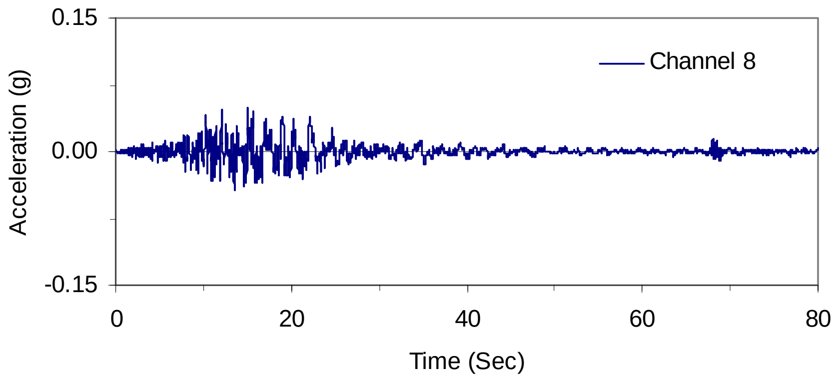

Northridge: Channel 9

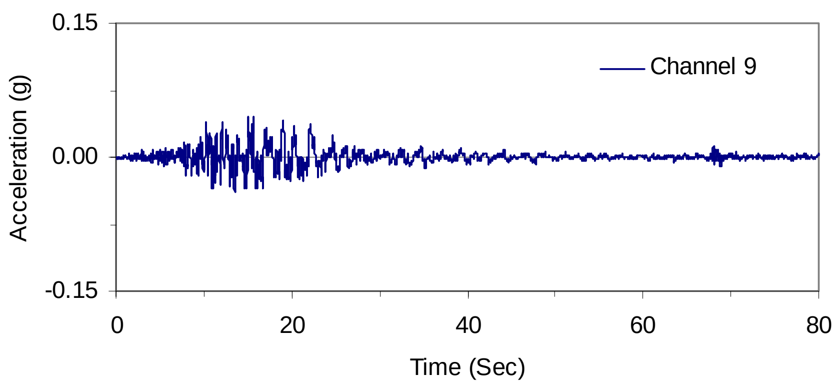

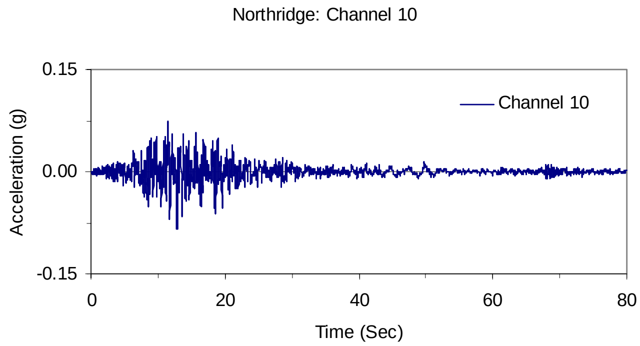
Northridge: Channel 10
Channel 10
0.15
0.00
-0.15
Acceleration (g)
0
20
40
60
80
Time (Sec)

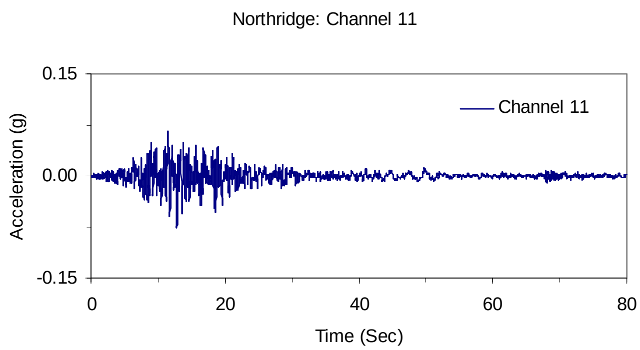
Northridge: Channel 11
Channel 11
0.15
0.00
-0.15
Acceleration (g)
0
20
40
60
80
Time (Sec)

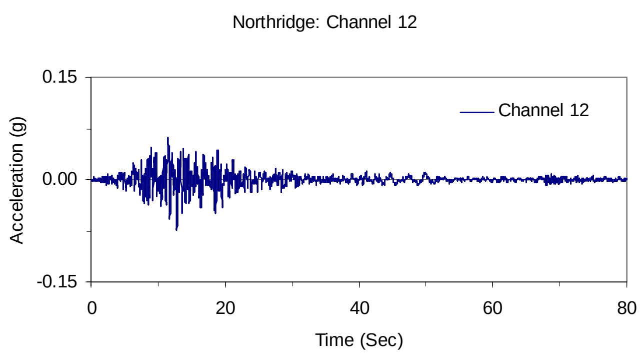
Northridge: Channel 12
Channel 12
0.15
0.00
-0.15
Acceleration (g)
0
20
40
60
80
Time (Sec)

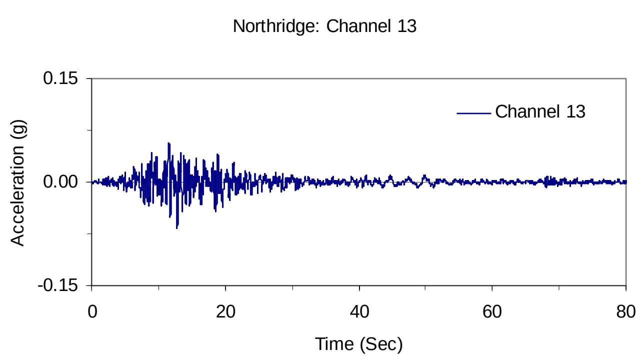
Northridge: Channel 13
Channel 13
0.15
0.00
-0.15
Acceleration (g)
0
20
40
60
80
Time (Sec)

APPENDIX A-6

Recorded Displacement Time Histories, Northridge, 3-Story Building

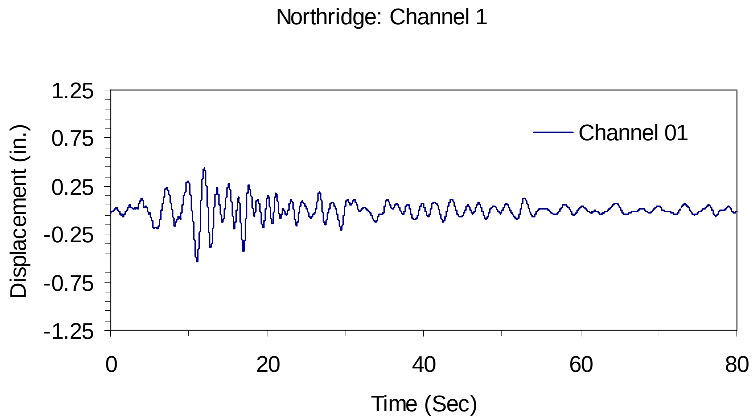

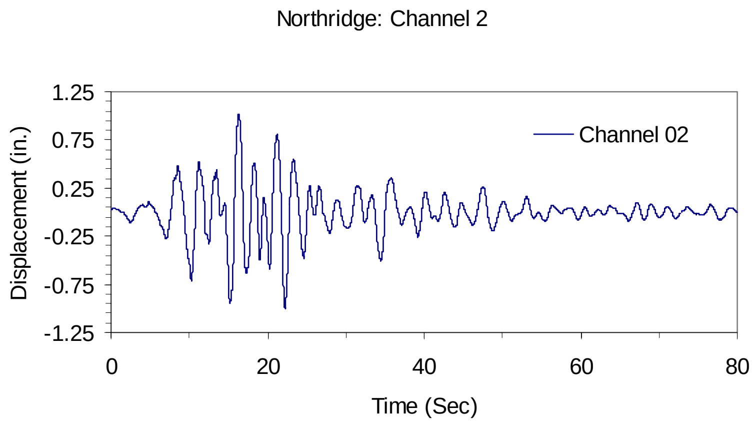

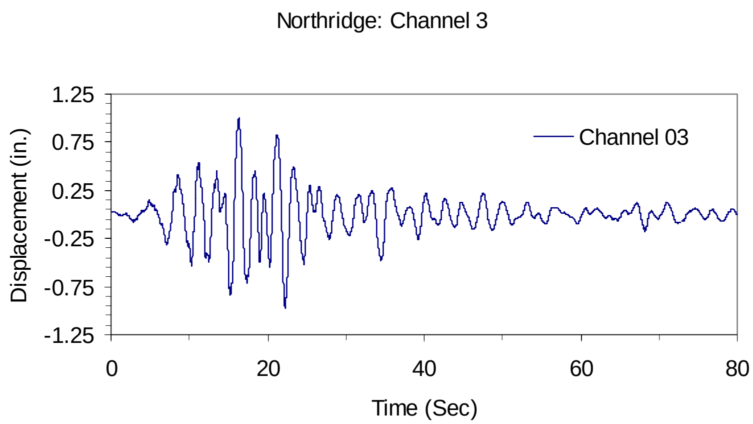

Northridge: Channel 4

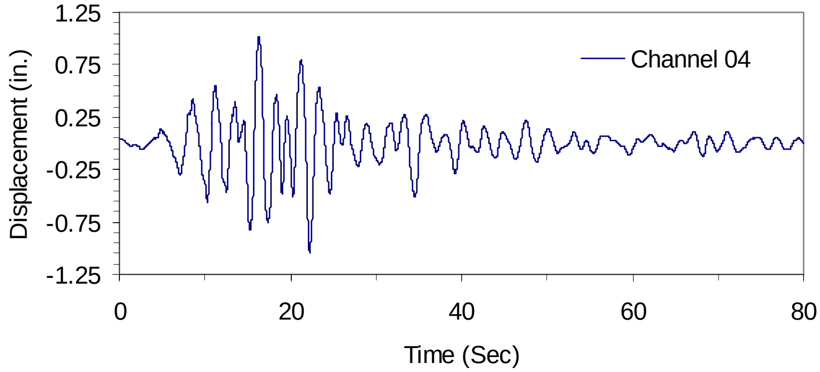

Northridge: Channel 5

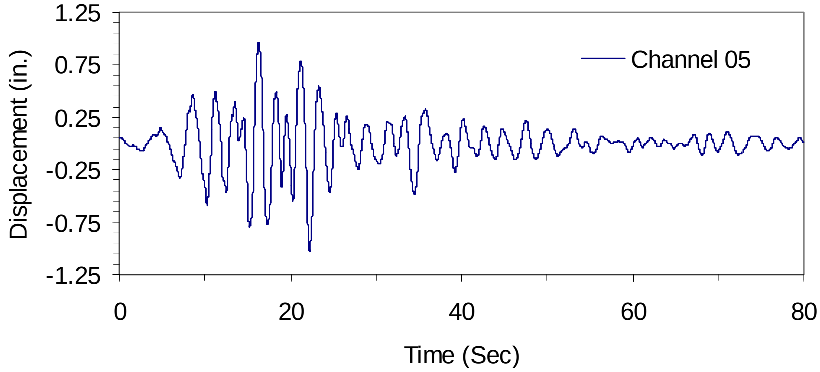

Northridge: Channel 6

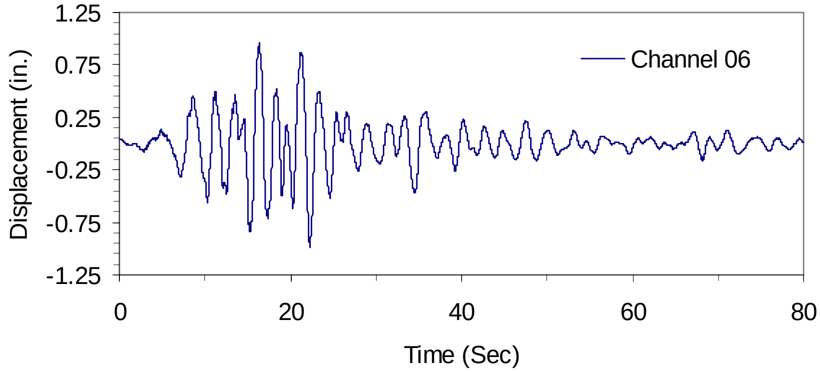

Northridge: Channel 7

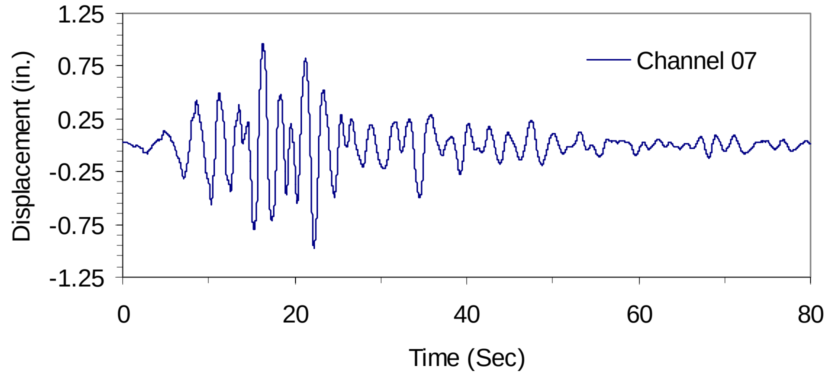

Northridge: Channel 8

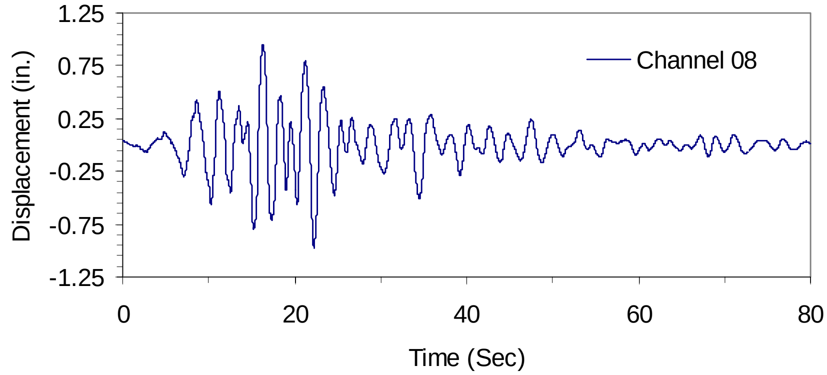

Northridge: Channel 9

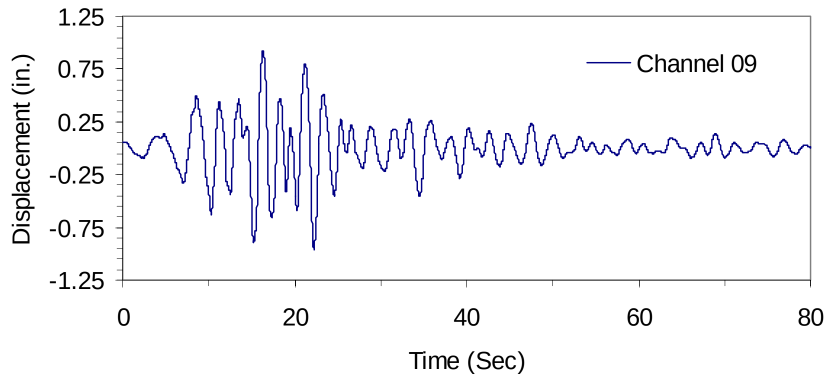

Northridge: Channel 10

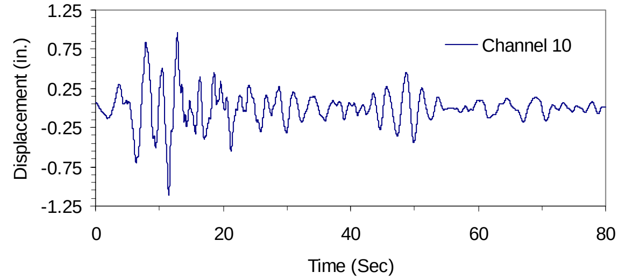

Northridge: Channel 11

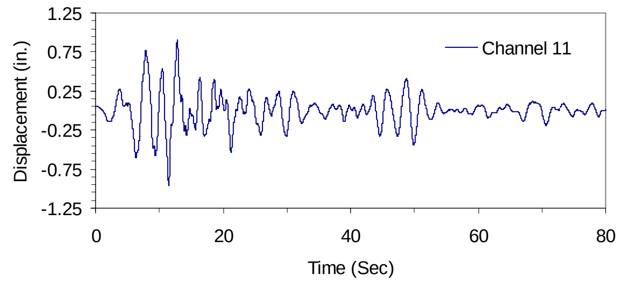

Northridge: Channel 12

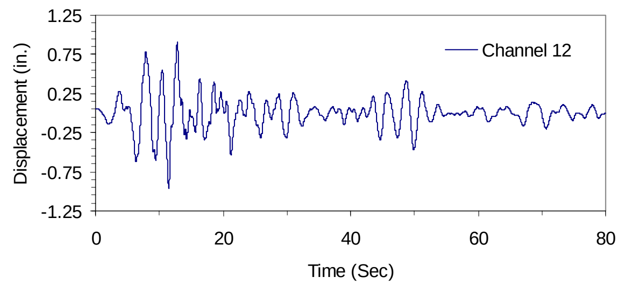

Northridge: Channel 13

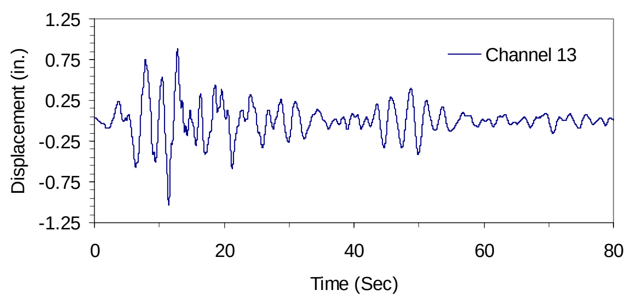

APPENDIX B-1

Recorded Acceleration Time Histories, Loma Prieta, 2-Story Building

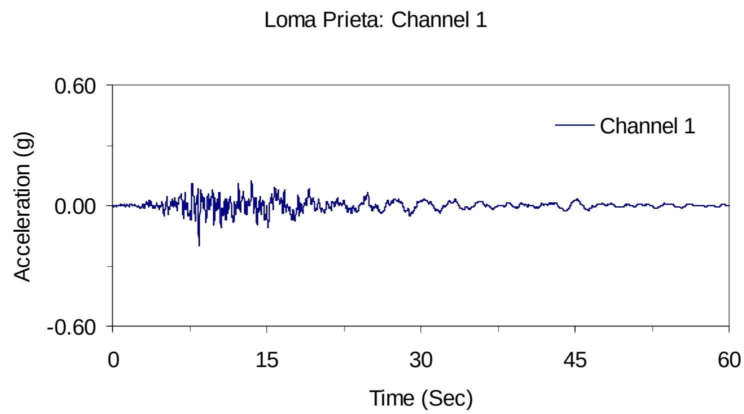

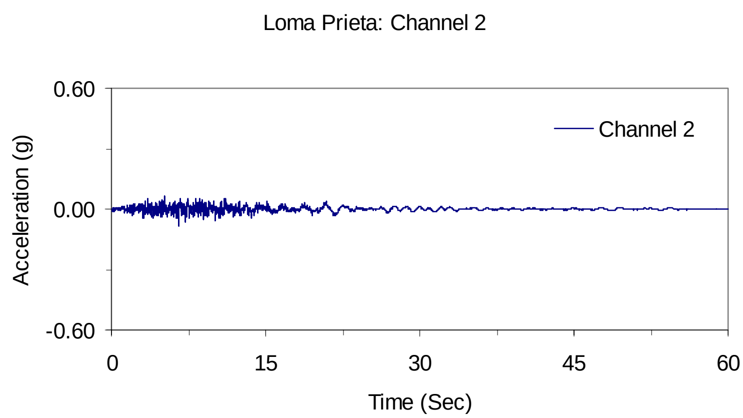

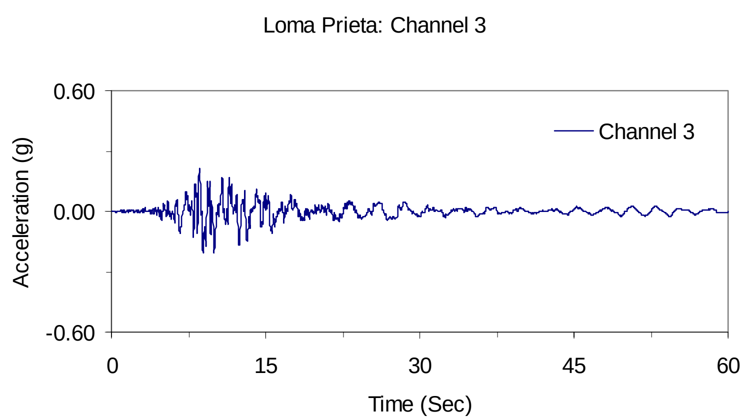

Loma Prieta: Channel 4

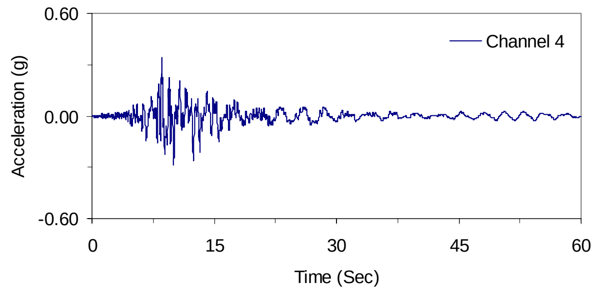

Loma Prieta: Channel 5

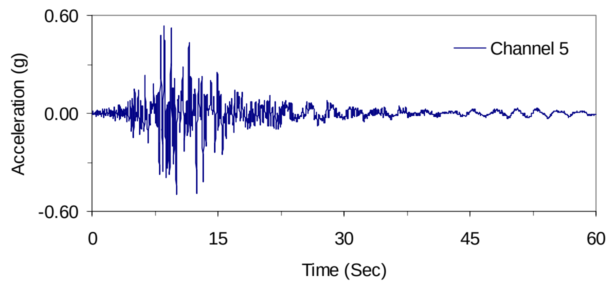

Loma Prieta: Channel 6

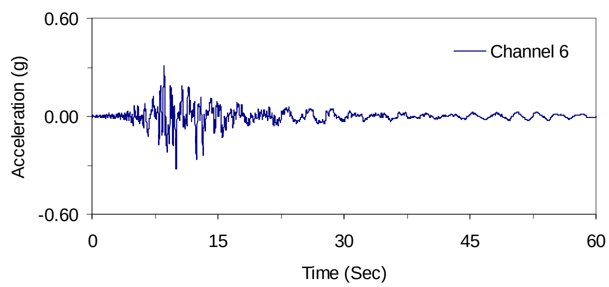

Loma Prieta: Channel 7

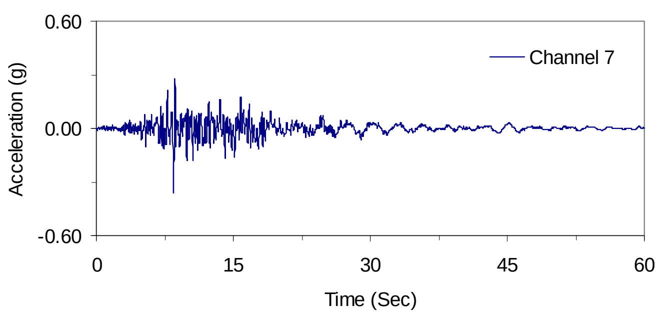

APPENDIX B-2

Recorded Displacement Time Histories, Loma Prieta, 2-Story Building

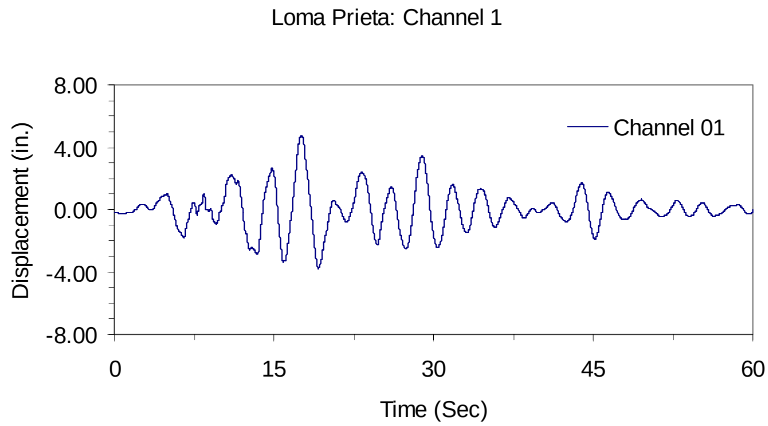

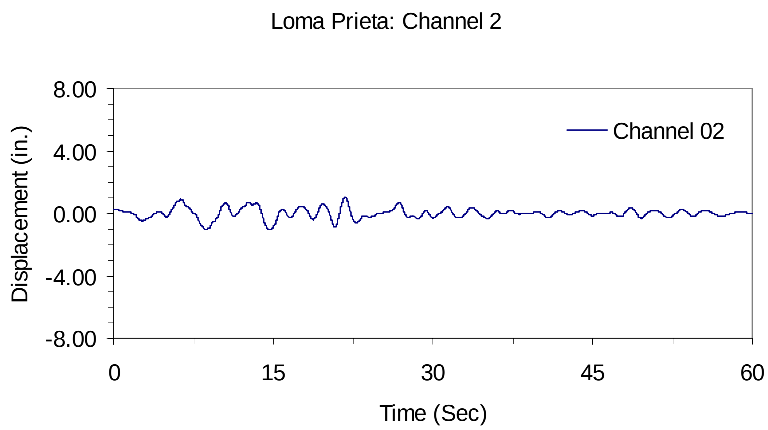

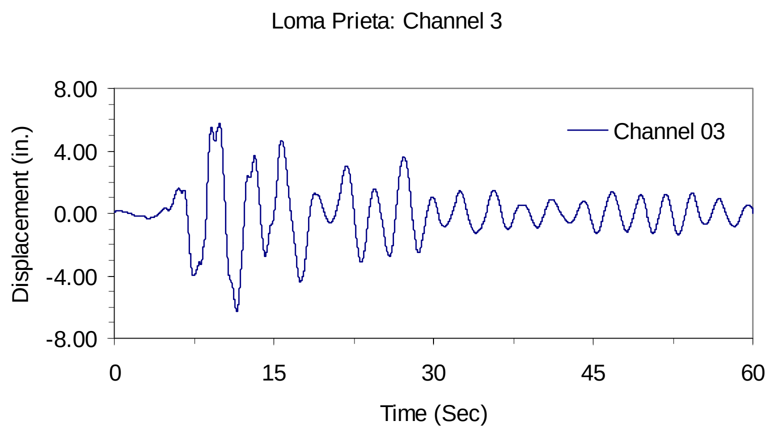

Loma Prieta: Channel 4

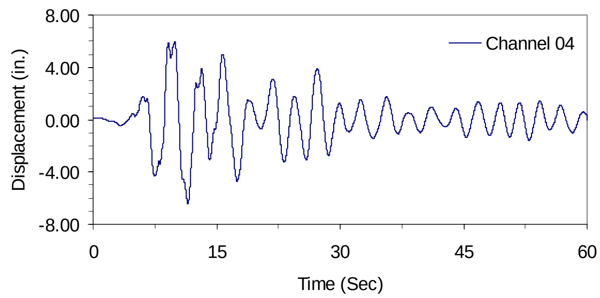

Loma Prieta: Channel 5

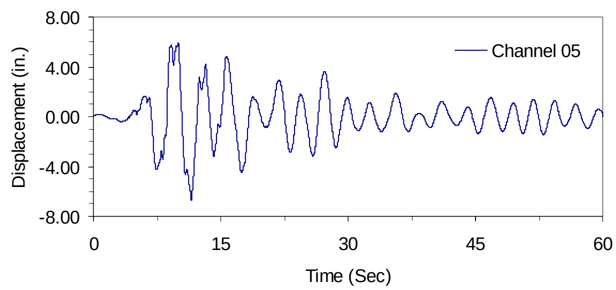

Loma Prieta: Channel 6

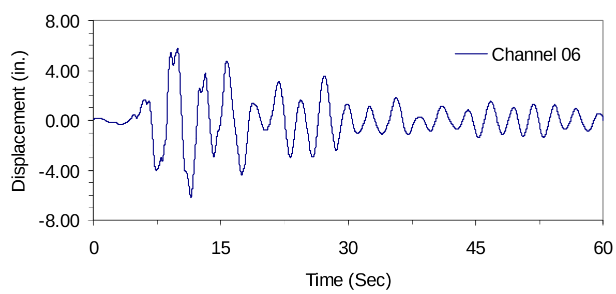

Loma Prieta: Channel 7

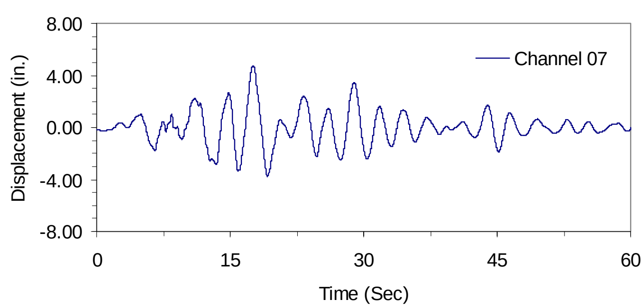

PEER REPORTS

PEER reports are available from the National Information Service for Earthquake Engineering (NISEE). To order PEER reports, please contact the Pacific Earthquake Engineering Research Center, 1301 South 46th Street, Richmond, California 94804-4698. Tel.: (510) 231-9468; Fax: (510) 231-9461.

PEER 2004/01 *Seismic Performance of Masonry Buildings and Design Implications.* Kerri Anne Taeko Tokoro, James C. Anderson, and Vitelmo V. Bertero. February 2004.

PEER 2003/18 *Performance Models for Flexural Damage in Reinforced Concrete Columns.* Michael Berry and Marc Eberhard. August 2004.

PEER 2003/16 *Seismic Demands for Performance-Based Design of Bridges.* Kevin Mackie and Božidar Stojadinović. August 2003.

PEER 2003/15 *Seismic Demands for Nondeteriorating Frame Structures and Their Dependence on Ground Motions.* Ricardo Antonio Medina and Helmut Krawinkler. May 2004.

PEER 2003/14 *Finite Element Reliability and Sensitivity Methods for Performance-Based Earthquake Engineering.* Terje Haukaas and Armen Der Kiureghian. April 2004.

PEER 2003/13 *Effects of Connection Hysteretic Degradation on the Seismic Behavior of Steel Moment-Resisting Frames.* Janise E. Rodgers and Stephen A. Mahin. March 2004.

PEER 2003/12 *Implementation Manual for the Seismic Protection of Laboratory Contents: Format and Case Studies.* William T. Holmes and Mary C. Comerio. October 2003.

PEER 2003/11 *Fifth U.S.-Japan Workshop on Performance-Based Earthquake Engineering Methodology for Reinforced Concrete Building Structures.* February 2004.

PEER 2003/10 *A Beam-Column Joint Model for Simulating the Earthquake Response of Reinforced Concrete Frames.* Laura N. Lowes, Nilanjan Mitra, and Arash Altoontash. February 2004.

PEER 2003/09 *Sequencing Repairs after an Earthquake: An Economic Approach.* Marco Casari and Simon J. Wilkie. April 2004.

PEER 2003/08 *A Technical Framework for Probability-Based Demand and Capacity Factor Design (DCFD) Seismic Formats*. Fatemeh Jalayer and C. Allin Cornell. November 2003.

PEER 2003/07 *Uncertainty Specification and Propagation for Loss Estimation Using FOSM Methods.* Jack W. Baker and C. Allin Cornell. September 2003.

PEER 2003/06 *Performance of Circular Reinforced Concrete Bridge Columns under Bidirectional Earthquake Loading*. Mahmoud M. Hachem, Stephen A. Mahin, and Jack P. Moehle. February 2003.

PEER 2003/05 *Response Assessment for Building-Specific Loss Estimation.* Eduardo Miranda and Shahram Taghavi. September 2003.

PEER 2003/04 *Experimental Assessment of Columns with Short Lap Splices Subjected to Cyclic Loads*. Murat Melek, John W. Wallace, and Joel Conte. April 2003.

PEER 2003/03 *Probabilistic Response Assessment for Building-Specific Loss Estimation.* Eduardo Miranda and Hesameddin Aslani. September 2003.

PEER 2003/02 *Software Framework for Collaborative Development of Nonlinear Dynamic Analysis Program.* Jun Peng and Kincho H. Law. September 2003.

PEER 2003/01 *Shake Table Tests and Analytical Studies on the Gravity Load Collapse of Reinforced Concrete Frames.* Kenneth John Elwood and Jack P. Moehle. November 2003

PEER 2002/24 *Performance of Beam to Column Bridge Joints Subjected to a Large Velocity Pulse.* Natalie Gibson, André Filiatrault, and Scott A. Ashford. April 2002.

PEER 2002/23 *Effects of Large Velocity Pulses on Reinforced Concrete Bridge Columns.* Greg L. Orozco and Scott A. Ashford. April 2002.

PEER 2002/22 *Characterization of Large Velocity Pulses for Laboratory Testing.* Kenneth E. Cox and Scott A. Ashford. April 2002.

PEER 2002/21 *Fourth U.S.-Japan Workshop on Performance-Based Earthquake Engineering Methodology for Reinforced Concrete Building Structures*. December 2002.

PEER 2002/20 *Barriers to Adoption and Implementation of PBEE Innovations.* Peter J. May. August 2002.

PEER 2002/19 *Economic-Engineered Integrated Models for Earthquakes: Socioeconomic Impacts.* Peter Gordon, James E. Moore II, and Harry W. Richardson. July 2002.

PEER 2002/18 *Assessment of Reinforced Concrete Building Exterior Joints with Substandard Details.* Chris P. Pantelides, Jon Hansen, Justin Nadauld, and Lawrence D. Reaveley. May 2002.

PEER 2002/17 *Structural Characterization and Seismic Response Analysis of a Highway Overcrossing Equipped with Elastomeric Bearings and Fluid Dampers: A Case Study.* Nicos Makris and Jian Zhang. November 2002.

PEER 2002/16 *Estimation of Uncertainty in Geotechnical Properties for Performance-Based Earthquake Engineering.* Allen L. Jones, Steven L. Kramer, and Pedro Arduino. December 2002.

PEER 2002/15 *Seismic Behavior of Bridge Columns Subjected to Various Loading Patterns.* Asadollah Esmaeily-Gh. and Yan Xiao. December 2002.

PEER 2002/14 *Inelastic Seismic Response of Extended Pile Shaft Supported Bridge Structures.* T.C. Hutchinson, R.W. Boulanger, Y.H. Chai, and I.M. Idriss. December 2002.

PEER 2002/13 *Probabilistic Models and Fragility Estimates for Bridge Components and Systems.* Paolo Gardoni, Armen Der Kiureghian, and Khalid M. Mosalam. June 2002.

PEER 2002/12 *Effects of Fault Dip and Slip Rake on Near-Source Ground Motions: Why Chi-Chi Was a Relatively Mild M7.6 Earthquake.* Brad T. Aagaard, John F. Hall, and Thomas H. Heaton. December 2002.

PEER 2002/11 *Analytical and Experimental Study of Fiber-Reinforced Strip Isolators*. James M. Kelly and Shakhzod M. Takhirov. September 2002.

PEER 2002/10 *Centrifuge Modeling of Settlement and Lateral Spreading with Comparisons to Numerical Analyses***.** Sivapalan Gajan and Bruce L. Kutter. January 2003.

PEER 2002/09 *Documentation and Analysis of Field Case Histories of Seismic Compression during the 1994 Northridge, California, Earthquake.* Jonathan P. Stewart, Patrick M. Smith, Daniel H. Whang, and Jonathan D. Bray. October 2002.

PEER 2002/08 *Component Testing, Stability Analysis and Characterization of Buckling-Restrained Unbonded Braces™.* Cameron Black, Nicos Makris, and Ian Aiken. September 2002.

PEER 2002/07 *Seismic Performance of Pile-Wharf Connections.* Charles W. Roeder, Robert Graff, Jennifer Soderstrom, and Jun Han Yoo. December 2001.

PEER 2002/06 *The Use of Benefit-Cost Analysis for Evaluation of Performance-Based Earthquake Engineering Decisions*. Richard O. Zerbe and Anthony Falit-Baiamonte. September 2001.

PEER 2002/05 *Guidelines, Specifications, and Seismic Performance Characterization of Nonstructural Building Components and Equipment*. André Filiatrault, Constantin Christopoulos, and Christopher Stearns. September 2001.

PEER 2002/04 *Consortium of Organizations for Strong-Motion Observation Systems and the Pacific Earthquake Engineering Research Center Lifelines Program: Invited Workshop on Archiving and Web Dissemination of Geotechnical Data, 4–5 October 2001*. September 2002.

PEER 2002/03 *Investigation of Sensitivity of Building Loss Estimates to Major Uncertain Variables for the Van Nuys Testbed.* Keith A. Porter, James L. Beck, and Rustem V. Shaikhutdinov. August 2002.

PEER 2002/02 *The Third U.S.-Japan Workshop on Performance-Based Earthquake Engineering Methodology for Reinforced Concrete Building Structures*. July 2002.

PEER 2002/01 *Nonstructural Loss Estimation: The UC Berkeley Case Study.* Mary C. Comerio and John C. Stallmeyer. December 2001.

PEER 2001/16 *Statistics of SDF-System Estimate of Roof Displacement for Pushover Analysis of Buildings.* Anil K. Chopra, Rakesh K. Goel, and Chatpan Chintanapakdee. December 2001.

PEER 2001/15 *Damage to Bridges during the 2001 Nisqually Earthquake.* R. Tyler Ranf, Marc O. Eberhard, and Michael P. Berry. November 2001.

PEER 2001/14 *Rocking Response of Equipment Anchored to a Base Foundation.* Nicos Makris and Cameron J. Black. September 2001.

PEER 2001/13 *Modeling Soil Liquefaction Hazards for Performance-Based Earthquake Engineering.* Steven L. Kramer and Ahmed-W. Elgamal. February 2001.

PEER 2001/12 *Development of Geotechnical Capabilities in OpenSees.* Boris Jeremic. September 2001.

PEER 2001/11 *Analytical and Experimental Study of Fiber-Reinforced Elastomeric Isolators*. James M. Kelly and Shakhzod M. Takhirov. September 2001.

PEER 2001/10 *Amplification Factors for Spectral Acceleration in Active Regions.* Jonathan P. Stewart, Andrew H. Liu, Yoojoong Choi, and Mehmet B. Baturay. December 2001.

PEER 2001/09 *Ground Motion Evaluation Procedures for Performance-Based Design.* Jonathan P. Stewart, Shyh-Jeng Chiou, Jonathan D. Bray, Robert W. Graves, Paul G. Somerville, and Norman A. Abrahamson. September 2001.

PEER 2001/08 *Experimental and Computational Evaluation of Reinforced Concrete Bridge Beam-Column Connections for Seismic Performance*. Clay J. Naito, Jack P. Moehle, and Khalid M. Mosalam. November 2001.

PEER 2001/07 *The Rocking Spectrum and the Shortcomings of Design Guidelines.* Nicos Makris and Dimitrios Konstantinidis. August 2001.

PEER 2001/06 *Development of an Electrical Substation Equipment Performance Database for Evaluation of Equipment Fragilities*. Thalia Agnanos. April 1999.

PEER 2001/05 *Stiffness Analysis of Fiber-Reinforced Elastomeric Isolators.* Hsiang-Chuan Tsai and James M. Kelly. May 2001.

PEER 2001/04 *Organizational and Societal Considerations for Performance-Based Earthquake Engineering.* Peter J. May. April 2001.

PEER 2001/03 *A Modal Pushover Analysis Procedure to Estimate Seismic Demands for Buildings: Theory and Preliminary Evaluation.* Anil K. Chopra and Rakesh K. Goel. January 2001.

PEER 2001/02 *Seismic Response Analysis of Highway Overcrossings Including Soil-Structure Interaction.* Jian Zhang and Nicos Makris. March 2001.

PEER 2001/01 *Experimental Study of Large Seismic Steel Beam-to-Column Connections.* Egor P. Popov and Shakhzod M. Takhirov. November 2000.

PEER 2000/10 *The Second U.S.-Japan Workshop on Performance-Based Earthquake Engineering Methodology for Reinforced Concrete Building Structures.* March 2000.

PEER 2000/09 *Structural Engineering Reconnaissance of the August 17, 1999 Earthquake: Kocaeli (Izmit), Turkey.* Halil Sezen, Kenneth J. Elwood, Andrew S. Whittaker, Khalid Mosalam, John J. Wallace, and John F. Stanton. December 2000.

PEER 2000/08 *Behavior of Reinforced Concrete Bridge Columns Having Varying Aspect Ratios and Varying Lengths of Confinement.* Anthony J. Calderone, Dawn E. Lehman, and Jack P. Moehle. January 2001.

PEER 2000/07 *Cover-Plate and Flange-Plate Reinforced Steel Moment-Resisting Connections.* Taejin Kim, Andrew S. Whittaker, Amir S. Gilani, Vitelmo V. Bertero, and Shakhzod M. Takhirov. September 2000.

PEER 2000/06 *Seismic Evaluation and Analysis of 230-kV Disconnect Switches.* Amir S. J. Gilani, Andrew S. Whittaker, Gregory L. Fenves, Chun-Hao Chen, Henry Ho, and Eric Fujisaki. July 2000.

PEER 2000/05 *Performance-Based Evaluation of Exterior Reinforced Concrete Building Joints for Seismic Excitation.* Chandra Clyde, Chris P. Pantelides, and Lawrence D. Reaveley. July 2000.

PEER 2000/04 *An Evaluation of Seismic Energy Demand: An Attenuation Approach.* Chung-Che Chou and Chia-Ming Uang. July 1999.

PEER 2000/03 *Framing Earthquake Retrofitting Decisions: The Case of Hillside Homes in Los Angeles.* Detlof von Winterfeldt, Nels Roselund, and Alicia Kitsuse. March 2000.

PEER 2000/02 *U.S.-Japan Workshop on the Effects of Near-Field Earthquake Shaking.* Andrew Whittaker, ed. July 2000.

PEER 2000/01 *Further Studies on Seismic Interaction in Interconnected Electrical Substation Equipment.* Armen Der Kiureghian, Kee-Jeung Hong, and Jerome L. Sackman. November 1999.

PEER 1999/14 *Seismic Evaluation and Retrofit of 230-kV Porcelain Transformer Bushings*. Amir S. Gilani, Andrew S. Whittaker, Gregory L. Fenves, and Eric Fujisaki. December 1999.

PEER 1999/13 *Building Vulnerability Studies: Modeling and Evaluation of Tilt-up and Steel Reinforced Concrete Buildings.* John W. Wallace, Jonathan P. Stewart, and Andrew S. Whittaker, editors. December 1999.

PEER 1999/12 *Rehabilitation of Nonductile RC Frame Building Using Encasement Plates and Energy-Dissipating Devices.* Mehrdad Sasani, Vitelmo V. Bertero, James C. Anderson. December 1999.

PEER 1999/11 *Performance Evaluation Database for Concrete Bridge Components and Systems under Simulated Seismic Loads.* Yael D. Hose and Frieder Seible. November 1999.

PEER 1999/10 *U.S.-Japan Workshop on Performance-Based Earthquake Engineering Methodology for Reinforced Concrete Building Structures.* December 1999.

PEER 1999/09 *Performance Improvement of Long Period Building Structures Subjected to Severe Pulse-Type Ground Motions*. James C. Anderson, Vitelmo V. Bertero, and Raul Bertero. October 1999.

PEER 1999/08 *Envelopes for Seismic Response Vectors.* Charles Menun and Armen Der Kiureghian. July 1999.

PEER 1999/07 *Documentation of Strengths and Weaknesses of Current Computer Analysis Methods for Seismic Performance of Reinforced Concrete Members.* William F. Cofer. November 1999.

PEER 1999/06 *Rocking Response and Overturning of Anchored Equipment under Seismic Excitations.* Nicos Makris and Jian Zhang. November 1999.

PEER 1999/05 *Seismic Evaluation of 550 kV Porcelain Transformer Bushings.* Amir S. Gilani, Andrew S. Whittaker, Gregory L. Fenves, and Eric Fujisaki. October 1999.

PEER 1999/04 *Adoption and Enforcement of Earthquake Risk-Reduction Measures.* Peter J. May, Raymond J. Burby, T. Jens Feeley, and Robert Wood.

PEER 1999/03 *Task 3 Characterization of Site Response General Site Categories*. Adrian Rodriguez-Marek, Jonathan D. Bray, and Norman Abrahamson. February 1999.

PEER 1999/02 *Capacity-Demand-Diagram Methods for Estimating Seismic Deformation of Inelastic Structures: SDF Systems*. Anil K. Chopra and Rakesh Goel. April 1999.

PEER 1999/01 *Interaction in Interconnected Electrical Substation Equipment Subjected to Earthquake Ground Motions.* Armen Der Kiureghian, Jerome L. Sackman, and Kee-Jeung Hong. February 1999.

PEER 1998/08 *Behavior and Failure Analysis of a Multiple-Frame Highway Bridge in the 1994 Northridge Earthquake.* Gregory L. Fenves and Michael Ellery. December 1998.

PEER 1998/07 *Empirical Evaluation of Inertial Soil-Structure Interaction Effects.* Jonathan P. Stewart, Raymond B. Seed, and Gregory L. Fenves. November 1998.

PEER 1998/06 *Effect of Damping Mechanisms on the Response of Seismic Isolated Structures.* Nicos Makris and Shih-Po Chang. November 1998.

PEER 1998/05 *Rocking Response and Overturning of Equipment under Horizontal Pulse-Type Motions.* Nicos Makris and Yiannis Roussos. October 1998.

PEER 1998/04 *Pacific Earthquake Engineering Research Invitational Workshop Proceedings, May 14–15, 1998: Defining the Links between Planning, Policy Analysis, Economics and Earthquake Engineering.* Mary Comerio and Peter Gordon. September 1998.

PEER 1998/03 *Repair/Upgrade Procedures for Welded Beam to Column Connections.* James C. Anderson and Xiaojing Duan. May 1998.

PEER 1998/02 *Seismic Evaluation of 196 kV Porcelain Transformer Bushings.* Amir S. Gilani, Juan W. Chavez, Gregory L. Fenves, and Andrew S. Whittaker. May 1998.

PEER 1998/01 *Seismic Performance of Well-Confined Concrete Bridge Columns.* Dawn E. Lehman and Jack P. Moehle. December 2000.